Hydrodynamic study of gas-solid flow in an internally circulating fluidized bed (ICFB) using experimental and CFD techniques.

Ravi K Gujjula

A Thesis Submitted to
Indian Institute of Technology Hyderabad
In Partial Fulfillment of the Requirements for
The Degree of Doctor of Philosophy

Department of Chemical Engineering

September, 2014

Declaration

I declare that this written submission represents my ideas in my own words and where others' ideas or words have been included, I have adequately cited and referenced the original sources. I also declare that I have adhered to all principles of academic honesty and integrity and have not misrepresented or fabricated or falsified any idea/data/fact/source in my submission. I understand that any violation of the above will be a cause for disciplinary action by the Institute and can also evoke penal action from the sources that have thus not been properly cited, or from whom proper permission has not been taken when needed.

_____

(Signature)

_____

(Ravi Kumar Gujjula)

_____

(CH09P002)

Approval Sheet

This thesis entitled **Hydrodynamic study of gas-solid flow in an internally circulating fluidized bed (ICFB) using experimental and CFD techniques** by Ravi Kumar Gujjula is approved for the degree of Doctor of Philosophy from IIT Hyderabad.

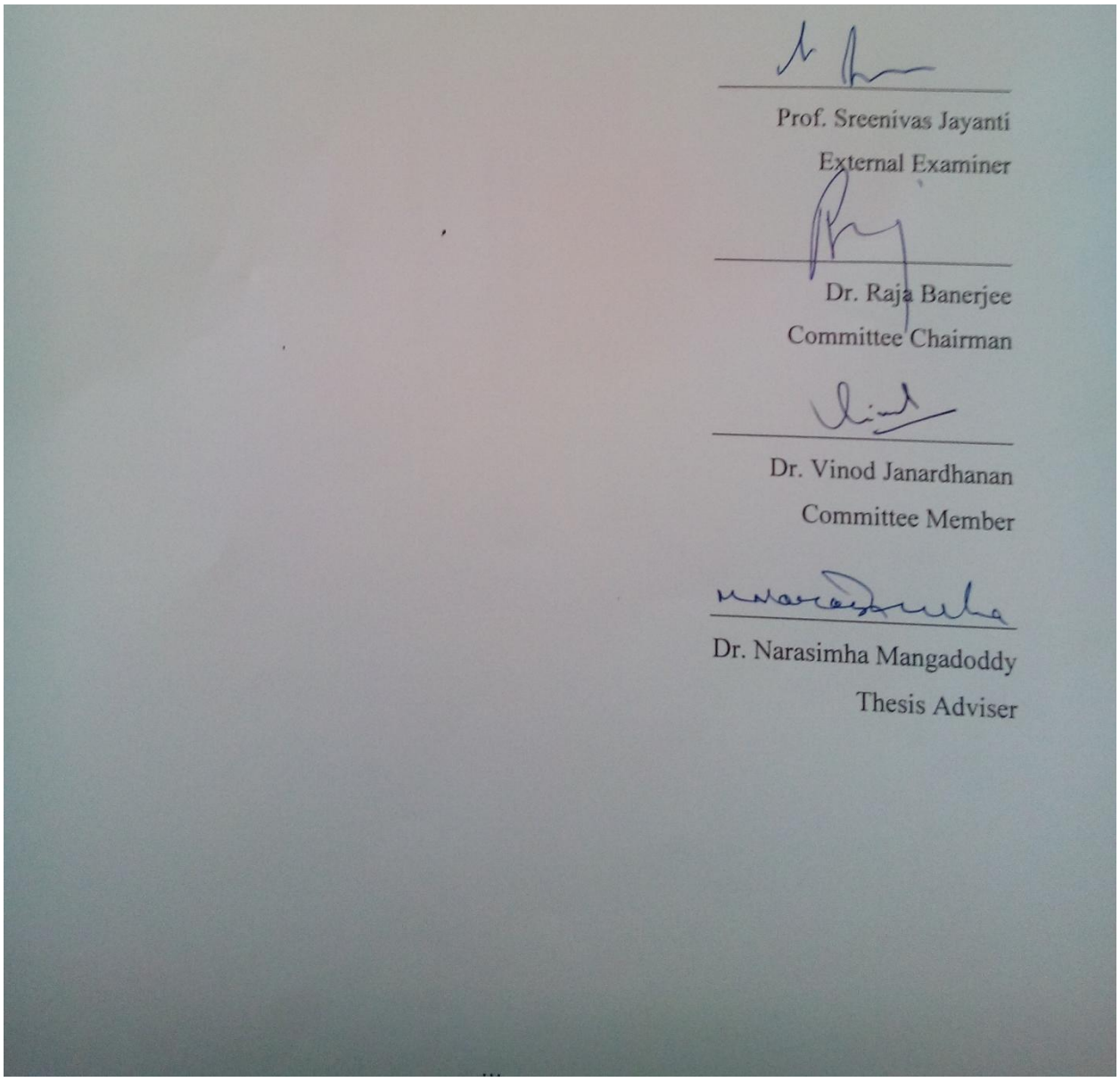

Prof. Sreenivas Jayanti
External Examiner

Dr. Raja Banerjee
Committee Chairman

Dr. Vinod Janardhanan
Committee Member

Dr. Narasimha Mangadoddy
Thesis Adviser

Acknowledgements

I have spent all the time in Indian Institute of Technology Hyderabad with joy of exploring the frontiers of science during my research work tenure. It's my pleasure to acknowledge all those who helped and supported me directly and indirectly.

First and foremost, I would like to express my sincere gratitude to Dr Narasimha Mangadoddy for his guidance, lively discussion, constructive and honest criticism, constant encouragement and expert advices. I am greatly indebted to him for giving me opportunity and excellent freedom to work under him.

I extent my sincere gratitude to Prof. PST Sai, Department of Chemical Engg, IIT Madras, , India, for his valuable suggestions during my initial stage of experimental setup and continuous support during my course work time in IIT Madras.

I am extremely grateful to my doctorial committee members Dr Anand Mohan, Dr Vinod Department of Chemical engineering, IIT Hyderabad, India and Dr Raja Benerjee, Department of mechanical Engg, IIT Hyderabad, India for their insightful suggestions and support throughout my work.

I would like to sincerely thank to Director, Indian Institute of Technology Hyderabad, Hyderabad, India for providing me financial support and facilities, residential quarters accommodation to carry out my research work.

I am extremely grateful to Dr Ramji, Department of mechanical Engg, and Sri K. Satyanarayana workshop in charge and workshop team for providing a place to setup my experimental work and continuous support during my experimental work at workshop, IIT Hyderabad.

I also extent my grateful thanks to my PhD colleagues Mr Teza, Mr BalRaju, Ms Asha , for their constant help and support.

I am grateful to my first batch PhD colleagues T. Durga Rao, Mr. Abdul, Harikishan, Mr. Ch. Kiran for their continuous support at various stages of my work.

I express my sincere thanks to my Dr Narasimha group lab mates Mr. Teza, Mr, V. BalRaja, Ms Asha, Mr. Mayank, Chaitanya, Ms Mandakini for their fruitful discussions to improve the quality of my work. And also mutual understanding and continuous exchange of thoughts among us helped to develop the research lab at boy's hostel in the initial stage.

I extent my sincere thanks to my Ph. D colleagues Mr. Sudhakare reddy, Mr. Chandrashekar, Mrs. Lakshmi, Mrs Vandana, Appari srinivas, Mr. Gowtham, Mr. Nanda for their continuous support and encouragement at various stages of my work.

I would like to sincerely thank to DST for providing me financial support to carry out my research work.

I express my sincere thanks to Teza for his help during thesis writing and pleasant company during my stay in the campus.

Finally, I am grateful to my parents whose encouragement and good wishes guided me through difficult times and Haritha & Nischay my lovely wife and son for all the support and understanding during at every stage of my work. I also thank all my family members, uncle and aunty for their love, affection and moral support throughout my research work.

Ravi K Gujjula

DEDICATION

To

MY BELOVED PARENTS

Abstract

Circulating fluidized bed (CFB) solid circulation systems are widely used in the process of catalyst regeneration, coal gasification, coking, thermal cracking, drying, incineration of solids waste as well as many other applications. However, conventional circulating fluidized beds require a tall tower as a solids riser and externally circulation of solids with the help of cyclones. Therefore to alleviate such problems encounter with CFB, several new generation fluidized beds have been developed. A circulating fluidized bed called as an internally circulating fluidized bed (ICFB) with a draft tube is one of the novel design. An ICFB is a type of fluidized bed with centrally located draft tube, which divides the bed into two sections called as annular section and draft tube riser. Because of simple and flexibility of operation have its own advantages. Literature review shows that there is still considerable uncertainty in establishing complete hydrodynamics of ICFB. Only few computational fluid dynamics (CFD) simulation studies were reported on ICFB and that to most of them considered 2D geometry of ICFB. Moreover, in all CFD simulations, particles were assumed to mono sized particles.

The main objective of the present research includes experimental and computational work followed by development of mathematical model for solids circulation rate to understand ICFB hydrodynamics. In the experimental study, an ICFB (0.3 mx3.0 m) with a draft tube (0.1 m x 0.6 m) is adopted to investigate the hydrodynamic characteristic of silica particles having wide range size distributions at cold bed test conditions. The particles with a moderately wide size distribution in the range of Geldart group B and Geldart group B-D nature are used in the experiments. U-tube manometer probes used to investigate the evolution of pressure drop across in the draft tube and the annular pressure drop. A complete pressure drop flow curves are established for wide range of static bed heights, draft tube gap height and gas superficial velocities. High speed camera was utilized to measure particle downward velocity in the annular moving bed region, which is useful to estimate solids recirculation rate in the ICFB. By assuming equal mass-flux between the draft tube's rising bed and the annulus downward moving bed, the draft tube gas bypassing fractions were estimated through the modified Ergun equation. The pressure drop in ICFB's draft tube found sharply decreases with superficial gas velocity after the minimum spouting fluidization, and then a cross-over is observed in the pressure drop of annular bed compared to the draft tube. Gas bypassing fraction increases with an increase in gap height and decreases with increased static bed height and mean particle size.

Hydrodynamic study of ICFB is also made by using the multi-phase CFD model for both 2D and 3D ICFB geometries. The model approach uses ANSYS's Fluent™ based two-fluid Eulerian model with kinetic theory of granular flow options to account particle-particle and particle-wall interactions. The model also uses the various drag laws to account the gas-solid phase interactions. These drag models are basically implemented into Fluent through UDFs. The 2D simulation results by various drag laws show that the Arastoopour and Gibilaro drag models predict the fluidization dynamics in terms of flow patterns, void fractions and axial velocity fields in close agreement with the Ahuja &Patwardhan (2008) experimental data. 3D simulations were also carried out for a large scale ICFB. The effect of superficial gas velocity and the presence of draft tube on solid hold-up distribution, solid circulation pattern, and gas bypassing dynamics for the 3D ICFB investigated extensively. The mechanism governing the solid circulation and the pressure losses in an ICFB has been explained based on gas and solid dynamics obtained from these simulations. Predicted total granular temperature distributions in 3D ICFB draft tube and the annular zone are qualitatively in agreement with the literature experimental data. The total granular temperature tends to increase with increasing solids concentrations and decrease with an increase of solids concentration. Additional CFD validation is also made w.r.to IITH's 3D ICFB geometry for 0.4 m bed condition with the identified suitable drag and granular options. The predicted pressure drop profiles and solids circulation rate well agree with ICFB experimental data.

A predictive mathematical model for solids recirculation rate of ICFB is established using the dimensionless approach. The coefficients of the dimensionless numbers were investigated using the multiple linear fitting routine by minimizing the sum of the squares of error between measured values to the predicted model values. The fitting routine estimates the parameter values in the equations tested. A very large number of equation forms were investigated. Each one was assessed in terms of goodness of fit, fitting statistics, significance of variables, and practical utility. The final model equation was found to be the best according to these criteria. These model predictions well matched with experimental data within ± 30% error limits.

List of publications

Publications (Reputed journals or referred conferences)

1. **Ravi Gujjula**, Narasimha M., Experimental Investigation of Hydrodynamics of gas-solid flow in an Internally circulating fluidized bed**, Canadian Journal of Chemical Engineering,** 2015 DOI: 10.1002/cjce.22233

2. **Ravi Gujjula,** Narasimha.M "Hydrodynamic study of gas-solid internally circulating fluidized bed using multi-phase CFD model**,** International journal of particulate science &Technology 2014, DOI:10.1080/02726351.2015.1013590

3. **Ravi Gujjula,** Narasimha.M., Prediction of solid recirculation rate and solid volume fraction in an internally circulating fluidized bed**,** International Journal of Computational Mechanics, 2014, DOI: 10.1142/S0219876215400058

4. Teja Reddy Vakamalla, Kedar S. Kumbhar**, Ravi Gujjula,** Narasimha Mangadoddy, Computational and experimental study of the effect of inclination on hydrocyclone performance**, Separation and Purification Technology,** 2014 (138) 104-117.

5. **Ravi Gujjula,** Narasimha.M., Hydrodynamics study of gas-solid flow patterns in an internally circulating **fluidized bed with a draft tube,** ***11th International conference on Fluidized bed Technology, 14-17th May 2014*, Beijing, China.** PP 167-174

6. **Ravi Gujjula,** Narasimha.M., Sai, P.S.T., CFD prediction of solid recirculation rate and solids volume fraction in an ICFB**, *5th Asia pacific congress on computational mechanics & 4th international symposium on computational mechanics (APCOM 2013 / ISCOM 2013) 10-14th, Dec. 2013*, Singapore.** PP 1886

Non-referred (Full papers) Conferences

1. **Ravi Gujjula,** Narasimha.M "Hydrodynamics of Internally Circulating Fluidized bed." ***India-UK International Summer School conference on Efficient Fossil Energy Technologies, July04-10, 2011*, IIT Guwahati & The University of Nottingham.**

2. **Ravi Gujjula,** Narasimha M "Simulating gas-solid flow patterns in an Internally Circulating Fluidized bed with draft tube" ***XII International conference on Mineral processing technology-MPT-2011*, Oct 20-23,2011,Udaipur, India.**

3. **Ravi Gujjula,** Narasimha.M."CFD modeling of gas-solid flow and its patterns in an ICFB with a draft tube" ***IV th International Congress on Computational Mechanics and Simulation (ICCMS)*- 10-12 December 2012, IIT Hyderabad.**

Nomenclature

Aa	Draft tube area
Ad	Annulus area
A_{Gap}	Gap area for the gas to flow
C_D	Drag coefficient (-)
d_p	Particle diameter (m)
e_s	Coefficient of restitution
g	Acceleration due to gravity (m/s2)
$g_o(\varepsilon_s)$	Radial distribution function
G_s	Solid recirculation rate (kg/m^2s)
$\boldsymbol{I}$	Unit tensor (-)
k	Diffusion coefficient of granular temperature (kg/ms)
P	Pressure (N/m2)
P_s	Granular pressure (N/m2)
R	Radius of ICFB (m)
r	Draft tube radius (m)
Re_p	Particle Reynolds number (-)
U_a	Superficial velocity in the annulus (m/s)
Uo, U_d	Superficial velocity in the draft tube (m/s)
U_{pr}	Particle velocity in the riser
V_{rs}	Terminal velocity (m/s)
v_s'	Ensemble averaged magnitude of the randomly fluctuating velocity of the solid particles (m/s)
v_s	Solid Velocity (m/s)
v_g	Air Velocity (m/s)

fps	Frames for second
W_s	Solid circulation rate

Greek Symbols

β	Inter-phase momentum transfer coefficient (kg/m3s)
λs	Granular bulk viscosity (g/ms)
μs	Solid viscosity (kg/ms)
μg	Gas viscosity (kg/ms)
π	Irrational number
Θs	Granular temperature (m2/s2)
Θt	Total granular temperature
εg	Air volume fraction
εs	Solid volume fraction
γ	Collisional dissipation of energy (kg/m3 s)
ϕs	Transfer rate of kinetic energy (kg/m3 s)
ρg	Air density (kg/m3)
ρs	Solid density (kg/m3)
ρ_b	Bulk density of a particle (kg/m3)
τg	Gas stress tensor (N/m2)
τs	Solid stress tensor (N/m2)
εmf	Minimum fluidization

μs, fr Frictional viscosity

μs, col Collisional viscosity

μs, kin Granular viscosity

Subscripts

g Gas phase

s Solid phase

Abbreviations

AD Arastoopour drag

BH Bed height

BFB Bubbling fluidized bed

CFB Circulating fluidized bed

FCC Fluid catalytic cracking

GH Gap height

ICFB Internally circulating fluidized bed

ID Internal diameter

KTFG Kinetic theory of granular flow

PSD Particle size distribution

PIV Particle image velocimetry

RCFB Recirculating fluidized bed

SRR Solid recirculation rate

SD Standard deviation

TFM Two fluid model

UDF User defined function

Contents

Chapter1

Introduction

Hydrodynamics study of gas-solid flow in internally circulating fluidized bed with a draft tube is studied in this current research work. An introduction to the research background, objectives & scope and thesis structure are presented in this chapter.

1.1. Research Background

Fluidization is a process whereby a bed of solid particles is transformed into something closely resembling a liquid. This is achieved by pumping a fluid either a gas or liquid upwards through the bed at a rate that is sufficient to exert forces on the particles that exactly counteracts their weight[1]. Fluidization operation mainly used in the gas-solid, liquid-solid and gas-solid-liquid contacting operation in the chemical processes industries. Gas solid fluidization has a wide range of industrial applications like catalytic reactions of combustion and gasification reactions to convert coal, biomass, and waste matter into useful fuels or synthesis gas, drying, coating etc. In a number of all this applications there is a particle size reduction during operations which is leading to several problems Associated with different particles sizes in terms of solids circulation rate via external cyclone are also influences by particle mean size, a tall tower required to fluidized particles, handling of smaller sized particles as bed material with high bulk density, larger particles significantly effect minimum bubbling fluidization velocity e.t.c.

Different hydrodynamic regime can be observed depending on the particle characteristics and the magnitude of the superficial gas velocity. With increasing gas velocity, these flow regimes are fixed bed, bubbling fluidization, slugging fluidization, turbulent fluidization, fast fluidization and pneumatic conveying regimes. The bubbling, slugging and turbulent fluidization regimes are considered as conventional fluidization. The main characteristic of the conventional fluidized beds is that the beds operate at relatively low superficial gas velocity (usually less than 1-2 m/s) with little solids entrainment.

Based on the definition, several modes of fluidized state are considered with respect to superficial velocity. Which are, fixed bed, bubbling fluidized bed, turbulent fluidized bed and fast fluidized beds or circulating fluidized bed [2]. First generation fluidized beds are fluidized bed combustor (FBC), which are

being operated is in the bubbling fluidization mode. The second generation ~~fluidization are~~fluidization is called circulating fluidized bed (CFB). FBC's are without recirculation of unconverted particles achieved less combustion efficiency. Recirculation of unburnt particles into the fluidized bed helps to achieve higher combustion efficiency as high as more than 90% [3]. These CFB's are also associated with significant heat losses.

The various problems associated with the particles of different size or change in particles size during the operation would be encountered in the fluidization operation beginning from first generation FBC to CFB's. Now a day's CFB is widely used in coal combustion coal gasification and petroleum refinery processes. However conventional CFB's in general require a very tall tower as a solids riser and an accompanying a cyclone to external recycle the separated solids from the gas stream. To alleviate above said typical operation with CFBs such as tall tower, external cyclone and solids residence time, several new types of circulating fluidized beds have been proposed to overcome CFB disadvantages. They are spouted bed, spouted bed with draft tube and internally circulating fluidized bed (ICFB) [3].

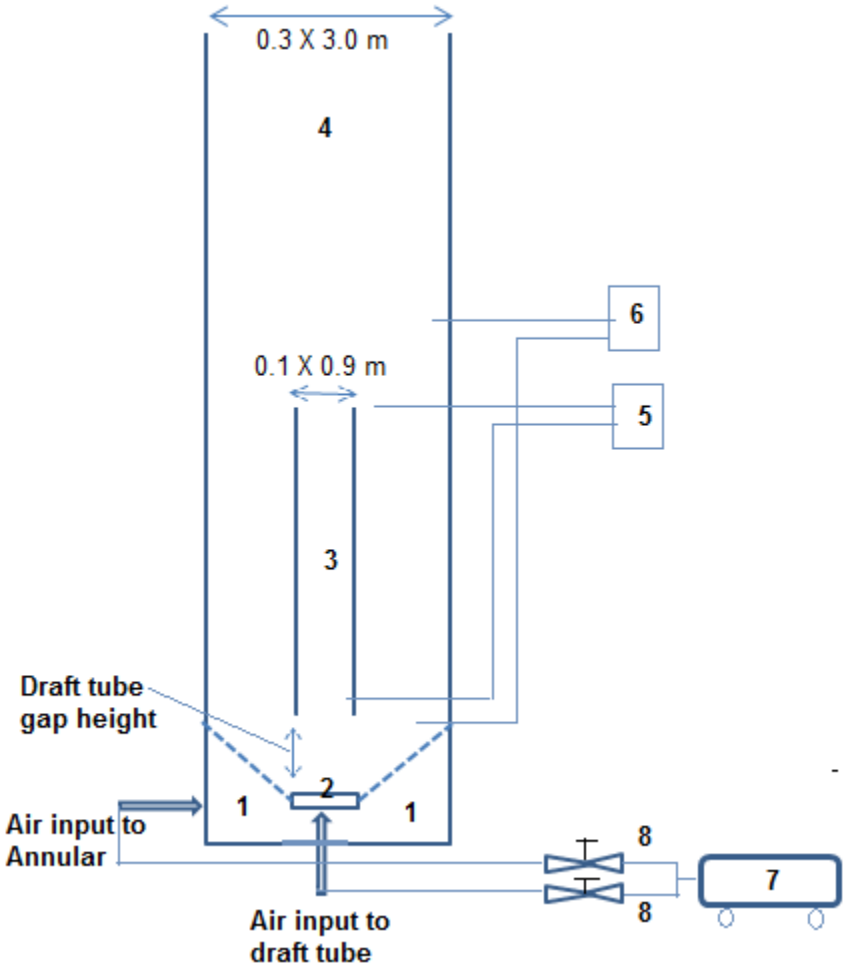

Figure 1: Schematic diagram of ICFB section. (1) annular air box (2) draft tube distributor (3) draft tube (4) ICFB (5) draft tube pressure measuring ports (6) annular bed pressure measuring ports (7) compressor (8) Air control value

ICFB was initially developed in the year 1987 [4], with a centrally located draft tube to divide the bed for internal solids circulation in a single vessel to reduce the height of conventional circulating fluidized bed and its construction cost. Draft tube acts as fluidized bed riser. Air input through the annular section will help smooth solids circulation or to avoid solids accumulation at the bottom of ICFB column. In the ICFB fluidized particles are spouting from the draft tube to fall on to the annular section and move downward to the bottom of the ICFB to enter into the draft tube through a gap height between the draft tube bottom and the draft tube air distributor as shown in the Fig. 1.

This ICFB reactor has several advantages such as its compact size, comparatively small heat loss from the reactor compared to conventional circulating fluidized beds (CFBs) since its riser is located inside the

reactor and its annular bed acts as a heat sink. Also, longer residence time of fine particles in the annulus section may provide higher conversion level compared to conventional fluidized bed combustors (FBCs) [5-7]. Therefore, ICFB reactors have been utilized for coal combustion , coal gasification of both high grade and low grade coal, incineration of solid wastes, continuous adsorption and desorption and desulfurization [6].

It has been noticed that ICFB divides the fluidized bed into two zones for internal circulation of solids in a single vessel with a significant reduction in column height compared to the conventional CFB [3, 8]. The gas velocities in the draft tube and annulus sections were different from the superficial gas velocities having with different gas distributors due to varying levels of gas bypassing between the draft tube and the annulus section [9]. The gas distribution between draft tube riser and annular section is controlled by inlet geometry. The solids circulation rate can be controlled by adjusting the input gas velocities to the draft tube and the annular section. Moreover that eruption motion of solids at the top of draft tube can reduce particle elutriation from the reactor significantly [10, 11]. Thus for the fine particles the residence time in the reactor is prolonged and conversion levels are increased as compared with the conventional fluidized beds. Most of the experimental studies in the literature have been targeted to measure pressure drop and descending annular bed particles velocity. Pressure drop is usually measured using pressure probes or manometers. The deceasing particle bed velocity is measured by tracer particles. However, limited literature available data is available on full pressure flow curves both in annulus & draft tube. Further, most of the studies have utilized either mono size or narrow size range particles. A few studies have also measured the gas bypassing fraction using online Gas chromatography [12, 13] and few are estimated gas bypassing using equal mass flux equations [14].

According to literature in the past the experimental and the computational fluidization simulation studies mainly focused on pressure drop fluctuation during the minimum fluidization, solids recirculation rate and gas bypassing fraction between draft tube and annulus section. In recent years growing interest is observed towards to the local dynamic behavior of gas-solid flow in ICFB in order to improve the understanding of the interaction between the two phases. With the increase of the computational power, the numerical simulation has become an additional tool for prediction of hydrodynamics of CFB's which are difficult to be revealed by current experimental measurement techniques.

In this thesis, author made an effort to study hydrodynamics of ICFB with appropriate configuration of draft tube gap height and different sized bed materials both by experimental and computational methods

and attempted to validate CFD data with ICFB experimental data. An attempt is made to develop an empirical model to predict solids recirculation rate for a given ICFB design and operating conditions.

1.2 Research objectives and scope

The following objectives are made to pursue in the thesis.

- To develop an accurate and reliable CFD model based on kinetic theory of granular flows for the ICFB hydrodynamics
- To establish an experimental method for reliable measurements of pressure drop with in the draft tube and annular regions and moving particle velocity in the annular region.
- To understand the hydrodynamics of the ICFB having Geldart B and B-D particles in terms of gas-solid flow field, voidage distribution, local solid segregation and solids fluctuating velocity field.
- To validate the CFD predicted data against the measured experimental data on large scale ICFB
- To develop a reliable one dimensional mathematical model for solids recirculation rate (G_s) based on dimensionless analysis.

1.3 Arrangement of thesis

The present work has been reported in this thesis comprising of seven chapters

Chapter 1 presents an introduction about fluidized bed features, internally circulating fluidized bed (ICFB) and current industrial importance of fluidization. It elaborates the gap areas for the novel second generation of fluidized bed as ICFB.

Chapter 2 presents a detailed literature review for different types of fluidized beds starting from fluidized bed combustors to spouted fluidized bed and circulating and internally circulating fluidized beds. Focused on hydrodynamic study of different types of measurement methods particularly in the case of pressure drop by pressure probes manometers etc, solids recirculation rate by thermister probes and hot solids tracer techniques, solids volume fraction by optical fiber probes and gas bypassing fraction by tracer gas techniques. This chapter also briefs on CFD modeling and available mathematical models of ICFB.

Chapter 3 summarizes detailed design of internally circulating fluidized bed fabrication, experimental methodology and CFD methodology using Elerian-Eulerian two fluid model with inclusion of kinetic theory of granular flow (KTGF) to predict hydrodynamics behavior of ICFB and granular temperature estimation calculation. It also presents determination of total pressure drop across the bed in both draft tube, and annular section, minimum spouting fluidization velocity under stable spouting operation conditions, solid recirculation rate and gas bypassing fractions.

Chapter 4 present CFD methodology that is implemented for 2D small scale of ICFB geometry. Ahuja & Patwardhan[15] 2D case was considered for the CFD simulation runs. The modeling approach adopted to simulate hydrodynamics of ICFB by using commercial software package ANSYS fluent 13.0. The Eulerian-Eulerian model or two fluid model (TFM) is used along with the kinetic theory of granular flow (KTGF) options for solid phase stress. Various drag models tested and finally identified the suitable drag model that predicts the gas-solid dynamics accurately for 2D ICFB. Grid independency check was made extensively identified the optimized mesh. 2D ICFB CFD simulation data validated against Ahuja & Patwardhan [15] experimental data. The model is then extended to 3D for Kim et al. [16] geometry with an appropriate feed flow rates and different particle sizes. Gas-solid flow hydrodynamics were simulated in terms of ΔP, ε_s, G_s and Θ for various superficial velocities and particle sizes.

Chapter 5 presents experimental data analysis of hydrodynamics of ICFB in terms of pressure flow curves for different size range of bed materials (Geldart B and Geldart B-D groups) and variation of gap height (7.5 cm to 14.5 cm) between the draft tube and air distributor. Pressure drop and solids recirculation rate were measured. The effect of superficial gas velocity, static bed height and the draft tube gap height on pressure drop profiles, solid circulation pattern, and gas bypassing dynamics for the ICFB investigated extensively.

Chapter 6 presents the validation of 3D IFCB CFD simulation data of with IITH's ICFB experimental data in terms of pressure drop, solids recirculation rate (SRR). The predicted pressure drop data validated with experimental data for different bed heights. A qualitative comparison is made for G_s

Chapter 7 This chapter presents the mathematical techniques of dimensional analysis, mathematical model development of ICFB for the solids recirculation rate. Model Equations for fluidized bed solid recirculation rate is proposed to evaluate the dependence of major design and operating variables on fluidized bed recirculation rate

Chapter 8 presents the conclusion of the research work and suggestions for further work.

Appendix: Appendix-I presents the experimental data sets, Appendix-II-CFD validation data, Appendix-III mathematical model for solids recirculation rate and Appendix-IV presents UDF software programming for drag models.

Chapter2

Literature review

2.1 Introduction

Particulate technology has played an important role in many industrial unit process and unit operations such as chemical processing, mineral processing, pharmaceutical production and many energy related process, etc and in particular, gas-solids fluidization has been widely employed in recent decades [17]. Particles contained in a column can be fluidized when gas is introduced via a gas distributor at the bottom of the column.

When a fluid is passed upwards through a bed of particles, the bed remains packed at low superficial fluid velocities. However, when the velocity of fluid is increased sufficiently to a point where the drag force on a particle is balanced by the net gravitational force, this is the point of incipient fluidization, and beyond which the bed is said to be fluidized. The superficial fluid velocity at the point of incipient fluidization is called the minimum fluidizing velocity. Different hydrodynamic regime can be observed depending on the particle characteristics and the magnitude of the superficial gas velocity as indicated in the Fig 2.1. At these excess velocities one of two phenomena will occur. The bed may continue to expand, and the particles move themselves uniformly, excess fluid may pass through the bed as bubbles, which is similar to the analogy of a boiling liquid. The former is known as particulate fluidization and in general occurs with liquid-solid systems. The latter, is concerned with the present work occurs with most gas-solid systems.

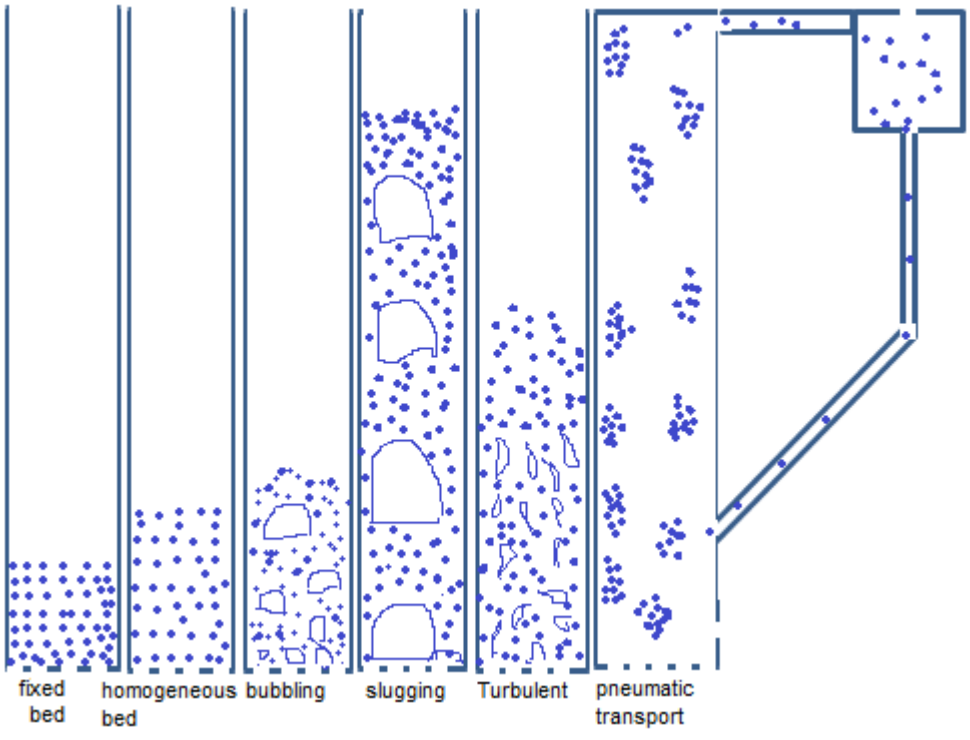

(a)

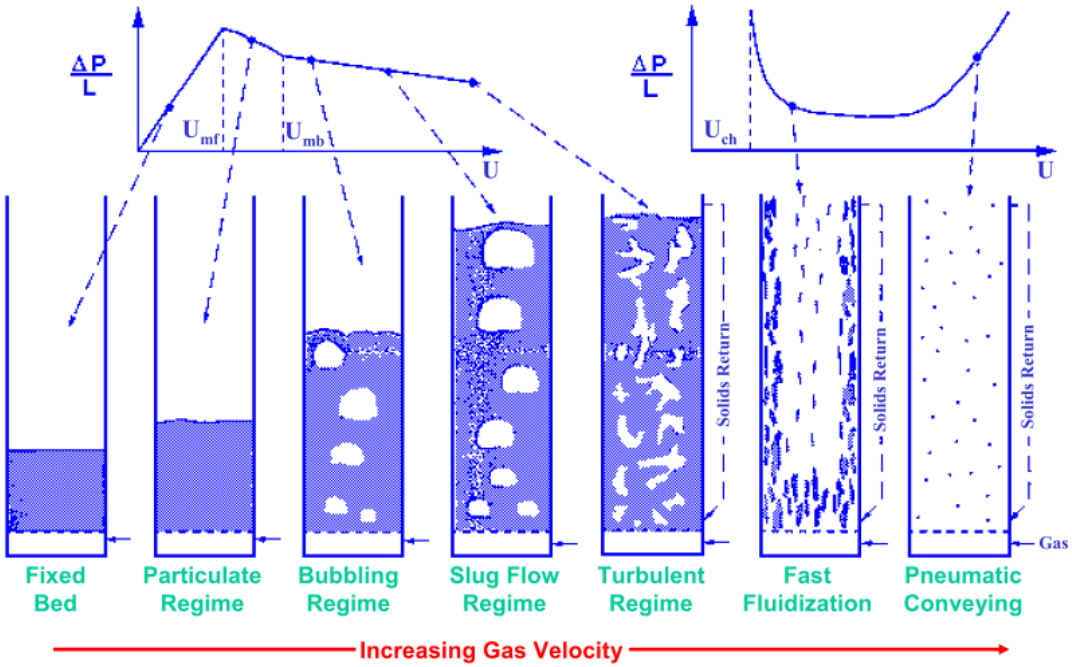

(b) Regimes of Fluidization

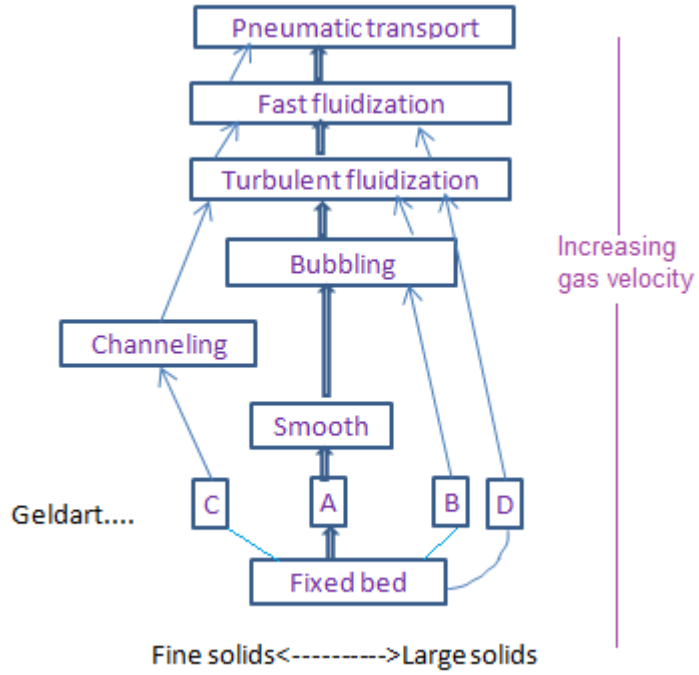

(c)

Figure 2.1 (a) Gas- solid flow classification according to Kunii and Levenspiel (1991) [2] based on the Geldart (1973) [18] particle classification.(c) Gas-solids contact (flow regimes) with change in gas velocity [2]

and is called aggregative fluidization [2]. Throughout this thesis the term fluidization is taken to mean as gas-solid fluidization. A fluidized bed is characterized by rapid particle movement, caused by the rising bubbles, and consequently good particle mixing, high rates of heat transfer and uniform temperature profiles are possible. These properties have led to the use of fluidized beds in a wide range of unit operations and unit processes including coating of metal with plastic, drying of solids, transportation, heating, adsorption, etc. Gas solid fluidization is widely used in chemical operations such as coal gasification, synthesis reactions, combustion and incineration, carbonization and gasification, roasting of sulphide ores, reduction of iron oxide, water split reaction into hydrogen, biochemical reactors, etc,.

2.2 Different types of non conventional fluidized beds and its development

The conventional fluidized beds also possess some serious deficiencies, however, the bubbles that are responsible for many benefits of a fluidized bed represent the fluid bypassing and reduction of fluid–solids contacting. The rapid mixing of solids in the bed leads to non-uniform solids residence time

distribution in the bed. The rigorous solids mixing in the bed also leads to attrition of bed material and increases the bed material loss from elutriation and entrainment. Thus for many industrial applications, the conventional fluidized beds have been modified to overcome those disadvantages. Those modifications, in many ways, alter substantially the operational characteristics of the fluidized beds and also change the design and engineering of the beds. It is the intent of this chapter to discuss about non-conventional fluidized beds in detail: CFB, the spouted bed, the recirculating fluidized bed (RCFB) with a draft tube. The development of fluidized bed technology from fluidized bed combustor to ICFB as mentioned below.

1921, Fritz Winkler, Germany, Coal Gasification

1938, Waren Lewis and Edwin Gilliland, USA, Fluid Catalytic Cracking, Fast Fluidized bed

1960, Douglas Elliott, England, Coal Combustion, BFB

1960 Ahlstrom Group, Finland, First commercial CFB boiler, 15 MW th , Peat

1974 Spouted bed Mathur and Epstein [19].

1983 The spouted fluid bed with a draft tube (Yang and Keairns [20])

1992 Internally circulating fluidized bed (Kim et al. [8])

The first extensive assimilation of the literature came from the publication of spouted Beds by Mathur and Epstein [19]. A more recent review can be found in Epstein and Grace [21]. A classical and conventional spouted bed is shown in Fig. 2.2. The fluid is supplied only through a centrally located input jet. If the fluid velocity is high and the bed is low enough, the fluid stream will punch through the bed as a spout as shown in Fig 2.2

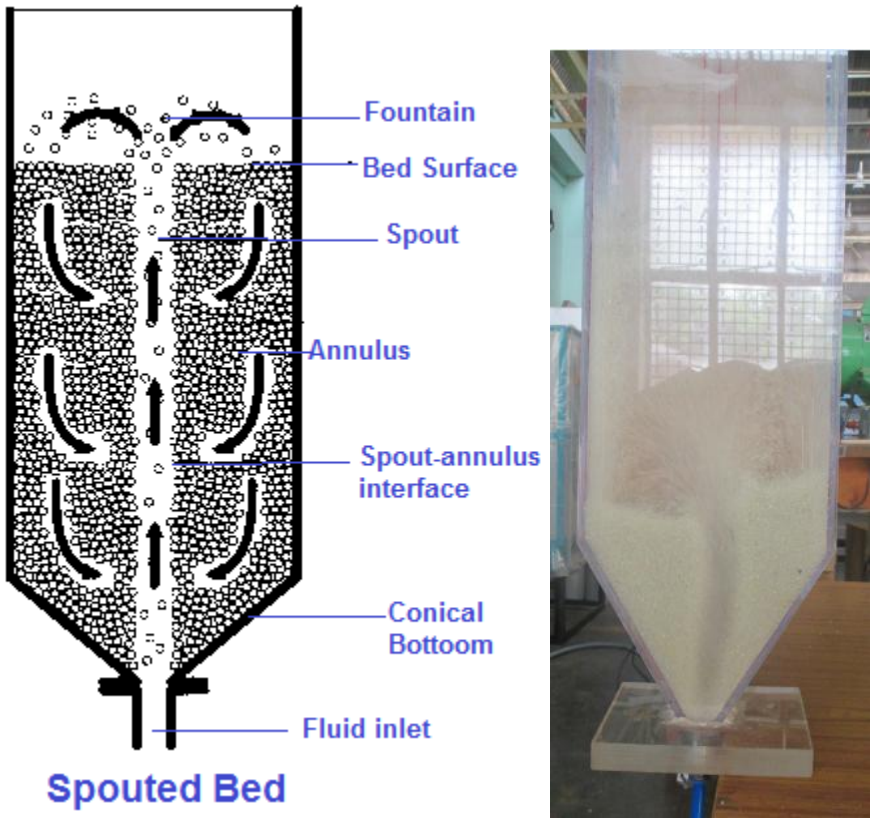

(a) (b)

Figure 2.2 Schematic spouted beds (Mathur and Epstein, 1974 [19] (a) Conventional spouted bed (b) Spouted bed (IITH's)

The words spouted bed and spouting were first coined by Mathur and Gishler [22] at the National Research Council of Canada during the development of a technique for drying wheat. The spout fluid will entrain solid particles at the spout–annulus interface and form a fountain above the bed. The spout fluid will also leak through the spout–annulus interface into the annulus to provide aeration for the particles in the annulus. The spouted bed is usually constructed as a cylindrical vessel with a conical bottom as shown in Fig. 2.2 to eliminate the stagnant region. Spouting in a conical vessel has also been employed. Solid particles can be continuously fed into the spouted bed through the concentric jet or into the annulus region and continuously withdrawn from the annulus region, just as in a fluidized bed.

First generation FBC boilers are in the bubbling fluidization mode and are, therefore, called stationary bubbling FBC boilers. Second generation FBC boilers employ the fast fluidization regime, and are consequently called CFBC boilers. Bubbling FBC boilers without recirculation of unburned particles achieve combustion efficiency of 90%. Recirculation of unburned particles and their reintroduction into

the furnace helps achieve combustion efficiency as high as 98%, depending on the coal type. Introduction of fly ash recirculation has enabled higher SO_2 retention and better limestone utilization.

Circulating fluidized bed has been widely used in coal combustion & gasification and petroleum refining processes. However, conventional circulating fluidized beds require a very tall main vessel as a solids riser and an accompanying tall cyclone to recycle separated solids from gas stream. To reduce the height of conventional circulating fluidized beds, construction costs, space and maintenance cost, several new types of circulating fluidized beds proposed to overcome above such problems by adopting draft tube mechanism in traditional fluidized bed. To avoid the above mentioned problems in CFB's, several novel types of CFB's have been explored in the past. One of the novel concept is called internally circulating fluidized bed (ICFB). The re-circulating fluidized bed with a draft tube concept is schematically illustrated in the Fig. 2.3.

2.3 Brief literature review

In this section literature reviewed separately for experimental studies, CFD simulations and mathematical model development with respect to the ICFB.

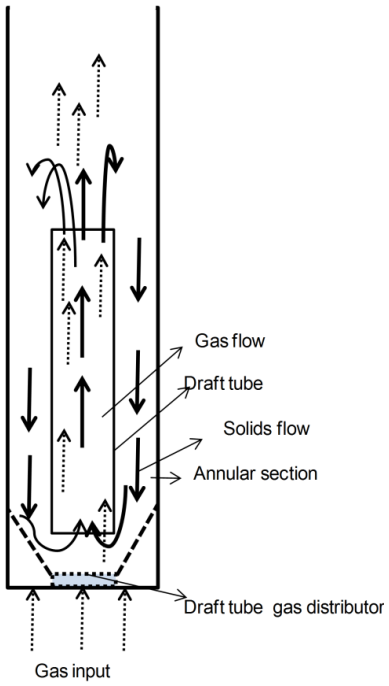

Figure 2.3 Recirculating fluidized bed

2.3.1 Experimental review

This ICFB concept was first called a recirculating fluidized bed by Yang and Keairns [20]. Several other names have also been used to describe the same concept: the fluid-lift solids recirculator [23], the spouted fluid bed with a draft tube [9, 24] the internally circulating fluidized bed [25, 26] or simply a circulating fluidized bed [3]. The addition of a tubular insert, a draft tube, in a spouted fluid bed changes the operational and design characteristics of an ordinary spouted bed. Notably, there is no limitation on the so-called ‘‘maximum spoutable bed height’’. Theoretically, a re-circulating fluidized bed with a draft tube can have any bed height desirable. It was observed that, when bed material are tested with bed depth exceeding the maximum spoutable bed height the region of stable flow pattern is narrow and a stable coherent spout or fountain cannot be obtained. Instead , periodic and in coherent spouting and spouting fluidization occurs [19].The so-called ‘‘minimum spouting velocity’’ will also be less for a re-circulating fluidized bed with a draft tube because the gas in the draft tube is confined and does not leak out along the spout height as in an ordinary spouted bed. There is considerably more gas-solid contacting operation and design flexibility for a re-circulating fluidized bed with a draft tube. The down comer region can be separately aerated. The gas distribution between the draft tube and the annular section can be adjusted by changing the design parameters at the draft tube inlet. Because the draft tube velocity and the down comer aeration can be individually adjusted, the solid circulation rate and particle residence time in the bed can be easily controlled. A detailed discussion of the re-circulating fluidized bed with a draft tube was made first by Yang [27]. Operating conditions for a re-circulating fluidized bed can be flexible as well. The bed height can be lower than the draft tube top or just cover the draft tube top so that a spout can penetrate the bed as in a spouted bed. The bed height can also be substantially higher than the draft tube top, so that a separate fluidized bed exists above the draft tube.

Operating the draft tube as a dilute-phase pneumatic transport tube, one can fluidize the solids inside the draft tube at lower velocities to induce the necessary recirculation of the solids. Several studies were conducted in this fashion [28]. The draft tube wall can also be solid or porous, although most of the studies in the literature employ a solid-wall draft tube [3]. Claflin and Fane [29] reported that a porous draft tube is suitable for applications in thermal disinfestation of wheat where control of particle movement and good gas/solid contacting could be accomplished at a modest pressure drop. The concept can also be employed as a liquid–solids and liquid–gas–solids contacting device [30].

Re-circulating fluidized bed [RCFB] or ICFB has some major advantages over the spouted fluidized bed like no constrain on the maximum spoutable height, uniform particle residence time in the riser etc.[31] The spouting velocity requirement is less comparatively with spouted beds since there is no dispersion of

gas [9]. The draft tube allows the particles to follow nearly a plug flow. Other advantages of RCFBs are compact size, high heat and mass transfer, uniform temperature and high mixing. The RCFBs have a variety of applications in coating, combustion and gasification of oil and coal [20]. Alappat and Rane [31] reported the use of RCFB for incineration of liquid waste-like distillery spent wash.. In recent years, a number of published articles have been reported valuable information about the hydrodynamics characteristics of ICFB with a draft tube. Riley and Judd [11] described a micro reactor which was developed to measure char-steam gasification kinetics under conditions which simulate the behavior of char in the fluidized bed with a draft tube. Chandal and Alappat [14] studied the effect of different operating conditions and design parameters such as flow rate, inventory of bed solids and draft tube gap height on the pressure drop profile for a re-circulating fluidized bed. Milne and Berruti [25] proposed a modified spout-fluid bed with draft tube called the ICFB, which eliminates gas bypassing from spouted bed to annular bed and helps in controlling the spout gas residence time. Zhong, Zhang and Jin [32] developed a novel method of particle tracking to measure solids circulation rate by combining with microwave heating and infrared thermal imaging technology in a flat-bottom spout-fluid bed.

Despite the wide applications of the RCFB, there are only a few studies reported in the literature on the hydrodynamics of the reactor operating with particle a size distribution. The brief literature on ICFB is tabulated in the Table 2.1. The listed investigations are mainly focused on the determination of pressure drop and solids circulation rate.

Very little attention was given to the detailed full pressure flow curves and its fluctuation in the draft tube and annular regimes. Most of the hydrodynamic studies limited to handle either mono size or a narrow sized particle distribution. A few studies have also measured the gas bypassing fraction using online Gas chromatography [13, 16] and few are estimated gas bypassing using equal mass flux equations [14]. Many of the researchers reported hydrodynamics by considering draft tube input superficial velocity only. Nevertheless, the characteristics of the gas-solid suspension flow in ICFBs are not yet fully understood due to their complicate turbulent flow and intensive phase interactions. In the view of ICFB as potential industrial applications there is a need of further investigation on hydrodynamic characteristics of this new generation fluidized bed. One can observe that ICFB divides the fluidized bed into two zones for internal circulation of solids in a single vessel with a significant reduction in column height compare to conventional CFB [8]. The gas velocities in the draft tube and annulus sections were different from the given superficial gas velocities with different gas distributors due to varying levels of gas bypassing between the draft tube and annulus sections [9]

Author	Particulate system & Experimental conditions	Column configuration	Measured quantities	Experimental observations
Lee et al.[33]	dp=0.25-0.46 mm, bed material sand particles, Vmf= 0.121 m/se mf=0.48	(0.3m-l.D.X0.6m- high) with a draft tube (0.1m-I.D. 0.3m-high) gap height 0.065-0.14 m	• Entrainment rate • Solids circulations rate	A predictive mathematical model based on pressure drop in the riser of an Internally Circulating Fluidized Bed (ICFB) is developed to predict solids circulation rate (G_s)
Kim et al.[7]	dp=130 µm, bed material PVC, Vmf= 0.008 m/s dp=210-610µm, bed material sand Vmf= 0.04 m/s- 0.27 m/s	Plexiglass column, Draft tube 0.1X0.3m Column 0.3X2.6m , gap height 0.14 m	• Entrainment rate • Transport disengaging height	The effects of gas velocity and particle size dp on the transport disengaging height (TDH),Fluidized bed with and without draft tube
Song et al. [12]]	Flat plate, conical plate, conical plate ring sparger.Bed material sand, dp=0.3 mm, Vmf= 0.1 m/s, e mf=0.48	Draft tube 0.1X0.3m Column 0.3X2.5m	• gas bypassing using co2 tracer • particle downward velocity measurement using thermister probes with hot sand as a tracer	The effects of gas distributor, draft tube height, gas velocity and gap height on the circulation of solids.
Ahn et al.[13]	Orifice diameter 15, 20, 25 & 30 mm, Bed material sand, dp=0.3, 0.39, 0.46 & 0.61 mm, Vmf= 0.1 m/s, e mf=0.48	Draft tube 0.1X0.9m Column 0.3X2.5m	• gas bypassing using co2 tracer • particle downward velocity measurement using thermister probes with hot sand as a tracer	The effects of orifice diameter in the draft tube, particle size, gas velocities and bed height on the circulation rate of solids
Kim et al.[16]	Average particle size, 86, 120, 170 & 288 µm,	0.1m and column diameter 0.3m, height	• Pressure drop using pressure transmitter • particle downward velocity	Hot solid tracer technique to determine solid circulation rate.

	Vmf= 0.1 m/s, e mf=0.48	2.6 m	measurement using two thermister probes with hot sand as a tracer	Effects of superficial gas velocities to a draft tube, to an annulus section and particle size on the solid circulation rate.
C.Y. Chu & S.J. Hwang [34]	Bed materials calcium sorbent 254, 385 and 460 µm their U mf= 19.3, 5.6, 12.4 and 17.0 cm/s, respectively & silica particles mean 460 µm, emf=0.5	Column 9cmX 2.5 m Draft tube height 30cm and diameter 4 cm	• Solid circulation rate measure using black silica particles as a tracer particles	Prediction of solids circulation rate in the riser of an internally circulating fluidized bed (ICFB)
Namkung et al. [35]	Bed material sand particles 185 µm	Column 0.355X2.5m Draft tube 0.078mX1.5m	• Pressure taps are used to measure pressure drop • Solids circulation rate by using thermocouple with hot solids as trace	effects of operating conditions and geometrical configuration on the solids circulation flux and gas bypassing
Rui Xiao et al [36]	Mean particle dia of glass beads 2.076mm,	Column 200mmX5000mm, draft tube 42 mm dia and 1 m height	• Solids circulation rate my solid sample collection method and gas bypassing by CO_2 trace method	Cylindrical column with cone type distributor, effects of operating conditions and geometrical configuration on the solids circulation flux and gas bypassing
Chandel and Alappat [14]	Geldart D particles, Coarse 1.7 mm & Fine (Geldart B) 0.6 mm, Vmf= 0.176 , e mf=0.378	Draft tube diameter 0.05 m, column diameter 0.15 m Draft tube height 1.0 m	• Pressure drop using U tube water manometer	pressure drop profile for a recirculating fluidized bed has been studied, inventory of solids and gap

		Gap height 0.03, 0.05, 0.095m		height
Ahuja G.N and Patwardhan A. W [15]	polypropylene particles (710–1000 µm), mean particle size 853 µm, Vmf= 0.176 , e mf=0.378	DD=0.1 m, height=0.158 m, column=0.186m , Height 1.2m	• Pressure drop • Solid hold-up measurement using Gamma ray tomography	The hydrodynamics of a gas–solid fluidized bed was studied by using with and without draft tube, complete and partial sparging, tomographic measurements of solid hold-up
Jin Hee Jeon et al. [37]	Bed material sand particles dp = 0.3mm, Umf =0.074 m/s	(0.28m×0.28mwidth×2.6mheight) with a centrally located draft tube (0.1m×0.1mwidth×0.9mheight), Distributor plate with 9 bubble caps	• Solids circulation rate measure with hot solid sand particle tracer technique with thermistor probe and gas bypassing fraction measured with CO2 tracer gas.	Square ICFB with orifice type draft tube
Nagashima et al. [38]	Silica 1950 µm and glass beads 1350 µm, Vmf= 0.86 & 0.74 m/s respectively, e mf=0.48 & e mf=0.41	column=100mm , Height 300mm	• Pressure drop using pressure transducer • Particle downward velocity measurement using colored tracer particles.	Hydrodynamic performance of Spouted beds with four different types of draft tubes Has been investigated experimentally

Yang [12]	Bed material dp=150 µm	Column 108 mm and 1092 mm high, with a draft tube 54.8 mm I.D., 60.3 mm O.D., and 1016 mm high	• Minimum fluidization velocity	Adsorption and reduction with hydrocarbons
Su, G. et al. [39]	Static bed height – 280,330,380 mm and Length of entrainment zone 10, 20 & 35 mm, dp =460.25 µm, Vmf = 0.16 m/s, e mf=0.44	Draft tube diameter, 20,30 &40 mm & column diameter 182 mm	• Pressure drop using capacitive differential pressure transducer	An experimental study on gas-particle flow behavior in a spout-fluid bed with a draft tube
Zhao et al. [40]	Bed material silica beads dp= 300 µm, Umf =0.074 m/s	Column height 800mm, dia 120mm, draft tube height 235-290, dia 70mm	• Pressure drop measurement using differential pressure drop transducers • Solid circulation rate by hot tracer method	Hydrodynamic behavior of an internally circulating fluidized bed with tubular gas distributors
Xingxing and Bi [41]	dp=0.155 mm , bed material, ZSM-5powder Vmf= 0.01 m/s,	Draft tube 50.8mmX1016, 101.6 mmX1092mm	• Gas bypass by tracer gas method • Solids circulation rate by optical fiber probe method	Experimental and modeling of ICFB

Table 2.1 Experimental Literature

2.4 CFD models

This section deals a detailed literature of the existing computational models used to estimate the hydrodynamics of CFB and ICFB's. Computer simulations provide an opportunity to look inside the fluidization process with great details of the flow, where as experimental measures may disturb the flow when target to extract phase characteristics with help of probes [42]. Within the group of numerical simulation techniques, there are two methods frequently adopted to study gas solid flow dynamics in fluidized beds. Discrete particle models (DPM) based on Euler–Lagrange approach and the continuum models (Euler–Euler approach) are the most common used methods to simulate majority of the multiphase flows.

Recently the Euler–Euler approach is being used for the simulation of large scale CFBs, the particulate solids phase is also treated as a continuum, whereas all phases can fully interpenetrate. The conservation equations in this approach can be considered as a generalization of the volume-averaged Navier–Stokes equations for interacting continuum approach [43]. In the discrete particle approach, the motion of each individual particle is modeled by solving the Newtonian equations of motion taking external forces and particle collisions into account.

In recent years due to advances in high performance computers and numerical algorithms, the computational fluid dynamics (CFD) technique has become a fundamental element of research in simulating gas–solid multiphase flow systems [44]. CFD is a powerful technique and holds great potential in providing detailed information of the complex flow dynamics in fluidized bed systems. The numerical models are more flexible and less expensive for performing parametric studies of different bed geometries and operating conditions. Further the CFD modeling can provide extensive data of bubble characteristics, volume fraction of solids for the entire reactor volume regardless of the complexity of the bed geometry and operating conditions. However, these numerical models still need to be validated against the experimental data for their improved model accuracy and predictability nature. Many researchers have put considerable effort in validating the CFD models in order to achieve fundamental and accurate predictions for these systems. One of the difficulties to validate CFD models with experiments is the computational effort needed to perform three-dimensional (3D) simulations of dynamic behavior of industrial scale fluidized beds.

The flow in fluidized bed involves minimum of two phases, typically fluid (gas or liquid) and solid associated with intensive phase interactions in turbulent conditions. Therefore, there is a need of multiphase model for efficient numerical modeling. A number of multiphase models are available in CFD for simulating such complex multi-phase fluidization systems. There are several examples of such models existing in the literature with most recent contribution by, [45-48]. These include the Eulerian-Eulerian multiphase approach and the Eulerian-Lagrangian approach. The Eulerian-Eulerian multiphase flow approach, where a set of continuity, momentum and turbulence equations is solved for each phase. This approach has been used for systems with very high dispersed phase concentrations, where solid-solid interactions carry a significant amount of the stress. To describe the particulate phase stress in the Eulerian–Eulerian approach, the kinetic theory of granular flow (KTGF) has been adopted. Kinetic theory of granular flow was developed by a number of researchers [49-52] to model the motion of a dense collection of nearly elastic spherical particles in various fluidization conditions.

In the past a number of computational studies indicated that the drag force between particle and fluid plays an important role in the prediction of the flow structure of a fluidization bed [53-57]. Several drag models have been developed to calculate the inter-phase momentum exchange in fluidized bed, such as the Wen and Yu , Syamlal & O'Brien and Gidaspow drag models [58-60]. Many researchers have successfully simulated the circulating fluidized bed of FCC particles using the classical drag models [47, 61-63]. However, few successful simulations were reported on dense fluidization of Geldart A particles. The CFD modeling of a bubbling fluid catalytic cracking (FCC) fluidized-bed reactor by Zimmermann and Taghipour [57] showed that the drag models of Syamlal–O'Brien and Gidaspow overestimated the momentum exchange between the gas and the solid phase and the bed expansion in comparison to the experimental data. The effect of various drag models on hydrodynamics behavior of gas–solid fluidized beds was also compared by van Wachem et al. [64]. They found that the expression suggested by Syamlal–O'Brien [59] predicted pressure drop, bed expansion and bubble diameter that were lower than the experimental data. McKeen and Pugsley [55] simulated a freely bubbling bed of FCC particles with two-fluid model. It was found that the generally poor simulation results for Geldart A, particles which could be attributed to the existence of significant cohesive inter-particle forces. Hosseini et al. [65] simulated the bubbling fluidized bed of FCC particles at high superficial gas velocities and demonstrated the sensitivity of their system to the model's parameters such as drag function, restitution coefficient, and maximum solid packing limits. They have observed significant errors between the predicted bed expansion ratios in comparison to the

experimental data. Using the Gibilaro's drag model [66] with a suitable scale factor, it was found more reasonable hydrodynamics results. In addition to the gravitational and the drag forces, several researchers have also shown that the frictional stresses play an important role in the modeling of a fluidization process [64, 67-70]. Abu-Zaid and Ahmadi [71] developed a simple kinetic model for flow of nearly elastic granular materials in the grain-inertia regime. They showed that frictional losses have the same effects as energy dissipation due to the inelasticity of granular particles [71].

In a gas-solid bubbling fluidized bed, Kuiper's [67, 72] observed that the prediction of the kinetic theory of granular flow (KTGF) was improved the simulations significantly when the effect of frictional stresses was included in the model. Huilin et al. [68] and Shuyan et al. [69] reported successful simulation results for conventional spouted beds by adopting combinations of frictional and kinetic stresses. Passalacqua and Marmo [70], Reuge et al. [73] and Hosseini et al. [65] found excellent simulation results using the frictional model of Srivastava and Sundaresan [74], when compared with the frictional models of Syamlal et al. [75] and Johnson and Jackson [76] for bubbling fluidized bed and spouted bed with a non-porous draft tube respectively.

Understanding of the hydrodynamics of ICFB is still far away from its maturity when compared to CFBs. However, only few researchers have attempted to study the flow patterns in the ICFB in which the most of studies are limited to two-dimensional cases. In the early 2000's numerical- model established based on the mass and momentum conservation equations to describe the complex hydrodynamics of ICFB reactor. Marschall and Mleczko [77] model was able to explain the effect of different reactor designs and various hydrodynamic parameters, e.g. height of the surrounding annulus, length of the entrainment region on the flow fields, i.e. volume fraction and velocity distributions. Zhao et al. [40] studied the particle motion in a two-dimensional thin slot-rectangular spouted bed with draft plates using particle image velocimetry (PIV) [49]. CFD simulations for grains of 0.22, 2.0, 3.7, and 1.0 mm diameter, Szafran and Kmiec [78] confirmed that fluctuations are caused by particle clusters originating at the bottom of the column. Solid particles were seen to cross into the jet, cover the column inlet, and be transported periodically through the draft tube, which is contrary to the findings of Zhao et al. [40]. The fluctuating solids inflow produces slugs and explains variations in fountain height and porosity. Modified and extended scaling relationships were proposed by Shirvanian and Calo [79] for conical-based rectangular spouted vessels with draft tube. The specific literature related to the ICFB is summarized in table 2.2. The effect of superficial gas velocity, position of the draft tube, and type of sparging action on the solid hold-up and the solid circulation patterns studied

through physical experiments and 2D CFD simulations by Ahuja & Patwardhan [15]. Hosseini et al. [80] predicted the hydrodynamics of ICFB reactor with 2D CFD integrating the kinetic theory of granular flow to achieve accurate simulation of the gas–solid fluidized beds. A number of drag models ranging from [59, 60, 81] drag formulations for Geldart B particles at a wide range of superficial gas velocities were adopted in this study [80]. The hydrodynamics in the gas–solid fluidized bed was investigated systematically using experimental measurements and CFD simulation incorporating the modified Gidaspow drag model to take into account in the formation of particle clusters [82]. The mechanism of governing solid circulation in an ICFB were explained based on gas and solid dynamics with an inclined gas distributor. They demonstrated with that the adopted CFD model can capture the key features of an ICFB system, fast fluidization in the reaction chamber, bubbling fluidization in the heat exchanger chamber and solid circulation between the chambers [83].

2.5 Summary of CFD simulations in an internally circulating fluidized bed

Table 2.2 List of CFD studies on ICFB

Author	**Experimental geometry data for validation**	**Remarks**
Ahuja and Patwardhan [15]	2D ICFB geometry (0.186m×0.9m), solids hold up measurements through Gamma ray tomography, bed particles (710–1000 µm), mean particle size 853 µm, V_{mf}= 0.176 , e_{mf}=0.378, DD=0.1m, height=0.158 m, column=0.186m , Height 1.2m	Euler–Euler two-fluid CFD model. Gidaspow drag model to estimate drage force KTFG Standard k–ε model was used. “SIMPLE” scheme for pressure–velocity coupling was used Solids hold-up profiles validated with experimental data of Ahuja 2008

		multi-fluid Eulerian–Eulerian approach based on kinetic theory of granular
Ishikura et al [84]	2D Geometry ICFB Column,0.1mX1.0m, draft tube , 0.3m length 0.3 dia 0.014-0.018m,	flow,Gidaspow drag model to estimate drage force KTFG
Feng et al. [83]	Solids circulation rate	Eulerian–Eulerian model (EEM) with kinetic theory of granular flow used to calculate solid stresses Gidaspow drag model
Hosseini et al. [80]	2D geometry and Eulerian model with KTGF	The circulation patterns for various operating conditions were discussed and CFD results showed that the drag model is an important hydrodynamics parameter for gas-fluidized beds with various gas distributors.
Moradi et al. [85]	2D geometry The modeling results were compared with the experimental work of Particle axial velocity validated with exp data	Eulerian model was employed to predict the flow behavior of the spouted bed Gidaspow drag model KTGF
		Along the wall, a no-

		slip condition is assumed

In a nutshell, based on CFD literature, we can conclude that numerical simulations using the computational fluid dynamics (CFD) technique and its validation with experimental data is a useful tool to understand the gas-solid multiphase flow systems. In the case of conventional type fluidized beds and spouted fluidized beds the simulation studies already developed and matured understanding of hydrodynamics of a gas-solid flow progressed significantly. Only a few simulation studies were reported on ICFB in the past and that to most of them considered 2D geometry. It can be seen from above listed literature table that, the experimental data that has been used for the validation of ICFB CFD model, were mainly limited to axial solids velocity profiles and voidage profiles from few sources. All the simulation studies were using the TFM approach, the gas inlet velocity was assumed to have an uniform or a parabolic profile, and the diameter of the bed bottom was assumed to be the same as the diameter of the gas inlet only, obviously it is different from experimental conditions. Moreover, in all CFD simulations, particles were assumed to be mono sized particles. There is a necessity to develop an accurate and reliable CFD model for both in 2D and 3D geometries to predict the hydrodynamics of novel fluidized beds such as ICFB.

2.6 Mathematical models

Table. 2.3. Summary of hydrodynamics models of internally circulating fluidized bed.

Author	**Bed geometry**	**models**
Chandel and Alappat [14]	Geldart D particles, Coarse 1.7 mm & Fine (Geldart B) 0.6 mm, Vmf= 0.176 , e mf=0.378	Solids circulation rate model & Riser pressure drop model
Xingxing Cheng, Xiaotao T. Bi [41]	dp=0.155 mm , bed material, ZSM-5powder Vmf= 0.01 m/s,	Solids flow and gas flow distribution model
Jeon et al. [86]	Sand particles dp =0.3mm, Umf =0.074 m/s, in square ICFB	Solids circulation rate and gas distribution model
S.D Kim et al. [16]	Average particle size, 86, 120, 170 & 288 μm, Vmf=	Correlation between

	0.1 m/s, e mf=0.48 0.1mX0.9m draft tube and column diameter 0.283mX height 2.0 m	Pressure drop and solids circulation rate
Song et al. [87]	Flat plate, conical plate, conical plate ring sparger.Bed material sand, dp=0.3 mm, Vmf= 0.1 m/s, e mf=0.48, Draft tube 0.1X0.3m Column 0.3X2.5m	Solid circulation rate correlation was developed
Y.T.Kim [8]	dp=130 µm, bed material PVC, Vmf= 0.008 m/s dp=210-610µm, bed material sand Vmf= 0.04 m/s- 0.27 m/s	TDH and entrainment models
Ahn et al. [13]	Orifice diameter 15, 20, 25 & 30 mm, Bed material sand, dp=0.3, 0.39, 0.46 & 0.61 mm, Vmf= 0.1 m/s, e mf=0.48	A model for flow of solids and gas through orifice
Su et al. [39]	Static bed height – 280,330,380 mm and Length of entrainment zone 10,20 & 35 mm, dp =460.25 µm, Vmf = 0.16 m/s, emf=0.44	Model for minimum fluidization

Some of hydrodynamic mathematical models used for internally circulating fluidized beds are summarized in the table 2.3. Most of the researchers validated their model with respect to their experimental data. Kim et al. [8] group developed a model to estimate TDH (transport disengaging height) and entrainment rate in the ICFB. In the Kim et al. experiment they used bed material as mono sized particles. They developed a model for solid circulation rate and pressure drop prediction and validated against their own experimental data. Their model is specific to their experimental geometry. Chandel and Alappat [14] considered a small geometry and an equation has been developed on the basis of dimensional analysis. It gives considerably good results for the same kind of experimental setup. This equation may not suitable for wide range of operating conditions and designs. If the ICFB reactor is of a totally different configuration setting and the ranges of the main parameters are entirely different and this equation may not be valid for such kind of case. Song et al. [87] developed a correlation for determining the solid circulation rate with pressure drop across the gap opening and the opening ratio using the orifice equation.

2.7 Way forward

Literature review summaries both experimental and computational works related to CFBs and ICFB. Despite the wide applications of the ICFB, there are only a few studies reported in the literature on the hydrodynamics of the reactor operating with particle a size distribution. The listed investigations are mainly focused on the determination of pressure drop and solids circulation rate. Very little attention was given to the detailed full pressure flow curves and its fluctuation in the draft tube and annular regimes. Most of the hydrodynamic studies limited to handle either mono size or a narrow sized particle distribution. Nevertheless, the characteristics of the gas-solid suspension flow in ICFBs are not yet fully understood due to their complicate turbulent flow and intensive phase interactions. In the view of ICFB as potential industrial applications there is a need of further investigation on hydrodynamic characteristics of this new generation fluidized bed both experimentally and computationally.

Based on brief CFD literature discussed in this chapter, one can conclude that in the case of conventional type fluidized beds and spouted fluidized beds the simulation studies already well developed and matured understanding of hydrodynamics of a gas-solid flow progressed significantly. Very few simulation studies are reported on ICFB in the past and that to most of them considered 2D geometry only. Moreover, in all CFD simulations, particles were assumed to be mono sized particles. It can be seen from above listed literature table that, the experimental data that has been used for the validation of ICFB CFD model, were mainly limited to axial solids velocity profiles and voidage profiles from few sources. It is understood that gas-solid fluidized beds should use the TFM approach, with appropriate boundary conditions for both gas and solid phases incorporating specific granular flow based closures. But the selection of appropriate interface forces and granular closures depends on local gas-solids dynamics, where in case ICFB, there is no detail computational studies were made in the past. Thus there is a necessity to develop an accurate and reliable CFD model for both in 2D and 3D geometries to predict the hydrodynamics of novel fluidized beds such as ICFB.

Despite an attempt is made in the past to develop a number of mathematical models for ICFB, but a generalized and reliable model for solids recirculation for ICFB yet to come. The problem with the above-mentioned mathematical models is that they cannot be used outside the range of conditions under which they were developed. Furthermore, any change to the design of the fluidized bed conditions means that the empirical constants have to be

refitted. In view of this shortcoming, there is necessity to build a model based on dimensionless approach using wide range of experimental data to establish the relationships between the variables, where this technique has the advantage of producing dimensionally consistent results for scale up

Chapter 3

Methodology

3.1 Introduction

As outlined in Chapter 2 the understanding of gas-solid flow behavior in internally circulating fluidized bed is very complex and not well understood. Problems like particles of different size or change in particles size during the operation, efficiency would be a serious problem encountered in the fluidization operation beginning from first generation FBC to CFB's. In the ICFB the gas bypass fraction and solid circulation rate measurement are very complicate mainly due to lack of intrusive measurement techniques inside the draft tube. This chapter describes about ICFB rig fabrication, commissioning and measurement techniques which are used in the measurements of pressure drop across the bed in the draft tube and in the annular section, and also measuring the solids recirculation rate using with high speed camera.

A multi-phase CFD model approach is adopted in this thesis to explore detailed investigation of gas-solid flow hydrodynamics in the ICFB. Further the review outlined in Chapter 2 indicated that the CFD simulation of the ICFB flow dynamics is very challenging. In this thesis, the author extended basic approach two-fluid model to 2D ICFB geometry simulations as a validation case to 3D ICFB geometry simulations to capture the complete hydrodynamics of gas solid flow behavior in the ICFB.

In the experimental literature, Table 2.1 shows that majority of literature was on small scale geometry except Kim et al. group [7]. Lee et al. [33] studied hydrodynamics of ICFB in a ratio of draft tube diameter to ICFB column diameter is 1/3, Chu & Hwang studied in a ratio of 1 / 2.5, Xiao et al. [36] studied in a ratio of 1 / 4.75 e t c., and Chandal & Alappat [14] studied in 1 / 10 ratio of leves. The hydrodynamics will be different in a large scale ICFB compared to the small scale ICFB. In our present research we have chosen draft tube to column ration as similar to the Kim et al.[7] group but with a wide particle size distribution as a bed material to study the complete hydrodynamics of ICFB.

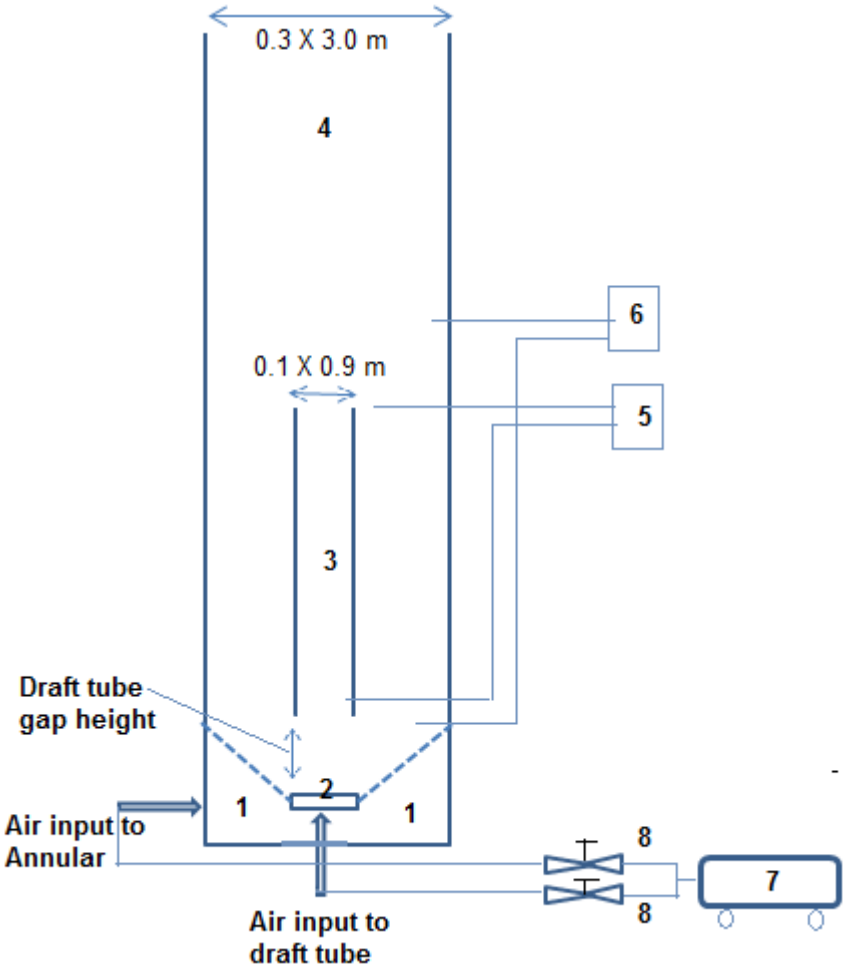

Figure 3.1: Schematic diagram of ICFB section. (1) annular air box (2) draft tube distributor (3) draft tube (4) ICFB (5) draft tube pressure measuring ports (6) annular bed pressure measuring ports (7) compressor (8) Air control value

3.2 Experimental setup

The experimental setup was a transparent acrylic cold model column. In the Fig. 3.1 show the schematic diagram of ICFB section, where all key parts and its connections and pressure measurements locations mentioned. The detailed description of the experimental rig facility shown in the Fig. 3.2. The experimental runs have been carried out in an acrylic column of 0.3 m ID and 3.0 m in height with a conical shape arrangement at the bottom and a draft tube of 0.1 m ID and 0.9 m height located centrally in main column. The detailed descriptions of the ICFB section and experimental rig have shown in the Fig. 3.2. The schematic diagram of Figure shows an internally circulating fluidized bed, a cylindrical draft tube which was installed in the center position of ICFB reactor. The experimental configuration and operating conditions are mentioned in the table 3.2. In an ICFB, a conical

acrylic air distributor with an angle 60^0 at the bottom to supply air to annulus and another separate air distributor is used to the draft tube and annuls sections respectively.

As shown in the Fig 3.3, a high end capacity compressor (30 HP, Chicago pneumatic compressor) equipped with two air filters followed by dryer was used to supply air as fluidizing gas. The ICFB column diameter and draft tube diameters have been selected such that for a given bed of solids (let's say sand particles) in the fast fluidization condition could be achieved for the selected capacity of a compressor. Initially air was directly supplied to the draft tube without air supplied to the annular section. Once the fluidization was initiated within the draft tube, a constant air inflow of 150 Lpm is maintained at the annular air distributor in all experimental runs. Turbine flow meter (Model TFM 1025 SG, Rockwin Flow meter India pvt. Ltd.,), having a flow range of 6.4 to 48 m^3/h, was used to measure air flow rate and was controlled by a gate valve to on and off air to the draft tube and annulus section. A pressure regulator was used for the storage cylindrical tank (1000 L) to avoid pressure fluctuations in the air flow rate. Sudden closing and opening valves were used for the cut down flow to the ICFB system in order to record the bed expansion leves. Two U-tube manometers with water medium were used to measure pressure difference within the draft tube and the annular section.

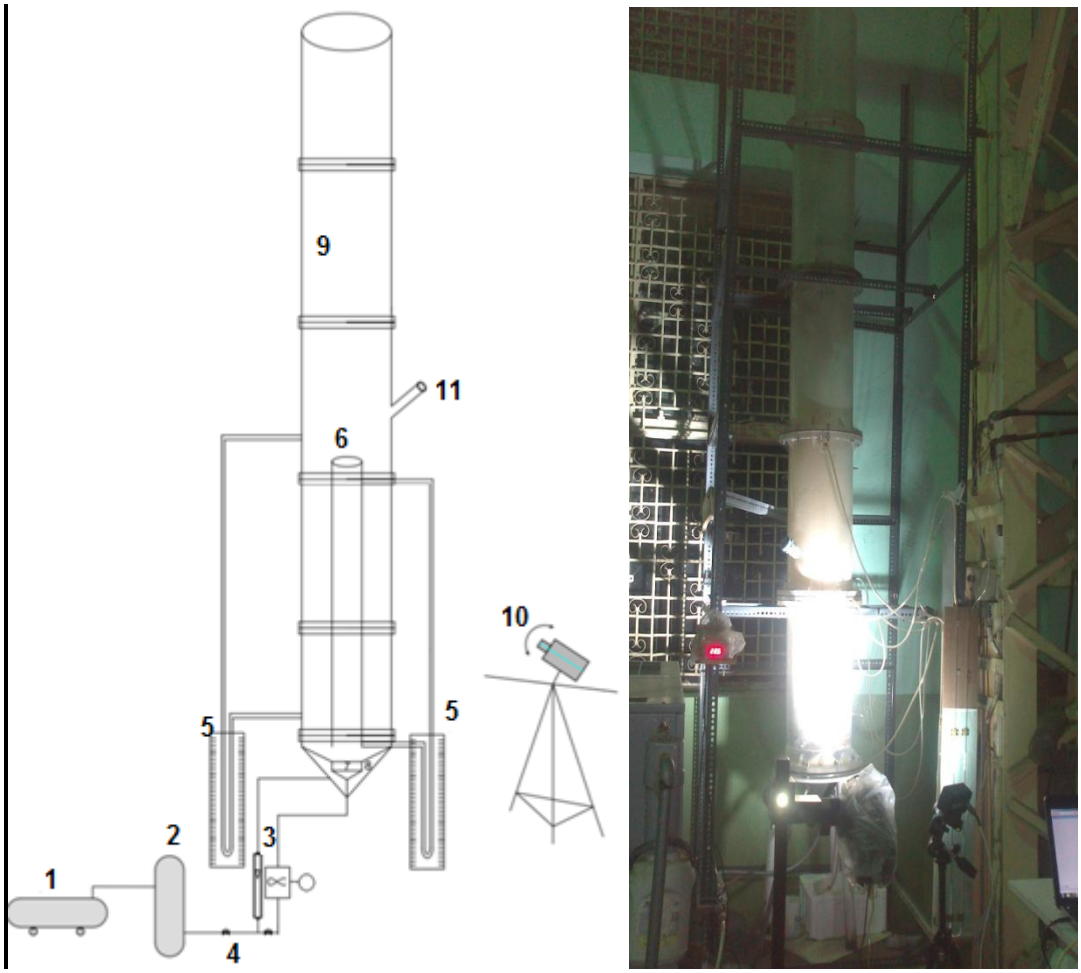

(a) (b)

Figure 3.2. Schematic diagram of ICFB experimental setup(a): (1) compressor (2) storage vessel (3) flow meter (4) control valve (5) manometers (6) draft tube (7) draft tube distributor (8) annulus distributor (9) ICFB column (10) High speed camera.(b) Laboratory experimental rig

Figure 3.3 Compressors and storage cylinder

3.2.1 Draft tube air distributor & Annular air distributor

Air supply to the ICFB column is divided into two sections. One section to the draft tube distributor and other one to the annulus section distributor separately by using control value. The two separate air distributor's snapshots are shown in the Fig. 3.4 (a) and (b). Draft tube distributor having seven bubble caps, each bubble cap having four holes (2.45 mm I.D.) and top of bubble cap cone shape arrangement is made to avoid accretion of solid particles on the cap. Annular air distributor conical in shape with an inclined angle of 60^{o} to prevent stagnant zones in the bottom of the ICFB and also which will provide easy to guide particles to enter into the draft tube through gap height which is provided at the bottom of the draft tube.

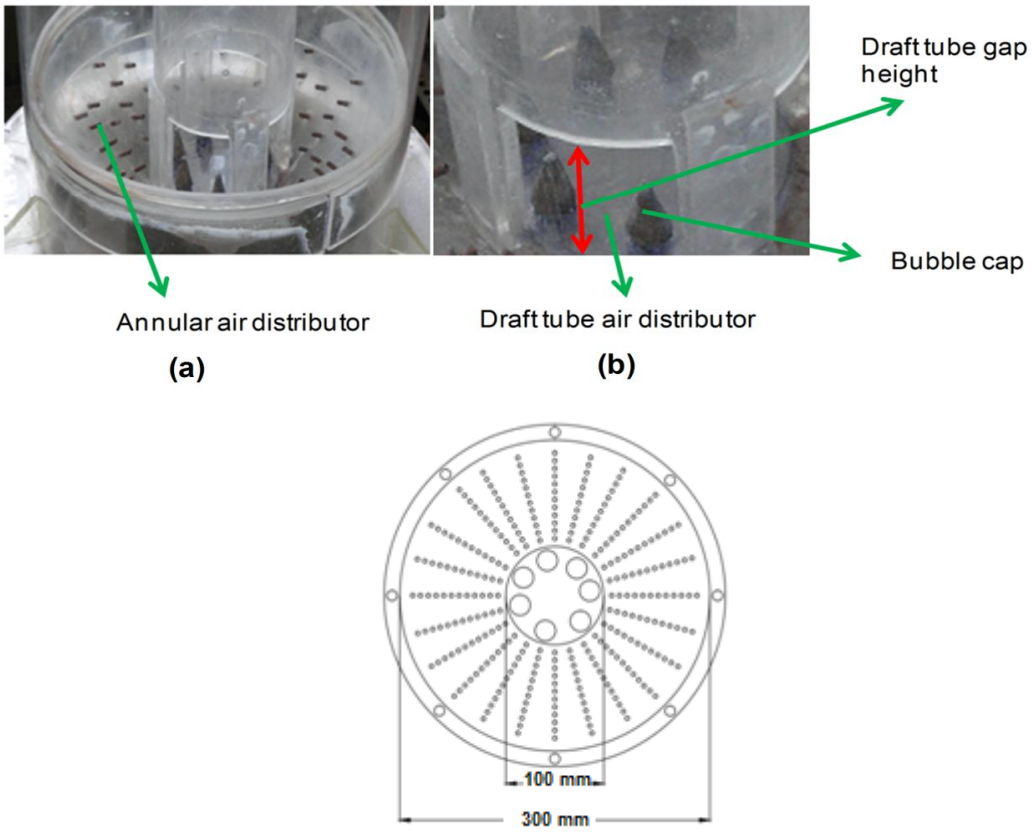

(c)

Figure 3.4 (a) annular distributor arrangements and (b) Draft tube (c) Schematic view of distributor's perforations arrangement

3.2.2 Pressure tap locations

The pressure taps were arranged to measure the pressure drop in the draft tube at the bottom and top locations (1 & 2) and also in annuls section bottom and top locations (3 & 4), as

shown in Fig. 3.5. To avoid particles entering into manometer leg with an arrangement of 100 microns screen mesh is made at the above mentioned all pressure tapings.

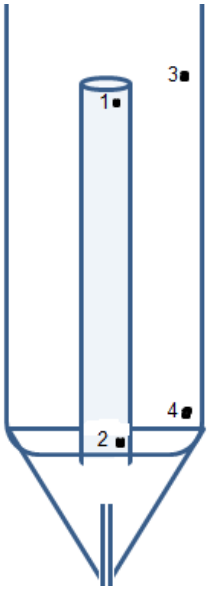

Figure 3.5. Location of pressure ports arrangements to measure pressure drop

3.2.3 Bed material properties

To study the effects of particle size on solid circulation and bed pressure drop profiles, two fractions of solids particles with a wide range of distribution have been used. The particle sizes of fraction are 75-995 µm and 150-1600 µm as shown in the Fig. 3.6.

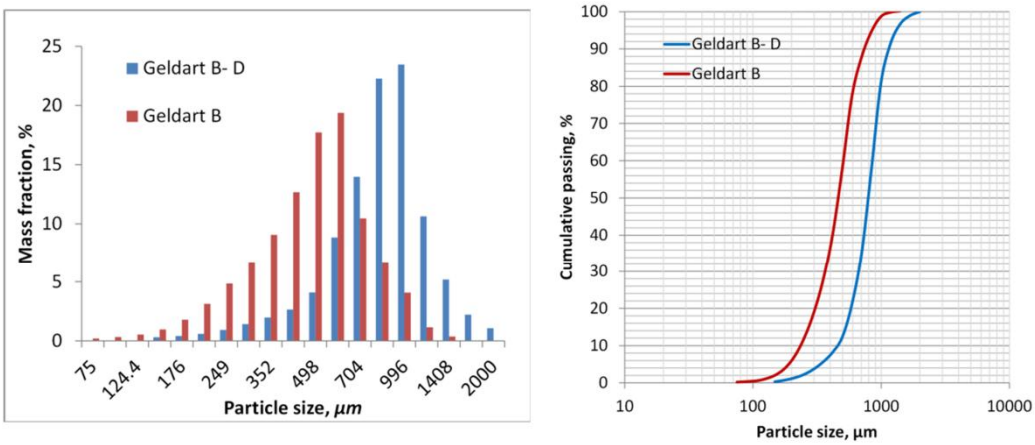

Figure 3.6: Particle size distribution of the two sand bed materials.

(a) **(b)**

Figure 3.7: Silica bed materials (a) Geldart group B (b) Geldart group B-D

The physical properties of silica particles are mentioned in the Table 3.1. Coarse particles come under the category of Geldart's Group B-D and a fine particle comes under Group B particles according to the Geldart's classification [18].

3.2.4 Particles characterization.

Geldart [18] has classified the behavior of solids particles fluidized by gases into four main groups A, B, C and D. Fig. 3.8 summarizes Geldart's classification. Group A consists of materials having small mean size and low particle density. Beds of powder in this group expand considerably before bubbling start and all bubbles rise faster than the interstitial gas. Cracking catalysts comes under this group of solids. Group B contains materials in the mean size ranging from 40 to 500µm and density greater than 1400 kg/m^3. There is no considerable bed expansion before bubbling start and most of the bubbles rise more quickly than the interstitial gas. Powders more cohesive in nature and consequently very difficult to fluidize belong to group C. Group D consists of large and dense articles. Larger bubbles rise slowly than the interstitial gas, so that the gas flows into the base of the bubbles and out of the top. The gas velocity in the dense phase of the bed is high and the flow regime around the particles may be turbulent. Group D particles are also capable of forming a stable spout.

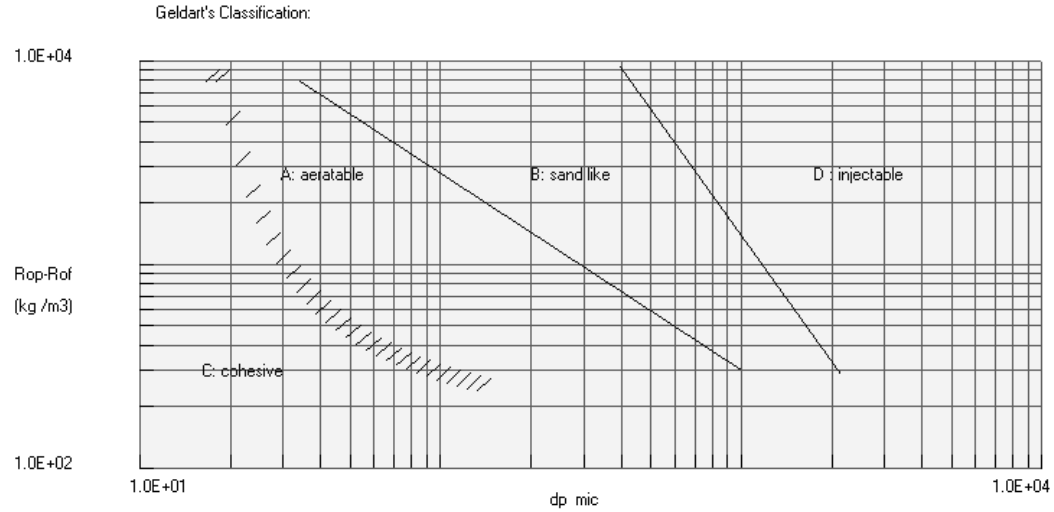

Figure 3.8 Powder classification diagram for fluidization by air at ambient conditions (from D.Geldart [18])

Geladart,(1973)[18] has proposed the following criterion for a particles to be in group D. The criterion is based on the fact that for group D particles, the bubble rise velocity is less than the interstitial gas velocity in the dense bed phase.

$$(\rho_p - \rho_g)(d_p)^2 \geq 10^{-3} \tag{3.1}$$

Where ρ_p, ρ_g are the densities of particles and gas respectively and d_p is the mean particle size. This criterion is only valid at atmospheric pressure and ambient temperatures and does not consider the effect of change in either the gas density or viscosity.

Table 3.1 Properties of bed particles

Solids type	Screen size	Avg size, μm	Ut, m/s	Umf, m/s	Density kg/m3	Bulk density kg/m3	Voidage
Geldart B	-75+950	475	3.44	0.158	2500	1350	0.46
Geldart B-D	-125+1150	805	5.59	0.385	2550	1410	0.44

The particle density and the packing voidage were measured using the water displacement method. First, particles (either loosely packed or tightly packed) were poured into a 500 ml volumetric flask of known weight. After measuring the total weight, the weight of particles was then calculated. Next, water was added slowly into the flask until the particles were just submerged with no bubble inside the flask. The volume of water added to the flask was recorded during this process and calculated by weighing the total weight (including particles, the flask and water). By subtracting the volume of water from the total volume, the volume of particles was obtained, and the density of particles could be calculated. The volume of water divided by the total volume gives the packing voidage. The properties of bed material are shown in the table 3.1

3.2.5 Annular falling particle velocity measurement

Experimentally, solid circulation rate can be measured from the vertical mass flux of solid particles passing through one or more of the regions across the bed using a number of methods [88], such methods are multi-fiber optical probes, radioactive tracer particles, and hot solid tracer techniques [89, 90]. In the current study the particle recirculation rate was investigated in a transparent Perspex ICFB cold model with silica sand particles as the bed material. Solid recirculation rates were measured by visual observation method using high speed camera. Downward moving bed particle velocity in the annuls is determined by visually following and timing a marked particle at the annulus wall interface over the fixed distance. Particle velocity was observed to vary at different positions along with the perimeter of the column due to local segregation and spouting particles piling on the surface of moving bed. As the bed seems to be packed bed in a moving bed condition, one can assume that the movement of the particles is fairly constant for a short distance of measurement. The movement of solid particle was found that the lowest at the curved surface junctions and at the bottom bed just near to the cone shape.

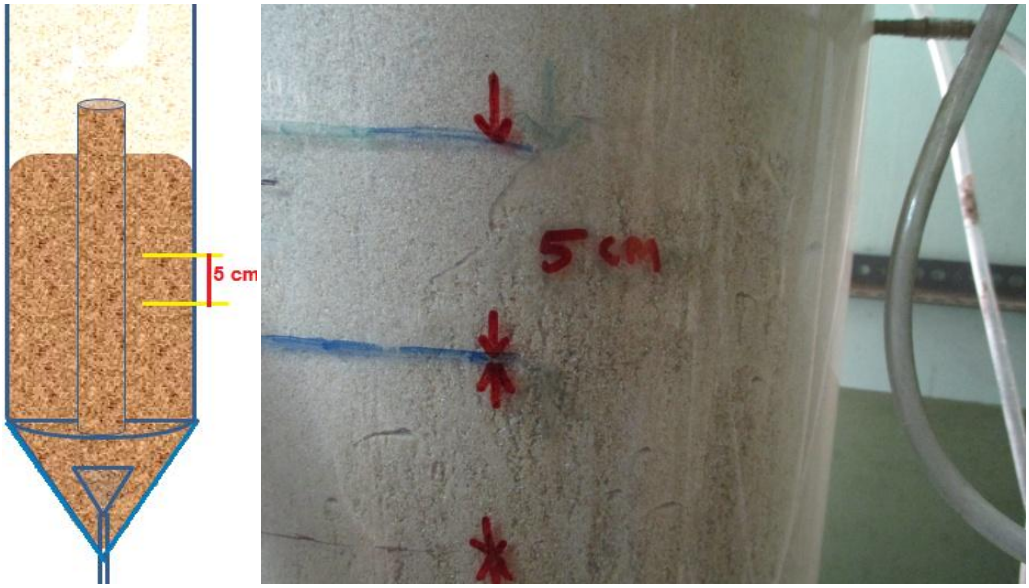

Figure 3.9 Annulus moving bed velocity measurement (a) schematic diagram (b) experimental measurement of annular velocity

Once downward particle velocity is calculated, solid recirculation rate (SRR) was quantified by using equation (3.2), in which silica particle velocity U_{PAn} was determined by measuring of the averaged time for a particles moving downward through a fixed distance of 50 mm in the annular section shown in the above Fig 3.9. This is measured with the help of the high speed camera (Photron's FASTCAM SA1.1 model 675K color), having a 5000 fps at one megapixels resolution. A series of sample frames indicating the trajectories of wall particles at different time periods is shown in Fig. 3.10. The same procedure was adopted at different locations along the circumference of annular section and then averaged out to minimize errors. All the experimental runs were conducted three times and averaged all three sets to compensate experimental reproducibility. In the annular section, the solids volume fraction ε_s, is assumed to be equal to the packed bed volume fraction, since the annular bed region is not in fluidized state, but behaves as descending nature bed in our current study.

$$G_s = u_{pAn}(1-\varepsilon_s)\rho_s \tag{3.2}$$

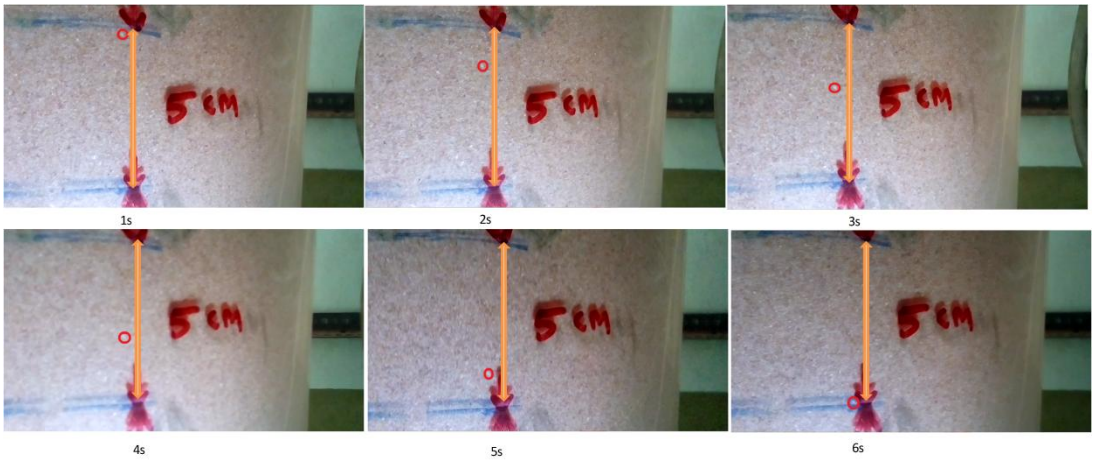

Figure 3.10 Annular downward particles tracking at a fixed distance of 5 cm at different time periods 1s, 2s, 3s, 4s, 5s and 6s

Equation (3.2) is correct if the velocity of solid and volume fractions is measured simultaneously, because the downward particle velocity in the annular section has a radial distribution of particles in case of a conventional spouted bed without a draft tube [91]. According to Hadzismajlovic et al. [24], the particle velocity in annulus section is uniform except in the conical section at the bottom of the ICFB. The flow of solid particles in the annular section was treated as plug flow except in the conical section [6]. Since the flow of solid particles in the annular section is not fluidized in our experiments, SRR could be calculated with Equation (3.2).

A number of experiments were performed as listed in Table 3.2. The effect of static bed height in three levels, the bed particle mean diameter in two levels, the gas superficial velocity in the range of 0-1.25 m/s (including 6 levels after the minimum spouting fluidization) and the draft tube gap height in three levels are varied for this ICFB in order to study the hydrodynamic behavior of a gas-solid system.

Table 3.2: ICFB experimental operation conditions

Item	Units	Values
Static bed height	cm	40, 50 & 60
Bed particle mean diameter	µm	470 & 800
Gas superficial velocity	cm/s	0-1.25
Draft tube gap height	cm	7.5, 10.5, 14.5

3.3 CFD approach

With the advent of increased computational facilities, hydrodynamic modeling of gas-solid flow is a new promising tool. At present it's a standard tool for single phase flows, it is at development stage for multiphase flow system, mainly for fluidized beds. Models developed and used in computational fluid dynamics codes (CFD) provides an understanding of phenomena involved in the system. Most of these models usually consist of a set of mathematical equations of continuity, momentum and energy. At present in fluidized bed multiphase flow research, there are two approaches for the numerical calculation of fluidized gas-solid flows, first one is the Euler-Lagrange approach based on molecular dynamics and other one is the Euler-Euler approach. Based on continuum mechanics treating the two phases an interpenetrating continuum. These two approaches have been examined and compared by Gera at al. [48]. Euler-Euler approach as outlined in chapter 2. For granular flows, such as flows in fluidized beds the Eulerian multiphase model with kinetic theory of granular flow is always the first choice to handle dense granular flow systems and also for my current simulations in this ICFB research.

3.3.1 CFD model

Hydrodynamic Modeling Using Kinetic Theory for Granular Flow (KTGF)

In the present study, it is proposed to solve the governing equations of mass, momentum and granular energy for both the gas and solids phase by means of a two-fluid model approach incorporating the Kinetic Theory of Granular Flow (KTGF) available in the commercial software package ANSYS's FLUENT^{TM}. To solve the set of equations, closures laws are required. In this work, it is proposed to apply the closure relations based on the (KTGF). The closure models, and the physical properties and simulation parameters used in this study are described in the following sections.

3.3.2 Eulerian–Eulerian model equations for gas–solid flow

Based on Eulerian multiphase model approach, the governing equations of mass and momentum for ICFB can be deduced by assuming phases as incompressible fluids having no mass transfer. External body force, lift force, as well as virtual mass force are ignored. The lift force mainly acts on the particles due to the velocity gradient in the primary flow field, so in case of dense fluidized bed inclusion of lift force is not appropriate. The partial differential TFM equations for explaining particle and fluid flows in the fluidized bed (Patankar) [92] are adopted for the ICFB.

The continuity equation in the absence of mass transfer between phases is give for each phase as follows

$$\frac{\partial}{\partial t}(\varepsilon_g \rho_g) + \nabla.(\varepsilon_g \rho_g v_g) = 0 \tag{3.3}$$

$$\frac{\partial}{\partial t}(\varepsilon_s \rho_s) + \nabla.(\varepsilon_s \rho_s v_s) = 0 \tag{3.4}$$

Where ε, ρ and *v* are the volume fraction, the density and the velocity in the both phase of gas-solid continuity eq. (3.3) & (3.4) respectively.

$$\varepsilon_g + \varepsilon_s = 1 \tag{3.5}$$

Each computational cell is shared by the interpenetrating phases, so that the sum overall volume fraction is unity.

The conservation of momentum equation for gas phase is described by

$$\frac{\partial}{\partial t}(\varepsilon_g \rho_g \upsilon_g) + \nabla.(\varepsilon_g \rho_g \upsilon_g \upsilon_g) = \nabla.\tau_g + \varepsilon_g \rho_g g - \varepsilon_g \nabla P + \beta(\upsilon_g - \upsilon_s) \tag{3.6}$$

The conservation of momentum equation for solid phase is described by

$$\frac{\partial}{\partial t}(\varepsilon_s \rho_s \upsilon_s) + \nabla.(\varepsilon_s \rho_s \upsilon_s \upsilon_s) = \nabla.\tau_s + \varepsilon_s \rho_s g - \nabla P_s - \varepsilon_s \nabla P + \beta(\upsilon_g - \upsilon_s) \tag{3.7}$$

In these equations β represents inter-phase momentum transfer coefficient between the gas and solid phases. When β multiplied by the slip velocity between the two phases, it yields an

interaction force between the phases. P is the pressure, g is the gravity and P_s is the granular pressure.

3.3.3 Drag models

An accurate account of drag force is required in the form of suitable drag model to close β in equations (3.6) & (3.7). The inter-phase momentum transfer between the two phases (gas-solid) represented by the drag force, plays an important role in any multiphase flow approach. Due to its high relevance, this phenomenon was frequently investigated in the literature. The ultimate goal of these works was to get an accurate drag model to predict exact draft force in the fluidized bed hydrodynamics.The drag force acting on a particle in fluid-solid systems can be represented by the product of a momentum transfer coefficient β, and the slip velocity (v_g-v_s) between the two phases. To cover the whole range of void fraction Gidaspow [60] proposed to combine the Wen-Yu [58] and Ergun equations [93] as shown in equations (3.12) & (3.13). Ergun equation is valid for fluidization conditions of $\varepsilon_g < 0.8$ as per the Gidapow's assumption. If the gas fraction is more than 0.8 then the phase is considered as gas bubble phase. The momentum exchange obtained from the correlation of Wen & Yu ($\varepsilon_g > 0.8$), where exchange takes place between that of bubble surrounded by particulate phase. The momentum exchange between the gas and dense phase takes place at lower values of gas fraction. Under those conditions momentum transfer can be considered to be given by Ergun equation. Generally, the drag force acting on a particle in gas–solid systems has been represented by various drag models like Syamlal-O'Brien [59], Gidaspow [60] , Gibilaro's [66] and Arastoopour [81]. The mathematical formulations of these four drag models that have been implemented as UDFs into Fluent are shown below mathematically.

Gidaspow's drag model [55].

Gidaspow drag is combination of precisely the Wen–Yu [58] and Ergun [93] equations. Here we considered the voidage as the volume fraction of gas phase. For voidage greater than 0.8, the Wen-Yu equation are recomended. For voidage less than 0.8 the Ergun equation was used.

$$\beta_{Wen-Yu} = \frac{3C_D \varepsilon_s \varepsilon_g \rho_g |\upsilon_g - \upsilon_s|}{4d_p} \varepsilon_g^{-2.65}, \qquad \varepsilon_g \geq 0.8 \qquad (3.8)$$

$$\beta_{Ergun} = 150\frac{\varepsilon_s^2 \mu_g}{\varepsilon_g d_p^2} + 1.75\frac{\varepsilon_s \mu_g |\upsilon_g - \upsilon_s|}{d_p}, \qquad \varepsilon_g < 0.8 \qquad (3.9)$$

Where C_D is Drag coefficient

$$C_D = \begin{cases} \frac{24}{\mathrm{Re}_p}[1+0.15(\mathrm{Re}_p)^{0.687}], & \mathrm{Re_p} < 1000 \\ 0.44 , & \mathrm{Re_p} > 1000 \end{cases} \quad (3.10)$$

$$\mathrm{Re}_p = \frac{\varepsilon_g \rho_g d_p |\upsilon_g - \upsilon_s|}{\mu_g} \text{ , Particle Reynolds Number} \quad (3.11)$$

The momentum exchange β at any point in the bed can be calculated with the above equations.

Arastoopour's drag model [81]

$$\beta_{gs} = \left(\frac{17.3}{\mathrm{Re}_p} + 0.336\right)\frac{\rho_g |\upsilon_g - \upsilon_s|}{d_p}(1-\varepsilon_g)\varepsilon_g^{-2.8}, \quad (3.12)$$

Syamlal–O'Brien [59] is expressed as

$$\beta_{gs} = \frac{3}{4}\frac{\varepsilon_g \varepsilon_s \rho_g}{\nu_{rs}^2 d_p} C_D\left(\frac{\mathrm{Re}_p}{\nu_{rs}}\right)|\upsilon_g - \upsilon_s| \quad (3.13)$$

Where C_D is the drag coefficient, and R_{es} is the solid Reynolds number defined as

$$C_D = \left(0.63 + \frac{4.8}{\sqrt{\mathrm{Re}_p / \nu_{rs}}}\right)^2 \quad (3.14)$$

$$\mathrm{Re}_p = \frac{\rho_g d_p |\upsilon_g - \upsilon_s|}{\mu_g} \quad (3.15)$$

The terminal velocity is V_{rs}

$$\nu_{rs} = 0.5\left[A - 0.06\mathrm{Re}_p + \sqrt{(0.06\mathrm{Re}_p)^2 + 0.12\mathrm{Re}_p(2B-A) + A^2}\right] \quad (3.16)$$

$$A = \varepsilon_g^{4.14}$$
$$B = \begin{cases} 0.8\varepsilon_g^{1.28} & for \varepsilon_g \le 0.85 \\ \varepsilon_g^{2.65} & for \varepsilon_g \ge 0.85 \end{cases} \quad (3.17)$$

Gibilaro's drag model [66]

$$\beta_{gs} = \left(\frac{17.3}{\mathrm{Re}_p} + 0.336 \right) \frac{\rho_g |\upsilon_g - \upsilon_s|}{d_p} (1-\varepsilon_g) \varepsilon_g^{-1.80} \tag{3.18}$$

$$\mathrm{Re}_p = \frac{\varepsilon_g \rho_g d_p |\upsilon_g - \upsilon_s|}{\mu_g} \tag{3.19}$$

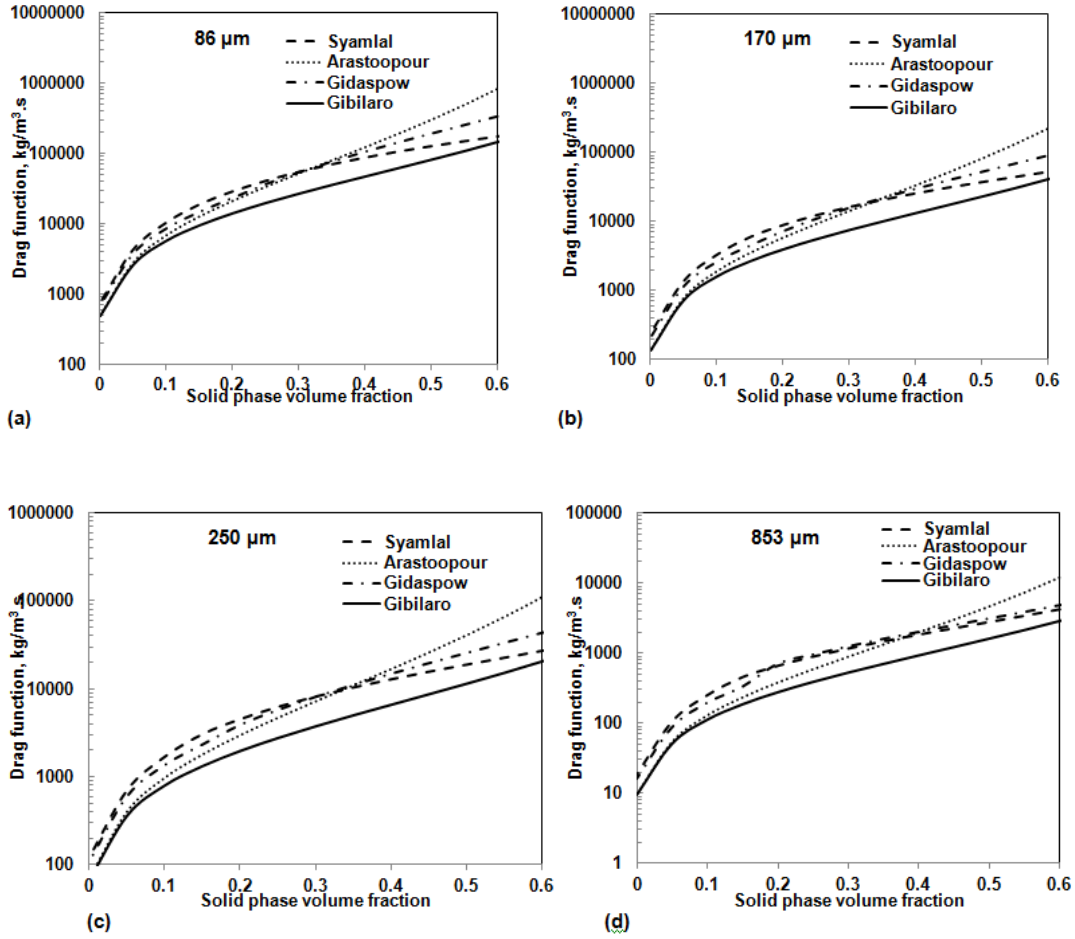

Figure 3.11 Comparison of different drag models for (a) 86 µm particles (b) 170 µm particles (c) 250 µm particles (d) 853 µm particles at a slip velocity of 1.04 m/s.

Fig.3.11. shows the relationship between the fluid-solid phase exchange coefficient, which is estimated for the available drag models in the literature as a function of solids volume fraction. For the various drag models Equation (3.8 -3.19) at fixed slip velocity of 1.04 m/s and for the 86 µm, 170 µm and 250 µm sized particles used in the present study calculations

and shownin Fig.3.11. It is observed that the Arastoopour and Gibilaro drag models predict larger values of gas-solids exchange coefficient at high of solids concentration compared to Syamlal-O'Brien and Gidaspow drag models. Both Gibilaro and Arastoopour drag models are actually based on Ergun equation defined an improved dependence of void to better match both packed bed and single particle drag. This means that the Arastoopour and Gibilaro drag models based predictions are significantly differ near the walls and drag coefficient will have the greatest influence on the model predictions. Fig.3.11 (d) shows the quantitative comparison of various drag models at fixed slip velocity of 1.04 m/s and for the 853μm particles used in Ahuja and Patwardhan [15] case in the present study as part of CFD validation. As it is seen there is a slight difference difference between drag coefficients at both low and very high solid concentration zones for the coarsest particles, i.e. 853 μm.
From the drag law comparison made in Fig 3.11 the following implications may be sought for ICFB. The presence of draft tube divides the solids flow once side as packed and annular region its lead/dilute fluidized bed in the draft tube. The adoption of Gibilaro and Arstoopour drag models for ICFB seems to be valid choice compared to Gidaspow and Syamlal OBriean drag laws due to consideration of extra dependence of void function (The same observations were observed as explained in the chapter 4)

3.3.4 Solid phase stress model formulations

To close the solid phase momentum transport equations, the solid phase stresses (τ_s & P_S) as described in Equation (3.6 and 3.7). The kinetic theory concept can be used for calculating the effective stresses of the solid phase resulting from direct collision and particle streaming could be calculated. These concepts are used when the granular motion is dominated by collisional interactions. In the modeling of granular flow, particles are modeled in analogy to gas molecules as described by kinetic theory of gases. A granular temperature may be defined in analogy to the temperature of the gas representing the kinetic energy levels. In this, a link exists between molecules random motion and temperature. The granular temperature is a measurement of the random fluctuations of the molecules in any substance. For gases random fluctuations will be occurred at a micro level between the molecules. This theory is extended to the macro scale where the molecules are substituted with particles. This approach is referred as the Kinetic Theory of Granular Flow (KTGF) and as described by Lun et al. [50] has become a very key tool for modeling gas-particle fluidized bed. Various studies on the hydrodynamics of gas-solid fluidized bed incorporating the

KTGF have shown this theory's potential in modeling of gas solid fluidized bed as summarized in the Chapter 2. These studies were also conducted by, Sinclair and Jackson [94], Ding and Gidaspow [52], Gidaspow [60], Benyahia et al. [47], Pain et al. [95, 96]. The kinetic energy of granular mean flow first degrades into the kinetic energy of random particle fluctuations, and then dissipates as heat because of inelastic collisions as depicted in the Fig 3.12. The granular temperature conservation equation is mentioned below. The particle velocity is decomposed into a mean v_s local velocity and superimposed fluctuating random velocity υ_s'.

A granular temperature is associated with the random fluctuation velocity. The solid phase transport equation for the granular temperature so-called granular temperature equation can be written as

$$\frac{3}{2}\left[\frac{\partial}{\partial t}(\varepsilon_s \rho_s \Theta_s) + \nabla.(\varepsilon_s \rho_s \upsilon_s \Theta_s)\right] = \tau_s : \nabla \upsilon_s - \nabla.(k\Theta_s \nabla \Theta_s) - \gamma_{\Theta s} - \phi_s \tag{3.20}$$

Granular temperature is defined as

$$\Theta_s = \frac{1}{3} < \overline{\upsilon_s' \upsilon_s'} > \tag{3.21}$$

In the above equation, V_s represents the ensemble-averaged magnitude of the randomly fluctuating velocity of the solid particles. Where τ_s solid stress tensor, $k\Theta_s \nabla \Theta_s$ flux of fluctuating energy-represents conduction due to the gradient of granular temperature, diffusion of the energy, $\gamma_{\Theta s}$ collisional dissipation of energy due to inelastic particle collisions. This term is represented by the expression derived by Lun et al [50]. ϕ_s is the transfer rate of kinetic energy between fluid-solid phases.

$$k_{\Theta s} = \frac{150 d_p \rho_S \sqrt{\Theta_s \pi}}{384(1+e) g_{OS}}\left[1 + \frac{6}{5}(1+e)\varepsilon_g g_o(\varepsilon_S)\right]^2 + 2 d_p \rho_S \varepsilon_s^{\,2}(1+2) g_o(\varepsilon_S) \tag{3.22}$$

$$\gamma_{\Theta s} = \frac{12(1-e_S^{\,2}) g_{OS}}{d_S \sqrt{\pi}} \rho_S \varepsilon_s^{\,2} \Theta_S^{3/2} \tag{3.23}$$

$$\phi_s = -3\beta \Theta_S \tag{3.24}$$

3.3.5 Solids pressure

The solid particles pressure is calculated independently and is used for the pressure gradient term ∇P_s is the solid granular phase momentum Eq. (3.7). The solid pressure is composed of a kinetic term and a second term due to particle collisions as follows Lun et al.[50].

$$P_s = \varepsilon_s \rho_s \Theta_s + 2\rho_s (1+e_s)\varepsilon_s^{\,2} g_o(\varepsilon_s)\Theta_s \tag{3.25}$$

Where Θ_s is the granular temperature, go (ε_s) is the radial distribution function, es is the coefficient of restitution for particle collisions. The coefficient e_s are 0.9 for a default value in the fluent, but the value can be adjusted to match the particle type. The granular temperature Θ_s is proportional to the kinetic energy of the fluctuating particle motion. τ_s-solid stress tensor can be expressed in Eq. (3.26) & (3.27) for gas-solid system respectively.

$$\tau_s = \varepsilon_s \mu_s \left(\nabla \upsilon_s + (\nabla \upsilon_s)^T\right) + \varepsilon_s (\lambda_s - \frac{2}{3}\mu_s)(\nabla . \upsilon_s).I \tag{3.26}$$

$$\tau_g = \varepsilon_g \mu_g \left(\nabla \upsilon_g + (\nabla \upsilon_g)^T\right) - \frac{2}{3}\varepsilon_g \mu_g (\nabla . \upsilon_g).I \tag{3.27}$$

Where μ_s and λ_s are the shear bulk granular bulk and viscosities for the solid phase, d_p is the particle diameter and I is the irrational number. The following model is developed from kinetic theory of granular flow by Lun's granular Kinetic theory [50] Eq. (3.28), the kinetic energy of granular mean flow first degrades into the kinetic energy of random particle fluctuations, and then dissipates as heat because of inelastic collisions.

The following sub models are used to account solid shear viscosity in the solid granular phase.

Solids bulk viscosity, [50] (Lun et al.)

$$\lambda_s = \frac{4}{3}\varepsilon_s \rho_s d_p g_0(\varepsilon_s)(1+e_s)\sqrt{\frac{\Theta_s}{\pi}} \tag{3.28}$$

Granular viscosity, [75] (Syamlal et al.)

$$\mu_{s,kin} = \frac{\varepsilon_s \rho_s d_s \sqrt{\Theta_s \pi}}{6(3-e_s)}\left[1+\frac{2}{5}(1+e_s)(3e_s-1)\varepsilon_s g_0(\varepsilon_s \right. \tag{3.29}$$

Frictional viscosity, [97] (Schaeffer's,)

$$\mu_{s,fr} = \frac{P_s Sin\phi}{2\sqrt{I_2 D}} \tag{3.30}$$

Collisional viscosity

$$\mu_{s,col} = \frac{4}{5}\varepsilon_s \rho_s d_p g_0(\varepsilon_s)(1+e_s)\sqrt{\frac{\Theta_s}{\pi}} \tag{3.31}$$

The function $g_0(\varepsilon_s)$ is a distribution function that governs the transition from the ‘‘compressible’’ condition with $\varepsilon_s<\varepsilon_{s,max}$, where the spacing between the solid particles can continue to decrease, to the ‘‘incompressible’’ condition with $\varepsilon_s>\varepsilon_{s,max}$ where no further decrease in the spacing can occur. The radial distribution function can be seen as a measure for the probability of inter-particle contact and estimated by the following equation.

$$g_o(\varepsilon_s) = \left[1 - \left(\frac{\varepsilon_s}{\varepsilon_{s,\max}}\right)^{\frac{1}{3}}\right]^{-1} \tag{3.32}$$

The radial distribution function g_0 (ε_s) is a correction factor that modifies the probability of collision close to packing as suggested by Sinclair and Jackson [94]. $\varepsilon_{s,max}$ is the maximum solids volume fraction for the packing limit.

Chapter 4

Gas-Solid flow analysis of ICFB using CFD model

4.1 Overview

In recent years, computational fluid dynamics (CFD) has been used extensively increasingly to improve chemical process design capabilities in many industrial applications, such as coal combustion and gasification, industrial drying processes and municipal wastewater sludge,

and other manufacturing and environmental products. Recent advancements in mathematical techniques and computer hardware, CFD has been found to be successful in predicting the hydrodynamic parameters of fluidized beds. The CFD solutions are being used to optimize and develop equipment and processing strategies in the process industry, replacing expensive and time-consuming experimentations. However, rigorous review on the application of CFD for the design, study, and evaluation of internally circulating fluidized bed is not yet available. The use of Eulerian-Eulerian model as mentioned in chapter 3 in the study of gas–solid multiphase flow in the ICFB is fully discussed in this chapter.

4.3 Grid and numerics

In this chapter 2D and 3D ICFB CFD simulations are being presented. First geometry, 2D ICFB, is considered from Ahuja & Patwardhan [15] work for the purpose of validation of the CFD model predictions. The second geometry, 3D ICFB, from IITH's, customized 30 cm diameter fluidization rig is used for parametric analysis. Ahuja & Patwardhan [15] experimented solid-gas flow patterns in an ICFB with a small geometry (Column 0.186 m X 1.2 m with a draft tube of 0.10 m X 0.158 m) using the gamma ray tomography. A particular case partial of sparging with a draft tube is considered here to simulate from Ahuja & Patwardhan [15]. Initially, 2D simulations run with the selected case in order to indentify correct CFD model strategy for turbulent fluidization. 2D simulations are performed using the chapter 3 specified two-fluid model along with no-slip boundary conditions adopted for both phases at the ICFB walls. Usually the wall treatment is possible by three ways as no slip, free lip and partial slip. Implementation of free and partial slip boundary conditions required the partial wall stress information and it is complicated. Experimentally as we have limited information available on wall particle dynamics, therefore boundary conditions are omitted here for sake of brevity, we have adopted here the no slip boundary conditions for particles. Since in this simulations the geometry of flow domain is large, the no slip wall boundary condition would effect the solids dynamics minimally. The bottom of the bed was defined as velocity inlet to specify a uniform superficial gas inlet velocity. Pressure outlet boundary conditions were employed at the top of the freeboard, which was set to a reference value of 1.01325 × 105 Pa. The settled bed was considered 0.186 m deep and initial solids volume fraction was defined as 0.62 with a maximum packing limit of 0.65. Simulations were initiated with uniform inlet superficial gas velocity of 2.24 m/s matching with the Ahuja & Patwardhan [15] experimental case. For

the prediction of drag force Syamlal and O'Brien, Gidaspow, Arastoopour and Gibilaro drag models are implemented into Fluent through the User Defined Functions (UDF).

Table 4.1 Simulation and model parameter for 2D ICFB

Parameter Description	**Value**
Particle density	956 (kg/m3)
Air density	1.225 (kg/m3)
Mean particle diameter	853 (μm)
Initial solid packing	0.52
Restitution coefficient	0.95
Boundary Condition	Outlet- pressure, walls-No slip

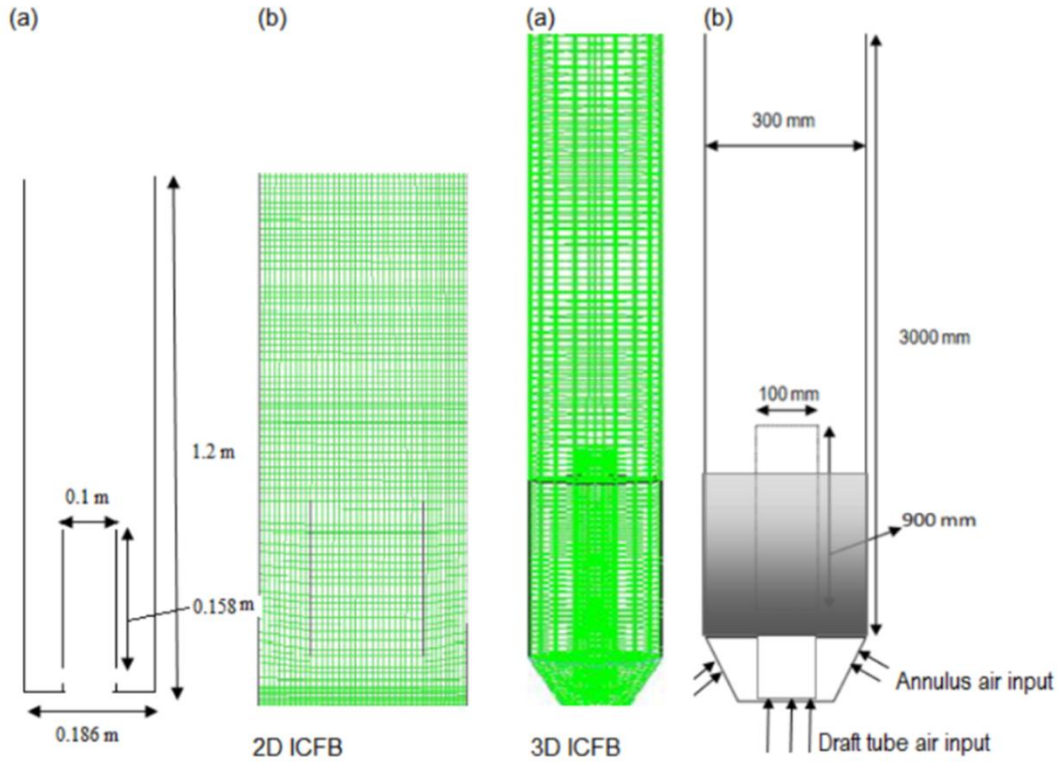

Figure 4.1. Schematic diagrams of 2D ICFB (a) Geometry (b) Grid and 3D ICFB (a) Grid (b) Geometry.

Table 4.2 Simulation and model parameter for 3D ICFB

Parameter Description	Value
Particle density	2500 (kg/m3)
Air density	1.225 (kg/m3)
Mean particle diameter	86,170 and 250 (μm)
Initial solid packing	0.62
Superficial air velocity	0.8, 1.0, 1.25, 1.5, 1.75 (m/s)
Fluidized bed column dimension	0.3 (m) x 3.0 (m)
Static bed height	0.8 (m)
Restitution coefficient	0.95
Boundary Condition	Outlet- pressure, walls-No slip

Once the 2D CFD model is validated, the same approach is then extended to study, the large scale 3D geometry. In this work, the 3D ICFB geometry with a configuration of 0.3 m diameter column having 3.0 m height and 0.1m diameter with 0.9 m height of draft tube as shown in Fig. 4.1 (a) is used. The same geometry & its computational mesh are created in GAMBIT, the presolver for Fluent, shown in the Fig. 4.1(b). Grid consists of total 54000 nodes and two cell zones. One is the static solids bed zone and another is free board zone. Two separate velocity inputs are created; one for the draft tube gas inlet and the other one is for annular gas input. Table 4.1 shows the simulation model parameters and its values used for the CFD simulation of the 3D ICFB. The initial bed height was 0.86 m and the initial solid volume fraction was defined as 0.62 with a maximum packing of 0.65. Simulations were initiated with uniform inlet superficial gas velocity to the draft tube set at 0.8, 1.25, 1.5 and 1.75 m/s with a constant uniform annular gas velocity of 0.2 m/s.

Simulations were run using ANSYS FLUENT 12.1.3 with standard k-ε model and Eulerain-Eulerian methods. Phase Coupled Semi Implicit Method for Pressure Linked Equations (PC-SIMPLE), which is an extension of SIMPLE algorithm to multiphase flows, is applied for pressure-velocity coupling. In this algorithm, the coupling terms are treated implicitly [92].QUICK scheme is used for discretizing the governing equations. Transient steady state simulations are run. A fixed time stepping of 0.001 seconds is used to advance the solution time.

4.4 Grid independence check

Grid independence check was initially performed for 2D 186 mm ICFB simulations. Based on assessment of analytical gas-solid exchange coefficient Arastoopour drag based CFD model simulations run. Four different mesh sizes comprising 5,000, 10,000, 30,000 and 70,000 nodes are used for this study. The simulated 2D ICFB results in terms of solids hold-up and solids axial velocity profiles by various grids are shown in Fig. 4.2 (a) (b) & 4.3. It is observed that simulations having grid size 30K and above are predicting the solid volume fractions close to the Ahuja's experimental data. Grid consisting 5K and 10K are under predicting the solid volume fractions across the radial position. Hence grid size of 30K nodes is selected as an optimum grid size for all 2D ICFB simulations.

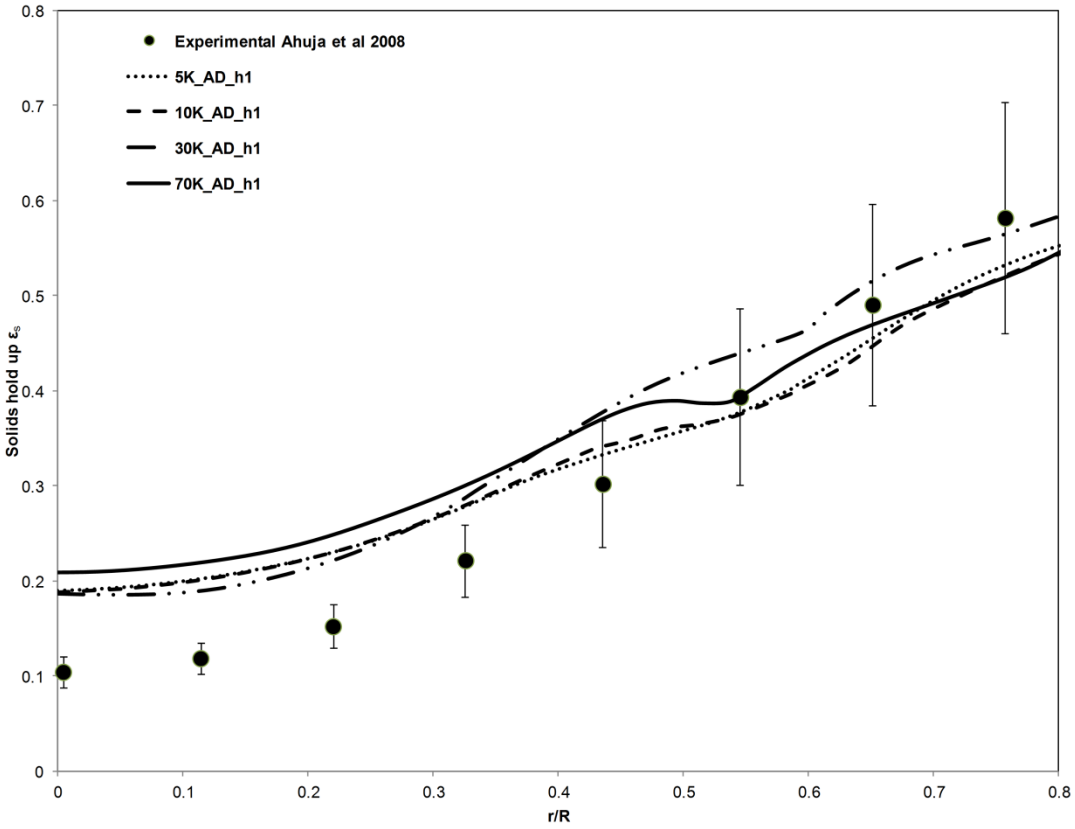

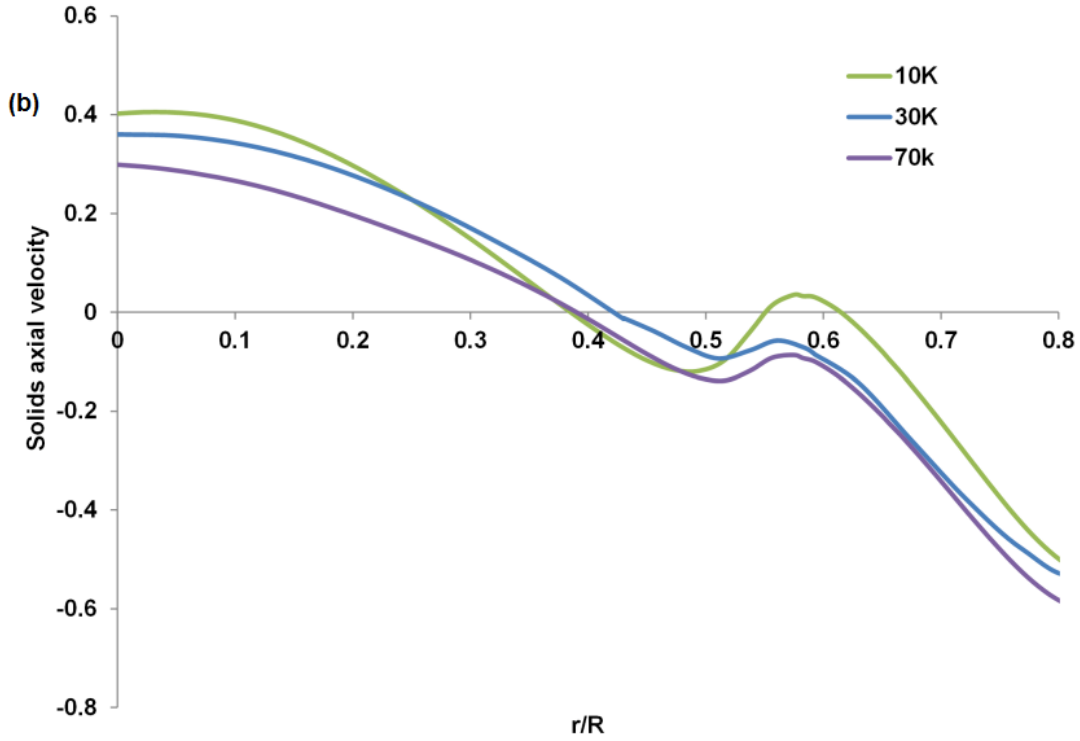

Figure 4.2. (a) Solids hold-up profiles for partial sparging with a draft tube comparison of different grid sizes with Arastoopour drag model. (b) Mean velocity profiles comparison of different grid sizes with Arastoopour drag model

4.5 2D CFD predictions for 186 mm ICFB & validation

In the current study, a number of momentum interface drag forces namely Gidaspow, Syamlal–O'Brien, Gibilaro and Arastoopour drag models are tested and compared with the Ahuja & Patwardhan [15] experimental data to identify the suitable drag model for modeling the turbulent fluidization of gas-solid particles. This present work assumes one case of Ahuja & Patwardhan [15] experiments having partial and complete sparging for 2D-ICFB CFD runs operating at a 2.24 m/s superficial velocity.

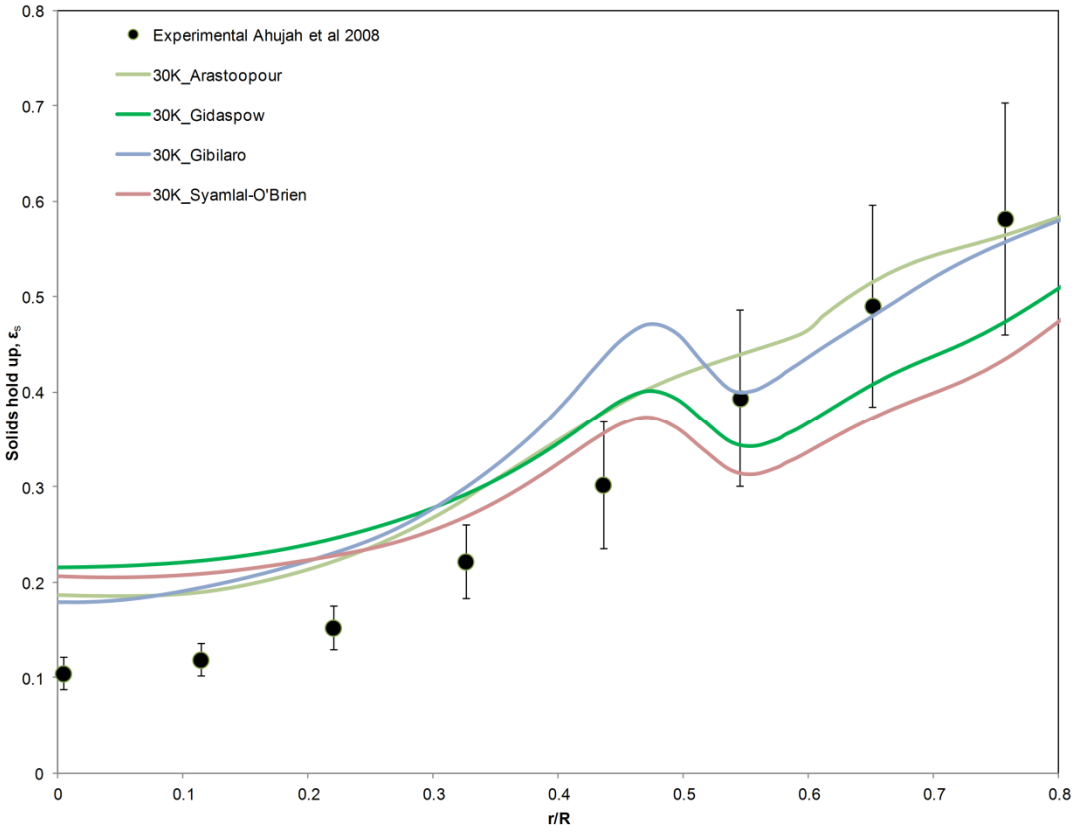

Figure 4.3. Solids hold-up profiles for partial sparging with a draft tube: Comparison of different drag models of 853 µm particles with 30K grid.

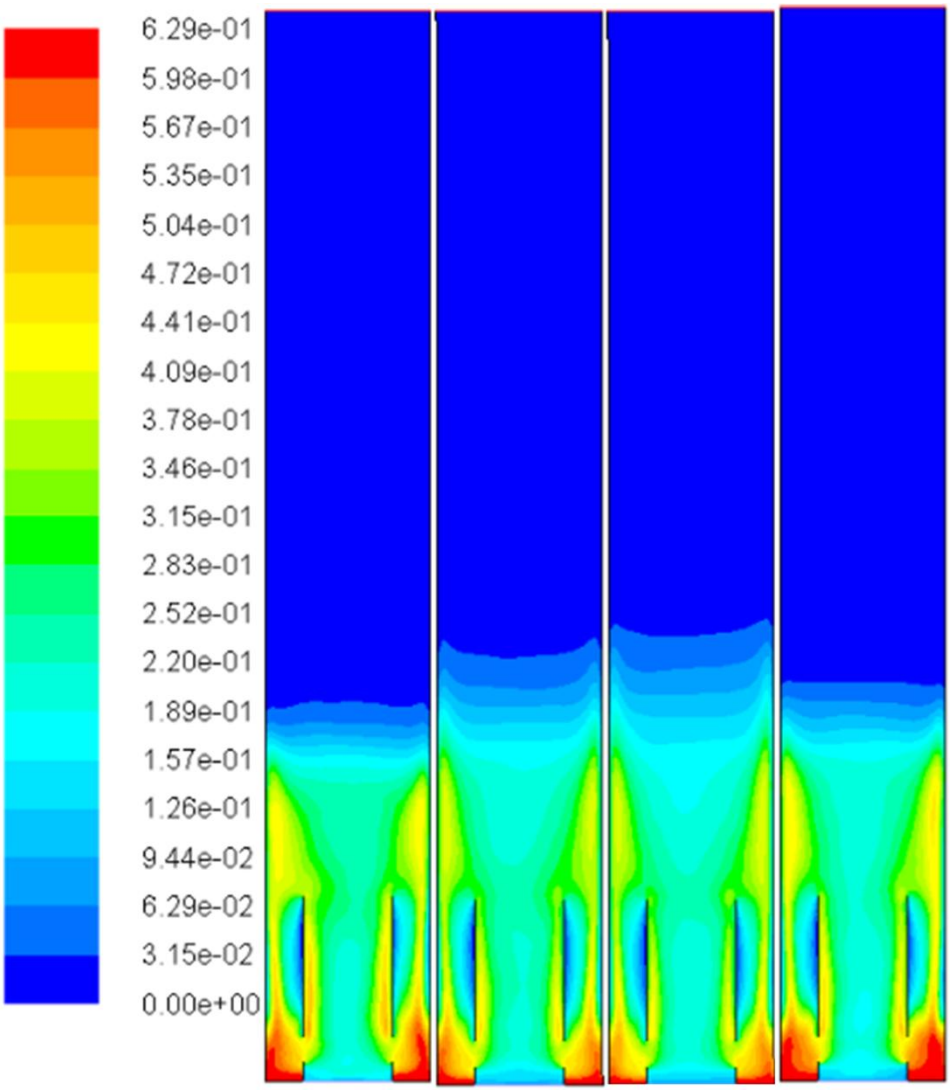

Figure 4.4. The Simulated solid volume fraction contours for various drag models for partially sparging with a draft tube (Uo=2.24 m/s) (a) Gibilaro drag model (b) Gidaspow drag model(c) Syamlal-O'Brien drag model and (d) Arastoopour drag model.

The effect of different drag models on local solid hold-up at a superficial gas velocity of 2.24 m/s, the restitution coefficient 0.95, solid maximum packing of 0.65 and h=0.0465 m are shown in Fig. 4.3. It is observed that the Gidaspow and Syamlal-O'Brien drag models show a significantly deviating volume fraction values from experimental values. Whereas. Arastoopour and Gibilaro drag models are predicting the solid volume fraction values much close to the experimental data. As observed from analytical comparison graph Fig. 3.11, the Gidaspow and Syamlal-O'Brien drag models under predict the gas-solids inter phase exchange coefficient at higher solids concentrations compared to the Arastoopour drag model. The drag forces accounted by the Gibilaro (1990) and Arastoopour et al. [81] are reasonably accurate and thus close predictions to experimental data are observed.

The simulated results in terms of solid volume fraction redial profiles and contours of the 2D ICFB are presented in Fig. 4.3-4.4. In Fig. 4.3. a comparison between the various drag model predictions is made based on mean solid volume fraction contours. These contours data analyzed in terms of expanded bed height and shape of fluidization pattern. The Gibilaro and Arastoopour drag model prediction represents the low bed expansion comparatively with other drag model predictions. The CFD models of Gidaspow and Syamlal-O'Brien drag models predict lean solids zone just above the gas distributor as seen in the Fig.4.4. Whereas in the case of Arastoopour & Gibilaro drag models, predicts dense zone at the bottom of draft tube which is just above the gas distributor.

A comparison of the predicted solid phase axial velocity using the four different drag models is made as shown in Fig. 4.5. Fig. 4.5 shows quantitative solids phase axial velocity profiles across the radial position for the case of partial sparging with a draft tube for various drag models with gas velocity of U_o= 2.24 m/s at h/H of 0.25. At smaller values of r/R, solids axial velocity is positive through the gas sparged area indicates solids phase in central zone is moving upwards in the draft tube along with the gas up to the value of r/R=0.35. At larger values of r/R (from 0.35 onwards) the solids axial velocity is negative, which indicate the downward solids flow in the annular region for the all drag models except in the case of Syamlal-O'Brien. In the Fig. 3.11, Arastoopour drag & Gibilaro drag laws indicates less resistance for the flow at lower solids concentration. The predicted solids axial velocities by these drag laws are higher as compared with Gidaspow & Syamlal-O'Brien drag models. At high solids concentration, the Arastoopour and Gibilaro drag show high flow resistance (high β_{gs}) hence lower axial velocity predictions. In case of Syamlal drag model, solid axial velocity changes from positive to negative at a value of r/R = 0.2 and again quickly changes from negative to positive at a value of r/R = 0.8 onwards. Overall, the Arastoopour and Gibilaro drag models estimated solids axial velocity profiles are closer to Ahuja's predicted solid axial velocity profiles. This velocity validation trend is consistent with solids-holdup profiles predicted by the same drag models.

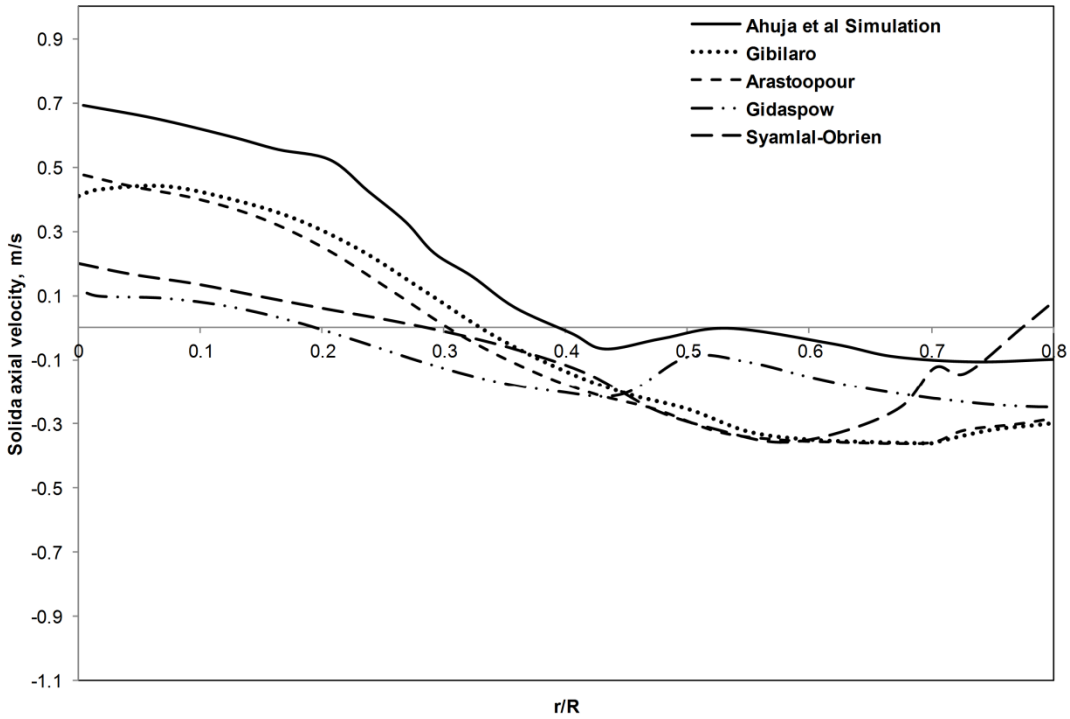

Figure 4.5 Comparison of predicted-Solids axial velocity profiles at U=2.24 m/s and h/H=0.25 for different drag models.

4.6 Motivation for 3D & large scale simulations

Although 2D experiments & simulations can be used to study particle fluid dynamics in fluidized beds, but 2D simulations may not completely represent the actual geometry and dynamic behavior of particles, as most of the realistic applications are in three dimensional and uses large diameter columns. However, for the real applications the trends estimated would be similar and the 2D-simulations are acceptable for the proof of concept of designs. 2D flow assumptions are widely used in fluidized bed simulations and extensive validations available in the literature for CFB. For bubbling fluidized bed, it has been suggested that 2D simulation is only good for qualitative study; whereas a 3D simulation is needed for quantitative estimation in the fluidized beds. Moreover, the 3D simulations are realistic in predicting the granular temperature and pressure than the 2D simulations since 3D simulations got more solid particles and available space [98]. In this work we attempted to simulate a large scale 3D laboratory ICFB for detailed fluidization dynamics in terms of flow patterns, pressure drop across the bed, void fractions, solids recirculation rates and granular temperatures.

4.7 300 mm ICFB 3D simulations:

4.7.1 Pressure drop in 3D ICFB

The pressure difference (ΔP) between the draft tube and annulus section is the driving force for solid recirculation in ICFB & CFB [99]. The predicted mean Δp value is plotted to compare pressure difference at across the length of the ICFB column both in draft tube top and bottom and in annular section top and bottom at various superficial velocities for three different sized particles as shown in the Fig.4.6 (a) (b) (c) and (d). When the draft tube superficial gas velocity is slowly increased for all size particles, the pressure drop of annular region becomes higher than that of the draft tube region. This type of phenomenon is caused by different bed density in different zones, namely, the draft tube zone has dilute flow and annular zone has dense solids flow. It can be seen that the pressure drop in the spout and fluidized zones are in same trend and this trend are analogous to literature reports for spout fluidized bed with or without draft tube [100]. For coarser size bed particles i.e 250 µm prevails higher pressure drop when compare with 86 & 170 µm size bed particles. The pressure drop between the draft tube and annular section also increased for coarser sized particles.

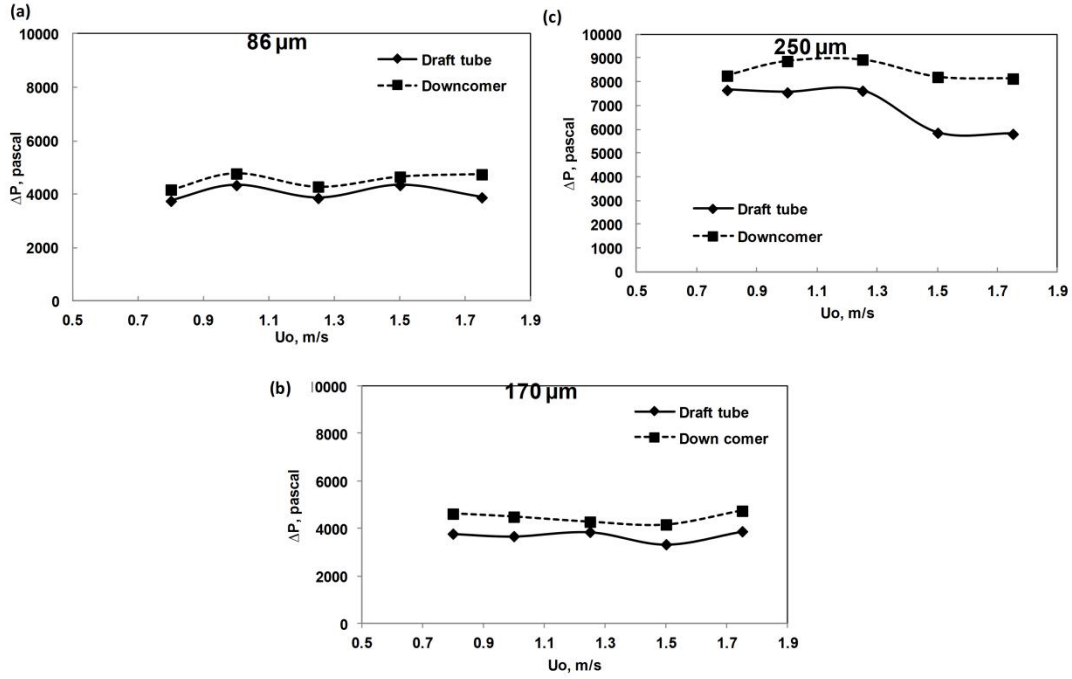

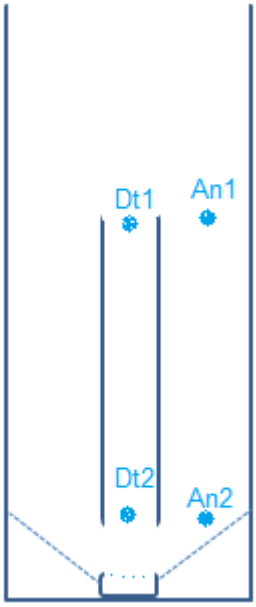

Figure 4.6. Pressure drop v_s draft tube velocity for the silica particle size (a) 86 µm (b)170 µm (c) 250 µm (d) Pressure difference location in the draft tube (Dt1 & Dt2) and annular section (An1 & An2) .

4.7.2 Solid Circulation Rate

Solid recirculation rate, Gs, is an important parameter to design any ICFB reactor with a suitable draft tube configuration. The effect of superficial gas velocity (Uo) on solid recirculation rate is shown in Fig.4.7 (a) (b) and (c). Solids recirculation rate Gs was actually calculated based on the product of mean volume fraction of solids, density of solids and the solid velocity magnitude. Gs increases with U_o due to the increase in the driving force for the circulation of solids between the draft tube and annular zone and as a result the increased bed voidage is observed in the draft tube. From Fig. 4.7 (a), it can be observed that solids recirculation rate increases with draft tube inlet velocity up to the velocity of 1.5 m/s and then declined at higher velocities. However, at higher superficial gas velocity specifically for 86 µm, Gs decreases due to an increase in air bypass from the draft tube to the annular region at a fixed gap height and also the rate of entrainment is more towards the annulus region from this gap height. The air inlet velocity to the draft tube is maintained higher than the annulus inlet velocity, which makes the density difference between annular and draft tube to increase at higher velocity. This might be providing the driving force for the solids recirculation between the draft tube to the annular section. Further it is also observed in the Figure 4.7 (a), (b) and (c), that the solid circulation rate of smaller particles steeply increases with the increase of superficial velocity than the coarser size particles.

This is due to the resistance of small particles entering the draft tube through the gap opening is lower than the large particles, thus more particles would enter the draft tube at the same superficial velocities. Less momentum required to transport the smaller particles from annular bed to draft tube column.

Solids circulation rate is calculated as a product of particle velocity, volume fraction and particle density. This G_s is calculated for each simulation having mono sized particles for different superficial velocities. As solids circulation rate G_s depends on local volume fraction and the different particle size, the simulations in the ICFB/CFB would lead to have different volume fraction distributions as shown in the Fig. 4.11 (which are governed by drag and local relative velocities). One would expect different solids circulation.

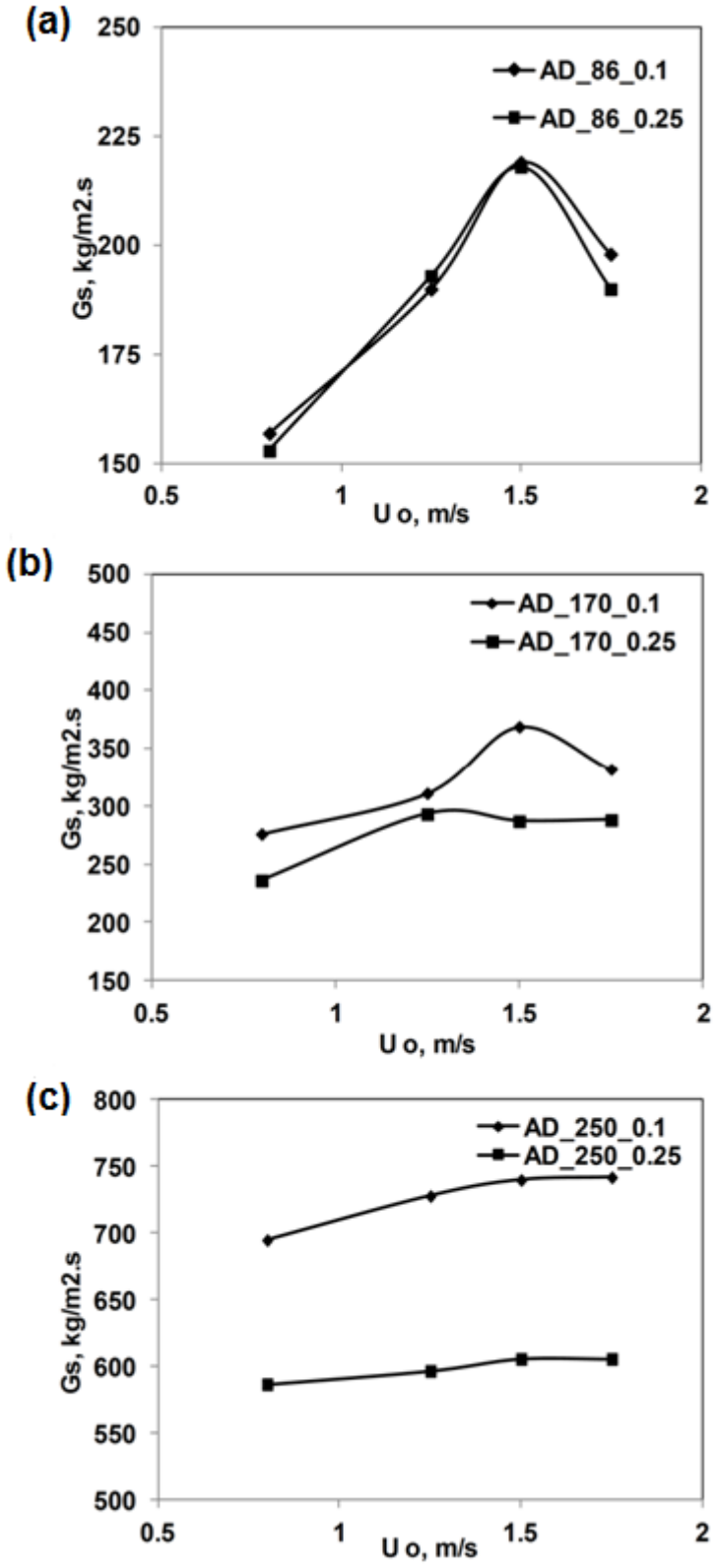

Figure 4.7. Solids circulation rate (Gs) versus draft tube velocity (U_o) at 0.1 m and 0.25 m axial locations and with Arastoopour drag (AD) (a) 86 µm (b) 170 µm (c) 250 µm.

4.7.3 Mean solids volume fraction distributions

Using the Arastoopour drag based CFD model, predicted contours of solid phase volume fractions are shown in Fig. 4.8, 4.9 & 4.10 for 86 µm 170 µm and 250 µm size silica particles at gas superficial velocities at 0.8, 1.25, 1.5 and 1.75 m/s respectively. The bed expansion height here actually refers the particle spread. The particle concentration beyond 0.01 volume fraction level are cut off for that bed expansion height. Alternatively one can also use voidage (below 99%) profiles to capture the bed height. For different size particles one can distinguish the solid spread from these contour plots. Fig. 4.8 is the simulation result for particle size of 86 µm. It is found that the particle spread is minimum at low superficial gas velocities. There exist a dense phase zone in the lower part of the ICFB and a dilute phase zone in the upper zone. However the dense phase bed level decreases gradually with increasing superficial gas velocity from 0.8 to 1.75 m/s. As shown in the Fig. 4.8 (a) (b) (c) (d), the solid distribution in the draft tube is significantly non-uniform. Fig. 4.8 (e) shows a quantitative prediction of solids volume fraction in the ICFB with respect to bed height. At the bottom of ICFB reactor, the solid volume fraction is high at low superficial velocity and decreases continuously along with the ICFB column height. In case of 250 µm size particles as expected, the height of the bed expansion is lower compared to 170 and 86 µm particle profiles due to the increased effective weight of the particles. The bed density in the bottom down comer has increased from average values of 0.28 to 0.45 solids volume fraction levels for 86 µm to 250 µm sized particles respectively. From Fig. 4.9 & 4.10 is it observed that the solids volume faction distributions of bed are certainly effected by particle size and gas superficial gas velocities.

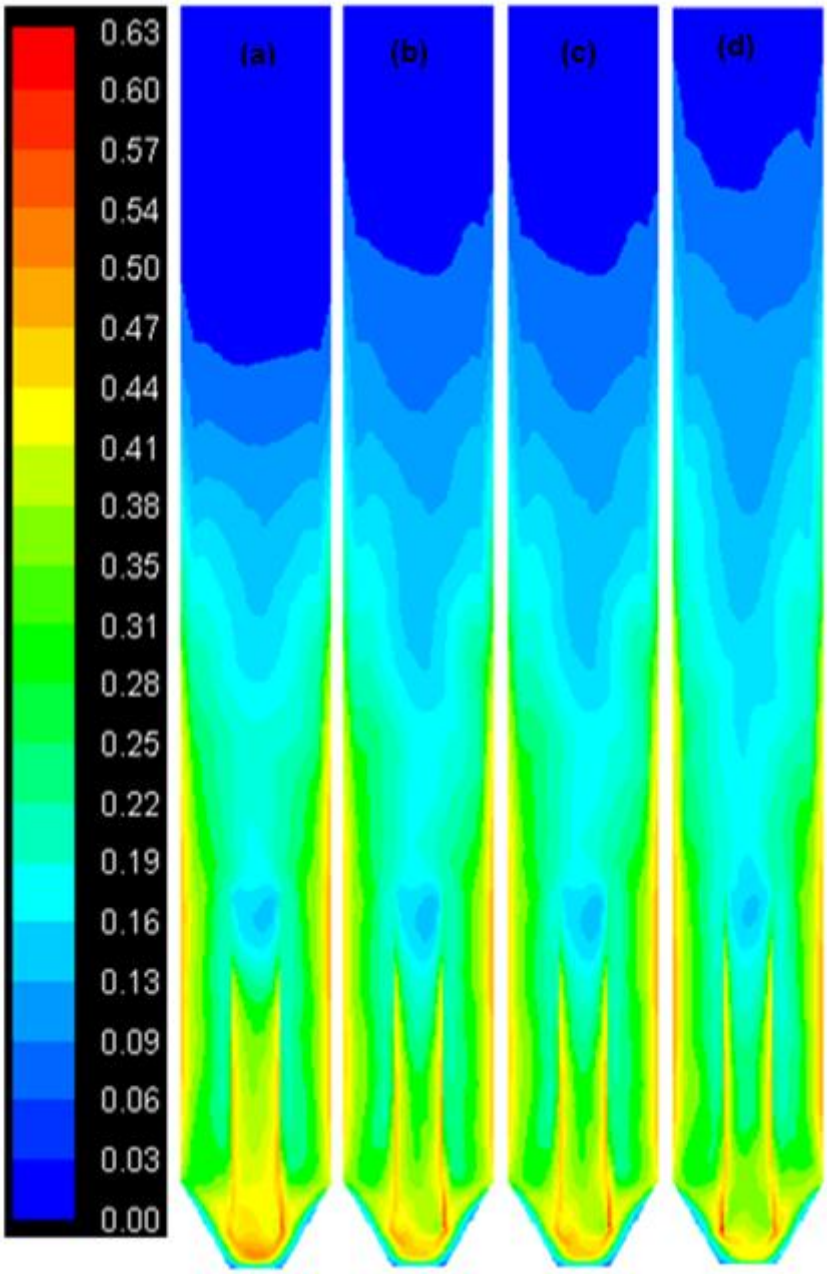
0.63
0.60
0.57
0.54
0.50
0.47
0.44
0.41
0.38
0.35
0.31
0.28
0.25
0.22
0.19
0.16
0.13
0.09
0.06
0.03
0.00
(a)
(b)
(c)
(d)

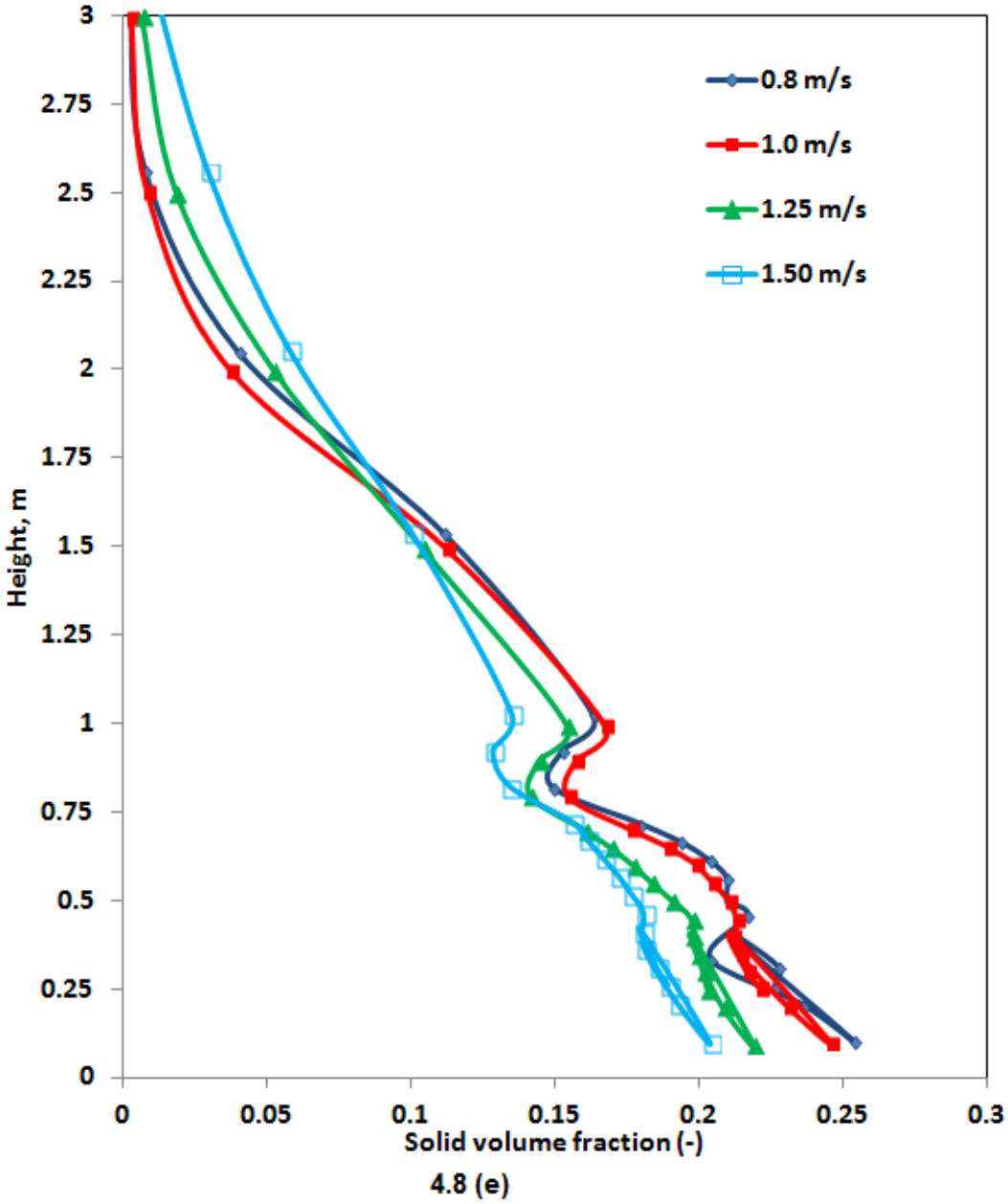

Figure 4.8 (a) Contour plot of solids volume fraction with different gas velocities of Silica particles of size 86 µm at a constant annulus input velocity (With Arastoopour drag model) Ua=0.2 m/s.(a) Ud=0.8 m/s (b) Ud=1.0 m/s (c) Ud=1.25 m/s (d) Ud=1.5 m/s. (e) Height versus solid volume fraction.

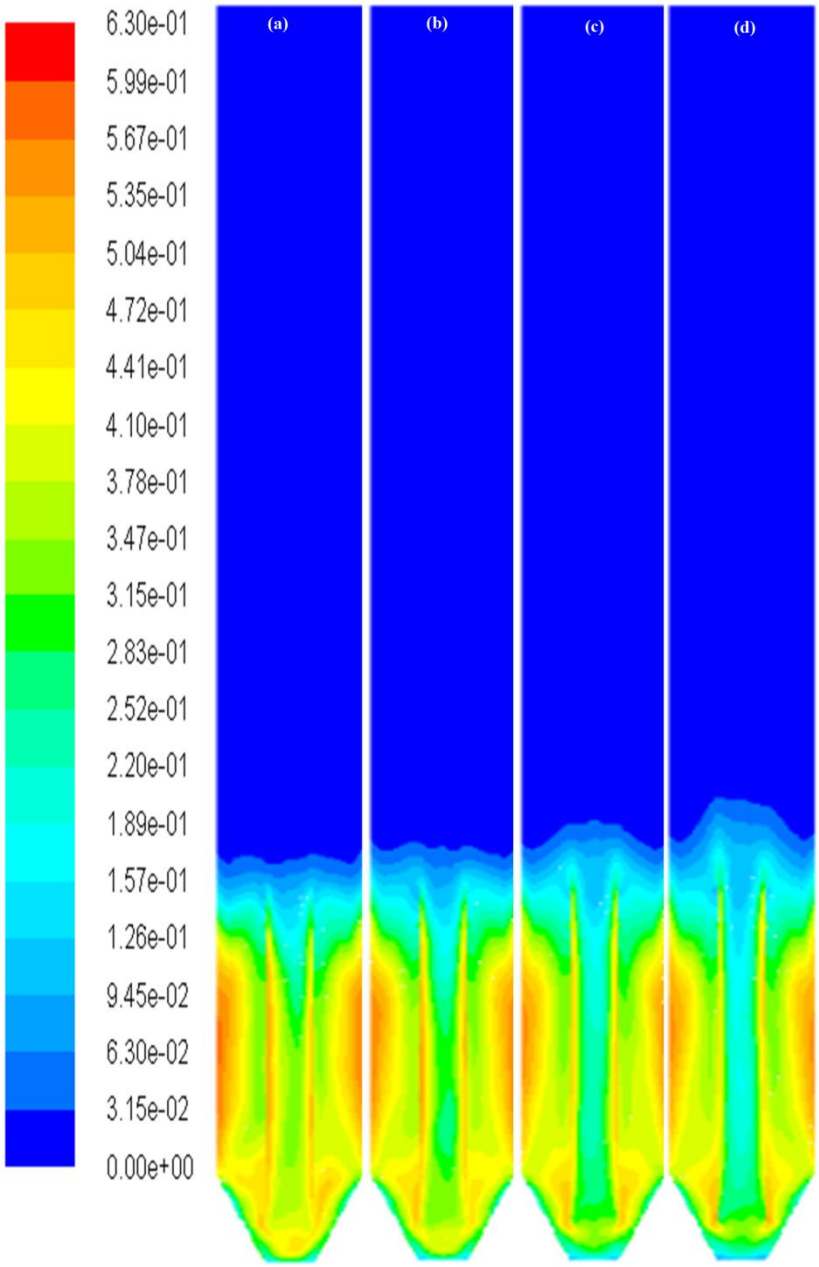

Figure 4.9. Contour plot of mean solids volume fraction with different gas velocities of Silica particles size 170 µm at constant annulus input velocity Ua=0.2 m/s (With Arastoopour drag model) (a) U_d=0.8 m/s.(b) U_d=1.25 m/s.(c) U_d=1.5 m/s.(d) Ud=1.75 m/s.

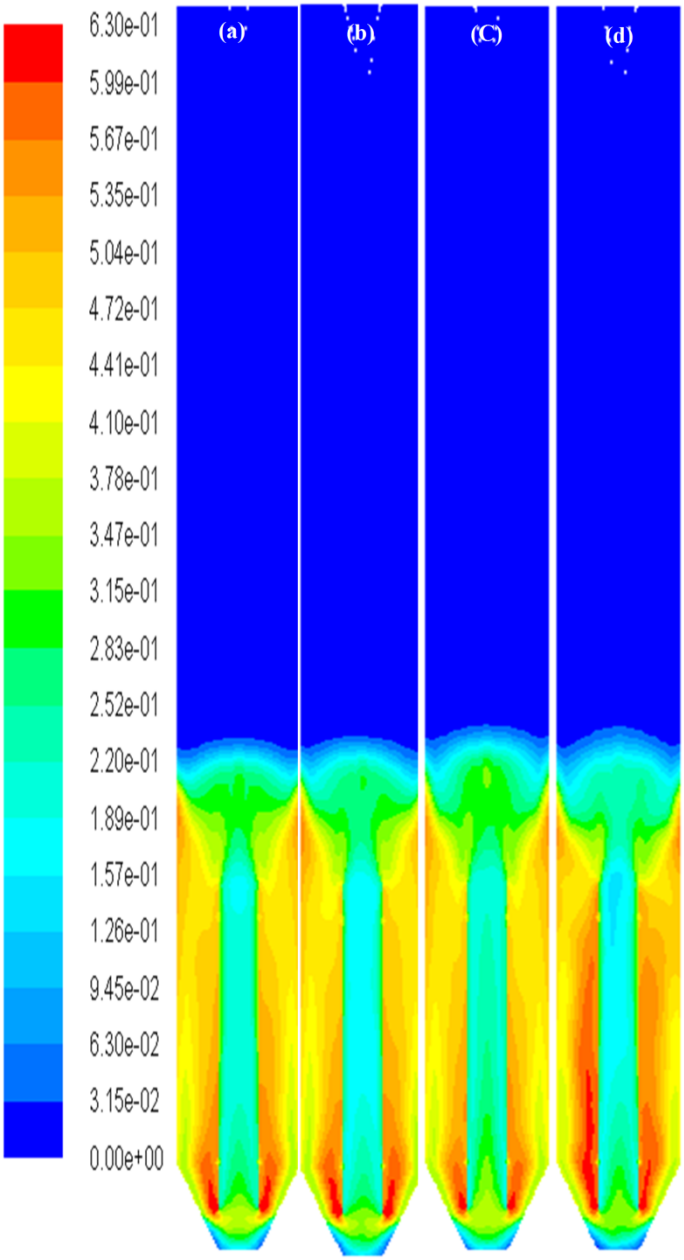

Figure 4.10. Contour plot of mean solids volume fraction with different gas velocities of Silica particles size 250 µm at constant annulus input velocity Ua=0.2 m/s (With Arastoopour drag model). (a) U_d=0.8 m/s. (b) U_d=1.25 m/s. (c) U_d=1.5 m/s. (d) U_d=1.75 m/s.

4.7.4 Radial profiles of solid volume fraction

(a) Within the draft tube

Using CFD tool, new insights in the hydrodynamic feature of ICFB can be analyzed in both draft tube and annular section. Fig. 4.10 shows the simulated time-averaged solids volume

faction profiles in the draft tube at different superficial gas velocity (0.8, 1.25, 1.5 and 1.75 m/s) for various diameter of the particles (86 μm, 170 μm & 250 μm). The data in Fig. 4.10 is extracted at a bed location of Z = 0.75 m (from the bottom of the draft tube). One can observer from these plots that the superficial gas velocity is significantly affecting the solid volume fraction distribution in the draft tube. With increasing draft tube superficial gas velocity, gas volume fraction in the draft tube increases and as the bed rises more and more the solid volume fraction levels decreases. Fig 4.11 (a), (b) and (c) shows that within the draft tube, relatively more volume fraction of particles occupied near the walls as compared to the central zone of the bed. The predicted radial non-uniform distribution of local solid phase volume fraction in the draft tube shows similar trend to that of the normal circulating fluidized beds (CFB) behavior. The non-uniform distribution of solid fraction is the resultant of the air velocity distribution, the collisions between particles and the wall, and particle-particle interactions. Fig. 4.11 shows that the solids volume fraction is much higher near the wall zone, due to the friction between solid phase and wall, which leads the clustering tendency among the particles. Therefore, most of the gas passes through the center region of a draft tube. The gas velocity might increase gradually towards the center of the draft tube, which makes upward drag force to act more on the solid particles. This gas distribution phenomena makes the particles can easily move upward along with the gas stream in the center region making the solid volume fraction low. At the center of the draft tube, the effect of superficial gas velocity on solids volume fraction is minimum, when moving towards to the wall there is a significant change in solids volume fraction. Similarly in case of 170 and 250 μm sized particles volume fraction increases from center of the draft tube to the wall with the increase in superficial velocity. For coarser size particles solid volume fraction near the walls much higher as compared to the 86 μm sized particles, But the influence of superficial gas velocities seems minimal compared to 86 μm sized particles.

(a)

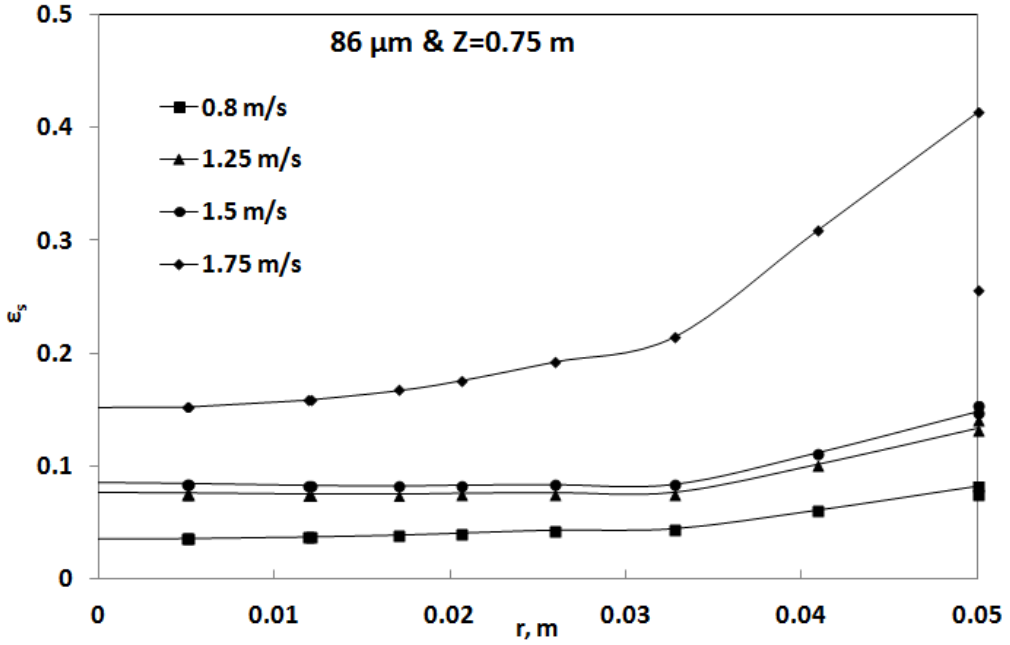
86 µm & Z=0.75 m
0.8 m/s
1.25 m/s
1.5 m/s
1.75 m/s
εs
r, m
0
0.1
0.2
0.3
0.4
0.5
0.01
0.02
0.03
0.04
0.05

(b)

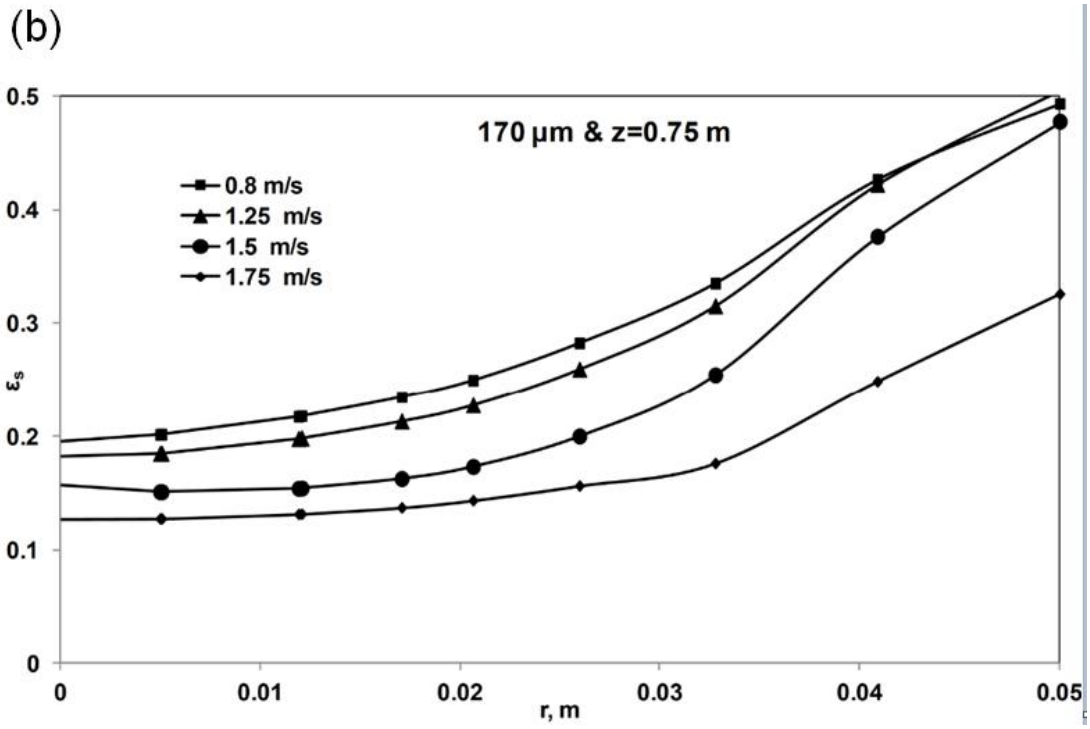
170 µm & z=0.75 m
0.8 m/s
1.25 m/s
1.5 m/s
1.75 m/s
εs
r, m
0
0.1
0.2
0.3
0.4
0.5
0.01
0.02
0.03
0.04
0.05

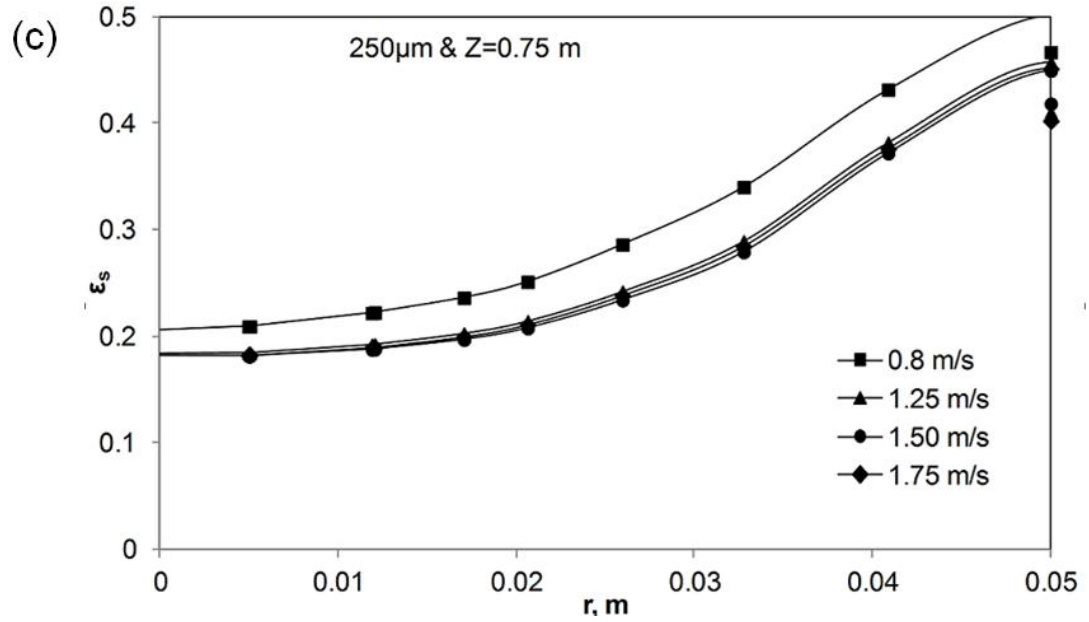

Figure 4.11. Solids volume fraction radial profiles in draft tube (a) 86 µm and (b) 250 µm(c) 170 µm at z=0.75 m axial location of 3D ICFB.

(b) In the annulus region

Fig. 4.13 gives the quantitative comparison of solids volume fraction profiles for different sized particles (86, 170 & 250 µm) at a location of Z = 0.75 m, and superficial gas velocities (0.8, 1.25, 1.5 and 1.75 m/s) in the annulus zone. From Fig 13 (a), (b) and (c), it can be observed that the radial distribution of a solid volume fraction in the annulus region is relatively uniform flattered when compared to the draft tube profiles shown in Fig. 12. Solid volume fraction values are high towards to the walls of both the draft tube and the down comer section, where as in the central zone of down comer the solids volume fraction is slightly lower than the wall region because of solids downward flow as result of gravity influence the gravity influence. This explains in the bed surface behavior, the dense bed surface will oscillate upward and downward due to the gas bubbles rising and breaking up, making the solid fraction lower in the central zone of annulus at higher Uo, say 1.75 m/s for the coarser size particles volume fraction is fairly constant across the radius of the annulus region. It is believed that annulus bed consisting the coarse size particles are not much affected by the gas bypass fraction flow rate results at the draft tube gap area.

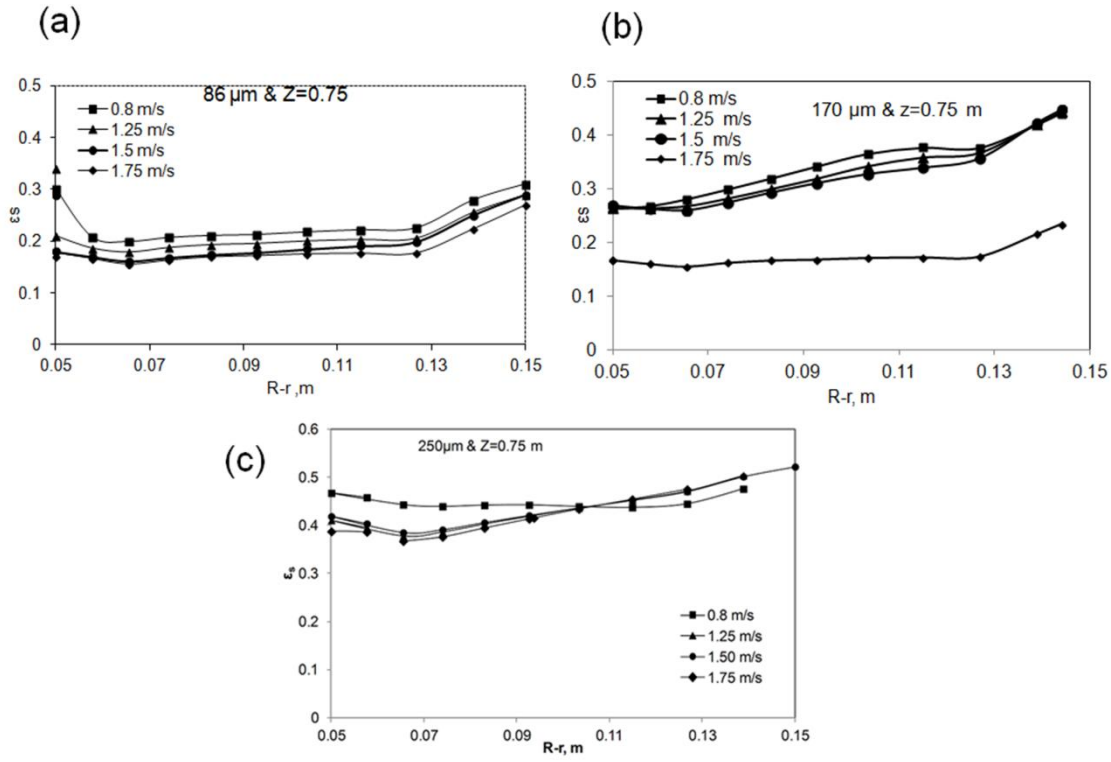

Figure 4.13. Solids fraction hold-up profiles in the Annulus (a) 86 µm (b) 250 µm and (c) 170 µm

4.8 Granular Temperature Profiles

The granular temperature concept was first introduced into the literature by Lun (1984). The granular temperature is computed by solving a fluctuating kinetic energy equation for the particles as already reviewed in the KTGF model section in Chapter 2 CFD methodology. The solid viscosity and granular pressure are computed as a function of granular temperature (Θ) in the CFD model itself, which are two kind of turbulence in fluidization [101]. These two kinds of turbulence give to two kinds of mixing, mixing on the level of particles and mixing on the level of bubbles or clusters. The classical or laminar granular temperature (Θ) is due to random oscillations of individual particles and turbulent granular temperature (Θ_t) is caused by the motion of clusters of particles or bubbles. The turbulent granular temperature is defined as the average of the normal Reynolds stresses [102], which is the average of the three squares of the velocity components in the three directions by using the following definition.

$$\Theta_t = \frac{1}{3}\overline{\upsilon_x'\upsilon_x'} + \frac{1}{3}\overline{\upsilon_y'\upsilon_y'} + \frac{1}{3}\overline{\upsilon_z'\upsilon_z'} \qquad (3.33)$$

Total granular temperature is the sum of laminar granular temperature (Θ) equation (19) and turbulent granular temperature

$$\Theta_{total} = \Theta + \Theta_t \tag{3.34}$$

4.8.1 Particles granular temperatures

Total granular temperature computed according to Eq (3.34) for different superficial velocities and particle sizes. The bigger sized particles give a low granular temperature due to the lower particle velocity fluctuations. At the wall the granular temperature decreases because of the wall friction resistance for the particles. At the center of draft tube riser, the solid-solid interactions by solid collisions were also low because of the low solid volume fraction. In the above draft tube section of the ICFB, the solid volume fraction decreases and causes the solid collisions to dominate the system.

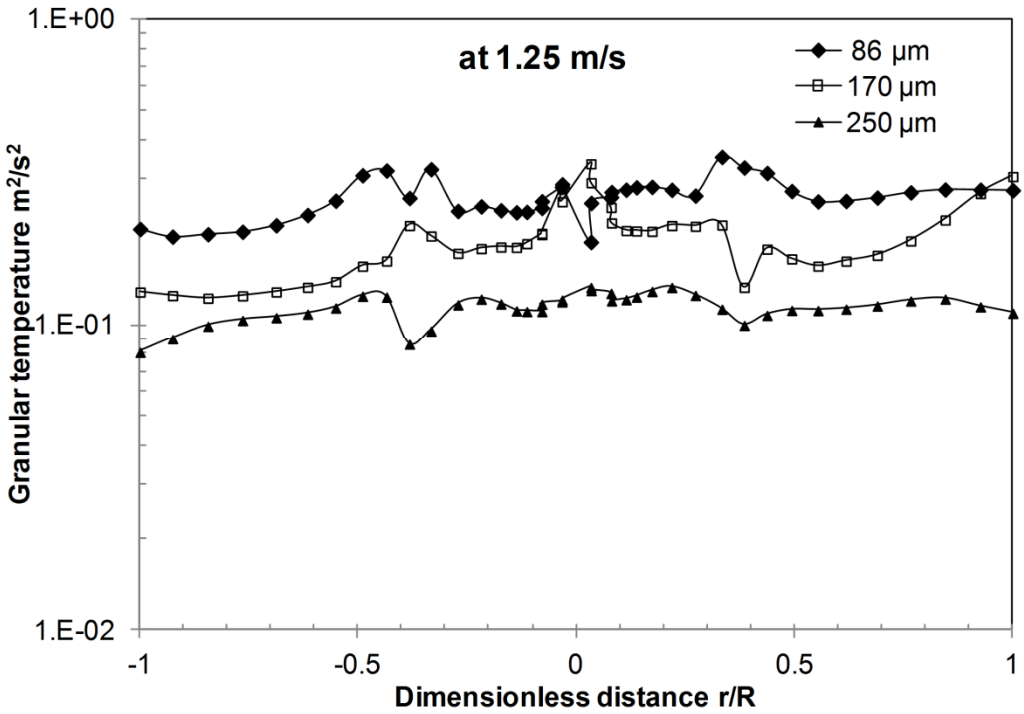

Figure 4.14. Granular temperature profiles for 86 170 & 250 µm particles at a velocity 1.25 m/s.

Fig. 4.14 shows the predicted solids granular temperature at superficial gas velocity of 1.25 m/s for different size range of solid particles (86 µm, 170 µm and 250 µm). The predicted results indicate that the smaller solid particles might have higher fluctuating velocities than the coarse particles because of this its granular temperature is higher than the other coarse particles. The bigger size solid particles have less fluctuating velocity due to high mass of solids thereby they exhibit low granular temperature. Fig. 4.15 shows the effect of superficial velocity on granular temperature for different size range of solid particles with in the draft tube. For 86-250 µm size particles, granular temperature decreases with superficial velocity due to the increased collisions between the smaller size particles than the higher sized particles at higher gas velocities.

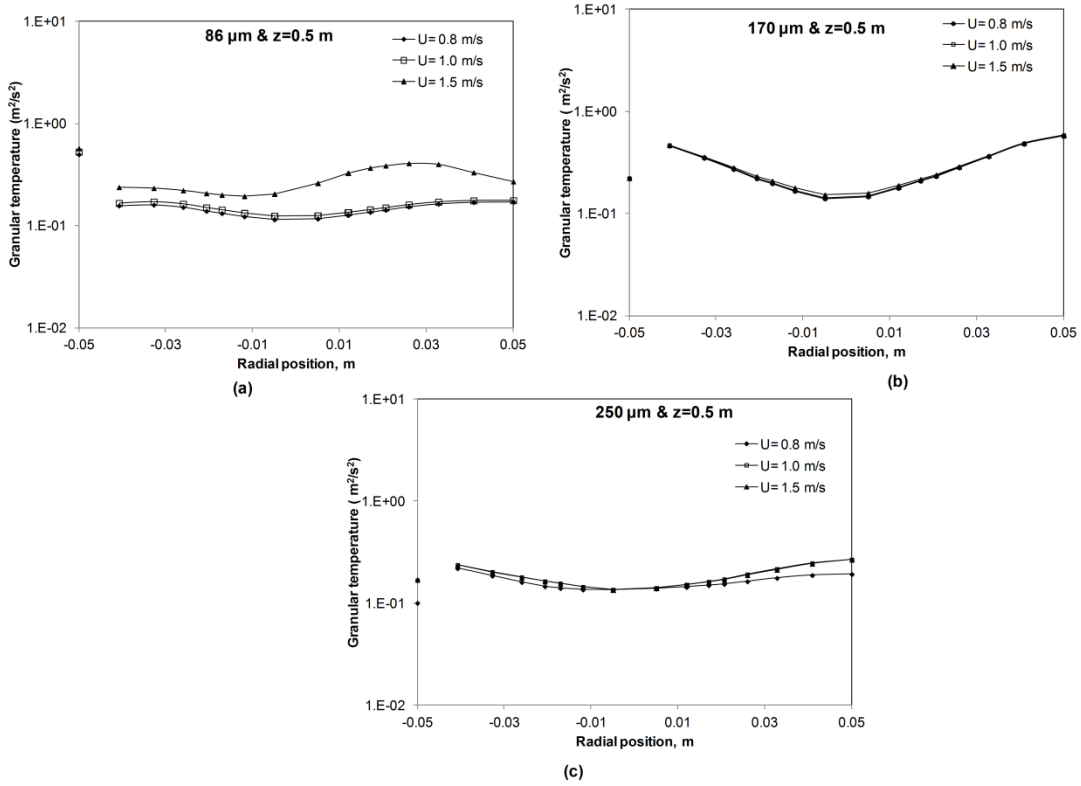

Figure 4.15 Granular temperature profiles in the draft tube at different superficial velocities (a) 86 µm and (b) 170 µm(c) 250 µm.

A comparison of the computed total granular temperatures with literature based experimental data for CFB [103-105] is shown in Fig. 4.16. It is interesting to observe the variations of predicted granular temperature at different superficial velocities in the draft tube riser. A correct trend is observed at low solids volume fractions is shown between the predicted total granular temperature and the 2 D experimental data obtained by Benjapon et

al. [98] with Plexiglas bubbling fluidized bed of 1.28 m height, 0.30 m width and 0.05 m thickness. Where they considered bed material as FCC catalyst with a mean particle diameter of 75 µm and a density of 1654 kg/m^3, classified as commonly used Geldart group A particles. There is a good agreement between the simulation results of 3D ICFB computational domains and with the experimental results from the literature at low solid volume fractions. too. The total granular temperature tends to increase with increasing solids concentrations($\varepsilon < 0.1$) in the dilute region and decreases with an increase of solids concentration in the dense region($\varepsilon > 0.1$). In the dense zone, the decrease in the granular temperature is mainly due to the reduction of the mean free path of the solid particles. As the zone becomes that of the packed bed (high solids concentration), the granular temperature becomes very lean. Our predicted trends and magnitude of the total granular temperature agree with experimental data.

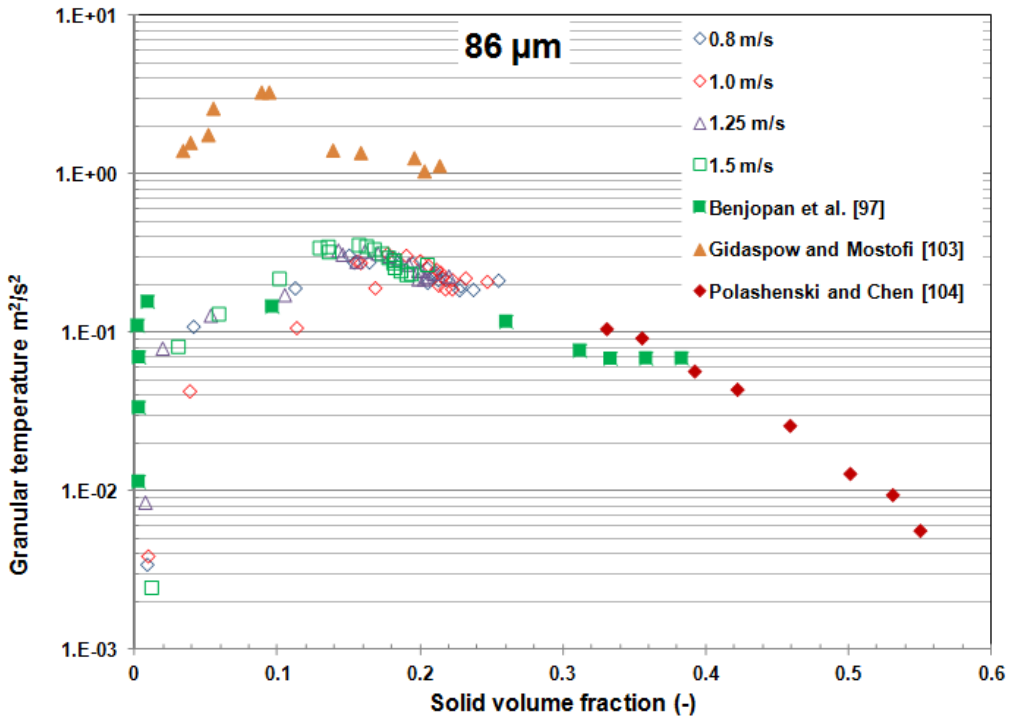

Figure 4.16: Comparison of the theoretical granular temperatures derived in this study and those experimentally derived in the literature.

4.9 Summary

The hydrodynamic characteristic of 2D & 3D ICFB reactors gas-solid flow was studied by an Eulerian-Eulerian CFD model with the solids stress closer from kinetic theory of granular flow. Four different drag models were considered for the simulations. Syamlal and O'Brien, Gidaspow, Arastoopour and Gibilaro drag models are implemented into Fluent through the User Defined Functions (UDF). 2D simulation of an internally circulating gas-solid fluidized bed with polypropylene particles was run based on Ahuja and Patwardhan [15] experimental case. Grid independence check is made with four grid sizes. The resulting hydrodynamic properties from 2D simulations are compared to Ahuja & Patwardhan experimental data. The simulation results by four different drag models show that the Arastoopour and Gibilaro drag models can accurately predict the flow pattern, voidage profiles, and velocity profiles in the ICFB. With the Arastoopour drag model the simulations are giving the best fits to the experimental data. The draft tube superficial gas velocity and the solids circulation rate have significant effect distribution of the solid volume fraction in each region. Increasing the draft tube superficial gas velocity can decreases solids volume fraction in the draft tube but has little effect in the annulus zone. The total granular temperature (Θ_{Total}) tends to increase with increasing solids concentrations($\varepsilon < 0.1$) in the dilute region and decreases with an increase of solids concentration in the dense region($\varepsilon > 0.1$). In the dense zone, the decreasing trend in the granular temperature is mainly due to the reduction of the mean free path of the solid particles. Even though the CFD simulation prediction close to the experimental data but still there is scope to go further do develop accurate CFD model

Chapter 5

Experimental Results and Data Analysis

5.1 Introduction

In this chapter, main focus is made on experimental analysis of the solids recirculation rate by using high speed cam and the pressure drop measurement by using U tube manometer. Using the measured solids velocity profiles in the annulus region, the gas bypassing fraction levels are calculated by adopting the equal mass flux balance.

A number of experiments were performed as listed in Table 5.1. The effect of static bed height in three levels as shown in the Fig 5.0, the bed particle mean diameter in two levels, the gas superficial velocity in the range of 0-1.2 m/s (including 4 levels after minimum fluidization) and the draft tube gap height in two levels are varied for this ICFB in order to study the hydrodynamic behavior of gas-solid system.

Table 5.1 ICFB experimental operation conditions

Item	Units	Values
Static bed height	cm	40, 50 & 60
Bed particle mean diameter	μm	470 & 800
Gas superficial velocity	m/s	0-1.3
Draft tube gap height	cm	7.5 , 10.5 &10.5

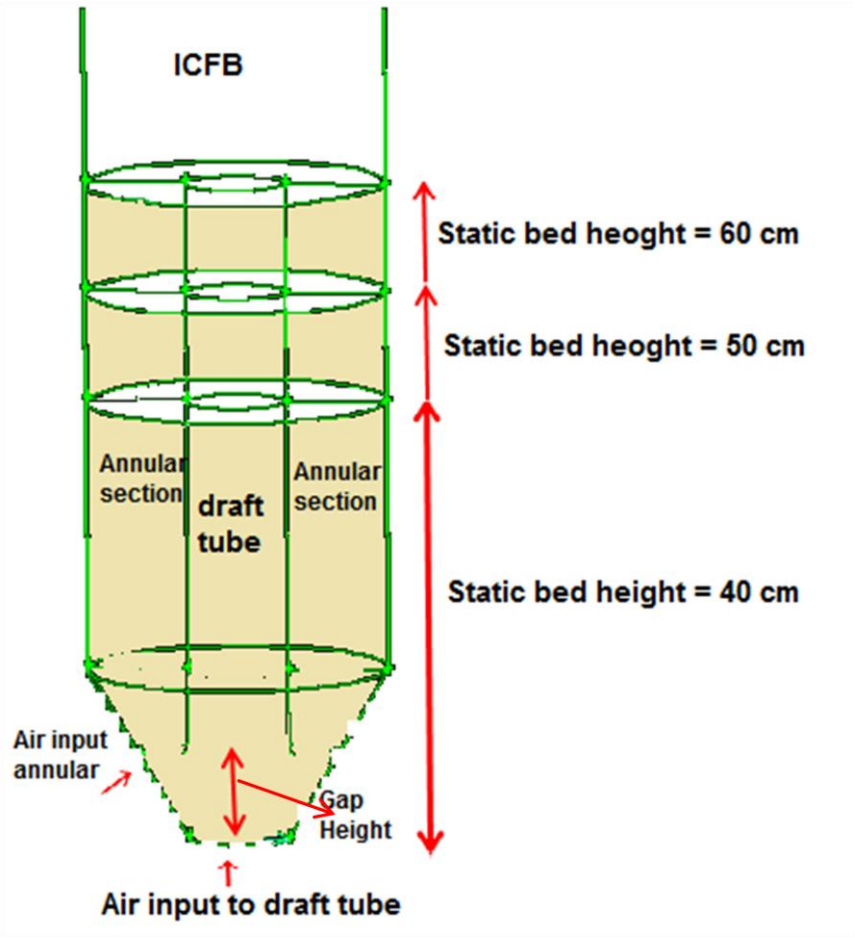

Figure 5.0 ICFB experimental configuration schematic view

5.2 **ICFB pressure flow curves**

5.2 **ICFB pressure flow curves**

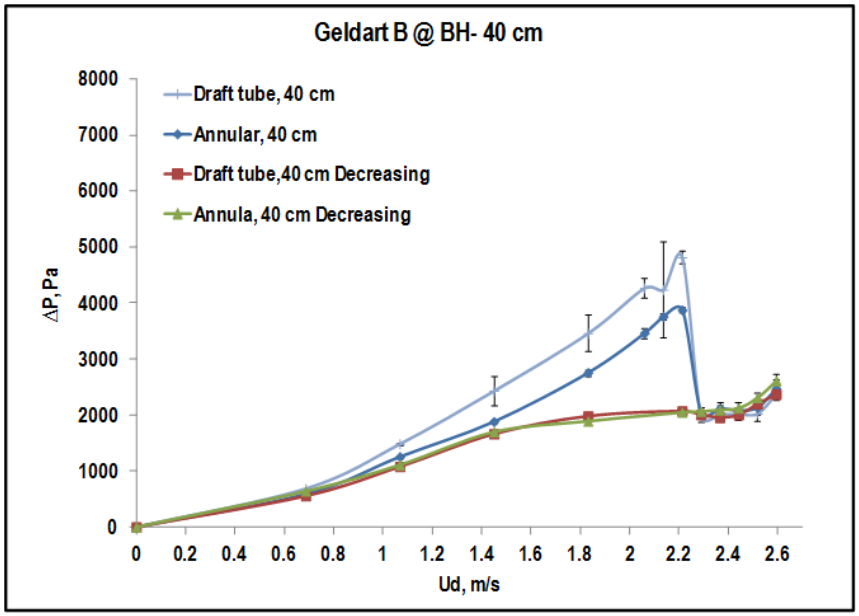

(a)

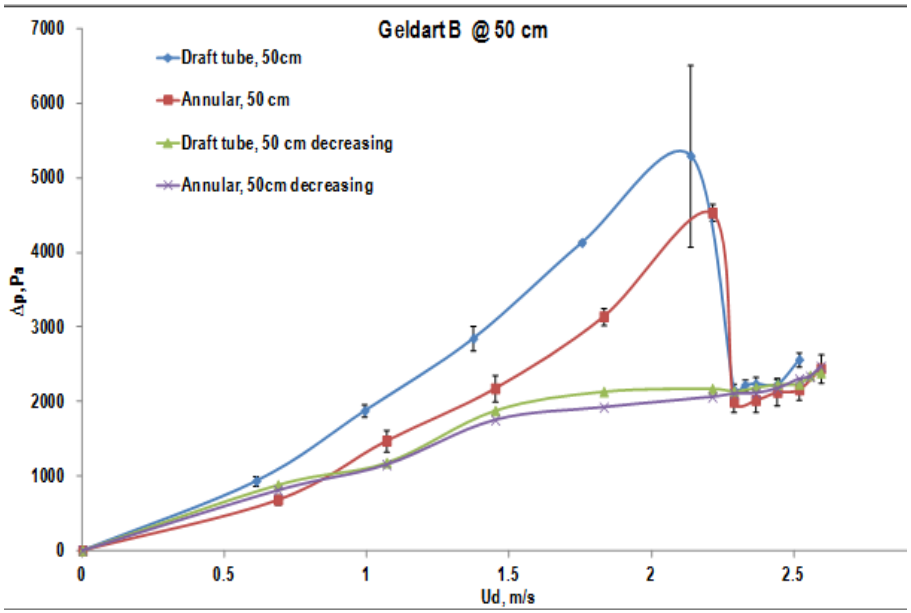

(b)

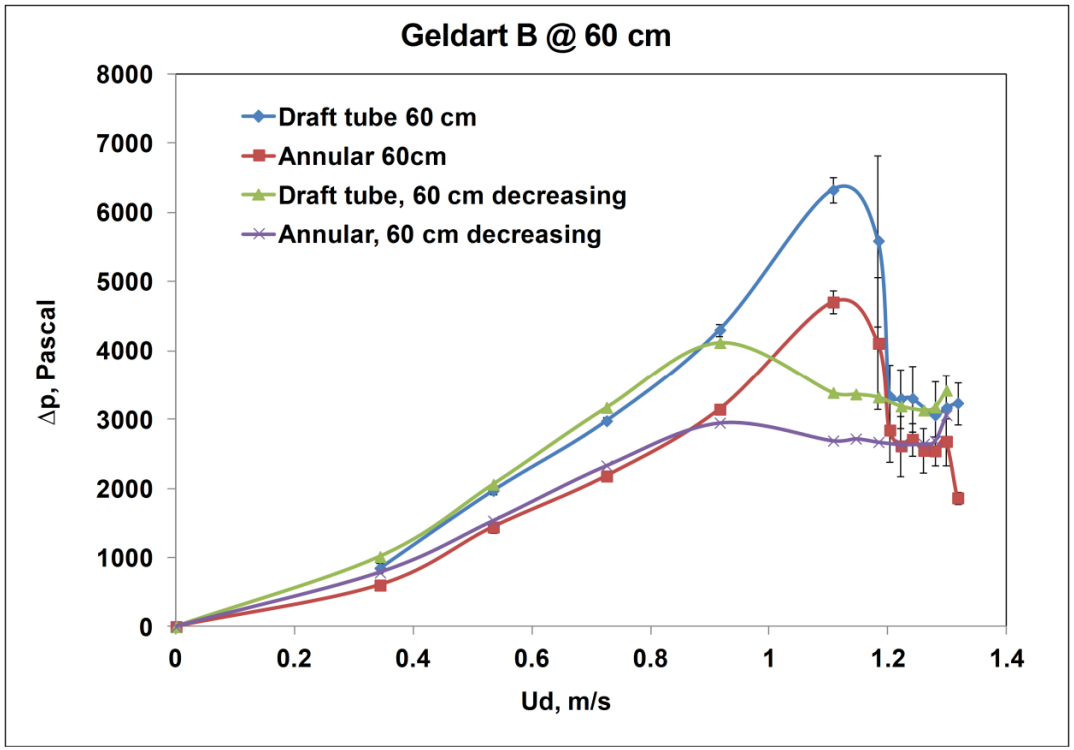

(c)

Figure 5.1 Pressure drop v_s superficial flow curve for (a) Bed height 40 cm (b) Bed height 50 cm and (c) Bed height 60 cm beds consisting of Geldart group B particles.

In every experimental run the measurement of bed pressure drop in the draft tube as well as in the annular section with superficial air velocity was carefully monitored from fixed bed to fluidizing bed conditions. Once the ΔP -U_o full curve is measured, the superficial velocity values are reversed to observe the hysteresis of the pressure drop. The same experiment is repeated thrice and the average data tabulated and also error bar are presented in the Fig. 5.1

Typical bed pressure drop versus gas superficial velocity (U_0) for Geldart B particles was shown in Fig. 5.1 (a) (b) & (c). It is observed that for a given initial bed height condition, the pressure drop increases with superficial velocity in both draft tube and annular bed similar to any packed bed condition. Then it reaches a maximum value near the minimum fluidized bed condition followed by sudden drop with superficial velocity. Unlike conventional CFB riser, in which the ΔP is fairly constant after the minimum fluidization, the draft tube's ΔP slightly increases with U_0 after the minimum fluidization and remains constant at higher fluidization velocities.

Similarly, in the annulus region, ΔP increases with U_0 till the minimum fluidization condition prevails in the draft tube. Once the minimum fluidized bed condition is achieved, the fluidized bed solids blow out from the draft tube and a fountain is created above the draft tube, which then experience neutrally buoyancy condition and will fall into the annulus region. As the maximum portion of solids falls into the annular zone, the bed of solids start descend due to effect momentum induced by annulus air-inflow and gas-bypassing flow from the draft to annular region near the gap area of draft tube bottom section. This phenomenon may lead to sudden drop in ΔP across the annulus bed particles.

Once annulus bed starts moving downward, the recirculation rate of solids from draft tube increases with fluidization velocities. This increased effective mass of annulus bed at higher velocities result an increasing $\Delta P_{Annulus}$. Before minimum fluidization, the $\Delta P_{Annulus}$ is much less than the ΔP_{Dt} and after initiating fluidization the $\Delta P_{Annulus}$ is slightly higher than the draft tube pressure drop. Once stable fluidization within the draft tube is achieved, when air flow rate to the draft tube gradually reduced the pressure drop slowly increase and immediately below the minimum fluidization velocity and bed height decreases. However, the final bed height may be greater than the initial value for the static bed. The pressure drops at low superficial velocities is less than that in the initial original fixed bed. A significant hysteresis is formed, which is due to the peak pressure drop and is much higher

than the column operating pressure drop and even further enhanced superficial air velocities than the minimum one is required to split the bed and initiate fluidization fountain.

5.3 Pressure fluctuating data-minimum spouting fluidization condition

The data presented in the pressure drop flow curves as shown in Fig. 5.2 (a) (b) & (c), also contains the pressure drop fluctuations, in terms of SD values. Fig. 5.2 shows the relation between the superficial gas velocity and standard deviation (SD) values of pressure drop in both draft tube and annular region of bed heights 40 cm, 50 cm and 60 cm. The pressure fluctuating curves in the draft tube and the annular region are very similar till the minimum spouting fluidization in the draft-tube condition. The value of SD is close to zero before the pressure drop starts to increase linearly with U_o. When the pressure drop fluctuates, significantly the value of SD increases, and after reaching a maximum value (SD value of draft tube of bed height 40 cm is 1420 Pascal, draft tube bed height 50 cm is 1225 Pascal and draft tube bed height 60 cm is 1185 Pascal) it decrease rapidly. This maximum pressure drop fluctuation indicates at which the draft tube's fixed bed change into fluidized condition. Based on this pressure fluctuating values, one can identify the minimum spouting fluidization velocity for a given bed of particles within the draft tube. In the end, the SD decrease slowly at a higher gas velocity. Combined with the experimental observation, it can be seen that the SD increases quickly when the draft tube region starts to fluidize. When the draft tube gas velocity is increased to a certain value, the bed starts to fluidize, and then the SD decreases correspondingly as shown in the Fig 5.2. These findings are similar to the experimental observations made with a spouting fluidized bed with a draft tube by Su et al. [39].

(a)

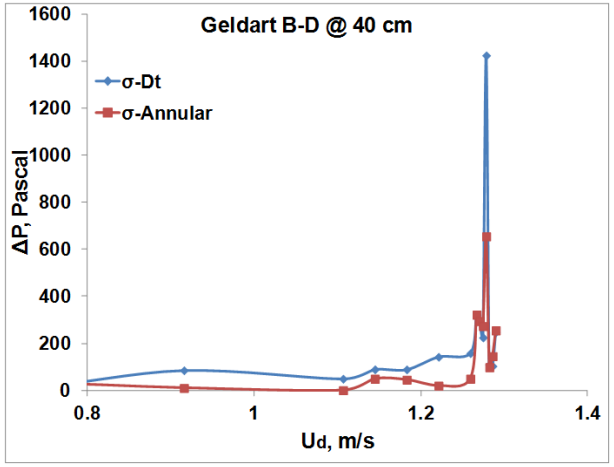

(b)

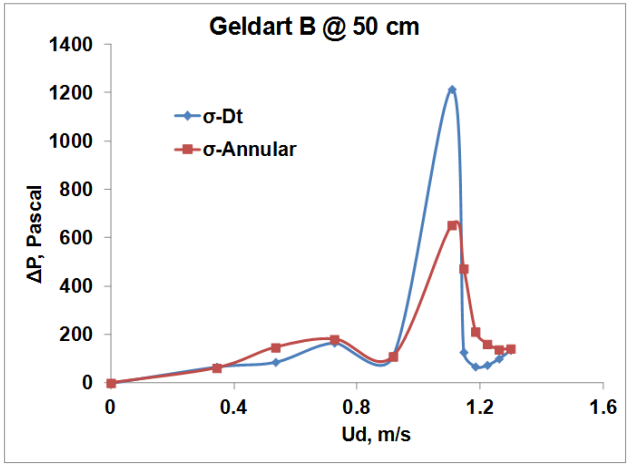

(c)

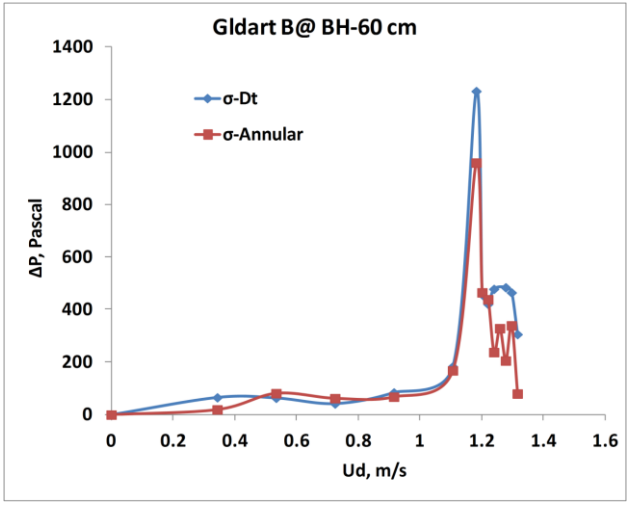

Figure 5.2: Standard deviation values of pressure drop vs superficial flow curve for (a) 40 cm (b) 50 cm and (c) 60 cm beds consisting Geldart B particles.

5.4 Influence of the superficial velocity

Fig. 5.3 shows the effect of superficial gas velocity on solid circulation rate measured repeatedly in comparison with its average values for the case of 40cm bed consisting Geldart group B particles at the gap height of 7.5 cm. Since the annulus bed was not fluidized in these ICFB experiments, the solid circulation rate could be calculated using Equation (3.2) with minimum possible error. The particle velocity in the annular zone, U_{pd}, was measured at three different positions with three repetitions each experiment along the circumference of the ICFB and was averaged and the error associated with its measurements is made in terms of standard deviation values. The annular bed voidage ε_d was assumed to be equal to the dense bed voidage (measured experimentally), as the annular bed was not fluidized in the present study. As reported in the Fig. 5.3, it is observed that the SD values of solids circulating rate are increasing with superficial velocity. For the above case, the three circumference positions having the associated maximum SDs are 2.51, 2.56, and 2.87 respectively. The averaged SD value for these measurements is 2.65. Hence, the assumption using the equation (3.2) does not result in any significant error. The solids bed height, the draft tube gap height and the superficial gas velocities were varied for a considerable range to study their effect on the solid circulation rate.

In the Fig. 5.3 solid circulation rate $G_{S,}$ slowly increases with the superficial gas velocity initially and then rapidly increases to large values as the annulus bed descents. With the increase in the superficial gas velocity U_0, there is an increase in the diameter of the jet produced in the entrainment region [6, 24]. This increases the solid circulation rate in the annulus region until the induced gas jet diameter is equal to the draft tube diameter. The maximum superficial gas velocity U_0 is maintained well below this limit always for all fluidization experiments conducted in this study. As reported by, further increase in U_0 will generally lead to an increase in the gas bypassing and a constant or small decrease in the solid circulation rate may possible.

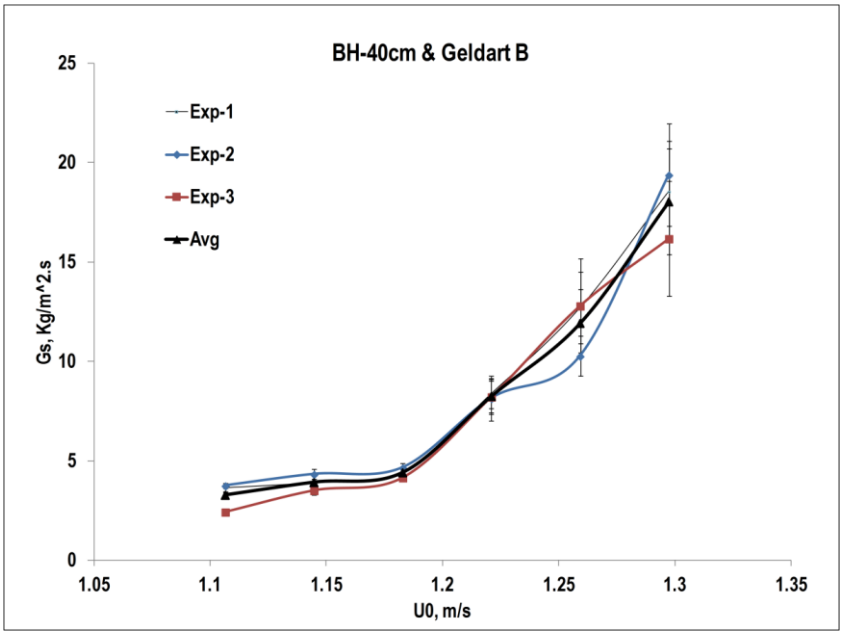

Figure 5.3: Solids circulation rate profile for 40 cm bed height consisting Geldart B particles ICFB at gap heights at 7.5 cm

5.5 Influence of the static bed height

Pressure drop profiles for 40, 50 and 60 cm static bed heights consisting Geldart B particles ICFB in the draft tube and the annular bed region are shown in Fig. 5.4. It is observed that as the static bed height increases the pressure drop across the draft tube and annular region increases due to its resultant increase in mass and bulk density of the bed. As the bed length increases, the bulk density and the effective mass loadings increases. The bed pressure drop increases with increasing bed height because more pressure forces is needed to fluidized more bed mass in the constant diameter bed, which is similar to Su et al.[39]. As reported in the general pressure flow curves in prior section, the maximum pressure fluctuations were found at peak pressure drop position, at which the minimum fluidization starts. This pressure drop certainly is influencing the solids recirculation rate in the annular bed zone.

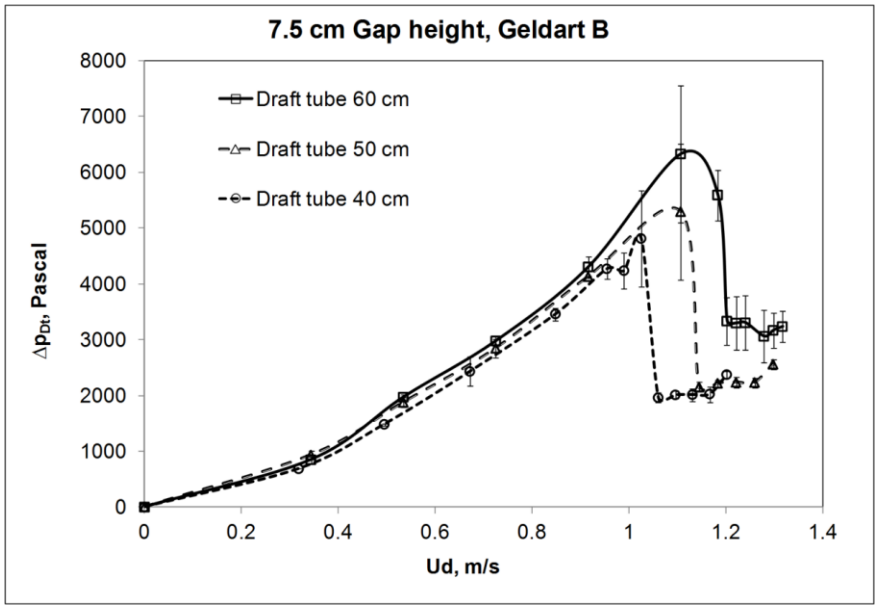
7.5 cm Gap height, Geldart B
Draft tube 60 cm
Draft tube 50 cm
Draft tube 40 cm
ΔpDt, Pascal
Ud, m/s
0
1000
2000
3000
4000
5000
6000
7000
8000
0
0.2
0.4
0.6
0.8
1
1.2
1.4

(a)

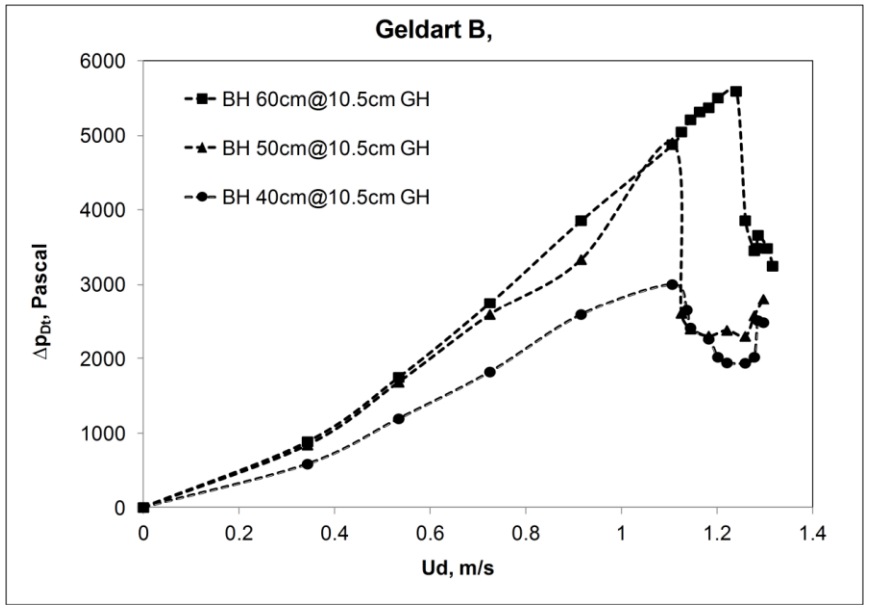
Geldart B,
BH 60cm@10.5cm GH
BH 50cm@10.5cm GH
BH 40cm@10.5cm GH
ΔpDt, Pascal
Ud, m/s
0
1000
2000
3000
4000
5000
6000
0
0.2
0.4
0.6
0.8
1
1.2
1.4

(b)

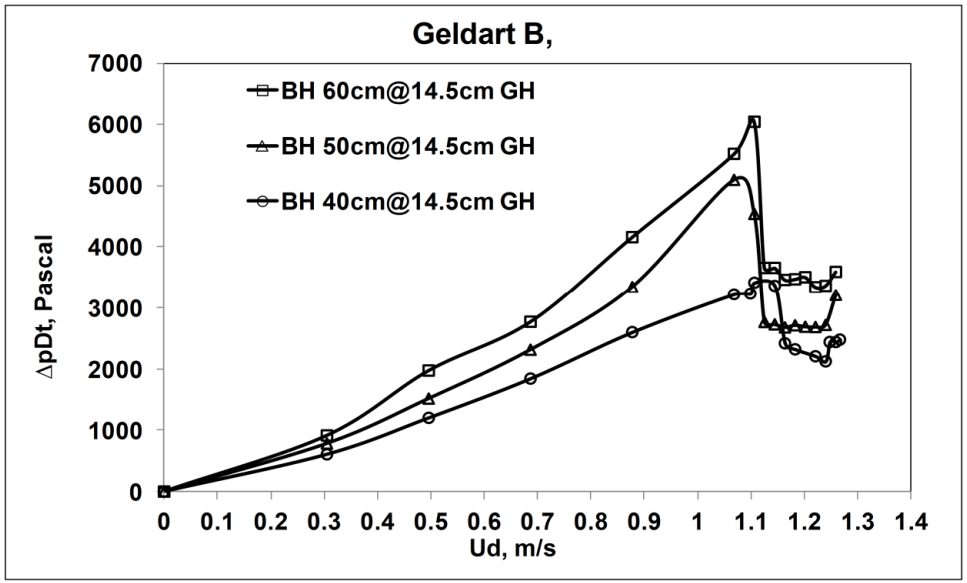

(c)

Figure 5.4 : Pressure profiles for 40, 50 and 60 cm bed heights consisting Geldart B particles ICFB in the (a) draft tube (b) gap height of 10.5 cm and draft tube pressure (c) gap height of 14.5 cm and draft tube pressure

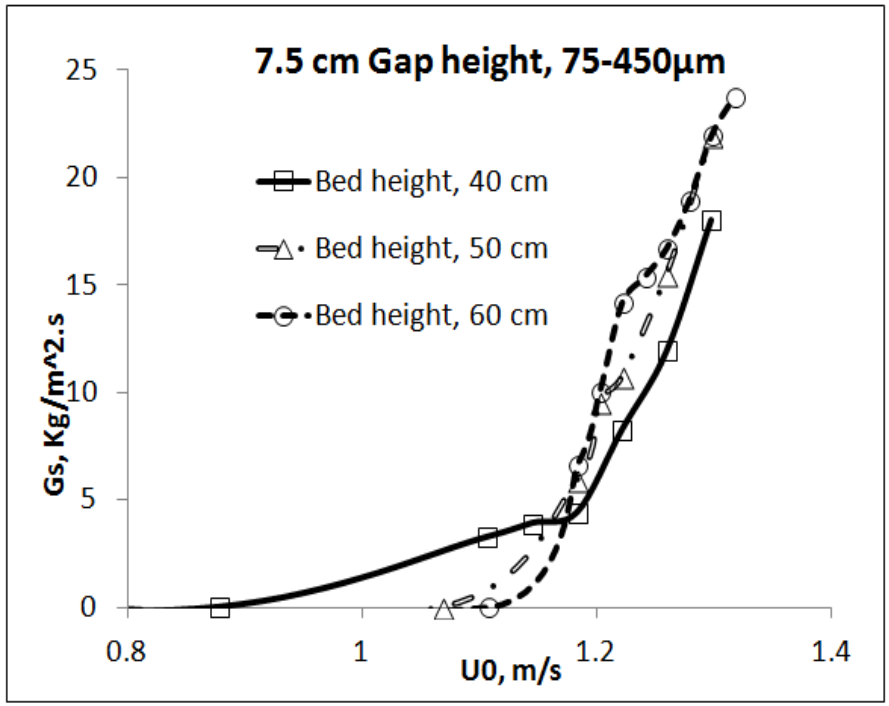

(a)

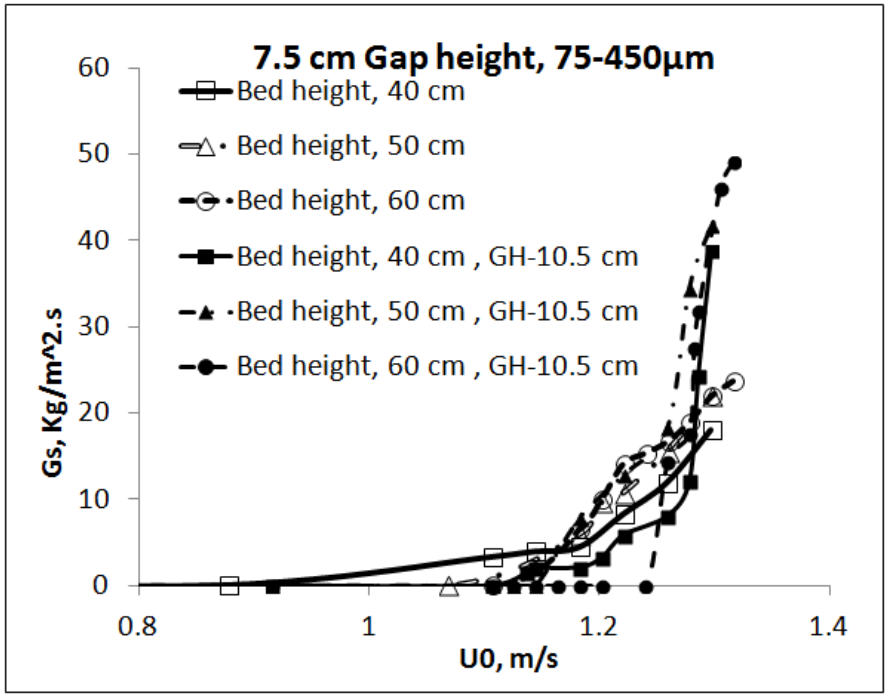

(b)

Figure 5.5: Solids circulation rate profiles for 40, 50 and 60 cm bed heights consisting Geldart B particles ICFB at a gap heights of (a) 7.5 cm (b) 7.5 cm & 10.5 cm.

- Fig. 5.5 shows the effect of static bed height on solid circulation rate for the bed consisting Geldart B particles of ICFB at gap heights of 7.5 cm & 10.5 cm. There is an increase in solid circulation rate with an increase in the height (mass) of solids for both draft tube height at 7.5 and 10.5 cm (Fig. 5.4 (a) and (b)). This phenomenon can be explained similar to Yang and Keairns [20] and from Fig. 5.4 observations due to resultant of increased bed mass loadings. An increase in bed of mass leads to an increase in the pressure difference between the draft tube bottom and the annular bed bottom and thereby an increase in the circulation of solids is possible. Further it is observed that annular bed recirculation start-up with gas velocity is also varying for ICFB's static bed heights at a fixed draft tube gap height. As the static bed height increase the recirculation start-up gas velocity increases due to increased bed mass that is responsible for higher pressure drop. At higher static bed conditions, once the draft tube bed is fluidized, the solids recirculation rate in the annular region significantly high and crosses over at much lower superficial velocities. This cross over is consistently observed for all the experiments conducted in this study. In the all experimental measurements the bed height effects do affect very little on the solid circulation rate.

5.6 Influence of the draft tube gap height

The gap height between the draft tube bottom and the gas distributor plate is an important parameter affecting the pressure drop and solids flow pattern both in the draft tube and the annular bed zone. Draft tube's pressure drop profiles for 40, 50 and 60 cm static bed heights consisting Geldart B particles of ICFB having different gap heights are shown in Fig. 5.6 (a). The pressure drop decreases with the increase in gap height for given bed of particles. An Increase in gap height leads to an increase in the gas bypassing and hence a decrease in the velocity of gas in the draft tube. This low gas velocity as a result of gas bypassing in the draft will further leads to lower pressure drop in the draft tube's packed bed solids in comparison to smaller gap height ICFB.

From Fig. 5.6 (b), the effect of draft tube gap height on the minimum fluidizing velocity for different static bed conditions in the riser can be observed. When the entrainment zone length increases (gap height), more and more gas enters into the annular bed region. Then it

needs more fluidizing gas, which leads to the increase of minimum fluidizing gas velocity. This implies that it needs more gas flow to form a fountain at the end of draft tube. This result is similar to the results reported by Nagashima et al. [38] for conical base spout-fluid bed with a draft tube. As described in previous section, the change in minimum fluidization velocity is very significant for large static beds compared to the lower bed heights.

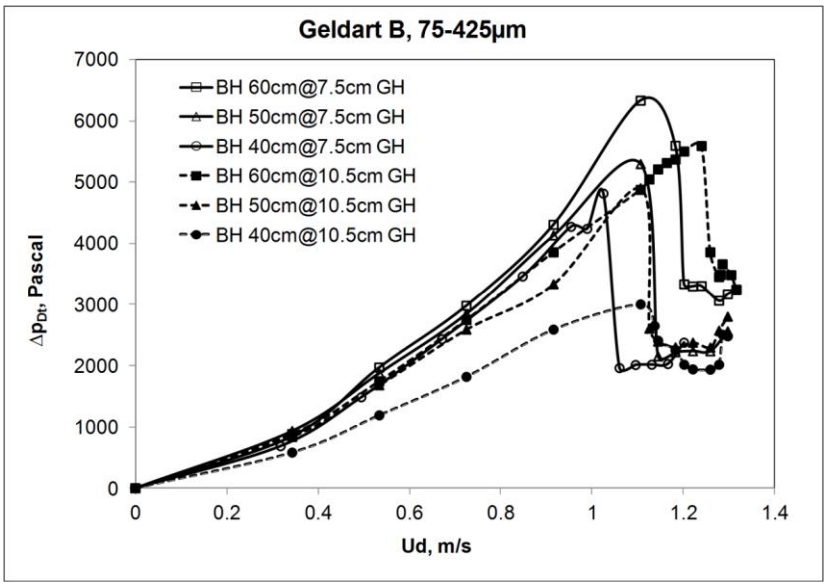

(a)

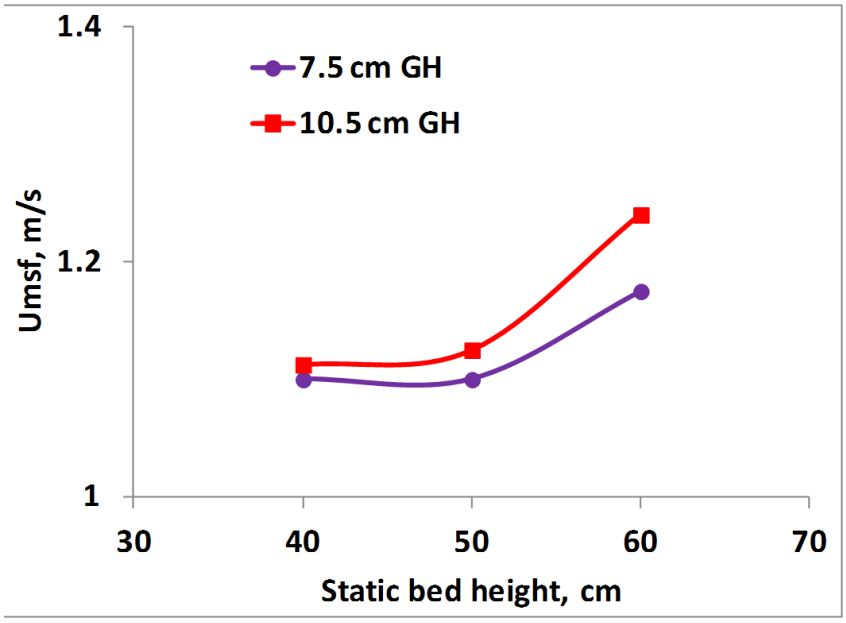

(b)

Figure 5.6: Pressure drop profiles across the draft tube at different gap heights consisting Geldart B particles ICFB at different gap heights for a static bed height (a) 40 cm, 50 cm, and 60 cm & gap height of 7.5 cm and 10.5 cm (b) U_{msf} versus gap height

From Fig. 5.7, an increasing trend in the solids circulation rate is observed for the gap height for ICFB. The increase in circulation rate is possibly due to an increased cross-sectional area and the availability of a higher pressure head across the gap area. Moreover, increased gap height will enhance gas bypassing through the clearance to the annular region, similar to Yang and Keairn's work [20]. This will lead to an increase in resistance across the clearance for the flow of solids. Possibly due to the bypassing of gas, the velocity of the gas in the draft tube will reduce, thereby increasing the concentration of solids in the draft tube and leading to increased pressure at the draft tubes gap edge position. Finally, the profile of solids circulation rate with gap height will depend on the pressure head available, the resistance across the clearance, the extent of gas bypassing through the gap, and the solid static bed height (the mass of the bed) which determines the pressure at the annular region near the draft tube gap. Further it is observed that the use of higher static bed height increases the pressure in the annular region near the gap height and thus reducing the bypassing of gas to the annular zone. That result an increase in solids circulation rate and use of higher superficial gas velocity increases the gas penetrating power making stable operation possible even at higher gap height. The present experimental data of SRR (Gs) is compared with the previous studies as shown in the Fig. 5.8. In all the studies the solids circulation rate increased with superficial velocity and the trend was nearly same for different types of draft tubes employed in the ICFB reactors. Solids circulation started at lower superficial velocity in the case of Lee et al. [33], Ahan et al. [13], Shih et al.[106] and Jin et al. [37]. Whereas in this study, the initial circulation of solids happened at higher superficial velocity i.e.U_o/ U_{mf} at 5.5. This is mainly due to coarse size particle fraction and wide particle size distribution used in the present study as compared with above all researchers work.

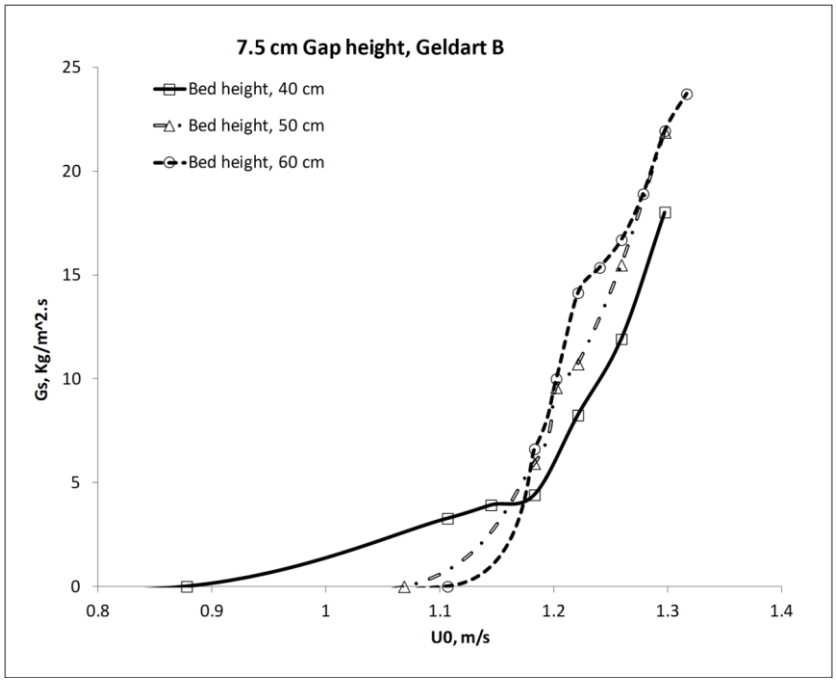

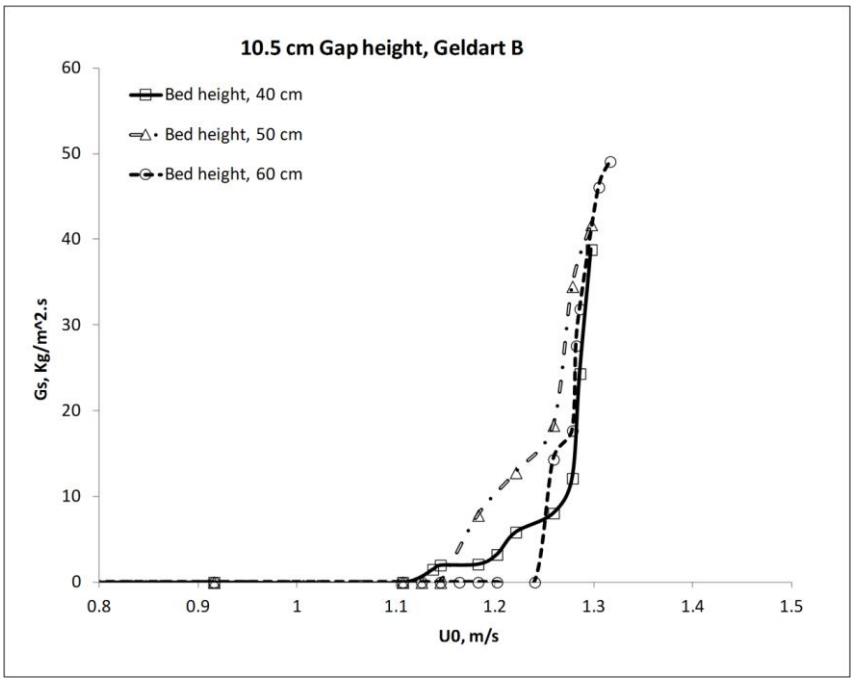

Figure 5.7: Solids circulation rate profiles for 40, 50 and 60 cm bed heights consisting Geldart B particles ICFB at different gap heights 7.5 cm and 10.5 cm

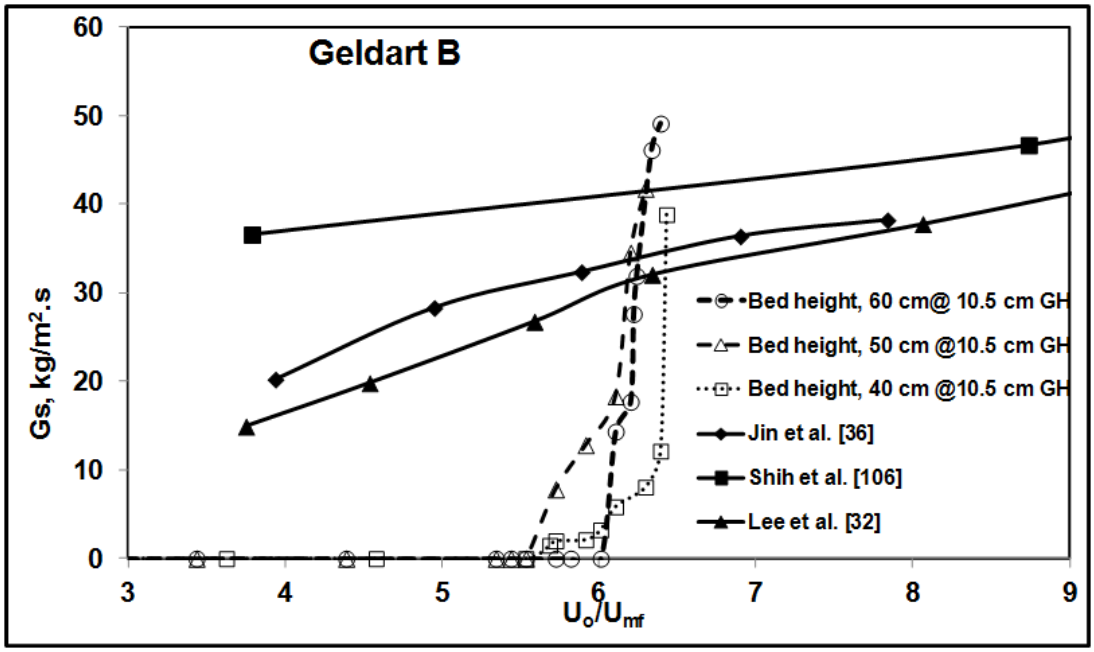

Figure 5.8: Comparison of solids circulation rate profiles at different U_o/U_{mf} for 40, 50 and 60 cm bed heights, at 10.5 cm as gap height.

5.7 Influence of the particle size distribution

It is believed that particle size also affects the fluidization pattern especially with fine particles (Geldart A, B and C) in the clustering phenomenon. Usually particle size significantly affects the cohesion and agglomeration of the solids. Using the two types of particles having fine and coarse size distributions, the measured pressure drop, solids circulation rate and gas bypass fraction were analyzed. A comparison of draft tube and annular bed pressure profiles for the two types of particle sizes considered for different static bed heights is shown Fig. 5.8. A general similar trend found for two particle distributions in terms of pressure flow curves up to peak pressure for both draft tube and annular beds, but the annular bed pressure drop is always lower than the draft tube. The draft tube pressure drop is higher for fine particles (Geldart B) than for the coarse particles (Geldart B-D). The same trend can be seen for all the static bed conditions. This may be due to the fact that small particles generate more friction than the coarse particles as they tend to leave little void space (more flow resistance to the gas flow) and agglomeration behavior. Further the coarse particles reach the fast fluidization regime at comparatively higher superficial gas velocity then the fine particles (see the table 3). This is believed due to the increased mass of bed for coarser particle at given static bed height.

Table 5.1: Measured minimum spouting fluidization velocities for all experimental conditions

S.No.	Gap height	Bed height	PSD	U_{mf}, m/s
1	7.5	40	Geldart B	1.10
2		50		1.08
3		60		1.09
4		40	Geldart B-D	1.28
5		50		1.28
6		60		1.28
7	10.5	40	Geldart B	1.06
8		50		1.07
9		60		1.20
10		40	Geldart B-D	1.28
11		50		1.28
12		60		1.28
13	14.5	40	Geldart B	1.13
14		50		1.08
15		60		1.11
16		40	Geldart B-D	1.12
17		50		1.25
18		60		1.25

The effect of particle size distribution on solids circulation (G_s) is shown in Fig. 5.9, where G_s decrease with increasing an effective particle mean size. Since the resistance of solid flow across the draft tube increases with particle size, the coarser solid particles will require higher momentum to fluidize in the draft tube, resulting reduced rate of solids into annular region would be possible. The static bed height seems to have a virtually no effect on G_s for coarse effective mean size particles. The Gs versus Uo curve for the coarse particle cases show a sudden increase in its solids circulation rate immediately after the minimum fluidization velocity, indicating an unstable bubbling fluidization condition. Whereas the fine effective particle size cases, a smooth and steady Gs curves is observed. It can be concluded that a smooth and stable fluidization within the draft tube may be possible mainly with Geldart B particle, while in the case of Geldart B-D particles the stable fluidization

occurs at a higher superficial velocity.

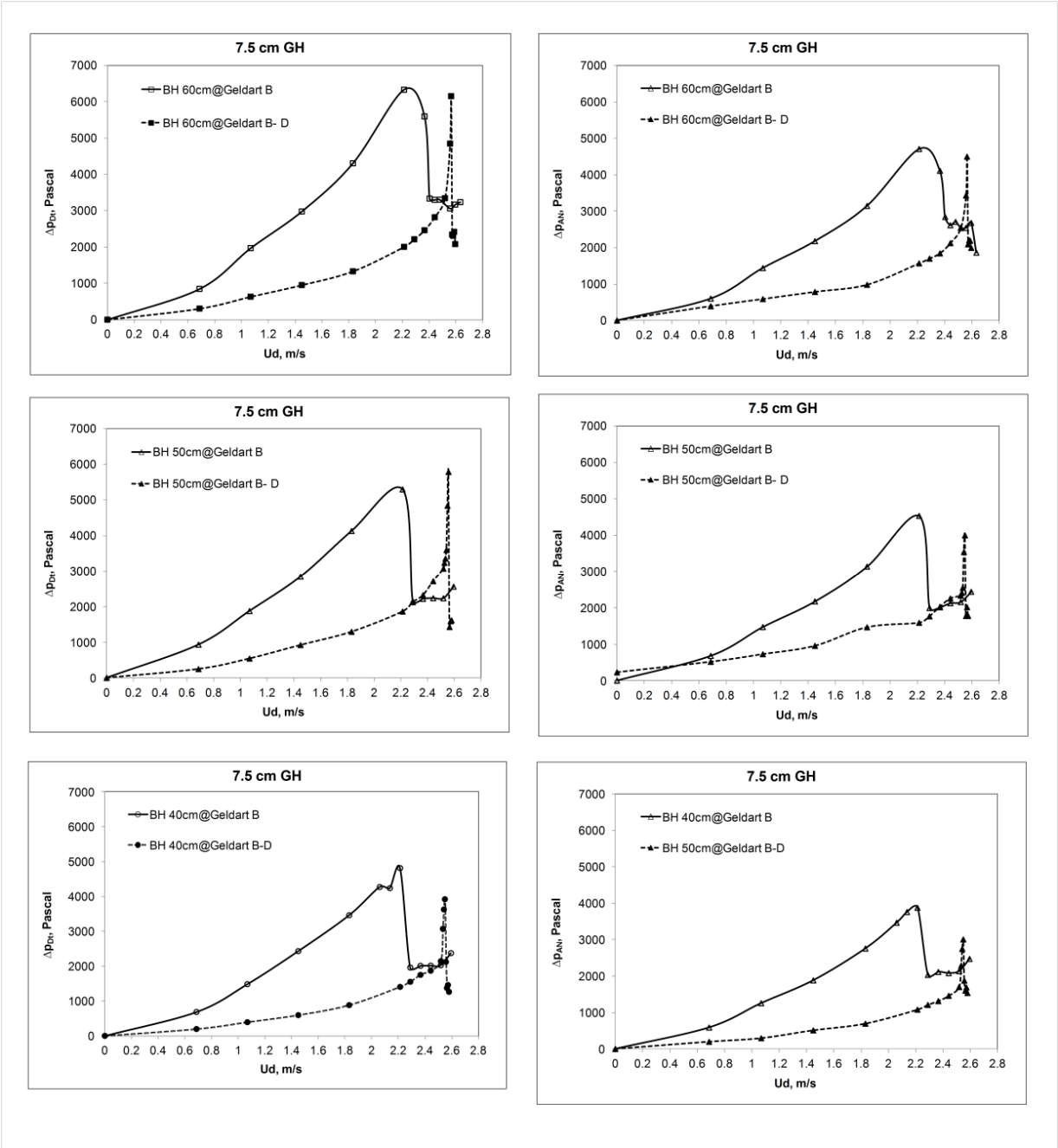

Figure 5.8: Pressure drop profiles across the draft tube and annular region for two different beds consisting Geldart B and Geldart B-D particles in ICFB for a static bed height of (a) 40 cm, (b) 50 cm, and (c) 60 cm

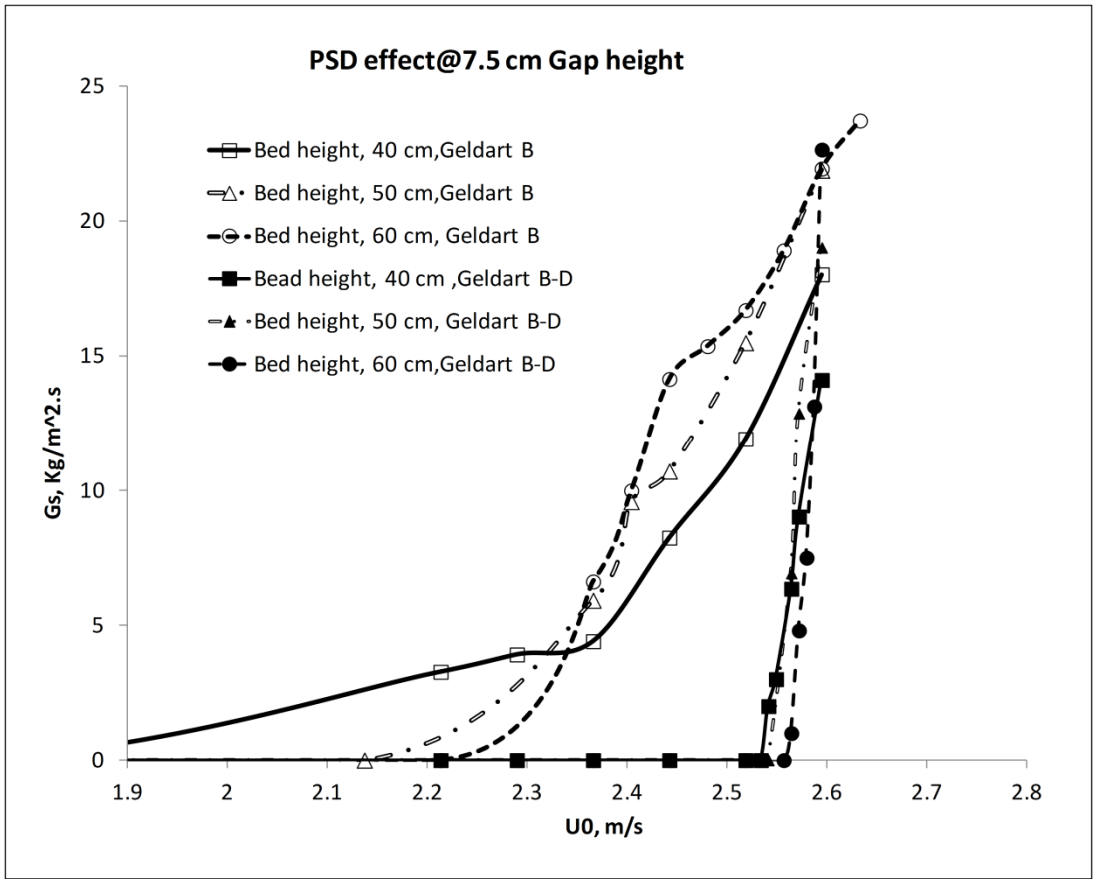

Figure 5.9: Solids circulation rate profiles for 40, 50 and 60 cm bed heights consisting two different particle size distributions at 7.5 cm gap height

5.8 Pressure drop in the annular zone

In the ICFB gas flow distribution between draft tube and annulus region is an important factor that will depends mainly on design and operation of ICFB. Annulus section of ICFB is different from the draft tube in terms of particle behavior. In the annulus section particles behavior like a fixed bed or fluidized bed will mainly depends on annulus input superficial gas velocity and also gas bypassing from the draft tube to annulus section. In our present experimental condition, the annulus section was not fluidized and the particles movement is always downwards and their velocity is very small (range from 0.0045 to 0.0163 m/s) when compared to the draft tube particle's velocity. Hence we assume that the behavior of annuls section as a fixed bed condition in entire experimental runs. The pressure drop per unit length for the annulus section can be calculated using Ergun equation [93]] at fixed bed condition. In the annular section, the particles are moving downwards and the air flowing upwards. Hence here we can use slip velocity instead of the U_o in the Eq (5.1). The

sphericity factor taken to be considered as the particles were not spherical in our present study. Then Eq (5.2) can be modified as the following.

$$\frac{\Delta P_{An}}{L} = \frac{150\mu(1-e_{An})^2 U_o}{e_{An}^3 d_p^2} + \frac{\rho_g 1.75(1-e_{An})U_o^2}{e_{An}^3 d_p} \text{-------} \quad (5.1)$$

Where e_{An} is voidage of the moving bed or fixed bed and is equal to e_{mf} for Geldart B and Geldart B-D powders [107].

$$\frac{\Delta P_{An}}{L} = \frac{150\mu(1-e_{An})^2 (U_{PAn} + U_{gAn})}{e_{An}{}^2 d_p{}^2 \phi_p{}^2} + \frac{\rho_g 1.75(1-e_{An})(U_{PAn} + U_{gAn})^2}{e_{An} d_p \phi_p} \text{ ..... (5.2)}$$

Yang & Keairns [20] have shown that Eq. (5.2) can be used for the predicting pressure drop in the annulus section.

5.9 Gas bypassing

Solids flow behavior in the draft tube and annulus mainly depends on gas bypassing fraction. Gas bypass fraction can be measured by applying various trace gas technique to the draft tube and as well as in the annulus section by injecting tracer gas across axial and radial positions. Yang and Keairns [21] has made first attempt to measure gas bypassing fraction by using the trace gas method experimentally.

Alternatively, using the measured pressure drop Δ_{PAN} one can calculate gas bypassing fraction by adopting modified Ergun equation for fixed bed conditions. Using above equation (5.2) actual velocity in the annuls section U_{gan} was estimated, with this Ugan information the amount of percentage of gas bypassing towards to the annuls section can be estimated as the ration of amount of flow diverted towards annular region to the total gas flow input to the system

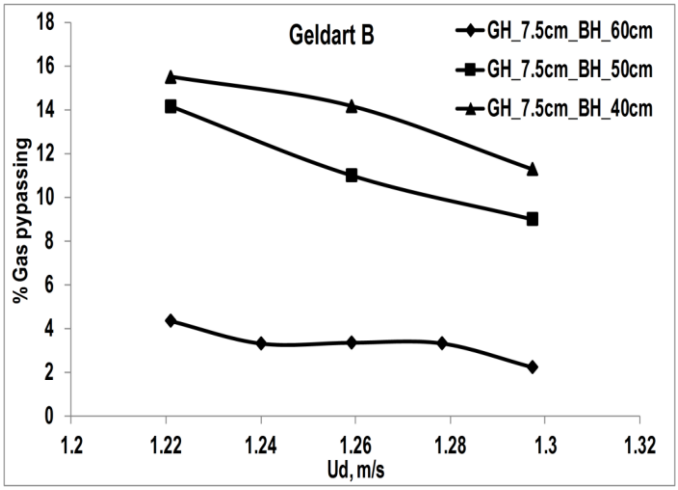

(a)

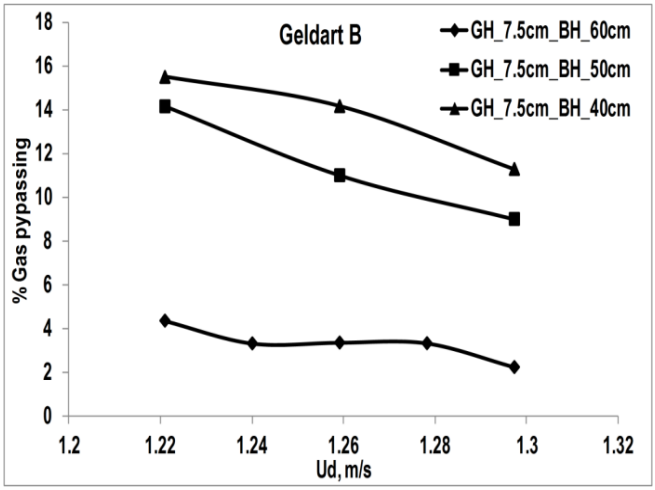

(b)

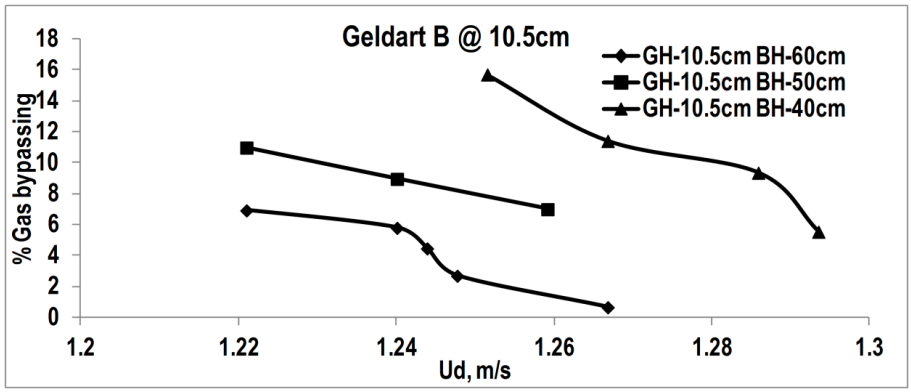

(c)

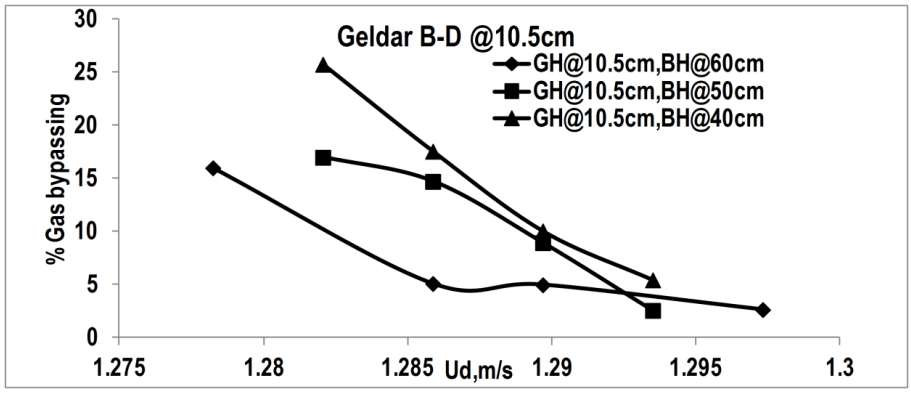

(d)

Figure. 5.10: Effect of gap height and static bed height on gas bypassing for (a) BH= 7.5 cm Geldart B (b) BH= 7.5 cm Geldart B-D (c) BH= 10.5 cm Geldart B (d) BH= 10.5 cm Geldart B-D.

5.9.1 Effect of superficial velocity

Gas bypassing decreases (from 16 percent to 11 percent) with an increase in superficial velocity (from 1.2 m/s to 1.3 m/s) due to lowered ΔP and lean solids concentration in the draft tube. At the higher superficial velocity bypass fraction becomes constant for maximum bed height. So once the system reaches a steady state, where bed pressure drop remain constant which might be leading to constant air bypassing which is shown in the Fig. 5.10 similar to Ahan et al. [13].As the bed height increases (BH = 40 cm to 60 cm) the bypassing fraction decreases for both Geldart B and Geldar B-D particles. This is mainly, because of increased mass of bed in the annular region. Increased bed mass offers more resistance to the air percolation towards to the annular region.

5.9.2 Effect of gap height

Gas bypass fraction increases with an increase in the gap height (GH = 7.5 cm to 10.5 cm) between the draft tube bottom and air distributor. The dispersion of air to the annular region increases with increased gap height leading to higher gas bypass.

5.9.3 Effect of particle size distribution

The Fig. 5.10 also shows the effect of particle size distribution (Geldart B & Geldart B-D size particles) on gas by passing fraction. Gas bypassing fraction increases with increased mean particle size. In the Fig 5.10 (c) at bed height of 40 cm for Geldart B particles have maximum gas bypassing fraction value around 16 percent. Where as in the case of Geldart B-D particles the maximum gas bypassing is 25 percentage. This is believed due to the fact that in the annulus bed consisting fine particles, the void fraction of the fixed bed is much smaller than the coarse size particles. Hence the flow resistance in case of fines is more than the coarse size particles. Larger sized particles offers less cohesion to the gas flow towards to the annular zone where as smaller sized particles offers more cohesion and hence offers larger resistance to the gas bypassing.

5.10 Conclusions

Hydrodynamic characteristics in an internally circulating fluidized bed with a draft tube was investigated experimentally using sand particles of group Geldart B and combined Geldart B-D. Pressure drop, solid circulation rate, gas bypassing and minimum fluidization velocities were considered as part of hydrodynamic study of gas solid flow in ICFB. Based on experimental results the following conclusions made.

- Pressure drop in the draft tube increases with an increase with bed height and also increases with gap height between the draft tube bottom and air distributor.
- Solid circulation rate Gs slowly increases with the superficial velocity initially and then rapidly increases to larger values as the annular bed descents. Gs increases with bed height due to increased bulk density and reduced void fraction that causes the higher bed pressure drop.
- Geldart B particles are having more pressure drop than the Geldart B-D particles due to the maximum possible packing and high frictional resistance of the fine particles for the gas flow. Gas bypassing fraction mainly depended on solids circulation rate, static bed height, superficial velocity, gap height and nature of bed material.
- Gas bypassing fraction increases with increased gap height and decreases with increased bed height. Gas bypassing fraction increases with increased mean particle size

Chapter 6

3D ICFB Simulations: Validation

6.1 3D ICFB CFD Simulations

This chapter mainly focus on 3D ICFB CFD model data validaton against the IITH's ICFB experimental data. In previous chapter 4, 2D ICFB simulations data is validated against to Ahuja & Patwardhan [15] experiments data with a small geometry. Although 2D pseudo simulations predict the hydrodynamic parameters reasonably correct, but the accurate prediction of solids volume fraction distributions and its associated fluctuate velocity components via granular temperature is mainly possible with 3D simulations. Very little literature exists on the granular temperature profiles of ICFB's, in which downward moving annular bed of solids significantly influence the draft tube riser solids dynamics unlike risers in the CFBs. 3D simulations of ICFB are virtually non exist. Usually fast fluidized beds or turbulent fluidized beds are always dynamic and turbulent in nature. To account this, turbulence 2D simulation may not able to predict the dynamics correctly due to less space availability in 2D. Because of the above said consideration we have performed 3D ICFB simulations and validation of the same against the IITH's ICFB experiments is attempted. The work reported in this chapter is aimed to validate a CFD-model for the hydrodynamic study of 3D- ICFB reactor. As described in chapter 3, The two-fluid CFD model along with the k-ε turbulence model and solid stress closer from KTGF is used for simulating the gas-solid flow pattern. The concept of energy of random particle motion is analogous to temperature and random motion of molecules in dense gases. The energy of random particle motion in granular flow as granular temperature "Θ" is indicated with equation (3.21). With the help of these simulations the instantaneous and the time-averaged pressure drop profiles and the solid volume fractions within the draft tube and the annulus section of ICFB are

predicted. Further, the flow fields, i.e. volume fractions and velocity distributions are analysed for the Geldart group B particles.

6.2. Simulation strategy and conditions

The geometry of 3D ICFB, which represents IITH's IFCB as described in the chapter 3, having column of 30 cm diameter and 300 cm height and draft tube of configuration of 0.1 m diameter and 0.6 m height of fluidization rig is used for parametric analysis. The same geometry and its computational mesh are created in the GAMBIT and as shown in the Fig 6.1. The mesh consist of 30K nodes. Relatively fine mesh is adopted in the draft tube section.3D simulations run with the selected case geometry in order to indentify correct CFD model for turbulent fluidization. 3D simulations are performed using above specified two-fluid model along with no-slip boundary conditions adopted for both phases at the ICFB walls. The bottom of the bed was defined as velocity inlet to specify a uniform superficial gas inlet velocity. Pressure boundary conditions were employed at the top of the freeboard, which was set to a reference value of 1.01325 × 105 Pa. The settled bed was considered 0.4 m, 0.5 m and 0.6 m deep and initial solids volume fraction was defined as 0.62 with a maximum packing limit of 0.65. Simulation was initiated with uniform inlet superficial gas velocity in the range of 1.2 m/s in order to simulate the flow curve starting from packed bed to the fluidized bed condition.

Table 6.1 Simulation and model parameter

Parameter Description	**Value**
Particle density	2650 (kg/m^3)
Air density	1.225 (kg/m^3)
Mean particle diameter	470 (μm) (Geldart B)
Initial solid packing	0.62
Superficial air velocity	0, 0.25, 0.5 0.75, 1.09, 1.14 & 1.2 (m/s)
Fluidized bed column dimension	0.3 (m) x 3.0 (m)
Static bed height	0.4, 0.5 & 0.6 (m)
Restitution coefficient	0.95
Boundary Condition	Outlet- pressure, walls-No slip for both

phases

The bed of particles and gas flow rates are listed in the table 6.1. 3D simulations were also run using ANSYS FLUENT 13.0 with standard k-ε model and Eulerain-Eulerian methods. Phase Coupled Semi Implicit Method for Pressure Linked Equations (PC-SIMPLE). QUICK scheme is used for discretizing the governing equations. A fixed time stepping of 0.001 seconds is used to advance the solution time.

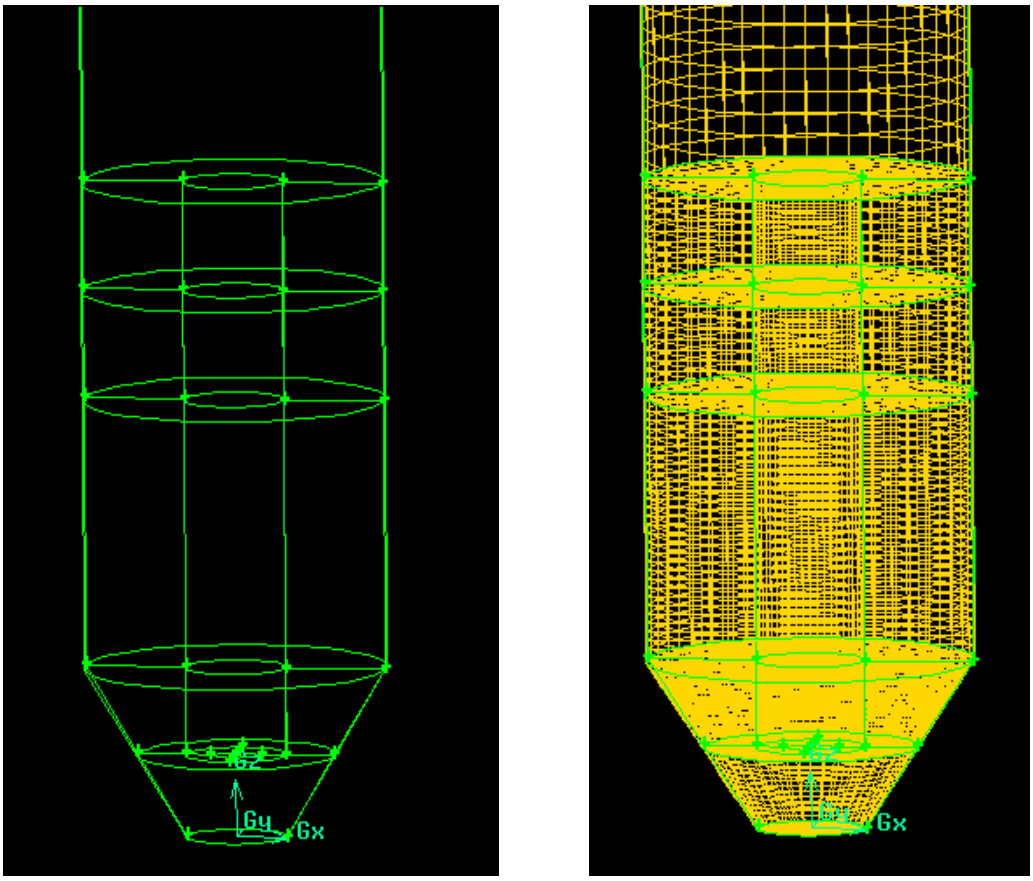

(a) (b)

Figure 6.1 Schematic diagrams of 3D ICFB (a) Geometry (b) Grid and 3D ICFB

6.3 (3D ICFB) pressure drop predictions and validation

The pressure drop (ΔP) between the draft tube and the annulus section is the driving force for solid recirculation in ICFB & CFB [99]. The predicted mean Δp value is plotted to compare pressure drop across the length of the ICFB column in both the draft tube and the annulus section at various superficial velocities varying from 0-1.2 m/s for the 470 µm mean sized particles at bed height of 40 cm and gap height 7.5 cm has shown in the Fig. 6.2.

The simulation data is actually averaged over minimum 2 seconds physical time, once it reaches transient steady state.

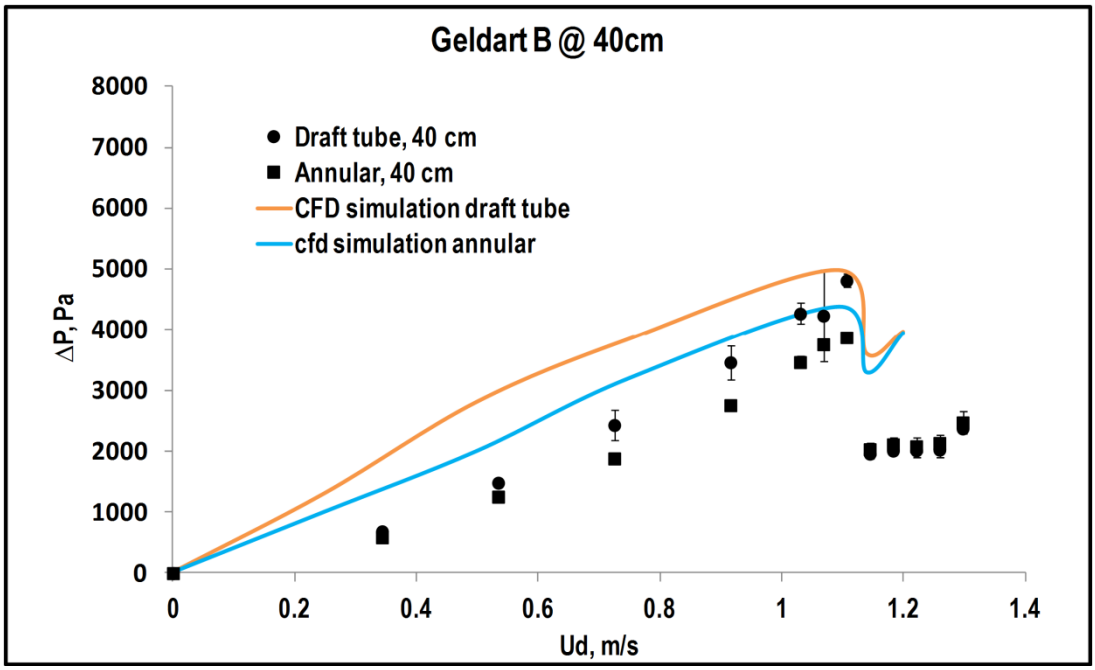

Figure. 6.2 Pressure drop v_s draft tube velocity for the silica particle size 470 µm at bed height of 40 cm and gap height of 7.5 cm.

When the draft tube superficial gas velocity is slowly increased for the bed of particles, the pressure drop in the draft tube and in the annular region slowly increased as shown Fig. 6.2. This type of phenomenon is caused by different bed bulk density in different zones, namely, the draft tube zone has dilute flow and annular zone has dense flow. It can be seen that the pressure drop in the spout and fluidized zones are in same trend and this trend are analogous to literature reports for spout fluidized bed with or without draft tube [100]. CFD predicted pressure drop with in the draft tube and in the annular section is following similar trend with IITH's ICFB experimental data of 470 µm and 40 cm bed height configuration. Similarly, predicted mean ΔP value is plotted to compare pressure drop across the length of the ICFB column in both draft tube and in down comer at various superficial velocities varying from 0-1.2 m/s for the 470 µm sized particles at bed height of 50 cm and gap height 7.5 cm has shown in the Fig 6.3. The pressure drop linearly increased with increased superficial velocity and once it reaches to maximum peak where minimum spout fluidization occurs. Once it reaches to maximum peak of pressure drop immediately pressure drop suddenly decreases sharply and remains constant for the further increases in superficial velocity. At

initial stage CFD predicted pressure drop is closely matches to IITH's ICFB experimental data up to minimum spouting velocity. After reaching minimum spout fluidized bed velocity, CFD data deviated from experimental data. In the experiments, the pressure fluctuations are significantly high especially at peak levels. We believe that the deviations between CFD data and experiments after the minimum spouting velocity is due to unaccounted particle size distribution in simulations where particle segregation would effect the bulk density thereby variation in the ΔP. Also in CFD the adopted particle frictional forces are default Schaeffer (1987) [97]. There is further scope to improve these simulations with improved frictional-collision constitutive relation such as Johnson and Jakson [76].

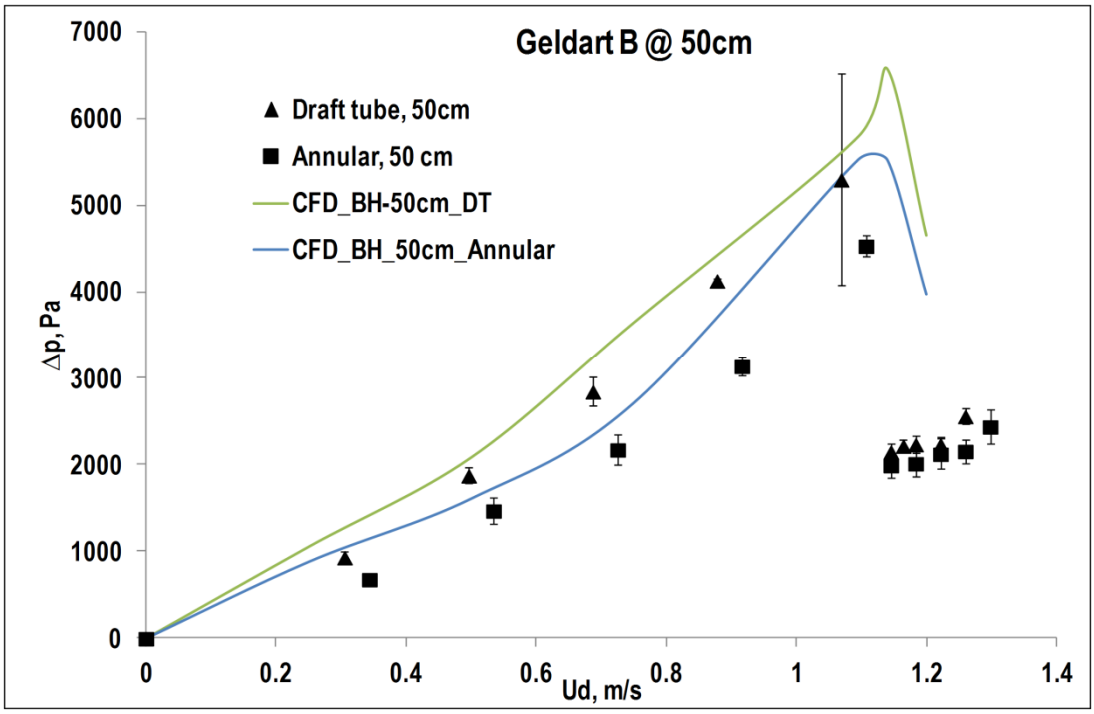

Figure 6.3: Pressure drop v_s draft tube velocity for the silica particle size 470 µm at bed height of 50 cm and gap height of 7.5 cm.

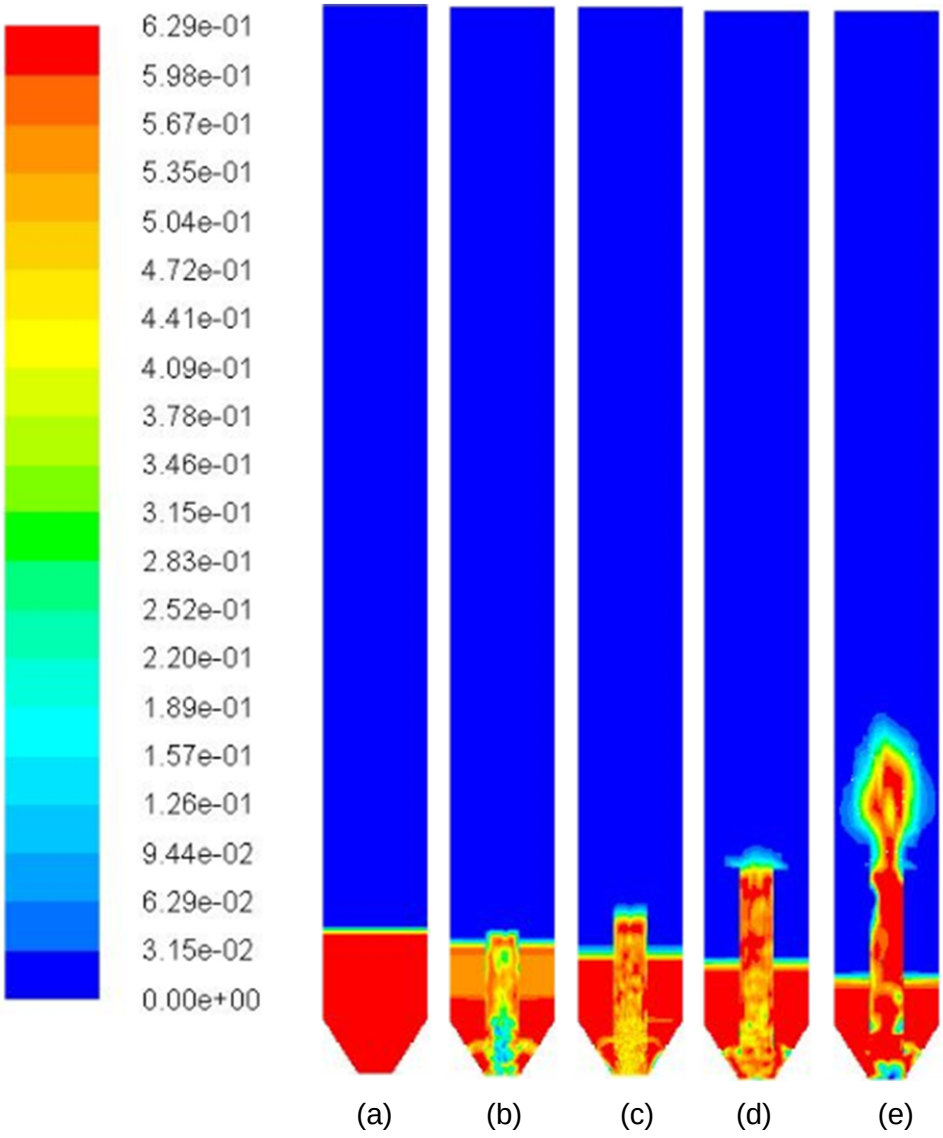

Figure. 6.4: Solids volume fraction for the silica particle size 470 µm at bed height of 40 cm and gap height of 7.5 cm at 0 s, 0.1 s, 0.15 s, 0.2s & 0.35 s.

6.4 Solid volume fraction Contours of 470 microns sized particles

Solid volume fraction contours at different time periods are shown in the Fig 6.4 for the silica silica particle size 470 µm at bed height of 40 cm and gap height of 7.5 cm. As the simulation time increases from time t = 0 s, slowly the bed moving from initial static bed condition to fluidization condition shown in the Fig 6.4 (a) to (e). In the draft tube solid particles are moving upward direction as the superficial velocity increases. After the

minimum fluidization condition the fluidized bed, solids blown out from draft tube and fountain is created. Depending on the particle size and density, at certain height above the draft tube the fountain will be risen. These particles will experience the neutrally buoyancy condition and will fall in to the annular region. In the Fig 6.4, one can observe qualitatively, a clearly fluidization condition occurs in the draft tube and moving packed bed condition happen in the annular section, which is very much similar to the experimental runs in the ICFB as discussed earlier in the experimental section.

6.5 Solids circulation rate

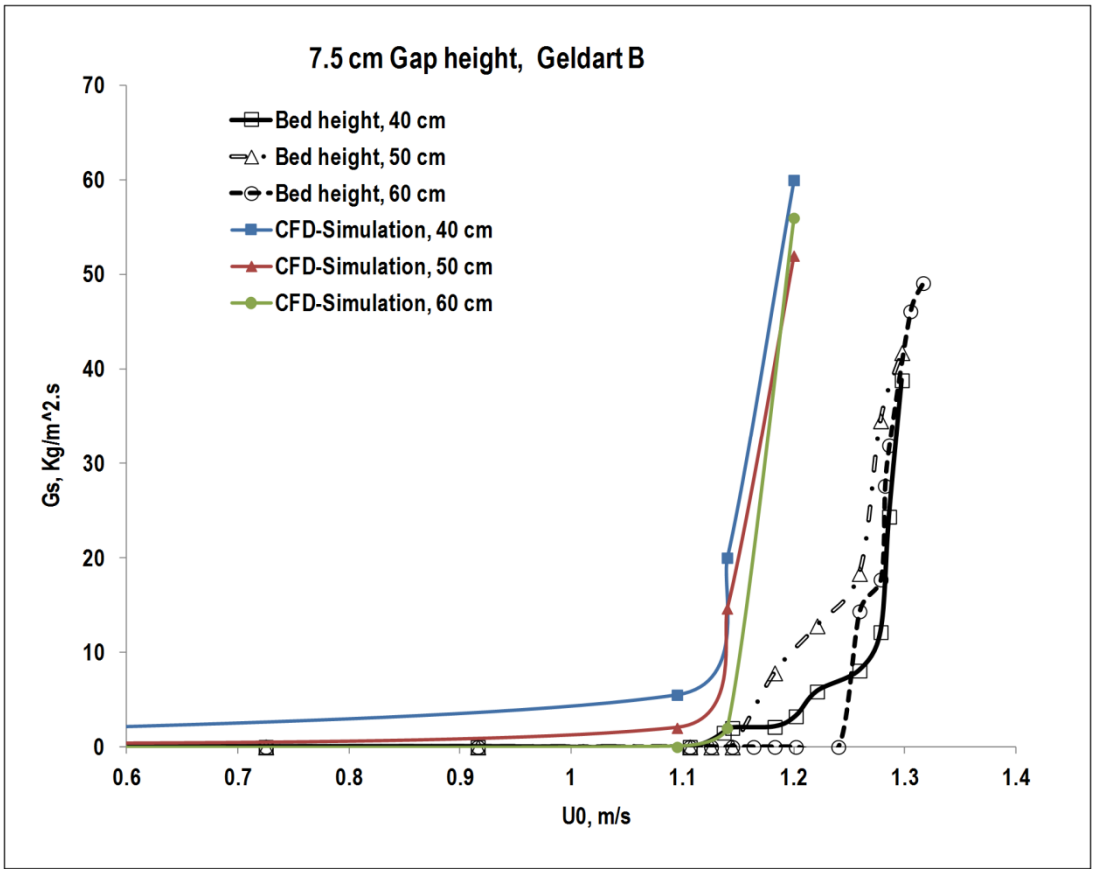

Figure. 6.5: Solids recirculation rate for the silica particle Geldart B at bed height of 40 cm 50 cm 60cm and a gap height of 7.5 cm.

Fig 6.5 shows that the comparison of experimental data and CFD computed data of solids recirculation rate (G_s). In both studies the solids circulation rate increases with superficial gas velocity. Initially at low superficial velocities there is no solids blown out from the draft tube but in the course of time bubbling fluidization occurs within the draft tube only. Once superficial velocity crosses to 1.0 m/s onwards initiation of solids circulation happens from

draft tube to annular section. As the bed height increases from 40 cm to 60 cm more superficial velocity is needed to lift the bed particles from draft tube to annular section, which is shown in the Fig 6.5. Predicted solids recirculation is showing similar trend with ICFB experimental data. The discrepancy between the CFD predictions and experimental data is large. As specified the basic reason for pressure drop deviation holds here too.

6.6 Solids volume fraction profiles in 3D ICFB

Solids volume fraction predicted for the silica particle of Geldart B group in the center of the draft tube along with height of ICFB at a gap height of 7.5 cm and bed height of 40 cm is shown in the Fig 6.6. Once input superficial velocity supplied to ICFB reactor, bed particles starts moving upward direction in the draft tube and at the same time, particles enter into the draft tube through a gap height of 7.5 cm which is provided at the bottom of draft tube distributor.

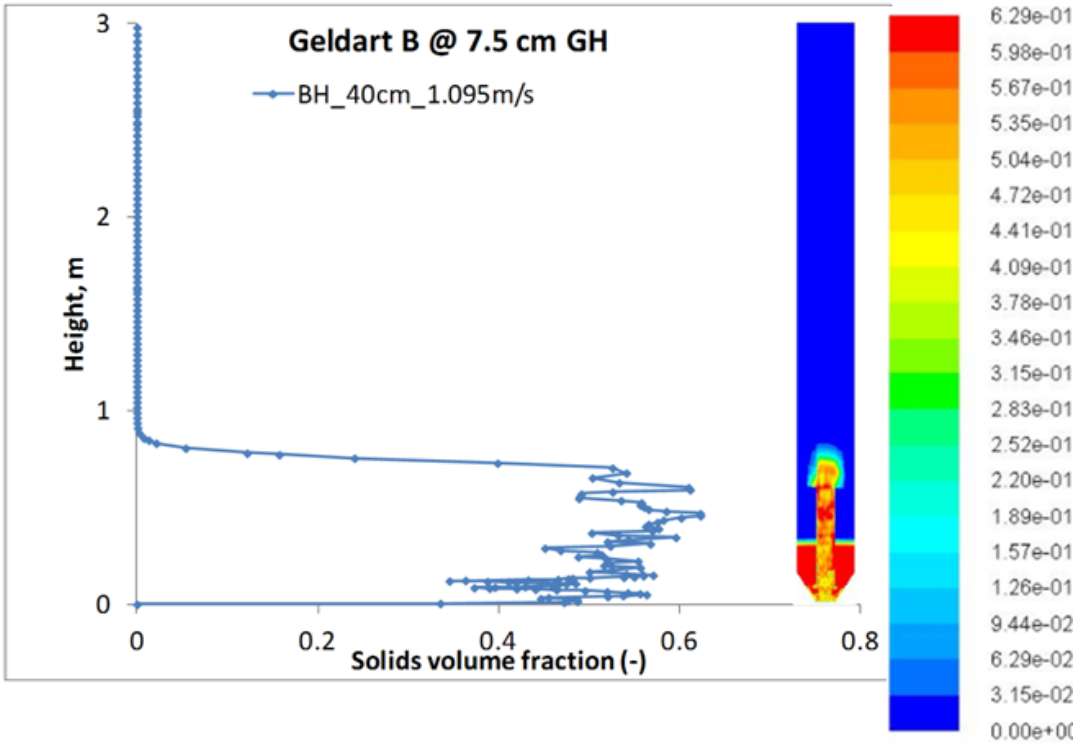

Figure. 6.6: Solids volume fraction for the silica particle of Geldart B group along with height of ICFB at a gap height of 7.5 cm and bed height of 40 cm.

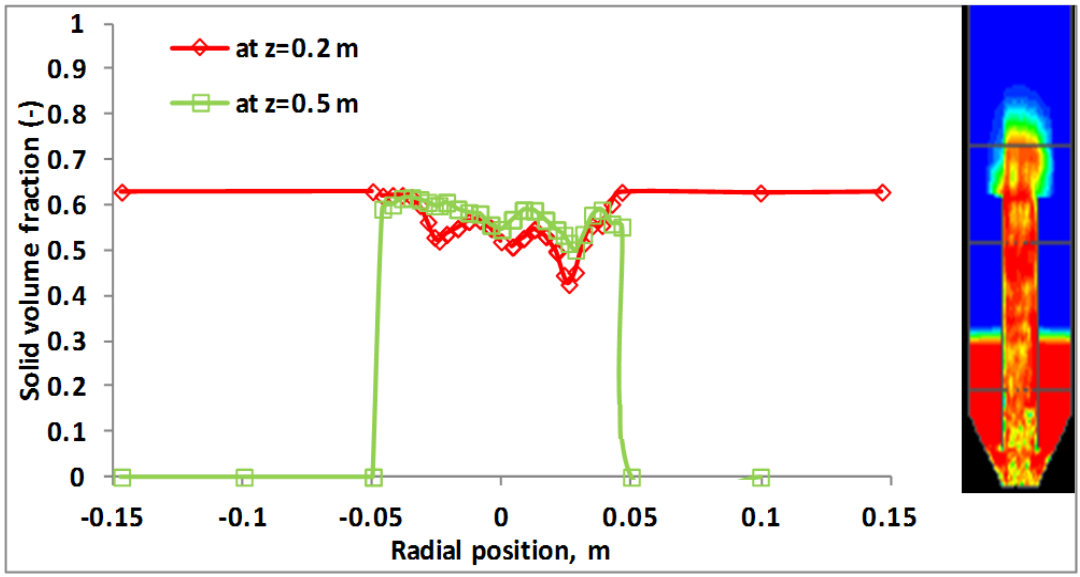

Figure 6.7 Solid volume fractions versus the radial direction at the height of 0.20 m and 0.5 m.

In the Fig 6.7 solid volume fractions plotted against radial position of ICFB reactor at different heights from the bottom of the reactor. At Z = 0.2 m, the solids concentration is much higher as compare with draft tube solids concentration. In the draft tube once minimum fluidization condition reached, bed start expanding and solids concentration become low which is shown in the contour of Fig 6.7. At a height of z =0.5 m, percentage of solids concentration in the annular section almost zero before spouting of bed particles as shown in the Fig. 6.7.

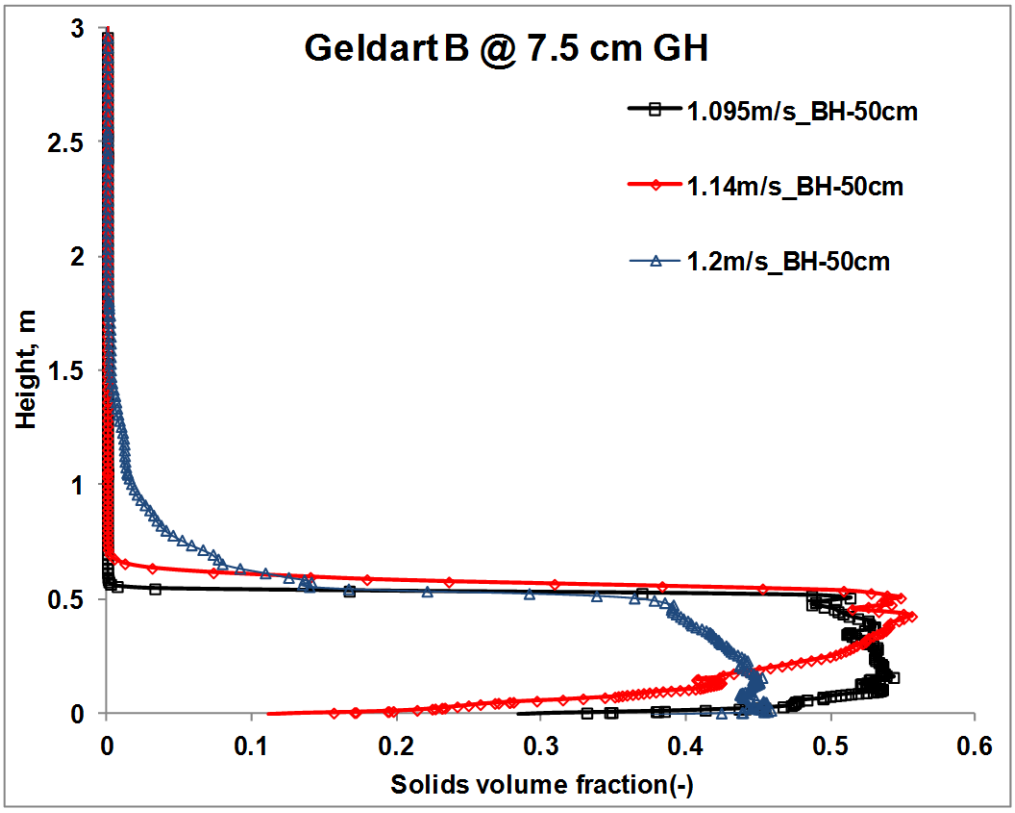

Figure. 6.8 Solids volume fraction for the silica particle of Geldart B group along with height of ICFB at a gap height of 7.5 cm and Bed height 50 cm.

Fig. 6.8. Shows the solids volume fraction along with the height of ICFB for the different superficial velocities. At low superficial velocity Uo = 1.095 m/s, silica bed expansion is minimum and solids volume fraction is maximum. As the superficial velocity increased to 1.2 m/s, bed expansion increases towards to the height of ICFB reactor and solids volume fraction levels decreases in the bottom of reactor and dilute bed extended along with the length of ICFB as shown in the Fig 6.8.

6.7 Conclusions

3D IITH's ICFB simulations were carried out using the two fluid model by incorporating the kinetic theory of granular flow (KTGF) using Ansys Fluent software. This model solves continuity and momentum equations phase wise along with additional closures such as transport equation for granular temperature (particulate turbulent kinetic energy)and granular pressure. Arastoopour drag model was utilized to take into account particle drag. The static bed was considered at three levels; 0.4 m, 0.5 m and 0.6 m deep and initial solids volume fraction was defined as 0.62 with a maximum packing limit of 0.65. Simulations were run with uniform superficial gas velocity of 0 to 1.2 m/s similar to the experimental conditions. The 3D CFD data validation against the IITH'S experiments is attempted. The

predicted values of pressure drop profiles both in the draft tube and annular section, and solids recirculation rate are basically in agreement with experimental results. At initial stage, the CFD predicted pressure drop profiles are close to IITH's ICFB experimental data up to minimum spouting velocity. After reaching minimum spout fluidized bed velocity, the CFD data deviated significantly from experimental data. In the experiments, the pressure fluctuations are significantly high especially at peak levels. In the experiments bed particles with various particle size distributions, where as in the case of CFD is mean size particles considered in all the simulations. Also in CFD the adopted only particle frictional forces are default Schaeffer (1987) [97]. Hence the CFD deviates hugely at peak fluidization condition. Predicted solids recirculation is showing similar trend with ICFB experimental data. The discrepancy between the CFD predictions and experimental data is large. As specified the basic reason for pressure drop deviation holds here too.

Chapter 7

Mathematical Model for Solids Recirculation Rate (G_S)

7.1 Introduction

This chapter presents the mathematical techniques of dimensional analysis whereby the parameters considered being likely to affect the flow can be combined into number of dimensional groupings and thereby testing model. The application of fluidized bed design, perhaps more than most engineering subjects relies on the use of empirical results built up from an extensive structure of experimental research. In many research areas empirical data are supplied in form of tables and graphs that the designer may use directly. However the tables and underlying experimental work become too cumbersome and time consuming if no way can be found establish the relationship between any two variables by generalized groupings. It is therefore the organization of the experimental work and the presentation of its results result that dimensional analysis plays such a key role. This dimensional technique, which is dealt with a survey of all the likely variables affecting any theoretical phenomenon and then suggests the formation of the groupings of more than one variable. In this chapter one dimensional mathematical model for solids circulation rate (G_S) is being developed based on dimensional analysis.

7.2 Dimensional Analysis

A dimensionless approach is used to establish the relationships between the variables, as this technique has the advantage of producing dimensionally consistent results for scale up. Furthermore, large quantum of experimentation is generally required to efficiently establish a relationship between the variable groups for a given range. Solid circulation rate in an ICFB is mainly depends on the physical and operating parameters. Therefore it can be useful if there is a relationship between these parameters. To establish the variables that had significant effects on the performance characteristics of ICFB many combinations of design and operating variables such as annulus diameter, draft tube diameter, height, superficial gas

velocity, bed height, solid particle diameter and density were tested and correlated in the present work.

A mathematical model is developed between solid circulation rate and various operating and design variables using dimensional analysis. The final coefficients are established on the basis of the experimental results in internally circulating fluidized beds. A wide range of data is used for the calculations of the coefficients so that the model can have a wide domain. The most commonly changed variables for internally circulating fluidized beds are superficial velocity u_o, annular velocity u_a, particle diameter d_P, bed height BH, density of solid ρ_s, density of fluid ρ_f, area of gap height A_{Gap}, area of annular section Aa, area of draft tube A_d, draft tube height H, viscosity μ. However, Yang and Keairns [9] showed that the effect of the distributor angle on solid circulation rate is negligible. A number of additional compound dimensionless groups like Reynolds number, Richardson number, and velocity, height and area ratios are defined in order to develop various fluidized bed model structures to predict the accurate values of solid recirculation rate. The definitions of these groups are discussed in the following section.

Reynolds Number

The conditions of flow in fluidized bed can be expressed in terms of Reynolds number R_e. The definition is generally chosen in terms of solid particle diameter, density, viscosity of the fluid and mean fluidization velocity, which is:

$$\mathrm{Re}_p = \frac{d_p u_{mf} \rho_f}{\mu}$$

The gas phase viscosity is used for the Re_p calculation. Whenever Re_p used for any model equations, the independent effect of viscosity was not included separately.

.

Richardson number

Richardson number is the dimensionless parameter which expresses the ratio of potential to kinetic energy. This number can be used as rough parameter of expected turbulence. Low values of Richardson number indicate presence of high turbulence.

$$R_i = \left(\frac{g\sqrt{A_d}}{u_{mf}^2} \right)$$

Buckingham's π theorem [108] states that if there is a physically meaningful equation for a system involving n number of physical variables, and k is the rank of the dimensional matrix, then the original expression is equivalent to an equation involving a set of p = n − k dimensionless parameters constructed from the original variables. This is a scheme for non-dimensionalisation. This provides a method for computing sets of dimensionless parameters from the given variables, even if the form of the equation is still unknown. However, the choice of dimensionless parameters is not unique: Buckingham's theorem only provides a way of generating sets of dimensionless parameters, and will not choose the most 'physically meaningful'.

The three primary dimensions (mass M, length L, and time T) of the operating and design parameters are used for the development of the dimensionless variables. The units and dimensions of various parameters are shown in Table 1.

Table 7.1: Parameters with units and dimensions

Parameter	Unit	Dimension
Solid circulation rate (Gs)	Kg/m^2s	$ML^{-2}T^{-1}$
Superficial gas velocity (u_0)	m/s	LT^{-1}
Velocity in annular section (u_a)	m/s	LT^{-1}
Mean fluidization velocity (umf)	m/s	LT^{-1}
Gap area for the gas to flow (AGap)	m^2	L^2
Bed height (BH)	m	L
Solid particle diameter (dp)	m	L
Solid particle density (ρs)	Kg/m^3	ML^{-3}
Fluid density (ρf)	Kg/m^3	ML^{-3}
Draft tube area (Aa)	m^2	L^2

Annulus area (Ad)	m^2	L^2
Draft tube height (H)	m	L
Fluid viscosity (μ)	Kg/ms	$ML^{-1}T^{-1}$
Acceleration due to gravity (g)	m/s^2	LT^{-2}

By using Buckingham π theorem [108]

Dimensionless variables are

$$\pi_1 = \frac{G_s}{(1-\varepsilon_{mf})u_{mf}\rho_s},\ \pi_2 = \frac{u_{mf}}{u_0},\ \pi_3 = \frac{u_a}{\sqrt{\frac{\Delta p}{(\rho_s - \rho_f)}}},\ \pi_4 = \frac{B_H}{\sqrt{A_d}},\ \pi_5 = \frac{d_p}{\sqrt{A_d}},$$

$$\pi_6 = \frac{\mu}{u_{mf}\rho_s d_p},\ \pi_7 = \frac{A_a}{A_d},\ \pi_8 = \frac{H}{\sqrt{A_d}},\ \pi_9 = \frac{g}{u_{mf}^2\sqrt{A_d}},\ \pi_{10} = \frac{A_{Gap}}{A_d}$$

The π terms can be represented as

$$f(\pi_1, \pi_2, \pi_3, \pi_4, \pi_5, \pi_6, \pi_7, \pi_8, \pi_9, \pi_{10}) = 0 \tag{7.2}$$

On the basis of dimensional analysis Equation can be rewritten as

$$\pi_1 = f_1(\pi_2, \pi_3, \pi_4, \pi_5, \pi_6, \pi_7, \pi_8, \pi_9, \pi_{10}) \tag{7.3}$$

The effect of the various operating and design parameters on the solid circulation rate of an ICFB can be shown in mathematical form as.

$$\frac{G_s}{\rho_s(1-\varepsilon_{mf})u_{mf}} = f_1\left(\frac{u_{mf}}{u_0}, \frac{u_a}{\sqrt{\frac{\Delta p}{(\rho_s - \rho_f)}}}, \frac{A_{gap}}{A_d}, \frac{d_p}{\sqrt{A_d}}, \frac{BH}{\sqrt{A_d}}, \frac{\mu}{\rho_f d_p u_{mf}}, \frac{A_a}{A_d}, \frac{H}{\sqrt{A_d}}, \frac{g\sqrt{A_d}}{u_{mf}^2}\right)$$

(7.4)

The main dependent Π_1 group is expressed in the undetermined function f1 comprising the other 9 π terms. For the generalized relationship, Equation is written as a nonlinear relationship and the p terms with coefficients i, j, k, m, o, s, p, q, w as shown in Equation:

$$\frac{G_s}{\rho_s\left(1-\varepsilon_{mf}\right)u_{mf}} \alpha \left(\frac{u_{mf}}{u_0}\right)^i \left(\frac{u_a}{\sqrt{\frac{\Delta p}{\left(\rho_s-\rho_f\right)}}}\right)^j \left(\frac{A_{gap}}{A_d}\right)^k \left(\frac{d_p}{\sqrt{A_d}}\right)^m \left(\frac{BH}{\sqrt{A_d}}\right)^o \left(\frac{\mu}{\rho_f d_p u_{mf}}\right)^s \left(\frac{A_a}{A_d}\right)^p \left(\frac{H}{\sqrt{A_d}}\right)^q \left(\frac{g\sqrt{A_d}}{u_{mf}^2}\right)^w \quad (7.5)$$

Equation can be rewritten as

$$\frac{G_s}{\rho_s\left(1-\varepsilon_{mf}\right)u_{mf}} = Con*\left(\frac{u_{pr}}{u_0}\right)^i \left(\frac{u_a}{\sqrt{\frac{\Delta p}{\left(\rho_s-\rho_f\right)}}}\right)^j \left(\frac{A_{gap}}{A_d}\right)^k \left(\frac{d_p}{\sqrt{A_d}}\right)^m \left(\frac{BH}{\sqrt{A_d}}\right)^o \left(\frac{1}{\mathrm{Re}_p}\right)^s \left(\frac{A_a}{A_d}\right)^p \left(\frac{H}{\sqrt{A_d}}\right)^q \left(\frac{g\sqrt{A_d}}{u_{mf}^2}\right)^w \quad (7.6)$$

7.2.1 Model equations

A generalized model for fluidized bed solid recirculation rate is proposed to evaluate the dependence of major design and operating variables on fluidized bed recirculation rate. Set of dimensionless variables included in the model are

Dimensionless variables are

Reduced particle diameter, $\left(\frac{d_p}{\sqrt{A_d}}\right)$ Reduced bed height, $\left(\frac{BH}{\sqrt{A_d}}\right)$

Reduced draft tube height, $\left(\frac{H}{\sqrt{A_d}}\right)$ Reduced gap area, $\left(\frac{A_{gap}}{A_d}\right)$

Reduced annular velocity, $\left(\frac{u_a}{\sqrt{\frac{\Delta p}{\left(\rho_s-\rho_f\right)}}}\right)$ Reduced annulus area, $\left(\frac{A_a}{A_d}\right)$ (7.7)

Reynolds number, $\left(\frac{d_p u_{mf} \rho_f}{\mu}\right)$ Richardson number, $\left(\frac{g\sqrt{A_d}}{u_{mf}^2}\right)$

Square root of draft tube area $\sqrt{Ad}$ is chosen as the characteristic dimension of length

The relationships between the dependent and independent variables are investigated using EXCEL SOLVER (Multiple linear fitting routine) by minimizing the sum of the squares error between measured values to the model predicted values. This is generally known as regression analysis. The fitting routine estimates the parameter values in the equation tested. Taking into account all the practical fluidized models developed by other researchers, together with the current state-of-art of all models and latest test results; the following constants are fitted and displayed in Table 7.2. The model equation (shown in Equation 7.6) is found to be the best according the fitting statistics. Solids circulation rate predicted by the fitted model for 470, 800 micron particles and corresponding experimental data is depicted in Figure 7.1. It can be observed that the model predictions are within the error limit of 30% of experimental data.

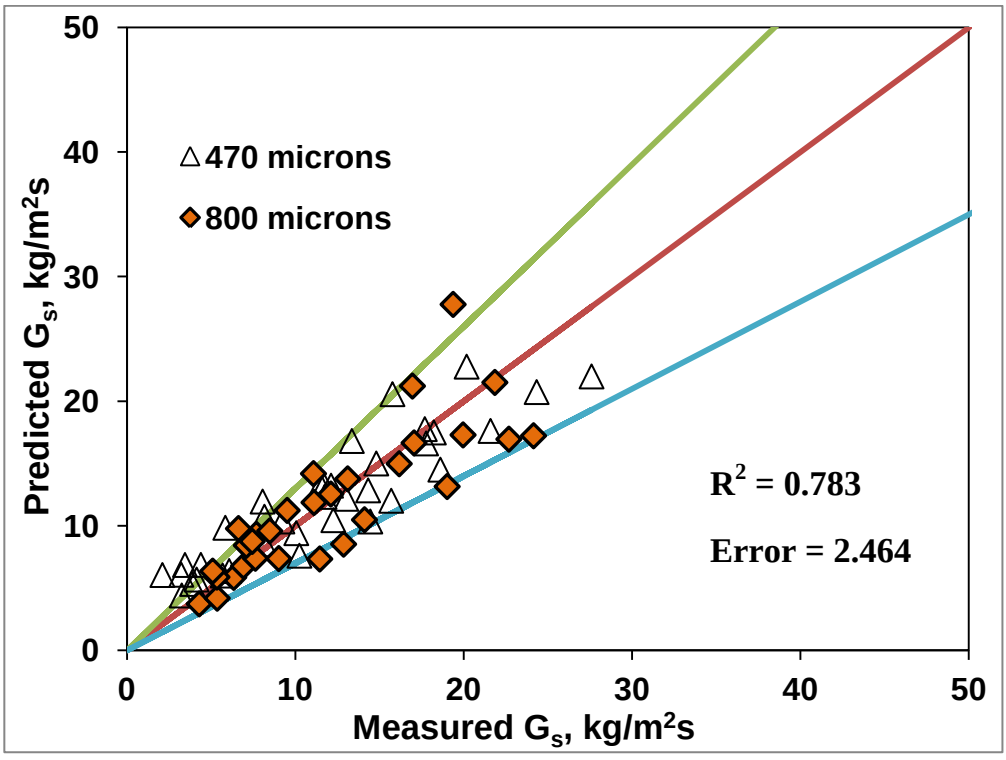

Figure 7.1: Predicted G_S by the model compared with experimental data

Table 7.2: Fitted constants from the experimental data

Parameter	i	j	k	m	o	s	p	q	w	Constant
Value	0.412	0.055	0.169	2.271	0.815	0.003	1.168	0.0734	1.255	5.54

$$\frac{G_s}{\rho_s\left(1-\varepsilon_{mf}\right)u_{mf}} = 5.54 * \left(\frac{u_{pr}}{u_0}\right)^{0.412} \left(\frac{u_a}{\sqrt{\frac{\Delta p}{\left(\rho_s-\rho_f\right)}}}\right)^{0.055} \left(\frac{A_{gap}}{A_d}\right)^{0.169} \left(\frac{d_p}{\sqrt{A_d}}\right)^{2.271} \left(\frac{BH}{\sqrt{A_d}}\right)^{0.815} \left(\frac{1}{\mathrm{Re}_p}\right)^{0.003} \left(\frac{A_a}{A_d}\right)^{1.168} \left(\frac{H}{\sqrt{A_d}}\right)^{0.0734} \left(\frac{g\sqrt{A_d}}{u_{mf}^2}\right)^{1.255} \quad (7.8)$$

To check the significance levels of the fitted constants, Analysis of Variance (ANOVA) technique is used to calculate F-number and their corresponding probabilities (P-values). If the significance levels (1-P) of at least one fitted constant is greater than 0.95 then one can say those constants are significant in the model. The significance levels of each parameter are clearly displayed in Table 7.3. The corresponding G_S model is assessed in terms of goodness of fit, fitting statistics, improvement over existing parameters. The final model after the significance test is shown in Equation 7.9. Solids circulation rate predicted by the modified model after the significant test for 470, 800 micron particles and corresponding experimental data is presented in Figure 7.2. It can be observed that the modified model predictions are also within the error limit of 30% of experimental data.

Model validation

The developed model (Equation 7.9) after the significance test is validated against the literature data of Chandel and Alappat [14] for 505 and 1543 micron particles. A total of ~110 data sets with variations in particle sizes, densities, fluidization velocities, bed heights, and gap heights is tested against developed mathematical model. The predicted G_s by using developed model is compared against measured experimental data and displayed in the Fig. 7.3. It can be observed that the model predictions are in good agreement with the experimental values within the error limits of ± 35%.

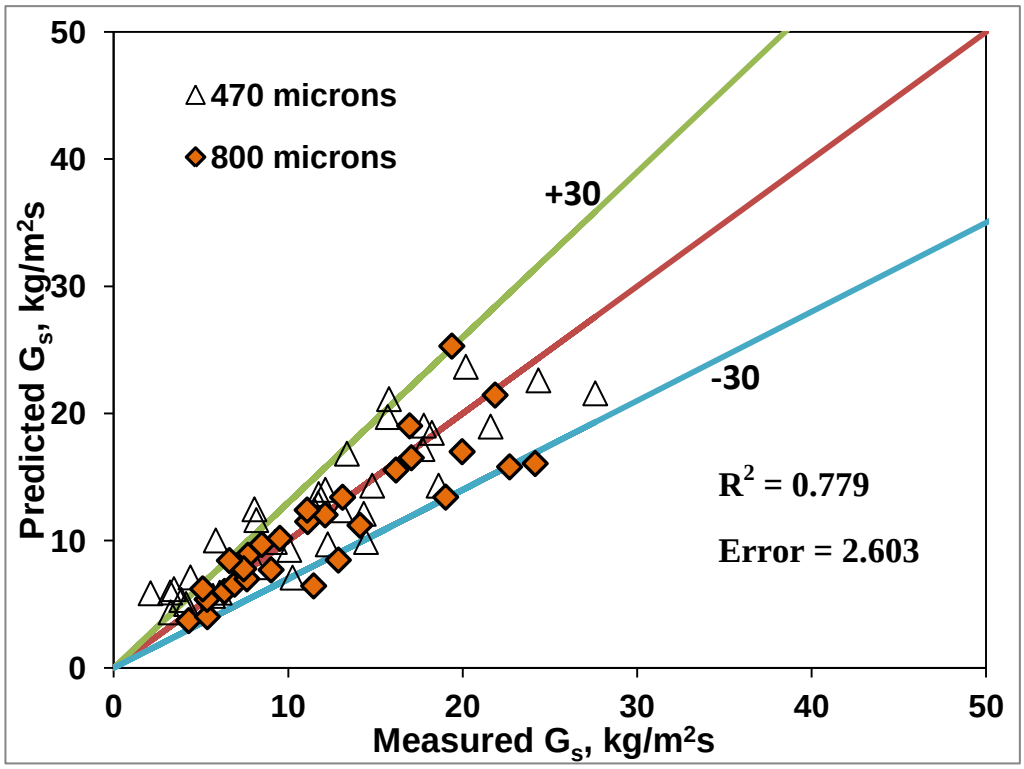

Figure 7.2: Predicted G_S by the model after the significance test compared with experimental data

Table 7.3: Fitted constants from the experimental data

Parameter	i	j	k	m	o	s	p	q	w	Constant
Value	0.412	0.055	0.169	2.271	0.815	0.003	1.168	0.0734	1.255	5.54
Significance level (1-P)	0.999	0.745	0.974	0.955	0.994	0.073	0.827	0.996	0.994	
Value after P-test	0.44	0	0.019	0.095	0.576	0	0	0.689	0.335	5.34

$$\frac{G_s}{\rho_s\left(1-\varepsilon_{mf}\right)u_{mf}} = 5.34*\left(\frac{u_{pr}}{u_0}\right)^{0.44}\left(\frac{A_{gap}}{A_d}\right)^{0.019}\left(\frac{d_p}{\sqrt{A_d}}\right)^{0.095}\left(\frac{BH}{\sqrt{A_d}}\right)^{0.576}\left(\frac{H}{\sqrt{A_d}}\right)^{0.689}\left(\frac{g\sqrt{A_d}}{u_{mf}^2}\right)^{0.335} \quad (7.9)$$

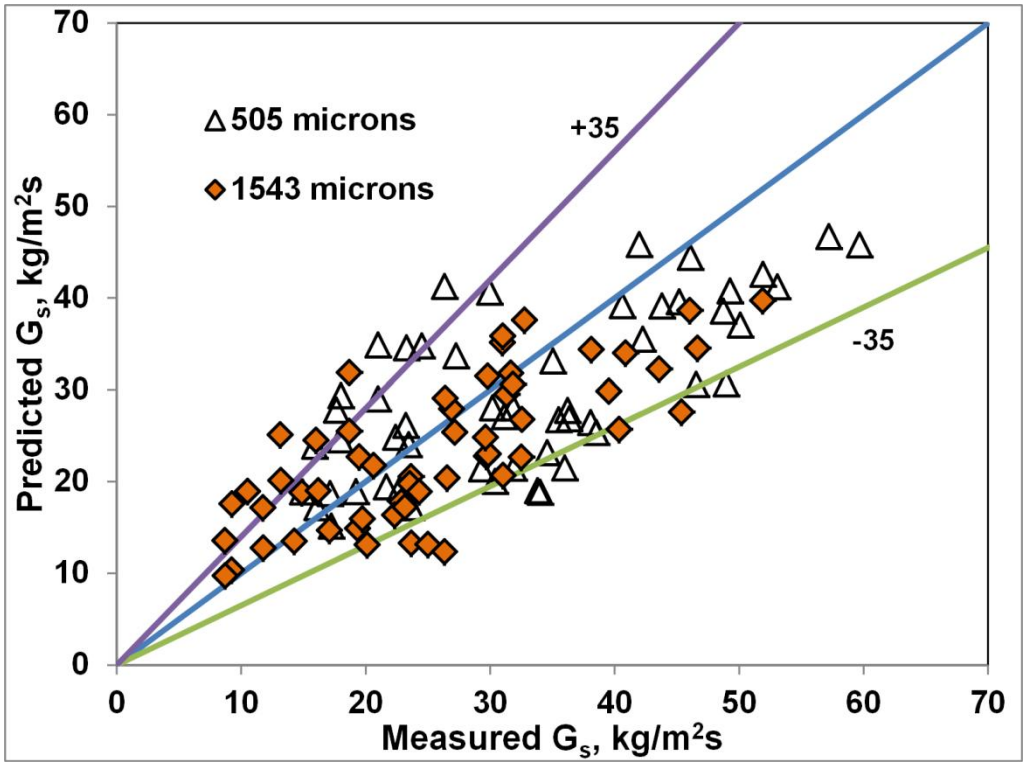

Figure 7.3: Validation of present mathematical model with the literature data of Chandel and Alappat [14] for solid circulation data (G_S)

7.3 Conclusions

A predictive mathematical model for solids recirculation rate of ICFB is established using the dimensionless approach. The coefficients of the dimensionless numbers were investigated using the regression analysis by the EXCEL SOLVER (multiple linear fitting routine). The fitting routine estimates the parameter values in the equations tested. The constants fitted for the recirculation rate (G_S) model is further assessed for the significance levels using ANOVA technique. After the P-test, insignificant variable are eliminated and final form of the equation also shown. Both the model predictions are well matched with the experimental data within ± 30% error limits. Developed mathematical model is further used to validate with the literature data on ICFB and observed good predictions with reasonable accuracy.

Chapter 8

Conclusions & future work

8.1 Conclusions

In this thesis, the main objective of research is the experimental and the CFD simulation study of an ICFB followed by development of mathematical model for solids circulation rate to understand ICFB hydrodynamics. The cold model internally circulating fluidized bed reactor was designed and fabricated with Acrylic transparent material to study hydrodynamic characteristics using silica bed materials of wide range size distributions. In the present study the effects of various operating and design parameters on the pressure drop and solids recirculation rate were studied for Geldart group B and Geldart group B-D particles.

ICFB Experimental work

Pressure drop, solid circulation rate, gas bypassing and minimum spouting fluidization velocities were considered as part of hydrodynamic study of gas solid flow in ICFB. Based on experimental results the following conclusions are made

- Pressure drop in the draft tube increases with an increase with static bed height and also increases with gap height between the draft tube bottom and air distributor.
- Solid circulation rate Gs slowly increases with the superficial velocity initially and then rapidly increases to larger values as the annular bed descents. Gs increases with static bed height due to increased bulk density and reduced void fraction that causes the higher bed pressure drop .

- Geldart B particles are having more pressure drop than the Geldart B-D particles due to the maximum possible packing and high frictional resistance of the fine particles for the gas flow. Gas bypassing fraction mainly depended on solids circulation rate, static bed height, superficial velocity, gap height and nature of bed material.
- Gas bypassing fraction increases with increased gap height and decreases with increased bed static height. Gas bypassing fraction increases with increased mean particle size.

CFD Simulations

The hydrodynamic characteristic of 2D & 3D ICFB reactors gas-solid flow was studied by an Eulerian-Eulerian CFD model with the stress closer from kinetic theory of granular flow. Four different drag models were considered for the simulations. Syamlal and O'Brien, Gidaspow, Arastoopour and Gibilaro drag models are implemented into Fluent through the User Defined Functions (UDF). 2D simulation of an internally circulating gas-solid fluidized bed with polypropylene particles was run based on Ahuja & Patwardhan (2008) experimental case. Grid independence check is made with four grid sizes. The resulting hydrodynamic properties from 2D simulations are compared to Ahuja & Patwardhan (2008) experimental data.

- The simulation results by four different drag models show that the Arastoopour and Gibilaro drag models can accurately predict the flow pattern, voidage profiles, and velocity profiles in the ICFB. With the Arastoopour drag model the simulations are giving the best fits to the experimental data.

- 3D simulations were also carried out for a large scale ICFB. The effect of superficial gas velocity and the presence of draft tube on solid hold-up distribution, solid circulation pattern, and gas bypassing dynamics for the 3D ICFB investigated extensively. The mechanism governing the solid circulation and the pressure losses in an ICFB has been explained based on gas and solid dynamics obtained from these simulations.

- Additional CFD validation is also made w.r.to IITH's 3D ICFB geometry for 0.4 m bed condition with the identified suitable drag and granular options. The predicted pressure drop profiles and solids circulation rate well agree with ICFB experimental data.

Mathematical model for solid recirculation rate

A mathematical model was developed for the solid recirculation rate in the ICFB by considering the effect of the various operating and design parameters. The model is based on the present experimental work. Dimensional analysis and nonlinear regression models are used to develop the model.

- A predictive mathematical model for solids recirculation rate of ICFB is established using the dimensionless approach. The final model equation was found to be the best according to these criteria. These model predictions well matched with experimental data within ± 30% error limits. Additional data sets from literature were used to validate the model by comparing the predictions of the model equations with the experimental results.

8.2. Future work

Based on the present study, the future research points are recommended as following.

- Mean size of particles used in the hydrodynamic simulation study. To generalize the result, the research on other particles (particle size and density) needed.
- To study in-depth of finer particle clustering concept required an accurate drag estimation using drags like EMMS, Filter grid drags is incorporating into CFD model.
- Experimental measurement of granular temperature gives an overview of particles collisional friction in the form of granular temperature. To measure granular temperature by using PIV and High speed camera
- In the solids circulation rate, the measurements are actually done near the wall of outside column but the movement of solid particles in the radial direction and void fraction might changes in the annular bed not considered in the measurement of solid circulation rate. May be needed to consider the measurement of void fraction dynamics by using sophisticated data acquisition system or intrusive techniques one has to use capture the dynamic bed change in the annular region.
- Accurate measurement of solids velocity in both in riser and falling in the annular section and measurement of concentration of solids using optical fiber probe (OFB) study is needed to further investigation in the ICFB hydrodynamics.

- Quantified validation of CFD models with respect to electrical conductance volume tomography (ECVT).

9. REFERENCES

[1] L.G. Gibilaro, Fluidization Dynamics. Butterworth-Heinemann, 2001 (2001).

[2] D. Kunii, O. Levenspiel, Fluidization Engineering, second edition ed., Butterworth-Heinemann, 1991.

[3] R.D. LaNauze, A Circulating fluidized bed. Powder technology 15 (1976) 117.

[4] E. Studsvik, Fast fluidized bed boiler and a method of controlling such a boiler, in, (1987) U.S. Patent.No. US4686939.

[5] J.M. Lee, Y.J. Kim, S.D. Kim, Catalytic coal gasification in an internally circulating fluidized bed reactor with draft tube. Appl. Therm. Eng. 18 (1998) 1013.

[6] L. Mukadi, C.A. Guy, R. Legros, Modeling of an internally circulating fluidized bed reactor for thermal treatment of industrial solid wastes. Can. J. Chem. Eng. 77 (1999) 420.

[7] Y.J. Kim, J.M. Lee, S.D. Kim, Modeling of Coal Gasification in an Internally Circulating Fluidized Bed Reactor with Draught Tube. Fuel 79 (2000) 69.

[8] Y.T. Kim, B.H. Song, S.D. Kim, Entrainment of solids in an internally circulating fluidized bed with draft tube. Chemical Engineering Journal 66 (1997) 105-110.

[9] W. Yang, D. Keairns, Studies on the solid circulation rate and gas bypassing in spouted fluid-bed with a draft tube. Journal of Chemical Engineering of Canadian 61 (1983) 349.

[10] O. Kinoshita, T. Kojima, T. Furusawa, Increased retension of fines in a circulating system of fluidized bed particles. J. Chem. Eng. Jpn 20 (1987) 641.

[11] R.K. Riley, M.R. Judd, The measurement of chat-steam gasification reaction for the designg of fluidized bed coal gasifier which contains a draft tube. Chem. Eng. Commun. 61 (1987) 151.

[12] T. Yang, T. Zhang, H.T. Bi, A novel continuous reactor for catalytic reduction of NOx – Fixed bed simulation. Canadian Journal of Chemical Engineering 86(3) (2008) 395-402.

[13] H.S. Ahn, W.J. Lee, Solid Circulation and Gas Bypassing in an Internally Circulating Fluidized Bed with an Orifice-Type Draft Tube. Chemical Engineering Journal of Korean 16 (1999) 618.

[14] M.K. Chandel, B.J. Alappat, Pressure drop and gas bypassing in recirculating fluidized beds. Chemical Engineering Science 61 (2006) 1489.

[15] G.N. Ahuja, A.W. Patwardhan, CFD and experimental studies of solids hold-up distribution and circulation patterns in gas–solid fluidized beds. Chemical Engineering Journal 143 (2008) 147–160.

[16] S.D. Kim, Y.H. Kim, S.H. Roh, D.H. Lee, Solid circulation characteristics in an internally circulating fluidized bed with orifice-type draft tube. chemical Engineering Journal of Korean 19 (2002) 911.

[17] J.R. Grace, High Velocity Fluidized Bed Reactors. Chem. Eng. Sci 45 (1990) 1953-1966.

[18] D. Geldart, Types of Gas Fluidization. Powder Technology 7 (1973) 285.

[19] K.B. Mathur, N. Epstein, Spouted beds, in, Academic Press, 1974.

[20] W.C. Yang, D.L. Keairns, Design of recirculating fluidized beds for commercial applications. AIChE Symposium Series 74 (1978) 218–228.

[21] N. Epstein, J.R. Grace, Spouting of particulate solids., in: Handbook of Powder Science and Technology, Chapman and Hall, New York. 1997, pp. 532.

[22] K.B. Mathur, N.A. Gishler, Technique for Contacting Gases with Coarse Solid Particles. . AlChE J. (1955) 157-164.

[23] R.H. Buchanan, B. Wilson, The fluid-lift solids recirculator. Mech Chem Eng Trans (Australia) (1965) 117–124.

[24] D. Hadzismajlovic, Z. Grbavcic, D.S. Povrenovic, D.V. Vukovic, R.V. Garic, H. Littman, The hydrodynamic behavior of a 0.95 m diameter spout-fluid bed with a draft tube, in: 7th engineering foundation conference on fluidization, Brisbane, Australia., 1992, pp. 337.

[25] B.J. Milne, F. Berruti, L.A. Behie, Solids circulation in an internally circulating fluidized bed (ICFB) reactor. , Engineering Foundation, New York, 1992.

[26] W. Lee, S. Kim, B. Song, Steam Gasification of an Australian Bituminous Coal in a Fluidized Bed. Chemical Engineering Journal of Korean 19 (2002) 1091.

[27] W.C. Yang, Engineering and applications of recirculating and jetting fluidized bed., Westwood, Noyes, 1999.

[28] M. Ishida, T. Shirai, Circulation of solid particles within the fluidized bed with a draft tube. . chemical Engineering Journal of Japan 8 (1975) 477–481.

[29] J.K. Claflin, A.G. Fane, Spouting with a porous draft-tube. Journal of Chemical Engineering of Canadian 61 (1983) 356-363.

[30] Oguchi Y, K.J. Junichi, Liquid-solid particle or liquid-gas-solid particle contacting method, in, Japan, 1973.1973.

[31] B.J. Alappat, V.C. Rane, Solid circulation rate in recirculating fluidized bed. Journal of energy Engineering 127 (2001) 51-68.

[32] W. Zhong, Y. Zhang, B. Jin, Y.Z. W. Zhong, B. Jin. Energy Fuels 2010 24, 5131., Novel method to study the particle circulation in a flat-bottom spout-fluid bed. Energy Fuels 24 (2010) 5131.

[33] W.J. Lee, Y.J. Cho, J.R. Kim, S.D. Kim, Coal Combustion Characteristics in a Fluidized-bed Combustor with a Draft Tube. Korean J. Chem. Eng. 9 (1992) 206.

[34] C.Y. Chu, S.J. Hwang, Attrition and sulfation of calcium sorbent and solids circulation rate in an internally circulating fluidized bed. Powder Technol. 127 (2002) 185–195.

[35] W. Namkung, S.W. Kim, S.D. Kim, Hydrodynamic Characteristics of a FCC Regenerator. . Korean J. Chem. Eng. 20(1) (2003) 110-115.

[36] R. Xiao, M. Zhang, B. Jin, X. Liu, Solids Circulation Flux and Gas Bypassing in a Pressurized Spout-fluid Bed with a Draft Tube. Can. J. Chem. Eng. 80 (2002) 800-808.

[37] J. Hee, S.D. Kim, S.J. Kim, Y. Kang, Solid circulation and gas bypassing characteristics in a square internally circulating fluidized bed with draft tube. Chemical Engineering process 47 (2008) 2351.

[38] H. Nagashima, T. Ishikura, M.A. Ide, M. Can, Flow Regimes And Vertical Solids Conveying In A Spout–Fluid Bed With A Draft Tube. Journal of Chemical Engineering 89 (2011) 264.

[39] G. Su, G. Huang, L. Ming, C. Liu, Study on the flow behavior in spout-fluid bed with a draft tube of sub-millimeter grade silicon particles. Chemical Engineering Journal (2014) 277.

[40] X.L. Zhao, S.Q. Li, G.Q. Liu, Q. Song, Q. Yao, Flow patterns of solids in a two-dimensional spouted bed with draft plates: PIV measurement and DEM simulations. Powder Technology 183 (2008) 79–87.

[41] C. Xingxing, X.T. Bi, Hydrodynamics of an i-CFB deNOx reactor. . Powder Technology 251 (2014) 25–36.

[42] N.G. Deen, M. Annaland, M.A. Hoef, J.A.M. Kuipers, Review of discrete particle modeling of fluidized beds. Chem. Eng. Sci. 62 (2007) 28-44.

[43] M. Goldschmidt, Hydrodynamic modelling of fluidised bed spray granulation, in, Twente University., The Netherlands 2001.

[44] A.S. Mujumdar, Z. Wu, Thermal drying technologies - Cost-effective innovation aided by mathematical modeling approach. Drying Technology 26 (2008) 146–154.

[45] J.A.M. Kuipers, K.J. van Duin, F.P.H. van Beckum, W.P.M. van Swaaij, A numerical model of gas-fluidized beds. Chemical Engineering Science 47 (1992) 1913.

[46] V. Mathiesen, T. Solberg, H. Arastoopour, H. Hjertager, Experimental and computational study of multiphase gas-particle in a CFB riser. AIChE Journal 45 (1999) 2503–2518.

[47] S. Benyahia, H. Arastoopour, T. Knowlton, H. Massah, Simulation of particles and gas flow behavior in the riser section of a circulating fluidized bed using the kinetic theory approach for the particulate phase. Powder Technology 112 (2000) 24–33.

[48] D.M. Gera, Y. Gautam, T. Tsuji, Kawaguchi, T. Tanaka, Computer simulation of bubbles in large-particle fluidized beds. Powder Technology 98 (1998) 38–47.

[49] G. Ahmadi, M. Shahinpoor, A kinetic model for rapid flow of granular materials. International Journal of Non-Linear Mechanics 19 (1983) 177–186.

[50] C.K.K. Lun, S.B. Savage, D.J. Jeffrey, N. Chepurniy, Kinetic theories for granular flow inelastic particles in Couette flow and slightly inelastic particles in a general flow field. Journal of Fluid Mechanics 140 (1984) 223–256.

[51] G. Ahmadi, D.N. Ma, A kinetic model for granular flows of nearly elastic particles ingrain-inertia regime. International Journal of Bulk Solid Storage Soils 2 (1986) 8-16.

[52] J. Ding, D. Gidaspow, A Bubbling Fluidization Model Using Kinetic Theory of Granular Flow. AIChE Journal 36 (1990).

[53] R. Beetstra, M.A. van der Hoef, J.A.M. Kuipers, Numerical study of segregation using a new drag force correlation for polydisperse systems derived from lattice-Boltzmann simulations. Chemical Engineering Science 62 (2007) 246–255.

[54] E. Helland, H. Bournot, R. Occelli, L. Tadrist, Drag reduction and cluster formation in a circulating fluidised bed. Chemical Engineering Science 62 (2007) 148–158.

[55] T. McKeen, T. Pugsley, Simulation and experimental validation of a freely bubbling bed of FCC catalyst. Powder Technology 129 (2003) 139–152.

[56] N. Yang, W. Wang, W. Ge, J. Li, CFD simulation of concurrent-up gas–solid flow in circulating fluidized beds with structure-dependent drag coefficient. Chemical Engineering Journal 96 (2003) 71–80.

[57] S. Zimmermann, F. Taghipour, CFD modeling of the hydrodynamics and reaction kinetics of FCC fluidized-bed reactors. Industrial & Engineering Chemistry Research 44 (2005) 9818–9827.

[58] C.Y. Wen, Y.H. Yu, Mechanics of fluidization. Chemical Engineering Progress Symposium Series 62 (1966) 100–111.

[59] M. Syamlal, T.J. O'Brien, Computer simulation of bubbles in a fluidized bed. AIChE Symposium Series 85 (1989) 22–31.

[60] D. Gidaspow, Multiphase flow and fluidizationdization : Continuum and kinetic theory description, in, New York : Academic Press, 1994.

[61] C.K. Chan, Y.C. Guo, K.S. Lau, Numerical modeling of gas-particle flow using a comprehensive kinetic theory with turbulence modulation. Powder Technology 150 (2005) 42–55.

[62] A. Neri, D. Gidaspow, Riser hydrodynamics: Simulation using kinetic theory. AIChE Journal 46 (2000) 52–67.

[63] Y. Zheng, X. Wan, Z. Qian, F. Wei, Y. Jin, Numerical simulation of the gas-particle turbulent flow in riser reactor based on k–ε–kp–_p–two-fluid model. Chemical Engineering Science 56 (2001) 6813–6822.

[64] B.G.M. van Wachem, J.C. Schouten, C.M. van den Bleek, R. Krishna, J.L. Sinclair, Comparative Analysis of CFD Models of Dense Gas–Solid Systems. AIChE Journal 47 (2001) 1035-1051.

[65] S.H. Hosseini, M. Zivdar, R. Rahimi, A. Samimi, CFD simulation of gas–solid bubbling fluidized bed containing the FCC particles. Korean J. Chem. Eng. 26 (2009) 1405–1413.

[66] L.G. Gibilaro, R. Di Felice, S.P. Waldram, Generalized friction factor and drag coefficient correlations for fluid–particle interactions. chemical Engineering Science 40 (1985) 1817–1823.

[67] D.J. Patil, M. van Sint Annaland, J.A.M. Kuipers, Critical comparison of hydrodynamics models for gas–solid fluidized beds—Part I: bubbling gas–solid fluidized beds operated with a jet. chemical Engineering Science 60 (2005) 57–72.

[68] L. Huilin, H. Yurong, L. Wentie, D. Jianmin, D. Gidaspow, J. Bouillard, Computer simulations of gas–solid flow in spouted beds using kinetic-frictional stress model of granular flow. chemical Engineering Science 59 (2004) 865–878.

[69] W. Shuyan, L. Xiang, L. Huilin, Y. Long, S. Dan, H. Yurong, D. Yonglong, Numerical simulations of flow behavior of gas and particles in spouted beds using frictional kinetic stresses model. Powder Technology 196 (2009) 184–193.

[70] A. Passalacqua, L. Marmo, A critical comparison of frictional stress models applied to the simulation of bubbling fluidized beds. Chemical Engineering Science 64(12) (2009) 2795–2806.

[71] S. Abu-Zaid, G. Ahmadi, A simple kinetic model for rapid granular flows including frictional losses. ASCE Journal of Engineering Mechanics 116 (1990) 379–389.

[72] D.J. Patil, M. van Sint Annaland, Critical comparison of hydrodynamic models for gas–solid fluidized beds—Part II: freely bubbling gas–solid fluidized beds. Chemical Engineering Science 60 (2005) 73-84.

[73] N. Reuge, L. Cadoret, C. Coufort-Saudejaud, S. Pannala, M. Syamlal, B. Caussat, Multi-fluid Eulerian modeling of dense gas–solid fluidized bed hydrodynamics; influence of the dissipation parameters. Chemical Engineering Science 22 (2008) 5540–5551.

[74] A. Srivastava, S. Sundaresan, Analysis of a frictional-kinetic model for gas–particle flow. Powder Technology 129 (2003) 72–85.

[75] M. Syamlal, W. Rogers, T.J. O'Brien, MFIX documentation: theory guide, in: Technical Report DOE/METC-94/1004 (DE9400087), Morgantown Energy Technology Centre, Morgantown, West Virginia, 1993.

[76] P.C. Johnson, R. Jackson, Frictional–collisional constitutive relations for granular materials with application to plane shearing. Journal of Fluid Mechanics 176 (1987) 67-93.

[77] K.J. Marschall, L. Mleczko, CFD modeling of an internally circulating fluidized-bed reactor. chemical Engineering Science 54 (1999) 2085-2093.

[78] R.G. Szafran, A. Kmiec, Periodic fluctuations of flow and porosity in spouted beds. Transport in Porous Media 66 (2007) 187–200.

[79] P.A. Shirvanian, J.M. Calo, Hydrodynamic scaling of a rectangular spouted vessel with a draft duct. Chemical Engineering Journal 103 (2004) 29–34.

[80] S. Hosseini, G. Ahmadi, c. Rahimi, c. Mortaza, Mohsen, CFD studies of solids hold-up distribution and circulation patterns in gas–solid fluidized beds. Powder Technology 200 (2010) 202-215.

[81] H. Arastoopour, P. Pakdel, M. Adewumi, Hydrodynamic analysis of dilute gas–solids flow in a vertical pipe. Powder Technology 62 (1990) 163–170.

[82] C. Yan, C. Lu, Y. Liu, R. Cao, Shi. M, Experiments and simulations of gas–solid flow in an airlift loop reactor. Particuology 9 (2011) 130–138.

[83] Y. Feng, T. Smith, P.J. Witt., C. Doblin, S. Lim, M. Phil Schwarz, CFD modeling of gas–solid flow in an internally circulating fluidized bed. Powder Technology 219 (2012) 78–85.

[84] T. Ishikura, H. Nagashima, Hydrodynamics of a Spouted Bed with a Porous Draft Tube Containing a Small Amount of Finer Particles. Powder Technology 131 (2003) 56-65.

[85] S. Moradi, A. Yeganeh, M. Salimi, CFD-modeling of effects of draft tubes on operating condition in spouted beds. Applied Mathematical Modelling 37 (2013) 1851-1859.

[86] J.H. Jeon, S.D. Kim, Hydrodynamic Characteristics of Binary Solids Mixtures in a Square Internally Circulating Fluidized Bed. Journal of Chemical Engineering of Japan 43 (2010) 126-131.

[87] B. Song, Y.T. Kim, S.D. Kim, Entrainment of solids in an internally circulating fluidized bed with draft tube. . Chem. Eng. J. 68 (1997) 115.

[88] T.D. Hadley, T.D. Doblin, J. Orellana, K. Lim, Experimental quantification of the solids flux in an internally circulating fluidized bed, in: , in: The 13th International Conference on Fluidization: New Paradigm in Fluidization Engineering, 2010.

[89] C. Yan, C. Lu, Y. Liu, R. Cao, M. Shi, Hydrodynamics in airlift loop section of petroleum coke combustor. Powder Technol. 192 (2009) 143–151.

[90] A. Benkrid, H.S. Caram, Solid flow in the annular region of a spouted bed. . A.I.Ch.E. Journal 35 (1989) 1328–1336.

[91] Y.L. He, S.-Z. Qin, C.J. Lim, J.R. Grace, particle velocity profiles and solid flow patterns in spouted beds. Journal of chemical Engineering of Canadian 72 (1994) 561.

[92] S.V. Patankar, Numerical Heat Transfer and Fluid Flow, Hemisphere Publishing Corporation, 1980.

[93] S. Ergun, Fluid flow through packed columns. Chemical Engineering Progress 48 (1952) 89–94.

[94] J.L. Sinclair, R. Jackson, Gas-particle flow in a vertical pipe with particle-particle interactions. AIChE Journal 35 (1989) 1473–1486.

[95] C. Pain, S. Mansoorzadeh, C.R.E.D. Oliveira, A.J.H. Goddard, Numerical Modeling of Gas-Solid Fluidized Beds Using the Two-Fluid Approach. . Int. J. Numer. Methods Fluids 36 (2001) 91-124.

[96] E.N. Taghipour, F. Wong C, Experimental and Computational Study of Gas-Solid Fluidized Bed hydrodynamics. Chem. Eng. Sci. 60 (2005) 6857-6867.

[97] D.G. Schaeffer, Instability in the Evolution Equations Describing Incompressible Granular Flow. Journal of Differential Equations 66 (1987) 19–50.

[98] C. Benjapon, D. Gidaspow, P. Piumsomboona, Two- and three-dimensional CFD modeling of Geldart A particles in a thin bubbling fluidized bed: Comparison of turbulence and dispersion coefficient. Chemical Engineering Journal 171 (2011) 301–313.

[99] Y.Q. Feng, Witt, P. Doblin, C. Lim, P. Schwarz, CFD modeling of gas-solids flow in an internally circulation fluidized bed, in: The 10th China-Japan Symposium on Fluidization, Tokyo, Japan., 2010.

[100] J. Xu, J. Tang, W. Wei, X. Bao, Minimum spouting velocity in a spout-fluid bed with a draft tube. Journal of Chemical Engineering of Canadian 87 (2009) 274-278.

[101] D. Gidaspow, J. Jonghwun, R.K. Singh, Hydrodynamics of fluidization using kinetic theory: an emerging paradigm-2002 Flour–Daniel lecture. Powder Technology 148 (2004) 123–141.

[102] J. Jung, D. Gidaspow, I.K. Gamwo, Measurement of Two Kinds of Granular Temperatures, Stresses and Dispersion in Bubbling Beds. Industrial & Engineering Chemistry Research 44 (2005) 1329-1341.

[103] B. Chalermsinsuwana, D. Gidaspow, b. Pornpote Piumsomboona, Two- and three-dimensional CFD modeling of Geldart A particles in a thin bubbling fluidized bed : Comparison of turbulence and dispersion coefficient. Chemical Engineering Journal 171 (2011) 301–313.

[104] D. Gidaspow, R. Mostofi, Maximum carrying capacity and granular temperature of A, B, and C particles. AIChE Journal 49 (2003) 831–843.

[105] W. Polashenski, J. Chen, Measurement of particle stresses in fast fluidized beds. Industrial & Engineering Chemistry Research 38 (1999) 705–713.

[106] H.H. Shih, C.Y. Chu, S.J. Hwang, Solids circulation and attrition rates and gas bypassing in an internally circulating fluidized bed. . Industrial & Engineering Chemistry Research 42 (2003) 2085–2093.

[107] M.J. Rhodes, D.A. Geldart, A model for the circulating fluidized bed. . Powder Technol. 53 (1987) 115.

[108] E. Buckingham, On physically similar systems; illustrations of the use of dimensional equations. Physical Review 4 (1914) 345.

Appendix-I

Experimental conditions: Geldart B, Bed height= 60 cm, Gap height=7.5 cm

Experimental conditions: Geldart B, Bed height= 60 cm, Gap height=7.5 cm

First experiment																		
Input velocity U_o, m/s	Draft tube pressure drop_P1	Draft tube pressure dropT_P2	Draft tube pressure drop-DT_P3	Avg Draft tube pressure drop_DT	Standard deviation	Annular pressure dropANN_p1	Annular pressure drop-ANN_p1	Annular pressure drop-ANN_p1	Avg-Annular pressure dropAnnu_Avg_p	Standard deviation (SD's)	Draft tube pressure drop-Dt Avg	Standard deviation (SD's)	Time-T1	Time-T2	Time-T3	Time-Tavg	Velocity Vavg	Solid circulation rate SRR
0	0	0	0	0	0	0	0	0	0	0	0	0	0	0	0	0	0	0
0.3434066	784	784	725.2	764.4	33.948196	588	588	588	588	0	847.15556	65.577876	0	0	0	0	0	0
0.534188	1960	2058	2018.8	2012.2667	49.325585	1470	1568	1568	1535.3333	56.580326	1968.7111	63.595213	0	0	0	0	0	0
0.7249695	2940	2940	3038	2972.6667	56.580326	2195.2	2234.4	2312.8	2247.4667	59.878989	2977.0222	42.088056	0	0	0	0	0	0
0.9157509	4214	4312	4214	4246.6667	56.580326	3136	3175.2	3234	3181.7333	49.325585	4303.2889	84.366054	0	0	0	0	0	0
1.1065324	6174	6272	6252.4	6232.8	51.856726	4508	4606	4664.8	4592.9333	79.212457	6328.6222	183.45758	0	0	0	0	0	0
1.1828449	6370	6468	6526.8	6454.9333	79.212457	4782.4	4900	4860.8	4847.7333	59.878989	5592.5333	1233.516	10.5	13.16	9.47	11.043333	0.0045276	6.5650468

1.2019231	2646	2744	2842	2744	98	2156	2254	2352	2254	98	3332	457.04157	8	7	6.87	7.29	0.0068587	9.9451303
1.2210012	2685.2	2744	2881.2	2770.1333	100.57939	2116.8	1960	2195.2	2090.6667	119.75798	3297.1556	420.91859	4.85	4.91	7.1	5.62	0.0088968	12.900356
1.2400794	2646	2606.8	2802.8	2685.2	103.71345	2116.8	2450	2254	2273.6	167.46247	3301.5111	478.20698	4.2	5.6	4.56	4.7866667	0.0104457	15.14624
1.2782357	2450	2489.2	2352	2430.4	70.668805	1960	2058	2156	2058	98	3059.7778	484.22755	4.38	3.8	4	4.06	0.0123153	17.857143
1.2973138	2489.2	2685.2	2548	2574.1333	100.57939	2254	2352	2195.2	2267.0667	79.212457	3166.4889	464.65965	3.18	3.6	3.25	3.3433333	0.0149551	21.684945
1.3163919	2842	2744	2940	2842	98	2352	2548	2450	2450	98	3234	306.0049	3.1	2.9	3.18	3.06	0.0163399	23.69281

Second experiment																		
Uo	DT_P1	DT_P2	DT_P3	Avg_DT	stdv	ANN_p1	ANN_p1	ANN_p1	Annu_Avg_p	stdv	Annular_P	Std v	T1	T2	T3	Tavg	Vavg	SRR
0	0	0	0	0	0	0	0	0	0	0	0	0	0	0	0	0	0	0
0.3434066	882	882	882	882	0	588	588	588	588	0	601.06667	19.6	0	0	0	0	0	0
0.534188	2058	1960	1960	1992.6667	56.580326	1450.4	1411.2	1372	1411.2	39.2	1439.5111	81.470431	0	0	0	0	0	0
0.7249695	3038	2998.8	2998.8	3011.8667	22.632131	2116.8	2156	2116.8	2129.8667	22.632131	2177.7778	62.324028	0	0	0	0	0	0
0.9157509	4214	4449.2	4410	4357.7333	126.01037	3214.4	3175.2	3175.2	3188.2667	22.632131	3144.7111	67.97493	0	0	0	0	0	0
1.1065324	6134.8	6174	6252.4	6187.0667	59.878989	4508	4625.6	4704	4612.5333	98.65117	4706.1778	168.16196	0	0	0	0	0	0
1.1828449	6330.8	6370	6409.2	6370	39.2	4547.2	4664.8	4704	4638.6667	81.601307	4109.4667	961.24962	11.44	12.6	13	12.346667	0.0040497	5.8720302
1.2019231	3626	3822	3724	3724	98	2940	3136	3332	3136	196	2842	464.85482	10.22	9.9	11.12	10.413333	0.0048015	6.9622279
1.2210012	3626	3528	3822	3658.6667	149.69747	2744	2940	3038	2907.3333	149.69747	2613.3333	438.70737	6.12	6.4	7.5	6.673333	0.0074925	10.864136
1.2400794	3724	3665.2	3782.8	3724	58.8	2646	2744	2744	2711.3333	56.580326	2706.9778	237.72716	6	5.9	5.84	5.913333	0.0084555	12.260428

1.2591575	3136	3430	3528	3364.6667	204.00327	2450	2646	2842	2646	196	2548	328.70199	5.1	5.78	5.88	5.5866667	0.0089499	12.977327
1.2782357	3234	3332	3234	3266.6667	56.580326	2548	2646	2744	2646	98	2541.4667	205.59249	4.9	4.71	5	4.87	0.0102669	14.887064
1.2973138	3332	3430	3234	3332	98	2744	2940	3136	2940	196	2678.6667	339.48196	3.8	3.95	4.17	3.9733333	0.0125839	18.246644
1.3163919	3430	3528	3332	3430	98	2940	2940	2940	2940	0	1862	80.016665	3	2.2	1.89	2.3633333	0.0211566	30.67701

Uo	DT_P1	DT_P2	DT_P3	Avg_DT	stdv	ANN_p1	ANN_p1	ANN_p1	Annu_Avg_p	stdv	T1	T2	T3	Tavg	Vavg	SRR
0	0	0	0	0	0	0	0	0	0	0	0	0	0	0	0	0
0.3434066	882	882	921.2	895.06667	22.632131	627.2	627.2	627.2	627.2	0	0	0	0	0	0	0
0.534188	1901.2	1901.2	1901.2	1901.2	0	1372	1372	1372	1372	0	0	0	0	0	0	0
0.7249695	2940	2940	2959.6	2946.5333	11.316065	2156	2156	2156	2156	0	0	0	0	0	0	0
0.9157509	4292.4	4312	4312	4305.4667	11.316065	3038	3057.6	3096.8	3064.1333	29.939495	0	0	0	0	0	0
1.1065324	6566	6566	6566	6566	0	4939.2	4900	4900	4913.0667	22.632131	0	0	0	0	0	0
1.1828449	3920	4116	3822	3952.6667	149.69747	2646	2842	3038	2842	196	12.33	13.4	12.51	0.0039968	5.7953637	11.8
1.2019231	3626	3528	3430	3528	98	2940	3136	3332	3136	196	6.8	7	6.71	0.0074516	10.804769	6.33
1.2210012	3626	3332	3430	3462.6667	149.69747	2744	3136	2940	2940	196	6.25	6.88	6.376666667	0.0078411	11.369577	6
1.2400794	3586.8	3430	3469.2	3495.3333	81.601307	2646	2744	2744	2711.3333	56.580326	5.18	5.98	5.713333	0.0087515	12.689615	5.98

													33			
1.2591575	3528	3528	3528	3528	0	2450	2646	2842	2646	196	5.72	6	5.706667	0.0087617	12.704439	5.4
1.2782357	3469.2	3547.6	3430	3482.2667	59.878989	2548	2646	2744	2646	98	4.12	5.89	4.97	0.0100604	14.587525	4.9
1.2973138	3528	3626	3626	3593.3333	56.580326	2940	3136	3332	3136	196	3.16	3.89	3.516667	0.014218	20.616114	3.5
1.3163919	3430	3528	3332	3430	98	2940	2940	3136	3005.3333	113.16065	1.67	2.6	2.156667	0.0231839	33.616692	2.2

Decreasing velocity experiment-First experiment										
Uo	**DT_P1**	**DT_P2**	**DT_P3**	**Avg_DT**	**stdv**	**ANN_p1**	**ANN_p1**	**ANN_p1**	**Annu_Avg_p**	**stdv**
0	0	0	0	0	0	0	0	0	0	0
0.3434066	784	784	784	784	0	686	686	686	686	0
0.534188	1568	1568	1568	1568	0	1274	1274	1274	1274	0
0.7249695	2371.6	2352	2352	2358.533	11.31607	2038.4	1960	1960	1986.133	45.26426
0.9157509	2842	2881.2	2842	2855.067	22.63213	2156	2234.4	2156	2182.133	45.26426
1.1065324	2744	2842	2744	2776.667	56.58033	2254	2391.2	2312.8	2319.333	68.83294

1.1446886	2646	2744	2842	2744	98	2352	2450	2312.8	2371.6	70.6688
1.1828449	2881.2	2802.8	2744	2809.333	68.83294	2312.8	2352	2508.8	2391.2	103.7135
1.2210012	2842	2646	2744	2744	98	2450	2548	2352	2450	98
1.2591575	2646	2744	2802.8	2730.933	79.21246	2352	2430.4	2548	2443.467	98.65117
1.2782357	2842	2940	2802.8	2861.6	70.6688	2312.8	2450	2548	2436.933	118.1432
1.2973138	3234	3332	3430	3332	98	2940	3234	3136	3103.333	149.6975
Second experiment										
Uo	**DT_P1**	**DT_P2**	**DT_P3**	**Avg_DT**	**stdv**	**ANN_p1**	**ANN_p1**	**ANN_p1**	**Annu_Avg_p**	**stdv**
0	0	0	0	0	0	0	0	0	0	0
0.3434066	1078	1078	1078	1078	0	784	784	784	784	0
0.534188	2254	2254	2254	2254	0	1568	1568	1568	1568	0
0.7249695	3528	3528	3430	3495.333	56.58033	2352	2352	2352	2352	0
0.9157509	4606	4606	4606	4606	0	3234	3234	3234	3234	0
1.1065324	3626	3724	3822	3724	98	2548	2744	2940	2744	196
1.1446886	3430	3626	3822	3626	196	2744	2940	3136	2940	196
1.1828449	3528	3626	3724	3626	98	2548	2744	2940	2744	196
1.2210012	3626	3528	3626	3593.333	56.58033	2744	2940	3038	2907.333	149.6975
1.2591575	3332	3234	3136	3234	98	2352	2548	2744	2548	196
1.2782357	3038	3136	3234	3136	98	2548	2842	3038	2809.333	246.6279
1.2973138	3332	3430	3234	3332	98	2744	2940	3136	2940	196
Third experiment										
Uo	**DT_P1**	**DT_P2**	**DT_P3**	**Avg_DT**	**stdv**	**ANN_p1**	**ANN_p1**	**ANN_p1**	**Annu_Avg_p**	**stdv**

0	0	0	0	0	0	0	0	0	0	0
0.3434066	1176	1176	1176	1176	0	882	882	882	882	0
0.534188	2352	2352	2352	2352	0	1764	1724.8	1764	1750.933	22.63213
0.7249695	3665.2	3724	3586.8	3658.667	68.83294	2646	2646	2646	2646	0
0.9157509	4900	4900	4900	4900	0	3430	3430	3430	3430	0
1.1065324	3724	3626	3626	3658.667	56.58033	2842	3038	3136	3005.333	149.6975
1.1446886	3626	3822	3724	3724	98	2646	2842	3038	2842	196
1.1828449	3528	3626	3430	3528	98	2548	3136	2940	2874.667	299.3949
1.2210012	3234	3332	3136	3234	98	2352	2548	2744	2548	196
1.2591575	3430	3528	3332	3430	98	2744	2940	3136	2940	196
1.2782357	3528	3626	3430	3528	98	2548	2842	3038	2809.333	246.6279
1.2973138	3528	3626	3626	3593.333	56.58033	2940	3136	3332	3136	196

Experimental conditions: Geldart B, Bed height =50 cm, Gap height=7.5 cm

Uo, m/s	DT_ P1	DT_ P2	DT_ P3	Avg_ DT	stdv	ANN_ p1	ANN_ p1	ANN_ p1	Annu_A vg_p	stdv	DT_avg	std	T1	T2	T3	Tavg	Vavg	SRR
0	0	0	0	0	0	0	0	0	0	0	0	0	0	0	0	0	0	0
0.343 407	980	980	960. 4	973.4 667	11.31 607	744.8	744.8	744.8	744.8	1.39E- 13	932.088 9	67.26 478	0	0	0	0	0	0
0.534 188	196 0	196 0	196 0	1960	0	1568	1568	1568	1568	0	1875.06 7	87.10 431	0	0	0	0	0	0
0.724 969	303 8	303 8	303 8	3038	0	2312. 8	2312. 8	2312. 8	2312.8	0	2844.17 8	167.0 158	0	0	0	0	0	0
0.915 751	411 6	411 6	411 6	4116	0	3292. 8	3292. 8	3253. 6	3279.73 3	22.63 213	4129.06 7	19.6	0	0	0	0	0	0

1.106532	5742.8	5742.8	2058	4514.533	2127.42	4606	4606	4606	4606	0	5294.178	1214.585	0	0	0	0	0	0
1.144689	2058	2156	2254	2156	98	1764	1960	2156	1960	196	2149.467	87.10431	12.12	13.4	12	12.50667	0.003998	5.796908
1.182845	2156	2254	2352	2254	98	1862	2058	2254	2058	196	2216.978	68.21	7.72	6.18	7.4	7.1	0.007042	10.21127
1.221001	2254	2156	2058	2156	98	1960	2156	2352	2156	196	2234.4	94.50778	5.16	4.86	5	5.006667	0.009987	14.48069
1.259158	2156	2254	2058	2156	98	1960	2058	2254	2090.667	149.6975	2232.222	83.98574	3	3.76	3.2	3.32	0.01506	21.83735
1.297314	2450	2646	2548	2548	98	2352	2548	2744	2548	196	2558.889	90.94015	3.9	3.72	3.53	3.716667	0.013453	19.50673
Second experiment																		
Uo,m/s	**DT_P1**	**DT_P2**	**DT_P3**	**Avg_DT**	**stdv**	**ANN_p1**	**ANN_p1**	**ANN_p1**	**Annu_Avg_p**	**stdv**	**Annular_avg**	**stdv**	**T1**	**T2**	**T3**	**Tavg**	**Vavg**	**SRR**
0	0	0	0	0	0	0	0	0	0	0	0	0	0	0	0	0	0	0
0.343407	842.8	842.8	842.8	842.8	0	627.2	627.2	627.2	627.2	0	679.4667	61.98064	0	0	0	0	0	0
0.534188	1764	1764	1764	1764	0	1274	1274	1274	1274	0	1470	147	0	0	0	0	0	0
0.724969	2646	2665.6	2646	2652.533	11.31607	1920.8	1920.8	1960	1933.867	22.63213	2173.422	180.8211	0	0	0	0	0	0
0.915751	4174.8	4116	4116	4135.6	33.9482	3038	3038	3038	3038	0	3138.178	109.7619	0	0	0	0	0	0
1.106532	5625.2	5664.4	5625.2	5638.267	22.63213	4351.2	4390.4	4390.4	4377.333	22.63213	4529.778	114.892	0	0	0	0	0	0
1.144689	2058	2156	2254	2156	98	1862	1960	2156	1992.667	149.6975	1992.667	138.5929	12.92	10.97	13.78	12.55667	0.003982	5.773825
1.182845	2254	2156	2156	2188.667	56.58033	1862	2058	2254	2058	196	2014.444	155.8101	6.72	7.12	6.98	6.94	0.007205	10.44669
1.221001	2156	2254	2352	2254	98	1960	2058	2156	2058	98	2123.333	176.672	6.52	6.69	7.12	6.776667	0.007378	10.69848

1.259158	2352	2254	2254	2286.667	56.58033	2156	2254	2352	2254	98	2156	138.5929	4.2	4.81	5.12	4.71	0.010616	15.39278
1.297314	2450	2548	2646	2548	98	2254	2352	2548	2384.667	149.6975	2439.111	192.5672	3.5	2.79	3.46	3.25	0.015385	22.30769
Third experiment																		
Uo	DT_P1	DT_P2	DT_P3	Avg_DT	stdv	ANN_p1	ANN_p1	ANN_p1	Annu_Avg_p	stdv			**T1**	**T2**	**T3**	**Tavg**	**Vavg**	**SRR**
0	0	0	0	0	0	0	0	0	0	0			0	0	0	0	0	0
0.343407	980	980	980	980	0	744.8	627.2	627.2	666.4	67.89639			0	0	0	0	0	0
0.534188	1901.2	1901.2	1901.2	1901.2	0	1568	1568	1568	1568	0			0	0	0	0	0	0
0.724969	2842	2842	2842	2842	0	2273.6	2273.6	2273.6	2273.6	0			0	0	0	0	0	0
0.915751	4135.6	4135.6	4135.6	4135.6	0	3096.8	3096.8	3096.8	3096.8	5.57E-13			0	0	0	0	0	0
1.106532	5703.6	5742.8	5742.8	5729.733	22.63213	4606	4606	4606	4606	0			0	0	0	0	0	0
1.144689	2058	2097.2	2254	2136.4	103.7135	1960	2156	1960	2025.333	113.1607			12.6	13.5	13.44	13.18	0.003794	5.500759
1.182845	2156	2214.8	2254	2208.267	49.32558	1862	1960	1960	1927.333	56.58033			8.1	7.8	6.9	7.6	0.006579	9.539474
1.221001	2254	2293.2	2332.4	2293.2	39.2	1862	2254	2352	2156	259.2836			5.6	4.8	5.23	5.21	0.009597	13.91555
1.259158	2254	2214.8	2293.2	2254	39.2	1960	2254	2156	2123.333	149.6975			4.82	3.84	3.78	4.146667	0.012058	17.48392
1.297314	2450	2646	2646	2580.667	113.1607	2156	2352	2646	2384.667	246.6279			3.12	2.58	3.76	3.153333	0.015856	22.99154

Uo	DT_P1	DT_P2	DT_P3	Avg_DT	stdv	ANN_p1	ANN_p1	ANN_p1	Annu_Avg_p	stdv	Annula_avg	stdv
0	0	0	0	0	0	0	0	0	0	0	0	0
0.343407	686	725.2	725.2	712.1333	22.63213	705.6	744.8	744.8	731.7333	22.63213	805.7778	131.643
0.534188	1176	1176	1176	1176	0	1097.6	1097.6	1097.6	1097.6	0	1149.867	51.85673
0.724969	1822.8	1822.8	1822.8	1822.8	0	1724.8	1724.8	1724.8	1724.8	0	1748.756	90.23335
0.915751	2214.8	2214.8	2214.8	2214.8	0	1862	1960	1960	1927.333	56.58033	1918.622	86.24247
1.106532	2254	2214.8	2214.8	2227.867	22.63213	1960	2058	2156	2058	98	2058	120.025
1.144689	2058	2156	2156	2123.333	56.58033	1960	2156	2058	2058	98	2101.556	99.35179
1.182845	2156	2254	2156	2188.667	56.58033	2058	2058	2254	2123.333	113.1607	2110.267	100.8972
1.221001	2254	2214.8	2254	2240.933	22.63213	2058	2254	1960	2090.667	149.6975	2173.422	139.7813
1.259158	2156	2254	2156	2188.667	56.58033	2058	2254	2352	2221.333	149.6975	2297.556	147.9046
1.278236	2254	2293.2	1760.08	2102.427	297.1281	2254	2352	2548	2384.667	149.6975	2330.222	194.6341
1.297314	2450	2646	2548	2548	98	2352	2548	2744	2548	196	2466.333	179.8151
Second experiment												
U0	DT_P1	DT_P2	DT_P3	Avg_DT	stdv	ANN_p1	ANN_p1	ANN_p1	Annu_Avg_p	stdv	DT-avg	stdv
0	0	0	0	0	0	0	0	0	0	0	0	0
0.343407	1078	1078	1078	1078	0	980	980	980	980	0	877.6444	13.06667
0.534188	1274	1274	1274	1274	0	1215.2	1215.2	1215.2	1215.2	0	1176	0
0.724969	2018.8	2018.8	2018.8	2018.8	0	1862	1862	1862	1862	0	1875.067	0
0.915751	2156	2156	2156	2156	0	1960	1999.2	2038.4	1999.2	39.2	2129.867	22.63213
1.106532	2156	2254	2156	2188.667	56.58033	2058	2156	2254	2156	98	2169.067	19.6
1.144689	2156	2254	2214.8	2208.267	49.32558	2156	2254	2058	2156	98	2134.222	17.8776
1.182845	2156	2254	2254	2221.333	56.58033	2058	2156	2254	2156	98	2182.133	13.06667
1.221001	2156	2254	2352	2254	98	2058	2254	2312.8	2208.267	133.4144	2227.867	37.74561

1.259158	2254	2214.8	2352	2273.6	70.6688	2156	2254	2352	2254	98	2234.4	24.69307
1.278236	2254	2352	2450	2352	98	2058	2156	2450	2221.333	204.0033	2345.031	110.8496
1.297314	2156	2254	2254	2221.333	56.58033	2254	2352	2548	2384.667	149.6975	2384.667	29.28813
Third experiment												
#VALUE!	DT_P1	DT_P2	DT_P3	Avg_DT	stdv	ANN_p1	ANN_p1	ANN_p1	Annu_Avg_p	stdv		
0	0	0	0	0	0	0	0	0	0	0		
0.343407	842.8	842.8	842.8	842.8	0	705.6	705.6	705.6	705.6	1.39E-13		
0.534188	1078	1078	1078	1078	0	1136.8	1136.8	1136.8	1136.8	0		
0.724969	1783.6	1783.6	1783.6	1783.6	0	1685.6	1646.4	1646.4	1659.467	22.63213		
0.915751	2018.8	1979.6	2058	2018.8	39.2	1764	1862	1862	1829.333	56.58033		
1.106532	2058	2156	2058	2090.667	56.58033	1862	1960	2058	1960	98		
1.182845	2058	2097.2	2058	2071.067	22.63213	1960	2156	2156	2090.667	113.1607		
1.221001	2156	2156	2097.2	2136.4	33.9482	1960	2038.4	2156	2051.467	98.65117		
1.259158	2254	2156	2156	2188.667	56.58033	2058	2352	2254	2221.333	149.6975		
1.278236	2214.8	2254	2254	2240.933	22.63213	2254	2450	2548	2417.333	149.6975		
1.297314	2450	2646	2646	2580.667	113.1607	2156	2352	2646	2384.667	246.6279		

Experimental conditions: Geldart B, Bed height =40 cm, Gap height=7.5 cm

U0	DT_P1	DT_P2	DT_P3	Avg_DT	stdv	ANN_p1	ANN_p1	ANN_p1	Annu_Avg_p	stdv	DT_avg	std	stdv	T1	T2	T3	Tavg	Vavg	SRR	SRRavg
0	0	0	0	0	0	0	0	0	0	0	0	0	0	0	0	0	0	0	0	0
0.343407	686	686	686	686	0	588	588	588	588	0	686	0	0	0	0	0	0	0	0	0
0.534	147	147	147	1470	0	1274	1274	1274	1274	0	1483.0	0	19.30	0	0	0	0	0	0	0

188	0	0	0								67		075							
0.724969	2293.2	2881.2	2881.2	2685.2	339.482	1920.8	1920.8	1920.8	1920.8	0	2430.4	113.1607	241.0662	0	0	0	0	0	0	0
0.915751	3430	3430	3430	3430	0	2646	2842	2842	2776.667	113.1607	3460.489	199.9172	284.486	0	0	0	0	0	0	0
1.03022	4253.2	4253.2	4253.2	4253.2	0	3528	3528	3528	3528	0	4270.622	75.44044	169.9428	0	0	0	0	0	0	0
1.068376	4508	4508	4508	4508	0	3724	3724	3724	3724	0	4237.956	18.86011	755.6121	0	0	0	0	0	0	0
1.106532	4802	4998	4998	4932.667	113.1607	3822	3822	3822	3822	0	4812.889	89.24699	109.0867	19.89	21.2	18.8	19.96333	0.002505	3.631658	3.260785
1.144689	1862	1862	1862	1862	0	1960	2058	2156	2058	98	1960	26.40415	81.21999	18.1	19	20	19.03333	0.002627	3.809107	3.876413
1.182845	1960	2058	2058	2025.333	56.58033	2058	2254	2254	2188.667	113.1607	2010.089	70.38688	62.12655	15.94	16.3	17.2	16.48	0.003034	4.399272	4.396513
1.221001	2058	2156	2058	2090.667	56.58033	2058	2156	2352	2188.667	149.6975	2014.444	56.58033	104.5457	9.3	7.89	8.9	8.696667	0.005749	8.336527	8.172468
1.259158	2058	2352	2058	2156	169.741	2254	2352	2254	2286.667	56.58033	2025.333	75.44044	128.4201	4.98	6.6	5.78	5.786667	0.008641	12.5288	11.74591
1.297314	2254	2450	2352	2352	98	2548	2646	2744	2646	98	2373.778	32.66667	56.29384	3.5	4.59	3.79	3.96	0.012626	18.30808	17.77462
Second experiment																				
Uo	DT_P1	DT_P2	DT_P3	Avg_DT	stdv	ANN_p1	ANN_p1	ANN_p1	Annu_Avg_p	stdv	Annu_P_avg	stdv		T1	T2	T3	Tavg	Vavg	SRR	SRRavg
0	0	0	0	0	0	0	0	0	0	0	0	0		0	0	0	0	00	00	0
0.343407	686	686	686	686	0	588	588	588	588	0	588	0		0	0	0	0	00	0	0
0.534188	1470	1470	1470	1470	0	1215.2	1215.2	1215.2	1215.2	0	1254.4	29.4		0	0	0	0	0	0	0
0.724969	2352	2352	2352	2352	0	1862	1862	1862	1862	0	1881.6	29.4		0	0	0	0	0	0	0

0.915751	3273.2	3273.2	4312	3619.467	599.7515	2744	2744	2744	2744	0	2754.889	58.89067		0	0	0	0	0	0	0
1.03022	4312	4312	4704	4442.667	226.3213	3528	3528	3528	3528	0	3462.667	98		0	0	0	0	0	0	0
0.003875	4566.8	4566.8	1960	3697.867	1505.037	3822	3822	3822	3822	0	3756.667	49		0	0	0	0	0	0	0
1.106532	4704	4704	4704	4704	0	3880.8	3880.8	3880.8	3880.8	5.57E-13	3874.267	42.71721		18.89	20.2	19	19.36333	0.002582	3.74419	3.625279
1.144689	1960	2058	1960	1992.667	56.58033	1960	2058	2156	2058	98	2031.867	102.315		16.52	17.92	15.98	16.80667	0.002975	4.313764	4.232264
1.182845	2058	2018.8	2058	2044.933	22.63213	1960	2058	2254	2090.667	149.6975	2112.444	121.1312		14.97	15.68	16.23	15.62667	0.0032	4.639505	6.394312
1.221001	1960	2156	2058	2058	98	1960	2058	2156	2058	98	2079.778	145.1738		10.44	8.76	7.88	9.026667	0.005539	8.031758	10.27667
1.259158	1960	2058	1960	1992.667	56.58033	1960	2058	2156	2058	98	2134.222	136.6545		6.47	7.88	7	7.116667	0.007026	10.18735	13.02006
1.297314	2352	2352	2450	2384.667	56.58033	2156	2352	2450	2319.333	149.6975	2471.778	175.1555		3.25	3.98	4.12	3.783333	0.013216	19.163	19.163

Third experiment																					
Uo	DT_P1	DT_P2	DT_P3	Avg_DT	stdv	ANN_p1	ANN_p1	ANN_p1	Annu_Avg_p	stdv				T1	T2	T3	Tavg	Vavg	SRR	SRRavg
0	0	0	0	0	0	0	0	0	0	0										
0.343407	686	686	686	686	0	588	588	588	588	0										
0.534188	1509.2	1509.2	1509.2	1509.2	0	1274	1274	1274	1274	0										
0.724969	2254	2254	2254	2254	0	1862	1862	1862	1862	0										
0.915751	3332	3332	3332	3332	0	2744	2744	2744	2744	0										
1.03022	4116	4116	4116	4116	0	3332	3332	3332	3332	0										
1.068376	4508	4508	4508	4508	0	3724	3724	3724	3724	0										
1.106532	4802	4802	4802	4802	0	3920	3920	3920	3920	0				29.8	32.6	27.98	30.12667	0.00166	2.406506	2.406506
1.106532	2058	1960	2058	2025.333	56.58033	1862	1960	2116.8	1979.6	128.5258				19.35	20.98	21.7	20.67667	0.002418	3.506368	3.506368
1.182845	1960	2058	1862	1960	98	1960	2058	2156	2058	98				17.5	18.1	16.8	17.46667	0.002863	4.150763	4.150763
1.221001	1862	1960	1862	1894.667	56.58033	1862	1960	2156	1992.667	149.6975				8	8.98	9.71	8.896667	0.00562	8.14912	8.14912
1.259158	1862	1960	1960	1927.333	56.58033	1960	2058	2156	2058	98				4.7	6.69	5.98	5.79	0.008636	12.52159	12.52159
1.297314	2352	2352	2450	2384.667	56.58033	2352	2548	2450	2450	98				3.75	4.69	5.28	4.573333	0.010933	15.85277	15.85277

Uo	**DT_P1**	**DT_P2**	**DT_P3**	**Avg_DT**	**stdv**	**ANN_p1**	**ANN_p1**	**ANN_p1**	**Annu_Avg_p**	**stdv**	**DT_Avg**	**Std**
0	0	0	0	0	0	0	0	0	0	0	0	0
0.343407	588	588	588	588	0	627.2	627.2	627.2	627.2	0	555.3333	0
0.534188	1176	1176	1176	1176	0	1176	1176	1176	1176	0	1078	0
0.724969	1666	1666	1666	1666	0	1764	1764	1764	1764	0	1661.644	7.544044
0.915751	2018.8	2018.8	2018.8	2018.8	0	1862	1862	1862	1862	0	1979.6	0
1.106532	2058	2156	2156	2123.333	56.58033	2058	2156	2058	2090.667	56.58033	2068.889	56.58033
1.144689	2058	2156	2058	2090.667	56.58033	2058	2058	2058	2058	0	2005.733	49.03628
1.182845	1960	1960	2018.8	1979.6	33.9482	2058	2156	2156	2123.333	56.58033	1955.644	30.17617
1.221001	2058	2058	1960	2025.333	56.58033	2058	2254	2254	2188.667	113.1607	2003.556	57.32022
1.259158	2156	2156	2058	2123.333	56.58033	2058	2156	2254	2156	98	2199.556	56.58033
1.297314	2254	2450	2450	2384.667	113.1607	2548	2646	2744	2646	98	2368.333	105.5803
0												
U0	DT_P1	DT_P2	DT_P3	Avg_DT	stdv	ANN_p1	ANN_p1	ANN_p1	Annu_Avg_p	stdv	Annu_avg	Std
0	0	0	0	0	0	0	0	0	0	0	0	0
0.343407	588	588	588	588	0	744.8	744.8	744.8	744.8	1.39E-13	640.2667	4.64E-14
0.534188	1078	1078	1078	1078	0	1176	1176	1176	1176	0	1110.667	0
0.724969	1666	1626.8	1666	1652.933	22.63213	1724.8	1724.8	1724.8	1724.8	0	1698.667	0
0.915751	1960	1960	1960	1960	0	1920.8	1960	1960	1946.933	22.63213	1890.311	7.544044
1.106532	2058	2156	2058	2090.667	56.58033	2058	2058	2156	2090.667	56.58033	2047.111	70.38688
1.144689	1960	2018.8	2018.8	1999.2	33.9482	2116.8	2156	2058	2110.267	49.32558	2064.533	35.30197
1.182845	1960	2058	2058	2025.333	56.58033	2058	2254	2254	2188.667	113.1607	2090.667	89.24699
1.221001	1901.2	1960	2018.8	1960	58.8	2058	2156	2058	2090.667	56.58033	2123.333	106.4795
1.259158	2156	2058	2058	2090.667	56.58033	2254	2352	2254	2286.667	56.58033	2308.444	89.24699
1.297314	2352	2254	2450	2352	98	2450	2548	2744	2580.667	149.6975	2613.333	123.8487
0												

Uo	DT_P1	DT_P2	DT_P3	Avg_DT	stdv	ANN_p1	ANN_p1	ANN_p1	Annu_Avg_p	stdv		
0	0	0	0	0	0	0	0	0	0	0		
0.343407	490	490	490	490	0	548.8	548.8	548.8	548.8	0		
0.534188	980	980	980	980	0	980	980	980	980	0		
0.724969	1666	1666	1666	1666	0	1607.2	1607.2	1607.2	1607.2	0		
0.915751	1960	1960	1960	1960	0	1862	1862	1862	1862	0		
1.106532	1960	1960	2058	1992.667	56.58033	1862	1960	2058	1960	98		
1.182845	1960	1862	1960	1927.333	56.58033	1960	2058	2058	2025.333	56.58033		
1.221001	1862	1862	1862	1862	0	1862	1960	2058	1960	98		
1.259158	1960	2058	2058	2025.333	56.58033	1960	2058	2254	2090.667	149.6975		
1.297314	2352	2352	2450	2384.667	56.58033	2352	2548	2548	2482.667	113.1607		

Experimental conditions: Geldart B-D, Bed height 50 cm, Gap height=7.5 cm

U0	DT_P1	DT_P2	DT_P3	Avg_DT	stdv	ANN_p1	ANN_p1	ANN_p1	Annu_Avg_p	stdv	DT_avg	STDV	T1	T2	T3	Avg time	V agv	SRR	avg_SRR
0	0	0	0	0	0	0	0	0	0	0	0	0	0	0	0	0	0	0	0
0.343407	196	196	196	196	0	196	196	196	196	0	248.2667	40.32713	0	0	0	0	0	0	0
0.534188	548.8	548.8	548.8	548.8	0	548.8	548.8	548.8	548.8	0	542.2667	42.71721	0	0	0	0	0	0	0
0.724969	803.6	803.6	803.6	803.6	0	744.8	744.8	744.8	744.8	1.39E-13	921.2	122.402	0	0	0	0	0	0	0
0.915751	1234.8	1234.8	1234.8	1234.8	0	980	980	980	980	0	1293.6	61.20098	0	0	0	0	0	0	0
1.106532	1862	1862	1862	1862	0	1470	1470	1470	1470	0	1862	0	0	0	0	0	0	0	0
1.144689	1960	1960	1960	1960	0	1528.8	1528.8	1528.8	1528.8	0	2123.333	129.6418	0	0	0	0	0	0	0
1.182845	2254	2254	2254	2254	0	1666	1666	1666	1666	0	2319.333	49	0	0	0	0	0	0	0
1.221001	2646	2646	2646	2646	0	1960	1960	1960	1960	0	2711.333	98	0	0	0	0	0	0	0

1.259158	3038	3038	3038	3038	0	2254	2254	2254	2254	0	3070.667	49	0	0	0	0	0	0	0
1.262973	3234	3234	3234	3234	0	2254	2254	2254	2254	0	3234	0	0	0	0	0	0	0	0
1.266789	3332	3332	3332	3332	0	2352	2352	2352	2352	0	3353.778	43.21394	0	0	0	0	0	0	0
1.270604	3626	3626	3626	3626	0	2548	2548	2548	2548	0	3593.333	138.5929	0	0	0	0	0	0	0
1.27442	4214	4214	4214	4214	0	2940	2940	2940	2940	0	4834.667	485.0753	0	0	0	0	0	0	0
1.278236	5978	5978	5978	5978	0	3920	3920	3920	3920	0	5782	162.5146	20	18	17	18.33333	0.002727	3.954545	4.711059
1.282051	1568	1568	1568	1568	0	1568	1764	1960	1764	196	1426.444	121.1312	10.53	15.9	11.9	12.77667	0.003913	5.674406	6.220837
1.285867	1470	1470	1470	1470	0	1666	1568	3430	2221.333	1047.882	1589.778	107.1048	7.89	10.59	12	10.16	0.004921	7.135827	10.13098
1.289683	1666	1666	1666	1666	0	1764	1862	1862	1829.333	56.58033	1611.556	71.19535	6.69	5.12	4.9	5.57	0.008977	13.01616	15.21504
Second experiment																			
U0	**DT_P1**	**DT_P2**	**DT_P3**	**Avg_DT**	**stdv**	**ANN_p1**	**ANN_p1**	**ANN_p1**	**Annu_Avg_p**	**stdv**	**Annu_avg**	**Stdv**	**T1**	**T2**	**T3**	**Avg time**	**V agv**	**SRR**	**avg_SRR**

0	0	0	0	0	0	0	0	0	0	0	0	0	0	0	0	0	0	0	0
0.343407	254.8	254.8	254.8	254.8	3.48E-14	235.2	235.2	235.2	235.2	0	228.6667	25.92836	0	0	0	0	0	0	0
0.534188	588	588	588	588	0	490	490	490	490	0	516.1333	25.92836	0	0	0	0	0	0	0
0.724969	882	882	882	882	0	686	686	686	686	0	725.2	29.4	0	0	0	0	0	0	0
0.915751	1274	1274	1274	1274	0	980	980	980	980	0	953.8667	39.2	0	0	0	0	0	0	0
1.106532	1862	1862	1862	1862	0	1470	1470	1470	1470	0	1463.467	9.8	0	0	0	0	0	0	0
1.144689	2156	2156	2156	2156	0	1666	1666	1666	1666	0	1587.6	61.20098	0	0	0	0	0	0	0
1.182845	2352	2352	2352	2352	0	1764	1764	1764	1764	0	1764	84.87049	0	0	0	0	0	0	0
1.221001	2646	2646	2646	2646	0	2058	2058	2058	2058	0	2025.333	49	0	0	0	0	0	0	0
1.259158	3038	3038	3038	3038	0	2254	2254	2254	2254	0	2254	0	0	0	0	0	0	0	0
1.262973	3234	3234	3234	3234	0	2352	2352	2352	2352	0	2330.222	65.33333	0	0	0	0	0	0	0
1.266789	3332	3332	3332	3332	0	2450	2450	2450	2450	0	2406.444	51.65054	0	0	0	0	0	0	0

1.270604	3430	3430	3430	3430	0	2548	2548	2548	2548	0	2548	0	0	0	0	0	0	0	0
1.27442	4998	4998	4998	4998	0	3822	3822	3822	3822	0	3538.889	450.2789	0	0	0	0	0	0	0
1.278236	5586	5782	5684	5684	98	4018	4018	4018	4018	0	3996.222	65.33333	14	12.56	13.22	13.26	0.003771	5.467572	
1.282051	1372	1372	1274	1339.333	56.58033	1568	1764	1960	1764	196	1774.889	172.8558	9.59	11.88	10.67	10.71333	0.004667	6.767268	
1.285867	1666	1568	1666	1633.333	56.58033	1764	1960	2058	1927.333	149.6975	2014.444	556.7726	4.61	5.76	6.2	5.523333	0.009053	13.12613	
1.289683	1568	1568	1666	1600.667	56.58033	1666	1764	1862	1764	98	1774.889	76.61012	3.8	4.69	4	4.163333	0.01201	17.41393	
Third experiment																			
#VALUE!	DT_P1	DT_P2	DT_P3	Avg_DT	stdv	ANN_p1	ANN_p1	ANN_p1	Annu_Avg_p	stdv									
0	0	0	0	0	0	0	0	0	0	0				0	0	0	0	0	0
0.343407	294	294	294	294	0	254.8	254.8	254.8	254.8	3.48E-14				0	0	0	0	0	0
0.534188	490	490	490	490	0	509.6	509.6	509.6	509.6	6.96E-14				0	0	0	0	0	0

0.724969	1078	1078	1078	1078	0	744.8	744.8	744.8	744.8	1.39E-13				0	0	0	0	0	0
0.915751	1372	1372	1372	1372	0	901.6	901.6	901.6	901.6	0				0	0	0	0	0	0
1.106532	1862	1862	1862	1862	0	1450.4	1450.4	1450.4	1450.4	2.78E-13				0	0	0	0	0	0
1.144689	2254	2254	2254	2254	0	1568	1568	1568	1568	0				0	0	0	0	0	0
1.182845	2352	2352	2352	2352	0	1862	1862	1862	1862	0				0	0	0	0	0	0
1.221001	2842	2842	2842	2842	0	2058	2058	2058	2058	0				0	0	0	0	0	0
1.259158	3136	3136	3136	3136	0	2254	2254	2254	2254	0				0	0	0	0	0	0
1.262973	3234	3234	3234	3234	0	2352	2450	2352	2384.667	56.58033				0	0	0	0	0	0
1.266789	3332	3430	3430	3397.333	56.58033	2450	2352	2450	2417.333	56.58033				0	0	0	0	0	0
1.270604	3626	3724	3822	3724	98	2548	2548	2548	2548	0				0	0	0	0	0	0
1.27442	5194	5292	5390	5292	98	3822	3920	3822	3854.667	56.58033				0	0	0	0	0	0
1.278	558	578	568	5684	98	4018	4116	4018	4050.66	56.58			16	13.	14.	14.61	0.003	4.962	

236	6	2	4						7	033				23	6		422	355	
1.282051	1372	1470	1274	1372	98	1568	1862	1960	1796.667	204.033			9.72	10.5	7.12	9.113333	0.005486	7.955377	
1.285867	1666	1568	1764	1666	98	1764	1862	2058	1894.667	149.6975			5.34	7.65	5.68	6.223333	0.008034	11.64971	
1.289683	1568	1470	1666	1568	98	1666	1764	1764	1731.333	56.58033			2.8	3.12	3.83	3.25	0.015385	22.30769	

Decreasing velocity

U0	DT_P1	DT_P2	DT_P3	Avg_DT	stdv	ANN_p1	ANN_p1	ANN_p1	Annu_Avg_p	stdv	DT_avg_decreasing	stdv
0	0	0	0	0	0	0	0	0	0	0	0	0
0.343407	98	98	98	98	0	196	196	196	196	0	130.6667	0
0.534188	196	196	196	196	0	490	490	490	490	0	215.6	2.01E-14
0.724969	392	392	392	392	0	686	686	686	686	0	424.6667	0
0.915751	588	588	588	588	0	882	882	882	882	0	620.6667	0
1.106532	882	882	882	882	0	1176	1176	1176	1176	0	914.6667	0
1.144689	1078	1078	1078	1078	0	1274	1274	1274	1274	0	1078	0
1.182845	1274	1274	1274	1274	0	1372	1372	1372	1372	0	1208.667	0
1.221001	1372	1274	1372	1339.333	56.58033	1372	1470	1372	1404.667	56.58033	1284.889	32.66667
1.259158	1470	1568	1470	1502.667	56.58033	1568	1666	1568	1600.667	56.58033	1454.756	19.6
1.278236	1372	1470	1372	1404.667	56.58033	1568	1666	1607.2	1613.733	49.32558	1578.889	1.52E-13
1.297314	1470	1764	1764	1666	169.741	1764	1862	1568	1731.333	149.6975	1649.667	60.38471
0												

Uo	DT_P1	DT_P2	DT_P3	Avg_DT	stdv	ANN_p1	ANN_p1	ANN_p1	Annu_Avg_p	stdv	Annula_avg_decreasing	stdv
0	0	0	0	0	0	0	0	0	0	0	0	0
0.343407	98	98	98	98	0	235.2	235.2	235.2	235.2	0	228.6667	25.92836
0.534188	196	196	196	196	0	392	392	392	392	0	437.7333	42.71721
0.724969	392	392	392	392	0	588	588	588	588	0	633.7333	42.71721
0.915751	588	588	588	588	0	784	784	784	784	0	829.7333	42.71721
1.106532	882	882	882	882	0	1078	1078	1078	1078	0	1123.733	42.71721
1.144689	980	980	980	980	0	1176	1176	1176	1176	0	1234.8	44.90924
1.182845	1078	1078	1078	1078	0	1274	1274	1274	1274	0	1313.2	44.90924
1.221001	1176	1176	1176	1176	0	1470	1274	1176	1306.667	149.6975	1361.111	103.3011
1.259158	1274	1234.8	1274	1260.933	22.63213	1372	1470	1372	1404.667	56.58033	1470	109.5673
1.278236	1568	1568	1666	1600.667	56.58033	1372	1568	1764	1568	196	1605.022	129.0643
1.297314	1666	1764	1470	1633.333	149.6975	1666	1764	1862	1764	98	1764	98
0												
U0	DT_P1	DT_P2	DT_P3	Avg_DT	stdv	ANN_p1	ANN_p1	ANN_p1	Annu_Avg_p	stdv		
0	0	0	0	0	0	0	0	0	0	0		
0.343407	196	196	196	196	0	254.8	254.8	254.8	254.8	3.48E-14		
0.534188	254.8	254.8	254.8	254.8	3.48E-14	431.2	431.2	431.2	431.2	0		
0.724969	490	490	490	490	0	627.2	627.2	627.2	627.2	0		
0.915751	686	686	686	686	0	823.2	823.2	823.2	823.2	1.39E-13		
1.106532	980	980	980	980	0	1117.2	1117.2	1117.2	1117.2	0		
1.144689	1078	1078	1078	1078	0	1254.4	1254.4	1254.4	1254.4	0		
1.182845	1176	1176	1176	1176	0	1293.6	1293.6	1293.6	1293.6	0		
1.221001	1274	1274	1274	1274	0	1470	1274	1372	1372	98		
1.259158	1372	1274	1372	1339.333	56.58033	1372	1470	1372	1404.667	56.58033		
1.278236	1568	1568	1666	1600.667	56.58033	1470	1666	1764	1633.333	149.6975		

1.297314	1764	1764	1666	1731.333	56.58033	1764	1764	1862	1796.667	56.58033	

Experimental conditions: Geldart B-D, Bed height 40 cm, Gap height=7.5 cm

Uo	DT_P1	DT_P2	DT_P3	Avg_DT	stdv	ANN_p1	ANN_p1	ANN_p1	Annu_Avg_p	stdv			DT_avg STDV		T1	T2	T3	Avg time	V agv	SRR	avg_SRR	Stdv
0	0	0	0	0	0	0	0	0	0	0			0	0	0	0	0	0	0	0	0	0
0.343407	196	196	196	196	0	196	196	196	196	0	16.5	16.5	196	0	0	0	0	0	0	0	0	0
0.534188	392	392	392	392	0	294	294	294	294	0	17.5	17.5	392	0	0	0	0	0	0	0	0	0
0.724969	588	588	588	588	0	490	490	490	490	0	18.5	18.5	594.5333	9.8	0	0	0	0	0	0	0	0
0.915751	882	882	882	882	0	686	686	686	686	0	20	20	882	84.87049	0	0	0	0	0	0	0	0
1.106532	1372	1372	1372	1372	0	1078	1078	1078	1078	0	22.5	22.5	1404.667	49	0	0	0	0	0	0	0	0

1.144689	1470	1470	1470	1470	0	1176	1176	1176	1176	0	23	23	1550.578	88.98294	0	0	0	0	0	0	0	0
1.182845	1666	1666	1666	1666	0	1274	1274	1274	1274	0	24	24	1748.756	88.62245	0	0	0	0	0	0	0	0
1.221001	1764	1764	1764	1764	0	1430.8	1430.8	1430.8	1430.8	0	24.5	24.5	1868.533	142.3532	0	0	0	0	0	0	0	0
1.259158	2058	2058	2058	2058	0	1666	1666	1666	1666	0	26	26	2142.933	157.7161	0	0	0	0	0	0	0	0
1.266789	3234	3234	3234	3234	0	2450	2450	2450	2450	0	32	32	3070.667	321.3145	0	0	0	0	0	0	0	0
1.270604	3822	3822	3822	3822	0	2940	2940	2940	2940	0	35	35	3626	294	0	0	0	0	0	0	0	0
1.27442	4018	4018	4018	4018	0	3136	3136	3136	3136	0	36	36	3920	224.5462	0	0	0	0	0	0	2.12	0
1.278236	1078	1078	1078	1078	0	1372	1470	1470	1437.333	56.58033	21.5	22	2123.333	1424.375	17.37	14.9	15.8	16.02333	0.00312	4.524652	4.824996	1.130983
1.282051	1470	1470	1470	1470	0	1666	1568	1666	1633.333	56.58033	23	23.5	1372	109.5673	13	12.12	10.98	12.03333	0.004155	6.024931	6.904816	0.959385
1.285867	1372	1372	1372	1372	0	1666	1568	1568	1600.667	56.58033	23	22.5	1459.111	103.3011	9.1	10.28	8.9	9.426667	0.005304	7.690948	10.32437	1.562113
1.289683	1470	1470	1470	1470	0	1764	1666	1568	1666	98	22.5	23	1263.111	247.1682	6.52	5.12	7.12	6.253333	0.007996	11.59382	15.37783	0.936203
Second experiment																						
U0	DT_P1	DT_P2	DT_P3	Avg_DT	stdv	ANN_p1	ANN_p1	ANN_p1	Annu_Avg_p	stdv			Annu_avg	Stdv								

0	0	0	0	0	0	0	0	0	0	0	0	0	0	0	0	0	0	0	0	0	0	
0.343407	196	196	196	196	0	196	196	196	196	0	16.5	16.5	196	0	0	0	0	0	0	0	0	
0.534188	392	392	392	392	0	294	294	294	294	0	17.5	17.5	294	0	0	0	0	0	0	0	0	
0.724969	607.6	607.6	607.6	607.6	0	548.8	548.8	548.8	548.8	0	18.6	18.6	509.6	29.4	0	0	0	0	0	0	0	
0.915751	784	784	784	784	0	705.6	705.6	705.6	705.6	1.39E-13	19.5	19.5	692.5333	9.8	0	0	0	0	0	0	0	
1.106532	1372	1372	1372	1372	0	1078	1078	1078	1078	0	22.5	22.5	1078	0	0	0	0	0	0	0	0	
1.144689	1509.2	1509.2	1528.8	1515.733	11.31607	1176	1176	1176	1176	0	23.2	23.3	1208.667	49	0	0	0	0	0	0	0	
1.182845	1705.2	1705.2	1744.4	1718.267	22.63213	1293.6	1293.6	1293.6	1293.6	0	24.2	24.4	1313.2	44.90924	0	0	0	0	0	0	0	
1.221001	1783.6	1783.6	1783.6	1783.6	0	1470	1470	1470	1470	0	24.6	24.6	1456.933	19.6	0	0	0	0	0	0	0	
1.259158	2018.8	2018.8	2018.8	2018.8	0	1666	1666	1666	1666	0	25.8	25.8	1698.667	49	0	0	0	0	0	0	0	
1.266789	3332	3332	3332	3332	0	2548	2548	2548	2548	0	32.5	32.5	2286.667	321.3145	0	0	0	0	0	0	0	

1.270604	3822	3822	3822	3822	0	2940	2940	2940	2940	0	35	35	2744	294	0	0	0	0	0	0	0	
1.27442	4116	4116	4116	4116	0	3234	3234	3234	3234	0	36.5	36.5	3005.333	272.8205	0	0	0	0	0	0	0	
1.278236	1274	1176	1372	1274	98	1372	1470	1470	1437.333	56.58033	21.5	22.5	1872.889	654.5572	16.18	14.98	15.4	15.52	0.003222	4.671392	0.367347	
1.282051	1274	1372	1470	1372	98	1666	1568	1666	1633.333	56.58033	22.5	23	1600.667	98	10.12	9.18	10.96	10.08667	0.004957	7.187707	0.365854	
1.285867	1372	1470	1470	1437.333	56.58033	1568	1568	1666	1600.667	56.58033	23	23	1687.778	145.1738	7.89	8.32	9.14	8.45	0.005917	8.579882	0.364372	
1.289683	1470	1372	1274	1372	98	1764	1666	1764	1731.333	56.58033	22.5	22	1535.333	254.6115	4.9	5.76	4.12	4.926667	0.010149	14.71583	0.362903	
Third experiment																						
U0	DT_P1	DT_P2	DT_P3	Avg_DT	stdv	ANN_p1	ANN_p1	ANN_p1	Annu_Avg_p	stdv												
0	0	0	0	0	0	0	0	0	0	0	0	0		0	0	0	0	0	0	0		
0.343407	196	196	196	196	0	196	196	196	196	0	16.5	16.5		0	0	0	0	0	0	0		
0.534188	392	392	392	392	0	294	294	294	294	0	17.5	17.5		0	0	0	0	0	0	0		
0.724969	588	588	588	588	0	490	490	490	490	0	18.	18.		0	0	0	0	0	0	0		

											5	5										
0.915751	980	980	980	980	0	686	686	686	686	0	20.5	20.5		0	0	0	0	0	0	0		
1.106532	1470	1470	1470	1470	0	1078	1078	1078	1078	0	23	23		0	0	0	0	0	0	0		
1.144689	1666	1666	1666	1666	0	1274	1274	1274	1274	0	24	24		0	0	0	0	0	0	0		
1.182845	1862	1862	1862	1862	0	1372	1372	1372	1372	0	25	25		0	0	0	0	0	0	0		
1.221001	2058	2058	2058	2058	0	1470	1470	1470	1470	0	26	26		0	0	0	0	0	0	0		
1.259158	2352	2352	2352	2352	0	1764	1764	1764	1764	0	27.5	27.5		0	0	0	0	0	0	0		
1.266789	2646	2646	2646	2646	0	1862	1862	1862	1862	0	29	29		0	0	0	0	0	0	0		
1.270604	3234	3234	3234	3234	0	2352	2352	2352	2352	0	32	32		0	0	0	0	0	0	0		
1.27442	3626	3626	3626	3626	0	2646	2646	2646	2646	0	34	34		0	0	0	0	0	0	0		
1.278236	4018	4018	4018	4018	0	2744	2744	2744	2744	0	36	36			18.56	19	20	19.18667	0.002606	3.778666		
1.282051	1176	1274	1372	1274	98	1372	1568	1666	1535.333	149.6975	22	22.5			13.8	11.47	12	12.42333	0.004025	5.835793		
1.285867	1470	1568	1666	1568	98	1764	1862	1960	1862	98	23.5	24			6	6.98	7.16	6.713333	0.007448	10.7994		
1.289683	882	980	980	947.3333	56.58033	1176	1176	1274	1208.667	56.58033	20.	20.			3.89	4.67	5	4.52	0.011062	16.03982		

											5	5										

Decreasing velocity

U0	DT_P1	DT_P2	DT_P3	Avg_DT	stdv	ANN_p1	ANN_p1	ANN_p1	Annu_Avg_p	stdv	Dt_avg_decreasing	Stdv
0	0	0	0	0	0	0	0	0	0	0	0	0
0.343407	58.8	58.8	58.8	58.8	8.7E-15	196	196	196	196	0	58.8	0
0.534188	98	98	98	98	0	294	294	294	294	0	111.0667	0
0.724969	196	196	196	196	0	392	392	392	392	0	215.6	53.67681
0.915751	392	392	392	392	0	588	588	588	588	0	392	21.47072
1.106532	588	588	588	588	0	784	784	784	784	0	601.0667	53.67681
1.144689	686	686	686	686	0	882	882	882	882	0	686	32.20609
1.182845	784	784	784	784	0	980	980	980	980	0	934.2667	32.20609
1.221001	882	882	882	882	0	1019.2	1019.2	1019.2	1019.2	1.39E-13	882	21.47072
1.259158	980	980	980	980	0	1078	1136.8	1078	1097.6	33.9482	1165.111	48.67224
1.278236	1078	1176	1274	1176	98	1666	1568	1666	1633.333	56.58033	1143.333	135.0837
1.297314	1372	1470	1568	1470	98	1568	1372	1764	1568	196	1393.778	235.3361
Second experiment												
Uo	DT_P1	DT_P2	DT_P3	Avg_DT	stdv	ANN_p1	ANN_p1	ANN_p1	Annu_Avg_p	stdv	Annular_avg_decreasingg	Stdv
0	0	0	0	0	0	0	0	0	0	0	0	0
0.343407	58.8	58.8	58.8	58.8	8.7E-15	196	196	196	196	0	196	0
0.534188	98	98	98	98	0	294	294	294	294	0	294	0
0.724969	196	196	196	196	0	392	392	392	392	0	424.6667	49
0.915751	392	392	392	392	0	588	588	588	588	0	601.0667	19.6
1.106532	588	588	588	588	0	784	784	784	784	0	816.6667	49

1.144689	686	686	686	686	0	882	882	882	882	0	901.6	29.4
1.182845	784	784	784	784	0	980	980	980	980	0	999.6	29.4
1.221001	882	882	882	882	0	1019.2	1019.2	1019.2	1019.2	1.39E-13	1006.133	19.6
1.259158	980	980	1078	1012.667	56.58033	1078	1136.8	1078	1097.6	33.9482	1112.844	43.58277
1.278236	1274	1176	1372	1274	98	1372	1470	1470	1437.333	56.58033	1426.444	190.4778
1.297314	1470	1372	1470	1437.333	56.58033	1764	1666	1764	1731.333	56.58033	1557.111	210.4403

Third experiment

Uo	DT_P1	DT_P2	DT_P3	Avg_DT	stdv	ANN_p1	ANN_p1	ANN_p1	Annu_Avg_p	stdv		
0	0	0	0	0	0	0	0	0	0	0		
0.343407	58.8	58.8	58.8	58.8	8.7E-15	196	196	196	196	0		
0.534188	137.2	137.2	137.2	137.2	0	294	294	294	294	0		
0.724969	254.8	254.8	254.8	254.8	3.48E-14	490	490	490	490	0		
0.915751	392	392	392	392	0	627.2	627.2	627.2	627.2	0		
1.106532	627.2	627.2	627.2	627.2	0	882	882	882	882	0		
1.144689	686	686	686	686	0	940.8	940.8	940.8	940.8	0		
1.182845	1234.8	1234.8	1234.8	1234.8	0	1038.8	1038.8	1038.8	1038.8	0		
1.221001	882	882	882	882	0	980	980	980	980	0		
1.259158	980	1764	1764	1502.667	452.6426	1078	1176	1176	1143.333	56.58033		
1.278236	882	980	1078	980	98	1176	1176	1274	1208.667	56.58033		
1.297314	1078	1274	1470	1274	196	1176	1372	1568	1372	196		

Experimental conditions: Geldart B-D, Bed height= 60 cm, Gap height=7.5 cm

U0	DT_P1	DT_P2	DT_P3	Avg_DT	stdv	ANN_p1	ANN_p1	ANN_p1	Annu_Avg_p	stdv	DT_avg	Stdv	T1	T2	T3	Tavg	Vavg	SRR	SRRAvg	Stdv
0	0	0	0	0	0	0	0	0	0	0	0		0	0	0	0	0	0	0	0
0.343407	294	294	294	294	0	392	392	392	392	0	304.8889	159.7226	0	0	0	0	0	0	0	0
0.534188	588	588	588	588	0	588	588	588	588	0	631.5556	279.7147	0	0	0	0	0	0	0	0
0.724969	921.2	921.2	921.2	921.2	0	784	784	784	784	0	951.6889	398.2365	0	0	0	0	0	0	0	0
0.915751	1274	1274	1274	1274	0	980	980	980	980	0	1330.622	547.41	0	0	0	0	0	0	0	0
1.106532	2058	2058	2058	2058	0	1568	1568	1568	1568	0	2003.556	813.6448	0	0	0	0	0	0	0	0
1.144689	2254	2254	2254	2254	0	1666	1666	1666	1666	0	2212.622	897.1208	0	0	0	0	0	0	0	0
1.182845	2450	2450	2450	2450	0	1803.2	1803.2	1803.2	1803.2	0	2460.889	999.5049	0	0	0	0	0	0	0	0
1.221001	2842	2842	2842	2842	0	2058	2058	2058	2058	0	2820.222	1146.637	0	0	0	0	0	0	0	0
1.259158	3234	3234	3234	3234	0	2312.8	2312.8	2312.8	2312.8	0	3342.889	1356.943	0	0	0	0	0	0	0	0
1.278236	5194	5194	5194	5194	0	3626	3626	3626	3626	0	4845.556	1977.433	0	0	0	0	0	0	0	0
1.282051	5978	5978	5978	5978	0	4468.8	4468.8	4468.8	4468.8	0	6152.222	2481.158	0	0	0	0	0	0	0	0

1.285867	2254	2254	2254	2254	0	1764	1960	2156	1960	196	2341.111	958.7217	10.84	12.14	13.16	12.04667	0.004151	6.018262	4.821631	0.745392
1.289683	2254	2156	2254	2221.333	56.58033	2058	2156	2254	2156	98	2308.444	943.4335	7.8	9	8.12	8.306667	0.006019	8.727929	6.70822	0.471813
1.293498	2254	2352	2352	2319.333	56.58033	2156	2058	2352	2188.667	149.6975	2417.333	980.6357	3.97	4.66	5.12	4.583333	0.010909	15.81818	12.74028	1.109045
1.297314	2254		2352	1535.333	69.29646	1960	1960	2058	1992.667	56.58033	2079.778	988.4401	2.38	1.98	3.01	2.456667	0.020353	29.51153	21.69135	3.732307

Second experiment

U0	DT_P1	DT_P2	DT_P3	Avg_DT	stdv	ANN_p1	ANN_p1	ANN_p1	Annu_Avg_p	stdv	Annu_P_avg		T1	T2	T3	Tavg	Vavg	SRR		
0	0	0	0	0	0	0	0	0	0	0	0	0	0	0	0	0	0	0	0	0
0.343407	294	294	294	294	0	392	392	392	392	0	392	0	0	0	0	0	0	0	0	0
0.534188	588	588	588	588	0	588	588	588	588	0	588	0	0	0	0	0	0	0	0	0
0.724969	921.2	921.2	921.2	921.2	0	784	784	784	784	0	784	0	0	0	0	0	0	0	0	0
0.915751	1313.2	1313.2	1313.2	1313.2	0	980	980	980	980	0	980	0	0	0	0	0	0	0	0	0
1.106532	1960	1960	1960	1960	0	1568	1568	1568	1568	0	1568	0	0	0	0	0	0	0	0	0
1.144689	2156	2156	2156	2156	0	1666	1666	1666	1666	0	1698.667	49	0	0	0	0	0	0	0	0
1.182845	2352	2352	2352	2352	0	1764	1764	1764	1764	0	1842.4	89.81848	0	0	0	0	0	0	0	0
1.221001	2646	2646	2646	2646	0	1960	1960	1960	1960	0	2123.333	176.672	0	0	0	0	0	0	0	0
1.259158	3234	3234	3234	3234	0	2352	2352	2352	2352	0	2534.933	304.2738	0	0	0	0	0	0	0	0

1.278236	4410	4410	4410	4410	0	2940	2940	2940	2940	0	3430	369.9419	0	0	0	0	0	0	0	0
1.282051	6174	6174	6174	6174	0	4508	4508	4508	4508	0	4494.933	19.6	0	0	0	20	0.0025	3.625	0	0
1.285867	2254	2254	2450	2319.333	113.1607	1960	2156	2352	2156	196	2090.667	196	14.12	15.48	16.79	15.46333	0.003233	4.68851	0	0
1.289683	2352	2156	2352	2286.667	113.1607	2156	2058	2450	2221.333	204.0033	2199.556	155.8101	7.12	8.47	6.92	7.503333	0.006664	9.662372	0	0
1.293498	2450	2450	2352	2417.333	56.58033	2254	2058	2254	2188.667	113.1607	2188.667	109.5673	5	4.89	5.79	5.226667	0.009566	13.87117	0	0
1.297314	2254	2254	2352	2286.667	56.58033	1960	2058	1960	1992.667	56.58033	1992.667	49	3.12	2.9	3.78	3.266667	0.015306	22.19388	0	0
Third experiment																				
Uo	DT_P1	DT_P2	DT_P3	Avg_DT	stdv	ANN_p1	ANN_p1	ANN_p1	Annu_Avg_p	stdv			T1	T2	T3	Tavg	Vavg	SRR		
0	0	0	0	0	0	0	0	0	0	0			0	0	0	0	0	0	0	0
0.343407	196	196	588	326.6667	226.3213	392	392	392	392	0			0	0	0	0	0	0	0	0
0.534188	588	588	980	718.6667	226.3213	588	588	588	588	0			0	0	0	0	0	0	0	0
0.724969	882	882	1274	1012.667	226.3213	784	784	784	784	0			0	0	0	0	0	0	0	0
0.915751	1274	1274	1666	1404.667	226.3213	980	980	980	980	0			0	0	0	0	0	0	0	0
1.106532	1862	1862	2254	1992.667	226.3213	1568	1568	1568	1568	0			0	0	0	0	0	0	0	0
1.144689	2097.2	2097.2	2489.2	2227.867	226.3213	1764	1764	1764	1764	0			0	0	0	0	0	0	0	0
1.182845	2450	2450	2842	2580.667	226.3213	1960	1960	1960	1960	0			0	0	0	0	0	0	0	0
1.221001	2842	2842	3234	2972.667	226.3213	2352	2352	2352	2352	0			0	0	0	0	0	0	0	0

1.259158	3430	3430	3822	3560.667	226.3213	2940	2940	2940	2940	0			0	0	0	0	0	0	0	0
1.278236	4802	4802	5194	4932.667	226.3213	3724	3724	3724	3724	0			0	0	0	0	0	0	0	0
1.282051	6174	6174	6566	6304.667	226.3213	4508	4508	4508	4508	0			0	0	0	0	0	0	0	0
1.285867	2254	2254	2842	2450	339.482	1960	2156	2352	2156	196			13.5	15.2	16.9	15.2	0.003289	4.769737	0	0
1.289683	2352	2156	2744	2417.333	299.3949	2156	2058	2450	2221.333	204.0033			6.75	9	8.2	7.983333	0.006263	9.08142	0	0
1.293498	2450	2352	2744	2515.333	204.0033	2254	2058	2254	2188.667	113.1607			4.5	5.23	5.89	5.206667	0.009603	13.92446	0	0
1.297314	2254	2352	2646	2417.333	204.0033	1960	2058	1960	1992.667	56.58033			2.5	2.9	3.45	2.95	0.016949	24.57627	0	0

Decreasing velocity

U0	DT_P1	DT_P2	DT_P3	Avg_DT	stdv	ANN_p1	ANN_p1	ANN_p1	Annu_Avg_p	stdv	Dt_avg_decreasing	stdv
0	0	0	0	0	0	0	0	0	0	0	0	0
0.343407	196	196	196	196	0	352.8	352.8	352.8	352.8	6.96E-14	261.3333	0
0.534188	490	490	490	490	0	548.8	548.8	548.8	548.8	0	555.3333	0
0.724969	842.8	842.8	842.8	842.8	0	784	784	784	784	0	868.9333	0
0.915751	1176	1176	1176	1176	0	980	980	980	980	0	1241.333	0
1.106532	1666	1666	1666	1666	0	1372	1372	1372	1372	0	1796.667	0
1.144689	1470	1470	1470	1470	0	1489.6	1489.6	1489.6	1489.6	2.78E-13	1862	0
1.182845	2058	2058	2058	2058	0	1607.2	1607.2	1607.2	1607.2	0	2254	0
1.221001	2450	2450	2450	2450	0	1862	1862	1862	1862	0	2515.333	0
1.259158	2842	2842	2842	2842	0	2058	2058	2058	2058	0	2842	0
1.278236	2254	2254	2156	2221.333	56.58033	2058	1960	2352	2123.333	204.0033	2765.778	80.49399

1.297314	2156	2254	2156	2188.667	56.58033	1960	1960	2156	2025.333	113.1607	2188.667	32.66667
Second experiment												
#VALUE!	DT_P1	DT_P2	DT_P3	Avg_DT	stdv	ANN_p1	ANN_p1	ANN_p1	Annu_Avg_p	stdv	Annu_avg-decreasing	stdv
0	0	0	0	0	0	0	0	0	0	0	0	0
0.343407	294	294	294	294	0	392	392	392	392	0	392	4.02E-14
0.534188	588	588	588	588	0	588	588	588	588	0	588	0
0.724969	882	882	882	882	0	784	784	784	784	0	816.6667	0
0.915751	1274	1274	1274	1274	0	1078	1078	1078	1078	0	1064.933	0
1.106532	1862	1862	1862	1862	0	1568	1568	1568	1568	0	1515.733	0
1.144689	2058	2058	2058	2058	0	1666	1666	1666	1666	0	1613.733	1.61E-13
1.182845	2352	2352	2352	2352	0	1764	1764	1764	1764	0	1744.4	0
1.221001	2548	2548	2548	2548	0	1960	1960	1960	1960	0	1960	0
1.259158	2842	2842	2842	2842	0	2156	2156	2156	2156	0	2156	0
1.278236	3038	3234	2842	3038	196	1764	1960	2254	1992.667	246.6279	2079.778	48.58239
1.297314	2254	2058	2254	2188.667	113.1607	1960	2156	2352	2156	196	2156	47.82732
3rd exp												
U0	DT_P1	DT_P2	DT_P3	Avg_DT	stdv	ANN_p1	ANN_p1	ANN_p1	Annu_Avg_p	stdv		
0	0	0	0	0	0	0	0	0	0	0		
0.343407	294	294	294	294	0	431.2	431.2	431.2	431.2	0		
0.534188	588	588	588	588	0	627.2	627.2	627.2	627.2	0		
0.724969	882	882	882	882	0	882	882	882	882	0		
0.915751	1274	1274	1274	1274	0	1136.8	1136.8	1136.8	1136.8	0		
1.106532	1862	1862	1862	1862	0	1607.2	1607.2	1607.2	1607.2	0		
1.144689	2058	2058	2058	2058	0	1685.6	1685.6	1685.6	1685.6	2.78E-13		
1.182845	2352	2352	2352	2352	0	1862	1862	1862	1862	0		

1.221001	2548	2548	2548	2548	0	2058	2058	2058	2058	0		
1.259158	2842	2842	2842	2842	0	2254	2254	2254	2254	0		
1.278236	3038	3234	2842	3038	196	2156	1960	2254	2123.333	149.6975		
1.297314	2254	2058	2254	2188.667	113.1607	2352	2156	2352	2286.667	113.1607		

Appendix-II

CFD Data

(1) Pressure profiles data

Velocity, m/s	**Draft tube**		**avg**		**avg**	**pressure drop**
Bh_40cm						
0	0	0	0	0	0	0
0.25	3978	4243	4110.5	258	129	2000
0.5	4079	4351	4215	268	134	3000
0.75	3837	4111	3974	269	134.5	3839.5
1.095	4975	5268	5121.5	292	146	4975.5
1.14	3594	3894	3744	292	146	3598
1.2	3961	4244	4102.5	282	141	3961.5
Annular section						
0	0	0	0	0	0	0
0.25	3978	4243	4110.5	258	129	2000
0.5	3807	4079	3943	269	134.5	3000
0.75	4111	4386	4248.5	269	134.5	4114
1.095	4390	4682	4536	292	146	4390
1.14	3294	3594	3444	292	146	3298
1.2	3953	4234	4093.5	282	141	3952.5
Bh_50cm	Draft tube					
0	0	0	0	0	0	0
0.25	1121	1243	1182	258	129	1053

0.5	2079	2351	2215	268	134	2081
0.75	3537	4011	3774	269	134.5	3639.5
1.095	6060	5850	5955	350	175	5780
1.14	6560	6905	6732.5	344	172	6560.5
1.2	4645	4889	4767	243	121.5	4645.5
Annular section						
0	0	0	0	0	0	0
0.25	989	1030	1009.5	258	129	880.5
0.5	1607	1879	1743	269	134.5	1608.5
0.75	2711	2986	2848.5	269	134.5	2714
1.095	5523	5868	5695.5	344	172	5523.5
1.14	5525	5865	5695	344	172	5523
1.2	4245	3985	4115	282	141	3974

(2) Solids volume fraction data at Bed height of 50cm

Height	U0=1.095m/s_BH_50cm		Height	U0=1.14m/s_BH_50cm	Height	U0=1.2m/s_BH_50cm
0	3.00082		0	3.00082	9.12E-07	3.00082
0	2.95734		0	2.95734	2.09E-06	2.95734
0	2.91429		0	2.91429	6.59E-06	2.91429
0	2.87167		0	2.87167	8.53E-06	2.87167
0	2.82947		0	2.82947	7.02E-06	2.82947
0	2.78769		0	2.78769	4.15E-06	2.78769

0	2.74633		0	2.74633	1.02E-06	2.74633
0	2.70538		0	2.70538	5.24E-07	2.70538
0	2.66483		0	2.66483	5.14E-07	2.66483
0	2.62469		0	2.62469	9.09E-07	2.62469
0	2.58495		0	2.58495	2.07E-06	2.58495
0	2.54561		0	2.54561	1.92E-06	2.54561
0	2.52659		0	2.52659	1.37E-06	2.52659
0	2.50666		2.32E-37	2.50666	7.95E-07	2.50666
0	2.46809		7.8E-10	2.46809	6.86E-07	2.46809
0	2.44488		2.21E-08	2.44488	8.64E-07	2.44488
0	2.43424		3.19E-08	2.43424	9.45E-07	2.43424
0	2.43148		3.45E-08	2.43148	9.67E-07	2.43148
0	2.42991		3.61E-08	2.42991	9.79E-07	2.42991
0	2.39211		7.82E-08	2.39211	1.65E-06	2.39211
0	2.35468		9.3E-08	2.35468	1.54E-06	2.35468
0	2.31763		1.06E-07	2.31763	1.16E-06	2.31763
0	2.28094		1.19E-07	2.28094	1.22E-06	2.28094
0	2.24462		1.29E-07	2.24462	8.76E-07	2.24462
0	2.20867		1.36E-07	2.20867	6.35E-07	2.20867
0	2.17307		1.4E-07	2.17307	3.6E-06	2.17307
0	2.13782		1.43E-07	2.13782	9.59E-06	2.13782
0	2.10293		1.47E-07	2.10293	1.76E-05	2.10293
0	2.06838		1.51E-07	2.06838	3.15E-05	2.06838
0	2.03417		1.56E-07	2.03417	5.33E-05	2.03417
0	2.00031		1.6E-07	2.00031	8.1E-05	2.00031
0	1.96678		1.64E-07	1.96678	0.000112	1.96678

0	1.93359		1.69E-07	1.93359	0.000149	1.93359
0	1.90073		1.72E-07	1.90073	0.000203	1.90073
0	1.86819		1.75E-07	1.86819	0.000296	1.86819
0	1.83598		1.78E-07	1.83598	0.000455	1.83598
0	1.80409		1.81E-07	1.80409	0.000695	1.80409
0	1.78635		1.84E-07	1.78635	0.000868	1.78635
0	1.77251		1.86E-07	1.77251	0.001002	1.77251
0	1.74572		1.9E-07	1.74572	0.001286	1.74572
0	1.74303		1.91E-07	1.74303	0.001315	1.74303
0	1.74162		1.91E-07	1.74162	0.001331	1.74162
0	1.74125		1.91E-07	1.74125	0.001336	1.74125
3.36E-32	1.7103		1.98E-07	1.7103	0.001643	1.7103
1.97E-10	1.67966		2.06E-07	1.67966	0.001875	1.67966
5.45E-09	1.64933		2.16E-07	1.64933	0.00202	1.64933
2.97E-08	1.61929		2.27E-07	1.61929	0.002077	1.61929
9.13E-08	1.58956		2.41E-07	1.58956	0.002076	1.58956
1.58E-07	1.56012		2.55E-07	1.56012	0.002066	1.56012
2.01E-07	1.53097		2.66E-07	1.53097	0.002084	1.53097
2.34E-07	1.50211		2.68E-07	1.50211	0.002162	1.50211
2.62E-07	1.47354		2.65E-07	1.47354	0.00242	1.47354
2.83E-07	1.44526		2.74E-07	1.44526	0.003063	1.44526
2.99E-07	1.41725		3.28E-07	1.41725	0.004086	1.41725
3.12E-07	1.38953		4.42E-07	1.38953	0.005128	1.38953
3.25E-07	1.36208		5.71E-07	1.36208	0.005886	1.36208
3.34E-07	1.3349		6.49E-07	1.3349	0.006487	1.3349
3.4E-07	1.30799		6.6E-07	1.30799	0.007245	1.30799

3.45E-07	1.28136		6.35E-07	1.28136	0.008272	1.28136
3.49E-07	1.25498		6.12E-07	1.25498	0.009439	1.25498
3.54E-07	1.22887		5.98E-07	1.22887	0.010476	1.22887
3.6E-07	1.20302		5.91E-07	1.20302	0.011184	1.20302
3.68E-07	1.17743		5.89E-07	1.17743	0.011553	1.17743
3.76E-07	1.15209		5.94E-07	1.15209	0.011706	1.15209
3.86E-07	1.127		6.06E-07	1.127	0.011851	1.127
3.97E-07	1.10216		6.25E-07	1.10216	0.012144	1.10216
4.64E-07	1.07757		8.02E-07	1.07757	0.012649	1.07757
7.87E-07	1.05322		1.65E-06	1.05322	0.013536	1.05322
8.21E-07	1.05041		1.74E-06	1.05041	0.0137	1.05041
7.87E-07	1.05322		1.65E-06	1.05322	0.013536	1.05322
8.68E-07	1.0466		1.86E-06	1.0466	0.013924	1.0466
8.71E-07	1.04637		1.87E-06	1.04637	0.013937	1.04637
1.08E-06	1.02912		2.42E-06	1.02912	0.014944	1.02912
1.14E-06	1.00526		2.57E-06	1.00526	0.016631	1.00526
1.2E-06	0.981629		2.72E-06	0.981629	0.018409	0.981629
1.27E-06	0.958237		2.86E-06	0.958237	0.020453	0.958237
1.35E-06	0.935078		2.99E-06	0.935078	0.022952	0.935078
1.44E-06	0.91215		3.08E-06	0.91215	0.025978	0.91215
1.54E-06	0.889449		3.16E-06	0.889449	0.029134	0.889449
1.67E-06	0.866975		3.24E-06	0.866975	0.031784	0.866975
2.53E-06	0.844723		3.33E-06	0.844723	0.034142	0.844723
8.04E-06	0.822694		3.43E-06	0.822694	0.036929	0.822694
2.24E-05	0.800883		3.55E-06	0.800883	0.040336	0.800883
4.48E-05	0.77929		3.69E-06	0.77929	0.045158	0.77929

8.11E-05	0.757911		3.91E-06	0.757911	0.051459	0.757911
0.000159	0.736745		4.32E-06	0.736745	0.057928	0.736745
0.000419	0.715789		5.1E-06	0.715789	0.065863	0.715789
0.001557	0.695042		6.63E-06	0.695042	0.072906	0.695042
0.004719	0.674501		9.4E-06	0.674501	0.076464	0.674501
0.012025	0.654165		1.47E-05	0.654165	0.079292	0.654165
0.030878	0.634031		3.28E-05	0.634031	0.091458	0.634031
0.07312	0.614097		0.000114	0.614097	0.108988	0.614097
0.140183	0.594362		0.000336	0.594362	0.125125	0.594362
0.179255	0.584335		0.000574	0.584335	0.135901	0.584335
0.235853	0.574308		0.001004	0.574308	0.140776	0.574308
0.308862	0.564281		0.002205	0.564281	0.134649	0.564281
0.383229	0.554254		0.006766	0.554254	0.139494	0.554254
0.452685	0.544227		0.03277	0.544227	0.166493	0.544227
0.508667	0.5342		0.167112	0.5342	0.220785	0.5342
0.527648	0.524173		0.36939	0.524173	0.291345	0.524173
0.538698	0.514146		0.486668	0.514146	0.337872	0.514146
0.548114	0.504119		0.513211	0.504119	0.363995	0.504119
0.537912	0.494092		0.50335	0.494092	0.377723	0.494092
0.53476	0.484065		0.489401	0.484065	0.385028	0.484065
0.541712	0.474039		0.486747	0.474039	0.39104	0.474039
0.525715	0.464012		0.495175	0.464012	0.389936	0.464012
0.514625	0.453985		0.502391	0.453985	0.389591	0.453985
0.532916	0.443958		0.50486	0.443958	0.390432	0.443958
0.549988	0.433931		0.508278	0.433931	0.393043	0.433931
0.555749	0.423904		0.512484	0.423904	0.39594	0.423904

0.55018	0.413877		0.518448	0.413877	0.397928	0.413877
0.546814	0.40385		0.525762	0.40385	0.400958	0.40385
0.541007	0.393823		0.52594	0.393823	0.402936	0.393823
0.539396	0.385635		0.526794	0.385635	0.403819	0.385635
0.540166	0.377446		0.53029	0.377446	0.406588	0.377446
0.538482	0.369257		0.529121	0.369257	0.410524	0.369257
0.537844	0.361069		0.523187	0.361069	0.413623	0.361069
0.535501	0.35288		0.513179	0.35288	0.415998	0.35288
0.535345	0.352472		0.513001	0.352472	0.41609	0.352472
0.535322	0.352411		0.512974	0.352411	0.416103	0.352411
0.533915	0.349017		0.512044	0.349017	0.416903	0.349017
0.532121	0.344691		0.510866	0.344691	0.417922	0.344691
0.52897	0.336503		0.514542	0.336503	0.418624	0.336503
0.525946	0.328314		0.517169	0.328314	0.420112	0.328314
0.524188	0.320125		0.520572	0.320125	0.422166	0.320125
0.523959	0.311937		0.523411	0.311937	0.422629	0.311937
0.522343	0.306519		0.525008	0.306519	0.423761	0.306519
0.521519	0.303748		0.525832	0.303748	0.42434	0.303748
0.517738	0.295559		0.529087	0.295559	0.42742	0.295559
0.515328	0.287371		0.531791	0.287371	0.428698	0.287371
0.512901	0.279182		0.532177	0.279182	0.42964	0.279182
0.510141	0.270993		0.531092	0.270993	0.430859	0.270993
0.506699	0.262805		0.530419	0.262805	0.432523	0.262805
0.503201	0.254616		0.530604	0.254616	0.43537	0.254616
0.499288	0.246427		0.530587	0.246427	0.438071	0.246427
0.493059	0.238239		0.530024	0.238239	0.440118	0.238239

0.486231	0.23005		0.530852	0.23005	0.442179	0.23005
0.479034	0.221861		0.533073	0.221861	0.441008	0.221861
0.472532	0.213673		0.535044	0.213673	0.437393	0.213673
0.466028	0.205484		0.53595	0.205484	0.436689	0.205484
0.457961	0.197296		0.534994	0.197296	0.438764	0.197296
0.450214	0.189107		0.5343	0.189107	0.441514	0.189107
0.44155	0.180918		0.535664	0.180918	0.444373	0.180918
0.432634	0.17273		0.536946	0.17273	0.446415	0.17273
0.42546	0.164541		0.538194	0.164541	0.44865	0.164541
0.42299	0.156352		0.543228	0.156352	0.452331	0.156352
0.408173	0.148164		0.527337	0.148164	0.446621	0.148164
0.407134	0.14549		0.526394	0.14549	0.445789	0.14549
0.413282	0.142816		0.533519	0.142816	0.448576	0.142816
0.417161	0.140142		0.53337	0.140142	0.450004	0.140142
0.420529	0.137468		0.530589	0.137468	0.450409	0.137468
0.423067	0.134794		0.528201	0.134794	0.450432	0.134794
0.424166	0.132121		0.524781	0.132121	0.450064	0.132121
0.423735	0.129447		0.521402	0.129447	0.449225	0.129447
0.422358	0.126773		0.520362	0.126773	0.44835	0.126773
0.420668	0.124099		0.521638	0.124099	0.447643	0.124099
0.418821	0.121425		0.523881	0.121425	0.446708	0.121425
0.416643	0.118751		0.526249	0.118751	0.445708	0.118751
0.414438	0.116077		0.528312	0.116077	0.445011	0.116077
0.412676	0.113404		0.529543	0.113404	0.444387	0.113404
0.411343	0.11073		0.531168	0.11073	0.44412	0.11073
0.409526	0.108056		0.533624	0.108056	0.443993	0.108056

0.406231	0.105382		0.535454	0.105382	0.443841	0.105382
0.401458	0.102708		0.535659	0.102708	0.444123	0.102708
0.39556	0.100034		0.534798	0.100034	0.444088	0.100034
0.38938	0.097361		0.533922	0.097361	0.443656	0.097361
0.38378	0.094687		0.532351	0.094687	0.442611	0.094687
0.378853	0.092013		0.52927	0.092013	0.440546	0.092013
0.374446	0.089339		0.524331	0.089339	0.438744	0.089339
0.370407	0.086665		0.518755	0.086665	0.437728	0.086665
0.366676	0.083991		0.513926	0.083991	0.437162	0.083991
0.362847	0.081318		0.510044	0.081318	0.437061	0.081318
0.358974	0.078644		0.506659	0.078644	0.437802	0.078644
0.355662	0.07597		0.503162	0.07597	0.438837	0.07597
0.352983	0.073296		0.499519	0.073296	0.439387	0.073296
0.350577	0.070622		0.494432	0.070622	0.438773	0.070622
0.343633	0.067948		0.494915	0.067948	0.439789	0.067948
0.328596	0.062934		0.494474	0.062934	0.443843	0.062934
0.314582	0.05792		0.483471	0.05792	0.447922	0.05792
0.296655	0.052907		0.477587	0.052907	0.45311	0.052907
0.28053	0.047893		0.475536	0.047893	0.45518	0.047893
0.277986	0.046898		0.475433	0.046898	0.454606	0.046898
0.277677	0.046767		0.475452	0.046767	0.454561	0.046767
0.270189	0.043846		0.475116	0.043846	0.45289	0.043846
0.267652	0.04288		0.474909	0.04288	0.452261	0.04288
0.257617	0.037867		0.474079	0.037867	0.446126	0.037867
0.249464	0.032853		0.472564	0.032853	0.443135	0.032853
0.241642	0.02784		0.46691	0.02784	0.442961	0.02784

0.233128	0.022826		0.454336	0.022826	0.444654	0.022826
0.231254	0.021743		0.450522	0.021743	0.446088	0.021743
0.231022	0.021607		0.449987	0.021607	0.44624	0.021607
0.226484	0.019022		0.440857	0.019022	0.449681	0.019022
0.224373	0.017813		0.436538	0.017813	0.451285	0.017813
0.213882	0.0128		0.413135	0.0128	0.458473	0.0128
0.197507	0.007786		0.384915	0.007786	0.456193	0.007786
0.194458	0.00721		0.380453	0.00721	0.454099	0.00721
0.193617	0.007051		0.37924	0.007051	0.45351	0.007051
0.171768	0.002989		0.348732	0.002989	0.439001	0.002989
0.170607	0.002773		0.347135	0.002773	0.438213	0.002773
0.156323	0.000917		0.331275	0.000917	0.424183	0.000917
0.132081	-0.00224		0.304253	-0.00224	0.400368	-0.00224
0.111451	-0.00725		0.284096	-0.00725	0.376226	-0.00725

Appendix-III

Solids re-circulation rate (G_s) model fit data

Gap height, m	dp	Umf,minimum	A_gap	BH(Bed height),m	Q input flow rate, m3/s	U0, m/s	Rep	ΔP draft, pa	ΔP annular, pa	Upd , m/s	Upr	εr	Gs, Measured	Predicted Gs	Error	Ws(30%)	Ws(-30%)
0.075	0.0004	0.180424	0.0306	0.4	0.008056	1.026185	11.78606	89.24699	3874.267	0.002514	0.023253	0.498378	3.260784651	4.418131286	0.354929	4.23902	2.282549
0.075	0.0004	0.180424	0.0306	0.4	0.008333	1.061571	11.78606	26.40415	2031.867	0.002762	0.036578	0.649583	3.876413032	5.345979852	0.379105	5.039337	2.713489
0.075	0.0004	0.180424	0.0306	0.4	0.008611	1.096957	11.78606	70.38688	2112.444	0.003137	0.069706	0.7912	4.396513441	6.873814442	0.563469	5.715467	3.077559
0.075	0.0004	0.180424	0.0306	0.4	0.008889	1.132343	11.78606	56.58033	2079.778	0.006337	0.210441	0.860273	8.172468227	10.73925802	0.314078	10.62421	5.720728
0.075	0.0004	0.180424	0.0306	0.4	0.009167	1.167728	11.78606	75.44044	2134.222	0.007576	0.30303	0.884	11.74591481	12.33073201	0.049789	15.26969	8.22214
0.075	0.0004	0.180424	0.0306	0.4	0.009444	1.203114	11.78606	32.66667	2471.778	0.014286	0.64	0.896429	17.77461536	16.62385763	0.064742	23.107	12.44223
0.075	0.0004	0.180424	0.0306	0.5	0.008333	1.061571	11.78606	2149.467	1992.667	0.003998	0.031183	0.405128	5.690497455	6.017296458	0.057429	7.397647	3.983348
0.075	0.0004	0.180424	0.0306	0.5	0.008611	1.096957	11.78606	2216.978	2014.444	0.007042	0.094885	0.655625	10.06580906	9.418227095	0.064335	13.08555	7.046066
0.075	0.000	0.1804	0.030	0.5	0.008889	1.13234	11.7860	2234.	2123.33	0.00	0.18	0.74	13.031	12.177	0.06	16.9	9.12

	4	24	6			3	6	4	3	9987	198	5366	57153	37037	5549	4104	21
0.075	0.0004	0.180424	0.0306	0.5	0.009167	1.167728	11.78606	2232.222	2156	0.01506	0.447504	0.843846	18.23801785	17.50097274	0.040413	23.70942	12.76661
0.075	0.0004	0.180424	0.0306	0.5	0.009444	1.203114	11.78606	2558.889	2439.111	0.013453	0.474809	0.868533	21.60198737	17.62498222	0.184104	28.08258	15.12139
0.075	0.0004	0.180424	0.0306	0.6	0.008611	1.096957	11.78606	5592.533	4109.467	0.004528	0.027166	0.226667	6.077480244	6.383416414	0.050339	7.900724	4.254236
0.075	0.0004	0.180424	0.0306	0.6	0.00875	1.11465	11.78606	3332	2842	0.006859	0.086636	0.632667	9.237375743	10.35568138	0.121063	12.00859	6.466163
0.075	0.0004	0.180424	0.0306	0.6	0.008889	1.132343	11.78606	3297.156	2613.333	0.008897	0.158165	0.739	11.71135611	13.24355731	0.13083	15.22476	8.197949
0.075	0.0004	0.180424	0.0306	0.6	0.009028	1.150035	11.78606	3301.511	2706.978	0.010446	0.28651	0.830833	13.36542763	16.81842357	0.258353	17.37506	9.355799
0.075	0.0004	0.180424	0.0306	0.6	0.009306	1.185421	11.78606	3059.778	2548	0.012315	0.477683	0.880375	15.77724389	20.57577172	0.304142	20.51042	11.04407
0.075	0.0004	0.180424	0.0306	0.6	0.009444	1.203114	11.78606	3166.489	2541.467	0.014955	0.616899	0.887515	20.18256773	22.78483292	0.128936	26.23734	14.1278
0.105	0.0004	0.180424	0.04284	0.4	0.008611	1.096957	11.78606	2256.178	1851.111	0.001916	0.0445	0.800222	2.112727015	6.060052455	1.868356	2.746545	1.478909
0.105	0.0004	0.180424	0.04284	0.4	0.00875	1.11465	11.78606	2014.444	1829.333	0.00171	0.0456	0.826	3.235934922	6.08141919	0.879339	4.206715	2.265154
0.105	0.0004	0.180424	0.04284	0.4	0.008889	1.132343	11.78606	1938.222	1916.444	0.004892	0.148458	0.847091	5.850069424	9.850148426	0.683766	7.60509	4.095049

0.105	0.0004	0.180424	0.04284	0.4	0.009167	1.167728	11.78606	1933.867	1840.222	0.006837	0.243087	0.8695	8.065950258	11.95661861	0.482357	10.48574	5.646165
0.105	0.0004	0.180424	0.04284	0.4	0.009306	1.185421	11.78606	2014.444	1905.556	0.007886	0.315457	0.884	12.13032599	13.23207573	0.090826	15.76942	8.491228
0.105	0.0004	0.180424	0.04284	0.4	0.009361	1.192498	11.78606	2504.444	2156	0.018844	0.927716	0.90575	24.34032469	20.74398052	0.147753	31.64242	17.03823
0.105	0.0004	0.180424	0.04284	0.5	0.008194	1.043878	11.78606	2602.444	2047.111	0.003034	0.023489	0.400667	4.147597254	5.695375401	0.373175	5.391876	2.903318
0.105	0.0004	0.180424	0.04284	0.5	0.008333	1.061571	11.78606	2391.2	2123.333	0.003444	0.037658	0.57561	3.452380952	6.865937561	0.988754	4.488095	2.416667
0.105	0.0004	0.180424	0.04284	0.5	0.008611	1.096957	11.78606	2297.556	2112.444	0.004744	0.065432	0.6636	8.182844244	8.518887221	0.041067	10.6377	5.727991
0.105	0.0004	0.180424	0.04284	0.5	0.008889	1.132343	11.78606	2373.778	2199.556	0.006637	0.108161	0.715273	14.46143617	10.35332423	0.284074	18.79987	10.12301
0.105	0.0004	0.180424	0.04284	0.5	0.009167	1.167728	11.78606	2293.2	2112.444	0.013032	0.248613	0.756774	18.62157534	14.51933666	0.220295	24.20805	13.0351
0.105	0.0004	0.180424	0.04284	0.6	0.009028	1.150035	11.78606	5588.178	4529.778	0.009202	0.0818	0.478	12.26697172	10.46048211	0.147265	15.94706	8.58688
0.105	0.0004	0.180424	0.04284	0.6	0.009167	1.167728	11.78606	3854.667	3565.022	0.009954	0.134583	0.656833	14.33276096	12.85491442	0.10311	18.63259	10.03293
0.105	0.0004	0.180424	0.04284	0.6	0.009306	1.185421	11.78606	3451.778	3734.889	0.015974	0.296337	0.749875	17.69851631	17.76953368	0.004013	23.00807	12.38896
0.105	0.000	0.1804	0.042	0.6	0.009333	1.18896	11.7860	3484.	3549.77	0.01	0.49	0.82	27.601	21.998	0.20	35.8	19.3

	4	24	84				6	444	8	9084	3938	0727	87755	49499	3007	8244	2131
0.145	0.0004	0.180424	0.05916	0.4	0.00875	1.11465	11.78606	3047.8	1429.167	0.003265	0.067409	0.77525	10.24976437	7.609360052	0.257606	13.32469	7.174835
0.145	0.0004	0.180424	0.05916	0.5	0.009167	1.167728	11.78606	2672.133	2308.444	0.007928	0.17759	0.792857	11.49577167	13.24153224	0.151861	14.9445	8.04704
0.145	0.0004	0.180424	0.05916	0.5	0.009306	1.185421	11.78606	2750.533	2635.111	0.010218	0.245232	0.806667	14.81607629	15.01371075	0.013339	19.2609	10.37125
0.145	0.0004	0.180424	0.05916	0.6	0.009167	1.167728	11.78606	3342.889	2450	0.01083	0.097473	0.484444	15.70397112	12.02039376	0.234563	20.41516	10.99278
0.075	0.0008	0.522732	0.0306	0.4	0.009306	1.185421	68.29406	2123.333	1872.889	0.00312	0.018266	0.207333	4.298600133	3.74223497	0.129429	5.58818	3.00902
0.075	0.0008	0.522732	0.0306	0.4	0.009333	1.18896	68.29406	1372	1600.667	0.004155	0.053904	0.642333	6.349476718	5.868471433	0.075755	8.25432	4.444634
0.075	0.0008	0.522732	0.0306	0.4	0.009361	1.192498	68.29406	1459.111	1687.778	0.005304	0.094295	0.739	9.023411165	7.37835904	0.182309	11.73043	6.316388
0.075	0.0008	0.522732	0.0306	0.4	0.009389	1.196037	68.29406	1263.111	1535.333	0.007996	0.219312	0.830833	14.11649062	10.49196151	0.256759	18.35144	9.881543
0.075	0.0008	0.522732	0.0306	0.5	0.009306	1.185421	68.29406	5782	3996.222	0.002727	0.016364	0.226667	5.368110889	4.199309413	0.217731	6.978544	3.757678
0.075	0.0008	0.522732	0.0306	0.5	0.009333	1.18896	68.29406	1426.444	1774.889	0.003913	0.049432	0.632667	6.927701653	6.771133088	0.0226	9.006012	4.849391
0.075	0.0008	0.522732	0.0306	0.5	0.009361	1.192498	68.29406	1589.778	2014.444	0.004921	0.087489	0.739	12.87457771	8.535618072	0.337018	16.73695	9.012204

0.075	0.0008	0.522732	0.0306	0.5	0.009389	1.196037	68.29406	1611.556	1774.889	0.008977	0.246217	0.830833	19.02557932	13.16092741	0.308251	24.73325	13.31791
0.075	0.0008	0.522732	0.0306	0.6	0.009361	1.192498	68.29406	2341.111	2090.667	0.004151	0.024903	0.226667	5.353386384	5.891964626	0.100605	6.959402	3.74737
0.075	0.0008	0.522732	0.0306	0.6	0.009389	1.196037	68.29406	2308.444	2199.556	0.006019	0.076033	0.632667	7.692937369	9.325644184	0.212234	10.00082	5.385056
0.075	0.0008	0.522732	0.0306	0.6	0.009417	1.199575	68.29406	2417.333	2188.667	0.010909	0.193939	0.739	13.11724252	13.77363703	0.050041	17.05242	9.18207
0.075	0.0008	0.522732	0.0306	0.6	0.009444	1.203114	68.29406	2079.778	1992.667	0.020353	0.558248	0.830833	21.85886142	21.51550367	0.015708	28.41652	15.3012
0.105	0.0008	0.522732	0.04284	0.4	0.009306	1.185421	68.29406	1317.556	1568	0.003713	0.057121	0.6984	5.099021183	6.368795474	0.249023	6.628728	3.569315
0.105	0.0008	0.522732	0.04284	0.4	0.009333	1.18896	68.29406	1626.8	1894.667	0.00625	0.156	0.814103	8.486344076	9.599403677	0.131159	11.03225	5.940441
0.105	0.0008	0.522732	0.04284	0.4	0.009361	1.192498	68.29406	1742.222	1720.444	0.011811	0.4519	0.878727	16.1779755	14.98829055	0.073537	21.03137	11.32458
0.105	0.0008	0.522732	0.04284	0.5	0.009333	1.18896	68.29406	4769.333	3593.333	0.004502	0.056022	0.627143	7.634360434	7.405568693	0.029969	9.924669	5.344052
0.105	0.0008	0.522732	0.04284	0.5	0.009361	1.192498	68.29406	1676.889	1589.778	0.008547	0.189702	0.790945	12.1172887	12.55831588	0.036397	15.75248	8.482102
0.105	0.0008	0.522732	0.04284	0.5	0.009389	1.196037	68.29406	1883.778	1774.889	0.012799	0.412859	0.85616	19.97041565	17.30358506	0.133539	25.96154	13.97929
0.105	0.000	0.5227	0.042	0.6	0.009361	1.19249	68.2940	1764	1698.66	0.00	0.03	0.63	11.458	7.3464	0.35	14.8	8.02

	8	32	84			8	6		7	2906	6713	2667	87885	87669	8883	9654	1215
0.105	0.0008	0.522732	0.04284	0.6	0.009444	1.203114	68.29406	1949.111	1676.889	0.010768	0.28715	0.826	24.15800432	17.23605289	0.286528	31.40541	16.9106
0.145	0.0008	0.522732	0.05916	0.4	0.009361	1.192498	68.29406	1862	2123.333	0.005394	0.101236	0.752787	7.098158333	8.437678271	0.188714	9.227606	4.968711
0.145	0.0008	0.522732	0.05916	0.4	0.009389	1.196037	68.29406	1655.111	1437.333	0.007665	0.225652	0.842391	11.11773791	11.88048506	0.068606	14.45306	7.782417
0.145	0.0008	0.522732	0.05916	0.4	0.009417	1.199575	68.29406	1829.333	1524.444	0.012225	0.510258	0.888833	17.05952381	16.65997336	0.023421	22.17738	11.94167
0.145	0.0008	0.522732	0.05916	0.5	0.009389	1.196037	68.29406	2112.444	1698.667	0.005857	0.070285	0.613333	7.448660152	8.756900988	0.175636	9.683258	5.214062
0.145	0.0008	0.522732	0.05916	0.5	0.009417	1.199575	68.29406	1907.733	1600.667	0.006693	0.128514	0.758333	9.523339139	11.24249482	0.18052	12.38034	6.666337
0.145	0.0008	0.522732	0.05916	0.5	0.009444	1.203114	68.29406	1831.511	1633.333	0.011783	0.34564	0.841818	22.69207792	16.96152444	0.252535	29.4997	15.88445
0.145	0.0008	0.522732	0.05916	0.6	0.009361	1.192498	68.29406	2330.222	2776.667	0.004283	0.066391	0.700645	6.631303739	9.783981719	0.475424	8.620695	4.641913
0.145	0.0008	0.522732	0.05916	0.6	0.009389	1.196037	68.29406	2286.667	1764	0.006957	0.158279	0.796044	11.08597733	14.19542666	0.280485	14.41177	7.760181
0.145	0.0008	0.522732	0.05916	0.6	0.009417	1.199575	68.29406	2526.222	1622.444	0.011468	0.414324	0.871571	16.96312405	21.22599353	0.251302	22.05206	11.87419
0.145	0.0008	0.522732	0.05916	0.6	0.009444	1.203114	68.29406	1687.778	1709.556	0.01906	0.786982	0.887625	19.38001862	27.77925303	0.433397	25.19402	13.56601

Appendix-IV

UDF’s drag models

Arastoopour drag & Gibilaro drag UDF’s -3D

```
#include "udf.h"
#include "sg_mphase.h"
#define pi 3.14
#define diam2 0.000470

DEFINE_EXCHANGE_PROPERTY(custom_drag_Gibi, cell, mix_thread, s_col, f_col)

{

        Thread *thread_g, *thread_s;

        real x_vel_g, x_vel_s, y_vel_g, y_vel_s, z_vel_g, z_vel_s, NV_slip, slip_x, slip_y, slip_z, rho_g, rho_s, mu_g, rep, void_g, tp,
k_g_s;

        thread_g = THREAD_SUB_THREAD(mix_thread, s_col);

        thread_s = THREAD_SUB_THREAD(mix_thread, f_col);


        x_vel_g = C_U(cell, thread_g);
        y_vel_g = C_V(cell, thread_g);
        z_vel_g = C_W(cell, thread_g);
        x_vel_s = C_U(cell, thread_s);
        y_vel_s = C_V(cell, thread_s);
```

```
        z_vel_s = C_W(cell, thread_s);


        slip_x = x_vel_g - x_vel_s;
        slip_y = y_vel_g - y_vel_s;
        slip_z = z_vel_g - z_vel_s;

        rho_g = C_R(cell, thread_g);
        rho_s = C_R(cell, thread_s);
        mu_g = C_MU_L(cell, thread_g);

        NV_slip = sqrt(slip_x*slip_x + slip_y*slip_y + slip_z*slip_z);

        tp = rho_s*diam2*diam2/18./mu_g;

        void_g = C_VOF(cell, thread_g);

        rep = rho_g*NV_slip*diam2*void_g/mu_g;

        k_g_s = (17.3/rep+0.336)*rho_g*NV_slip*pow(void_g, -1.8)*(1.-void_g)/diam2;

        return k_g_s;
}

DEFINE_EXCHANGE_PROPERTY(custom_drag_Arast, cell, mix_thread, s_col, f_col)

{

        Thread *thread_g, *thread_s;
```

```
real x_vel_g, x_vel_s, y_vel_g, y_vel_s, z_vel_g, z_vel_s, NV_slip, slip_x, slip_y, slip_z, rho_g, rho_s, mu_g, rep, void_g, tp,
k_g_s;

thread_g = THREAD_SUB_THREAD(mix_thread, s_col);

thread_s = THREAD_SUB_THREAD(mix_thread, f_col);

x_vel_g = C_U(cell, thread_g);
y_vel_g = C_V(cell, thread_g);
z_vel_g = C_W(cell, thread_g);
x_vel_s = C_U(cell, thread_s);
y_vel_s = C_V(cell, thread_s);
z_vel_s = C_W(cell, thread_s);

slip_x = x_vel_g - x_vel_s;
slip_y = y_vel_g - y_vel_s;
slip_z = z_vel_g - z_vel_s;

rho_g = C_R(cell, thread_g);
rho_s = C_R(cell, thread_s);

mu_g = C_MU_L(cell, thread_g);

NV_slip = sqrt(slip_x*slip_x + slip_y*slip_y + slip_z*slip_z);

tp = rho_s*diam2*diam2/18./mu_g;

void_g = C_VOF(cell, thread_g);

/*rep = rho_g*NV_slip*diam2*void_g/mu_g;*/

rep = rho_g*NV_slip*diam2/mu_g;
```

```
    k_g_s = (17.3/rep+0.336)*rho_g*NV_slip*pow(void_g, -2.8)*(1.-void_g)/diam2;
    return k_g_s;
}
```

2D Arastooapour drag & Gibilaro drag for 853 Micron size particles

```
#include "udf.h"
#include "sg_mphase.h"
#define pi 3.14
#define diam2 0.000853

DEFINE_EXCHANGE_PROPERTY(custom_drag_Gibi, cell, mix_thread, s_col, f_col)

{

    Thread *thread_g, *thread_s;

    real x_vel_g, x_vel_s, y_vel_g, y_vel_s, NV_slip, slip_x, slip_y, rho_g, rho_s, mu_g, rep, void_g, tp, k_g_s;

    thread_g = THREAD_SUB_THREAD(mix_thread, s_col);

    thread_s = THREAD_SUB_THREAD(mix_thread, f_col);


    x_vel_g = C_U(cell, thread_g);
    y_vel_g = C_V(cell, thread_g);
    x_vel_s = C_U(cell, thread_s);
```

```
        y_vel_s = C_V(cell, thread_s);

        slip_x = x_vel_g - x_vel_s;
        slip_y = y_vel_g - y_vel_s;

        rho_g = C_R(cell, thread_g);
        rho_s = C_R(cell, thread_s);
        mu_g = C_MU_L(cell, thread_g);

        NV_slip = sqrt(slip_x*slip_x + slip_y*slip_y);

        tp = rho_s*diam2*diam2/18./mu_g;

        void_g = C_VOF(cell, thread_g);

        rep = rho_g*NV_slip*diam2*void_g/mu_g;
        k_g_s = (17.3/rep+0.336)*rho_g*NV_slip*pow(void_g, -1.8)*(1.-void_g)/diam2;
        return k_g_s;
}

DEFINE_EXCHANGE_PROPERTY(custom_drag_Arast, cell, mix_thread, s_col, f_col)

{
        Thread *thread_g, *thread_s;
        real x_vel_g, x_vel_s, y_vel_g, y_vel_s, NV_slip, slip_x, slip_y, rho_g, rho_s, mu_g, rep, void_g, tp, k_g_s;
        thread_g = THREAD_SUB_THREAD(mix_thread, s_col);
```

```
thread_s = THREAD_SUB_THREAD(mix_thread, f_col);


x_vel_g = C_U(cell, thread_g);
y_vel_g = C_V(cell, thread_g);
x_vel_s = C_U(cell, thread_s);
y_vel_s = C_V(cell, thread_s);

slip_x = x_vel_g - x_vel_s;
slip_y = y_vel_g - y_vel_s;

rho_g = C_R(cell, thread_g);
rho_s = C_R(cell, thread_s);

mu_g = C_MU_L(cell, thread_g);

NV_slip = sqrt(slip_x*slip_x + slip_y*slip_y );

tp = rho_s*diam2*diam2/18./mu_g;

void_g = C_VOF(cell, thread_g);


/*rep = rho_g*NV_slip*diam2*void_g/mu_g;*/


rep = rho_g*NV_slip*diam2/mu_g;

k_g_s = ((17.3/rep)+0.336)*rho_g*NV_slip*pow(void_g, -2.8)*(1.-void_g)/diam2;
```

```
        return k_g_s;
}

DEFINE_EXCHANGE_PROPERTY(custom_drag_Beestra, cell, mix_thread, s_col, f_col)

{

        Thread *thread_g, *thread_s;

        real x_vel_g, x_vel_s, y_vel_g, y_vel_s, NV_slip, slip_x, slip_y, rho_g, rho_s, mu_g, rep, void_g, tp, k_g_s, phi, f ;

        thread_g = THREAD_SUB_THREAD(mix_thread, s_col);

        thread_s = THREAD_SUB_THREAD(mix_thread, f_col);


        x_vel_g = C_U(cell, thread_g);
        y_vel_g = C_V(cell, thread_g);
        x_vel_s = C_U(cell, thread_s);
        y_vel_s = C_V(cell, thread_s);

        slip_x = x_vel_g - x_vel_s;
        slip_y = y_vel_g - y_vel_s;

         if (slip_x

        rho_g = C_R(cell, thread_g);
        rho_s = C_R(cell, thread_s);

        mu_g = C_MU_L(cell, thread_g);
```

```
        NV_slip = sqrt(slip_x*slip_x + slip_y*slip_y);
        void_g = C_VOF(cell, thread_g);
        phi = void_g ;
        //Non-dimensional drag force
        f = (10*phi/(pow(1-phi,2))) + (pow(1-phi,2)*(1+1.5*pow(phi,0.5))) /*(1+ ((((0.413*rep)/(24*pow(1-phi,2)))*((1/(1-phi) +
        3*phi*(1-phi) + 8.4*pow(rep,-0.343))))/(1+pow(10,3*phi)*pow(rep,-(1+4*phi)/2))))*/;
        f = f/(1-phi);
        //Corrects definition from drag only to total solid-fluid force
         //Interphase momentum exchange coefficient
        k_g_s = f;
         //Update momentum source UDM
        return k_g_s;

}
```